

NASA-CR-178973

J. T. Woodbridge EP25
P-185

AEROJET STRATEGIC PROPULSION COMPANY
P.O. BOX 15699C
SACRAMENTO, CALIFORNIA 95813

SRB/SLEEC (SOLID ROCKET BOOSTER/
SHINGLE LAP EXTENDIBLE EXIT CONE)
FEASIBILITY STUDY


Period of Performance
23 September 1985 to 19 September 1986

Published 19 September 1986

FINAL REPORT
Contract NAS8-36571
Report No. SRB-CLE-F

Volume 1 of 2 Volumes

(NASA-CR-178973) SRB/SLEEC (SOLID ROCKET BOOSTER/SHINGLE LAP EXTENDIBLE EXIT CONE) FEASIBILITY STUDY, VOLUME 1 Final Report, 23 Sep. 1985 - 19 Sep. 1986 (Aerojet Strategic Propulsion Co.) 185 p	N88-28964 Unclas CSCL 21H G3/20 0164894
---	---

 Date for general release Sept. 1988

Prepared for

GEORGE C. MARSHALL SPACE FLIGHT CENTER
MARSHALL SPACE FLIGHT CENTER, ALABAMA 35812

(NASA-CR-178973) SRB/SLEEC (SOLID ROCKET BOOSTER/SHINGLE LAP EXTENDIBLE EXIT CONE) FEASIBILITY STUDY, VOLUME 1 Final Report, 23 Sep. 1985 - 19 Sep. 1986 (Aerojet Strategic Propulsion Co.) 185 p	N88-28964 Unclas CSCL 21H G3/20 0164894
---	---



Final Report SRB-CLE-F

SRB/SLEEC (SOLID ROCKET BOOSTER/ SHINGLE LAP EXTENDIBLE EXIT CONE)

Feasibility Study

Volume 1 of 2

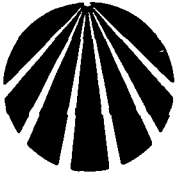
Contract NAS8-36571

Period of Performance

23 September 1985 to 19 September 1986

Published 19 September 1986

Aerojet Strategic Propulsion Company



Final Report SRB-CLE-F

SRB/SLEEC (SOLID ROCKET BOOSTER/ SHINGLE LAP EXTENDIBLE EXIT CONE)

Feasibility Study

Contract NAS8-36571

Period of Performance

23 September 1985 to 19 September 1986

Published 19 September 1986

Prepared By:

Approved By:

W.H. Baker, Jr.
Engineering Manager

C.V. Landrith
Program Manager

Prepared for:

George C. Marshall Space Flight Center
Marshall Space Flight Center, Alabama 35812

Aerojet Strategic Propulsion Company

P.O. Box 15699C Sacramento, California 95813

FOREWORD

This SRB/SLEEC Feasibility Study final report is submitted in accordance with the requirements of Attachment J-2 to Contract NAS8-36571. This report covers the period from 23 September 1985 to 19 September 1986. The program was sponsored by the National Aeronautics and Space Administration's George C. Marshall Space Flight Center (NASA/MSFC). The technical program monitor was J.T. Woolridge.

The program was conducted by Aerojet Strategic Propulsion Company (ASPC) under the direction of Craig V. Landrith, Program Manager. William (Bill) H. Baker, Jr. was the Project Engineer and Principal Investigator. Garrett Pneumatic Systems Division, Tempe, Arizona completed a design study of the Shingle Lap Extendible Exit Cone (SLEEC) actuation system while under subcontract to ASPC. A complete copy of this study is contained in Volume II, (Appendix A), of this report. John W. Merritt was GPSD's Project Engineer.

ABSTRACT

A preliminary design and analysis was completed for a SLEEC which could be incorporated on the Space Transportation System (STS) Solid Rocket Booster (SRB). Studies were completed which predicted weights and performance increases and development plans were prepared for the full-scale bench and static test of SLEEC. In conjunction with the design studies, a series of supporting analyses were performed to assure the validity and feasibility of performance, fabrication, cost, and reliability for the selected design. The feasibility and required amounts of bench, static firing, and flight tests considered necessary for the successful incorporation of SLEEC on the Shuttle SRBs were determined. Preliminary plans were completed which define both a follow-on study effort and a development program.

TABLE OF CONTENTS

	<u>Page No.</u>
FOREWORD	i
ABSTRACT	ii
TABLE OF CONTENTS	iii
FIGURE LIST	iv
LIST OF REFERENCES	viii
LIST OF APPENDICES	ix
1.0 INTRODUCTION/SUMMARY	1.0-1
2.0 OBJECTIVES	2.0-1
3.0 SCOPE	3.0-1
4.0 WORK ACCOMPLISHED	4.0-1
4.1 DESIGN STUDIES	4.1-1
4.1.1 Establish Design Requirements	4.1-1
4.1.2 Preliminary Design Layouts	4.1-2
4.1.2.1 Prepare Design Layouts	4.1-2
4.1.2.2 Analyze Designs	4.1-5
4.1.2.3 Determine Actuation Loads	4.1-8
4.1.2.4 Design Actuation System	4.1-8
4.1.3 System Integration Studies	4.1-11
4.1.3.1 Launch Systems	4.1-11
4.1.3.2 SRB Nozzle	4.1-11
4.1.3.3 SRB TVC System	4.1-12
4.2 SUPPORTING ANALYSES	4.2-1
4.2.1 Trajectory/Payload	4.2-1
4.2.2 Fabrication Feasibility and Cost	4.2-5
4.2.3 Reliability	4.2-8
4.3 TEST FEASIBILITY	4.3-1
4.3.1 Bench Test	4.3-1
4.3.2 Static Test	4.3-2
4.3.3 Flight Test	4.3-2
4.4 DEVELOPMENT PROGRAM DEFINITION	4.4-1
4.5 RECOMMENDATIONS	4.5-1

FIGURE LIST

Figure No.	Figure Title
Figure 1.0-1	Artist's Concept of SLEEC as Originally Conceived
Figure 1.0-2	SLEEC Model Deployment
Figure 1.0-3	Artist's Concept of SLEEC on SRB
Figure 1.0-4	Summary of Current SRB/SLEEC Performance Benefits and Costs
Figure 1.0-5	Suggested Schedule for Follow-On Study Effort
Figure 1.0-6	1981 Preliminary Layout of SLEEC on SRB High Performance Nozzle
Figure 1.0-7	SLEEC Tested December 1983
Figure 1.0-8	SLEEC Deploying During Static Test
Figure 3.0-1	SRB/SLEEC Feasibility Study Program Schedule
Figure 4.1-1	General SLEEC Geometry Defined
Figure 4.1-2	Existing SRB Configuration Showing Post Envelope and Shingle C/L
Figure 4.1-3	Overall SRB Configuration Showing Relocated Blast Shield
Figure 4.1-4	Existing Exit Cone, Compliance Ring and Linear Shaped Charge
Figure 4.1-5	Suggested Modifications to Linear Shaped Charge Insulators
Figure 4.1-6	Recommended Heat Shield and LSC Cover Modifications
Figure 4.1-7	View of Aft HPN Exit Cone Assembly with SLEEC Installed
Figure 4.1-8	Shingle-to-Exit Cone Geometry
Figure 4.1-9	Detail of Shingle-to-Exit Cone "Lapped" Region
Figure 4.1-10	Inner Shingle Detail
Figure 4.1-11	Outer Shingle Detail
Figure 4.1-12	Machined Build Up on Exit Cone Looking Aft
Figure 4.1-13	SRB/SLEEC System Looking Aft
Figure 4.1-14	SRB/SLEEC System Looking Forward
Figure 4.1-15	Detailed View of "Steps"
Figure 4.1-16	Cutaway Isometric View of SRB/SLEEC System

Figure No.	Figure Title
Figure 4.1-17	Enlarged Detail of Cutaway SRB/SLEEC Isometric View
Figure 4.1-18	Full Isometric View of Stowed SRB/SLEEC
Figure 4.1-19	Full Isometric View of Extended SRB/SLEEC
Figure 4.1-20	Details of Shingle Clip and Guide
Figure 4.1-21	View of SRB/SLEEC Looking Aft With Actuation System Installed
Figure 4.1-22	View of SRB/SLEEC Looking Aft With Protective External Heat Shields Installed
Figure 4.1-23	Thermal Response Prediction Procedures
Figure 4.1-24	Surface Regression and Char Depth vs Time for SLEEC Station 1
Figure 4.1-25	SLEEC Thermal Analysis Results
Figure 4.1-26	Typical SLEEC Internal Pressure Distribution
Figure 4.1-27	SLEEC Actuation Loads Defined
Figure 4.1-28	Side View Layout of Cable Actuation System
Figure 4.1-29	Preliminary Drawing of Actuation System Saddle Bracket
Figure 4.1-30	View Looking Aft, Layout of Cable Actuation System
Figure 4.1-31	Turnbuckle and "T" Bar Configuration
Figure 4.1-32	"Drift" Contours Used in Conjunction with "Smooth Post" to Define SLEEC "Build" Envelopes
Figure 4.1-33	SLEEC "Build" Contours as Constructed Using Defined "Drift" Contours
Figure 4.1-34	Limiting "Build" Envelope for SLEEC Constructed Using VC72-000020 "Drift" Contour
Figure 4.1-35	Intersection of Post Clearance "Build" Envelope and Outer Shingle
Figure 4.1-36	Calculated SRB/SLEEC Add-On Weights
Figure 4.1-37	Calculated SRB/SLEEC Add-On Inertia
Figure 4.1-38	Model Used for External Aerodynamic Force Studies
Figure 4.1-39	Axial Pressure Distributions Along SLEEC External Surface at 15 and 30 Seconds

Figure No.	Figure Title
Figure 4.1-40	Axial Pressure Distributions Along SLEEC External Surface at 44 and 60 Seconds
Figure 4.1-41	Axial Pressure Distributions Along SLEEC External Surface at 74 and 90 Seconds
Figure 4.2-1	SLEEC Performance Model
Figure 4.2-2	Predicted Vacuum Delivered Isp vs SLEEC Extension as a Function of Chamber Pressure for Initial Throat Area (T= 0 sec)
Figure 4.2-3	Predicted Vacuum Delivered Isp vs SLEEC Extension as a Function of Chamber Pressure for Final Throat Area (T= 122 sec)
Figure 4.2-4	SLEEC Internal Wall Pressure vs Extension Distance as a Ratio of Chamber Pressure
Figure 4.2-5A	Western Test Range Trajectory Used in Study (Sheet 1 of 4)
Figure 4.2-5B	Western Test Range Trajectory Used in Study (Sheet 2 of 4)
Figure 4.2-5C	Western Test Range Trajectory Used in Study (Sheet 3 of 4)
Figure 4.2-5D	Western Test Range Trajectory Used in Study (Sheet 4 of 4)
Figure 4.2-6	Nominal Chamber Pressure vs Time
Figure 4.2-7	SLEEC Extension vs Time
Figure 4.2-8	Vacuum Delivered Specific Impulse vs Time, With and Without SLEEC
Figure 4.2-9	SRB/SLEEC Expansion Ratio vs Extension Distance
Figure 4.2-10	Vacuum Thrust Coefficient vs Extension Distance
Figure 4.2-11	Delivered Specific Impulse vs Flight Time, With and Without SLEEC
Figure 4.2-12	SRB/SLEEC Performance Comparison
Figure 4.2-13	Preliminary ROM Fabrication Costs
Figure 4.2-14	SLEEC Actuation System Detail
Figure 4.2-15	HPN Aft Exit Cone Assembly Prior to Modification
Figure 4.2-16	Modified HPN Aft Cone Assembly
Figure 4.2-17	Shingle Lay-up Tool Surface Showing 12° Wedge
Figure 4.2-18	Shingle "B" Staged Standard Density Carbon Phenolic Liner

Figure No.	Figure Title
Figure 4.2-19	Shingle "B" Staged Standard and Low Density Carbon Phenolic Liners
Figure 4.2-20	Shingle with Graphite Phenolic Shell in Place
Figure 4.3-1	Bench Deployment/Loads Plan
Figure 4.3-2	Deployment Load Test Set-Up
Figure 4.3-3	Leakage Test Set-up
Figure 4.3-4	T-24 SRB Static Test Stand
Figure 4.3-5	Jet Pipe Diffuser Schematic
Figure 4.4-1A	Development Program Schedule, Page 1 of 3 pages
Figure 4.4-1B	Development Program Schedule, Page 2 of 3 Pages
Figure 4.4-1C	Development Program Schedule, Page 3 of 3 Pages

LIST OF REFERENCES

Reference No.	Reference
1	"A Practical Design Guide to Extendible Exit Cone (EEC) Selection and Design", W.H. Baker, Jr., AIAA-80-1298
2	"Design Features and Current Status of a Uniquely Packaged, Variable Area Extendible Exit Cone", W.H. Baker, Jr. and S.A. Brown, Pages 31-39, Aerojet Technology, Vol. I No. 1, 1983.
3	"Advanced Extendible Exit Cone Concepts Program", Final Report, Report No. AFRPL-TR-84-033, June 1984, Air Force Rocket Propulsion Laboratory, Edwards AFB, CA.
4	"Nonelectric Parts Reliability Data, -2", 1981, Reliability Analysis Center, Rome Air Development Center, Griffiss AFB, NY.

LIST OF APPENDICES

Appendix	Title
A	Volume 2 of SRB/SLEEC Feasibility Study Final Report, Report No. SRB-CLE-F, 19 Sept 1986, "Design Study for a SLEEC Actuation System", Prepared by Garrett Pneumatic Systems Division, Tempe, Arizona 85282
B	Stress Analysis of the SRB/SLEEC

1.0 INTRODUCTION/SUMMARY

This SRB/SLEEC Feasibility Study final report is submitted in accordance with the requirements of Attachment J-2 to Contract NAS8-36571. This report covers the period from 23 September 1985 to 19 September 1986. The program was sponsored by the National Aeronautics and Space Administration's George C. Marshall Space Flight Center (NASA/MSFC). The technical program monitor was J.T. Woolridge.

The program was conducted by Aerojet Strategic Propulsion Company (ASPC) under the direction of Craig V. Landrith, Program Manager. William (Bill) H. Baker, Jr. was the Project Engineer and Principal Investigator. Garrett Pneumatic Systems Division, Tempe, Arizona completed a design study of the Shingle Lap Extendible Exit Cone (SLEEC) actuation system while under subcontract to ASPC. A complete copy of this study is contained in Volume II, (Appendix A), of this report. John W. Merritt was GPSD's Project Engineer.

The objectives of the program were to complete a preliminary design of the SLEEC, predict the STS performance gain (if any), and prepare plans for a follow-on development effort and preliminarily verify structural and thermal margins of safety.

A preliminary design and analysis was completed for a SLEEC which could be incorporated on the Space Transportation System (STS) Solid Rocket Booster (SRB). Studies were completed which predicted weights and performance increases and development plans were prepared for the full-scale bench and static test of SLEEC.

SLEEC is a unique EEC that continuously varies its exit area. Figures 1.0-1 and 1.0-2 depict both an artist's conception and a photograph of a SLEEC model "growing" through its deployment sequence. SLEEC consists of 12 longitudinal shingles, a fixed cone, an actuation system, and thermal insulation. Six inner and six outer shingles are packaged around the fixed exit cone in an overlapping fashion. They are extended in an analog manner (i.e., continuously and not in discreet jumps) by an actuation system which simultaneously extends the shingles axially and radially. Because of the unique packaging and extension features, SLEEC is able to fit in volume limited spaces and still provide an optimum expansion ratio (within extension limits) during rocket ascent. Figure 1.0-3 depicts an early sketch of the SLEEC on the SRB.

The current study determined that SLEEC can provide a net payload increase into low earth orbit (LEO) of approximately 2471 lbm and indicated that the cost of procuring and installing a shipset of two SLEECs on the STS would be approximately 2.2 million dollars. Thus the cost per pound of increased payload capability to LEO amounts to approximately \$890, making SLEEC a viable alternative for increasing STS performance compared to some other solutions. Figure 1.0-4 summarizes the weights, performance gains and estimated costs associated with incorporating a SLEEC shipset (i.e., two SLEECs, one for each SRB) which resulted from this study. The study did not examine safety and reliability issues in depth. These are areas of great importance requiring further investigation.

The STS payload increase described above is but one of many potential advantages that SLEEC offers. These cover the broad areas of performance, manufacturing, cost, and flexibility.

PERFORMANCE

Although not examined in this study, in addition to the payload increase, SLEEC has the potential of being throttled, i.e., extended and/or retracted over the exhaust plume. Thus it could help reduce STS structural stresses encountered at max q. This potential feature may even provide a system benefit to the SSME. Similarly, it is so tightly packaged that it provides a lower external drag profile than other EEC concepts.

MANUFACTURING

There are numerous manufacturing advantages. The process of making shingles can be automated, thus greatly increasing industrial productivity. The shingles can be physically manufactured and shipped easily, and when assembled, the resulting cone size can far exceed the current size capability of current industrial and transportation facilities. Thus, larger cones can be constructed than those now available. The quantity of acceptable material will greatly increase since a defect would cause only a small portion of a cone (a shingle) to be rejected. The advantages multiply when one considers the possibility of retrofitting the SLEEC to existing SRMs with only minor hardware changes.

COST

The cost advantages include those associated with simplified manufacturing processes and the use of state-of-the-art materials and actuation systems. Much of the SLEEC actuation system derived during this study is comprised of hardware currently in use for thrust reversers and flaps on large passenger aircraft. Performance is therefore based on extremely reliable, demonstrated components. A further potential advantage accrues with the possibility of salvaging the jettisoned actuation system. Future studies will determine that these parts should be reusable, contributing significant cost savings. Finally, a SLEEC development program should be far less extensive than those associated with less developed components.

FLEXIBILITY

These potential advantages are underscored by SLEEC's flexibility. It has potential application to the SSME or any system needing heavy lift, altitude compensation capability.

Finally, the current study defined a follow-on program which outlines the development of SLEEC through design, fabrication and bench and static test. The objective of the program is to fully demonstrate the survivability and reliability of a full-scale SLEEC and to completely qualify it for the SRB. The program would be conducted over a five year period and is estimated to cost approximately 15 million dollars, not including the cost of motors and testing. Section 4.4 of this report details the schedule and estimated costs for the various program phases.

In summary, the objectives of this feasibility study program have been met. STS performance gains have been predicted, costs estimated, and development plans prepared. However, such studies sometimes raise as many issues as are answered. Final designs must be agreed upon with NASA/MSFC and design influencing issues resolved. Final performance and reliability numbers must be jointly agreed upon for use in a man-rated system. It is recommended that a follow-on study program be conducted to more fully address these issues. This program is outlined in Figure 1.0-5 and presents a suggested schedule and estimated costs.

1.1 BACKGROUND

The Shingle Lap Extendible Exit Cone (SLEEC) was invented in 1978 to fill the need for a variable area Extendible Exit Cone (EEC). No EEC concept before or since has demonstrated this capability. The term "variable area" means that (within the limits of its geometry and size) the exit or exhaust area of the extending system can be varied in a continuous or analog manner to permit the exhaust pressure of the gases at the nozzle exit plane to exactly match local ambient pressure at altitude during boost operation. This feature permits an approximate 10% delta performance gain over the more conventional extending systems that accomplish the same geometric expansion in one or more steps (Reference 1 describes most of these "conventional" EECs).

An equally important feature of SLEEC is the unique way in which it is manufactured, packaged (or stowed) and deployed (extended). First, SLEEC is manufactured in longitudinal segments of a cone called shingles. This means that SLEEC is not subject to fabrication and transportation limitations normally associated with very large monolithic exit cones.

Second, the nesting (overlapping) of the shingles in the stowed position permits SLEEC to be installed or retrofitted within existing envelopes for which conventional EECs (1), could not be considered, or (2), would lessen their performance because of their reduced size compared to SLEEC.

Finally, the shingles are simultaneously deployed in both the axial and radial directions along the fixed nozzle exit cone, which presents a low external drag profile while providing the desired variable area. The complete design details and benefits of SLEEC are given in Reference 2.

When first conceived, it was thought that the primary use for SLEEC would be on the liquid main engines of the shuttle orbiter. These engines are overexpanded at sea level and do not achieve optimum performance until an altitude of approximately 50,000 ft has been reached. Additionally, the exit cones are positioned so close to each other that any EEC must be tightly packaged so as not to cause interference with adjacent cone(s). SLEEC promised

increased performance since the installation would permit initial expansion ratios of about 30:1 instead of the present 77:1. The final 77:1 area ratio could then be achieved in an optimum, variable area manner without physical cone-to-cone interference. An additional benefit would be the ability to retract the cones for reentry or throttling.

It soon became apparent that SLEEC could increase the performance of the Shuttle Solid Rocket Booster (SRB) for just the opposite reason. The nozzle exit cone of the SRB is designed in the conventional fashion for solid rocket booster stages; that is, the exit area is essentially sized to provide optimum performance near sea level and then become less and less efficient as altitude increases. For the SRB application, SLEEC is packaged around the High Performance Motor (HPM) nozzle exit cone and extends during ascent as the ratio of ambient pressure (or SLEEC exit plane pressure) to chamber pressure dictates.

In 1981, Aerojet decided that the increased performance promised through incorporation of SLEEC on the SRB was substantial enough to warrant the expenditure of company funds for a preliminary performance assessment. The results of that study was shown in Figure 1.0-3, the artist's concept of SLEEC positioned on the SRB, and in Figure 1.0-6, a preliminary layout of the cross-section of the SLEEC assembly on the High Performance Nozzle (HPN) exit cone. The predicted performance gains for incorporating SLEEC on the shuttle SRB were determined in 1981 by "flying" the combination in a flight simulation program. The results of the simulation are shown below.

1981 Preliminary SRB/SLEEC Performance Predictions

Baseline Specific Impulse	270.7 sec
Ave Specific Impulse Calculated for SLEEC	281.2 sec
Ave Specific Impulse Gain "Flying" SLEEC	6.28 sec
Calculated SLEEC "Add-On" Weight (ea of two)	3990 lbm
Calculated SLEEC Weight Loss During Burn (ea)	300 lbm
Predicted Net Payload Increase to Park Orbit	3750 lbm

In November 1981, Aerojet presented these results to MSFC. The consensus of those attending the presentation was that, although SLEEC on Shuttle SRB was a good idea, Aerojet should return after the concept had been demonstrated. Concurrently, a contract (F04611-80-C-0059) had been awarded to Aerojet by the Air Force Rocket Propulsion Laboratory (AFRPL), Edwards AFB, to demonstrate the SLEEC concept in a test firing at simulated altitude conditions. This successful test took place 20 December 1983. The SLEEC, shown in Figure 1.0-7, was extended from the stowed to the fully deployed position in about 15 seconds, uniformly increasing motor performance by 4% during deployment. A picture of SLEEC deployment during the test is shown in Figure 1.0-8. The complete program results are described in Reference 3.

Having successfully demonstrated the concept, Aerojet submitted a proposal to NASA/MSFC for a study program to determine the feasibility of incorporating SLEEC on the Shuttle SRBs. This report presents the results of that feasibility effort.

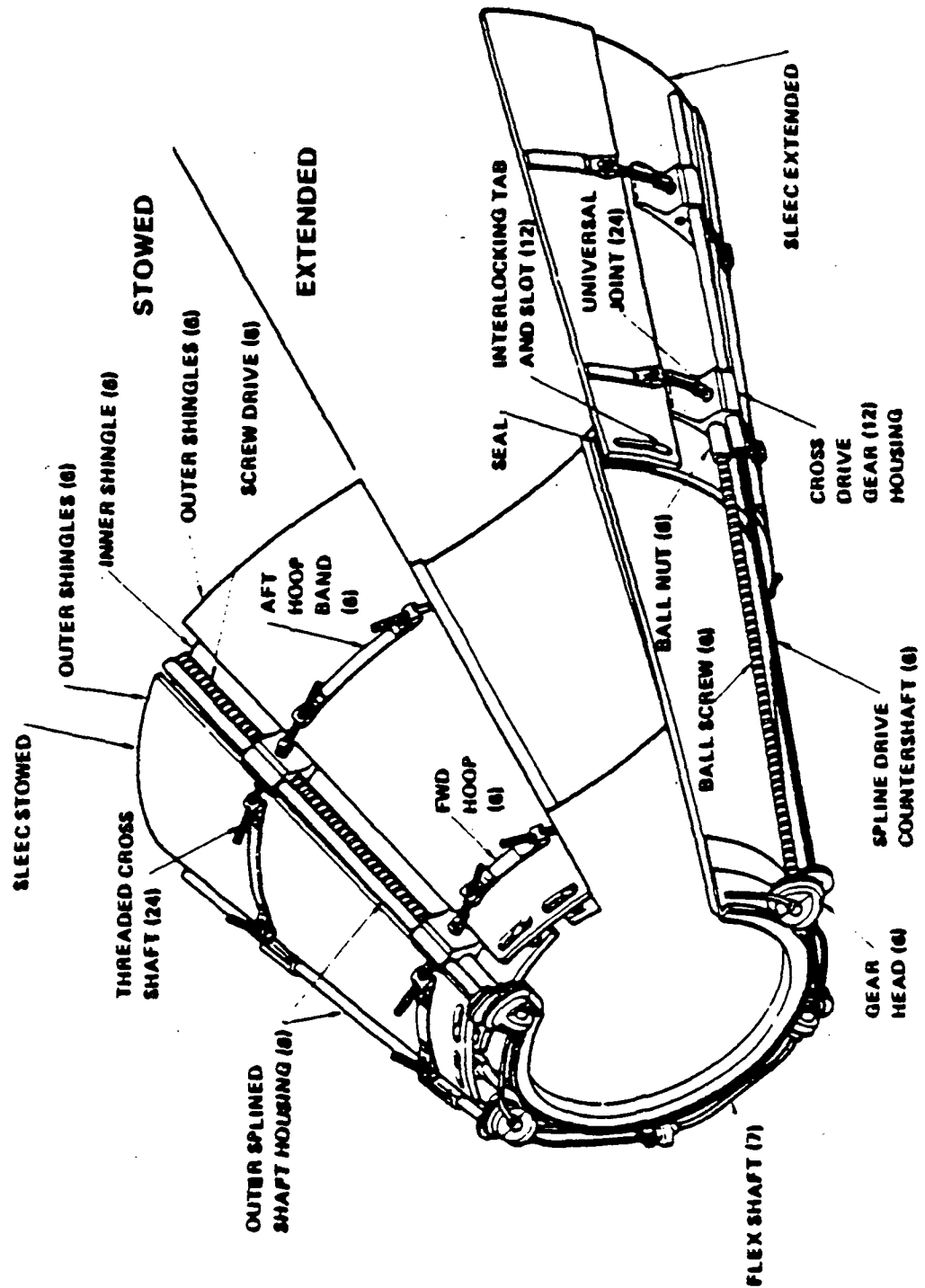


Figure 1.0-1 Artist's Concept of SLEEC as Originally Conceived

ORIGINAL PAGE IS
OF POOR QUALITY

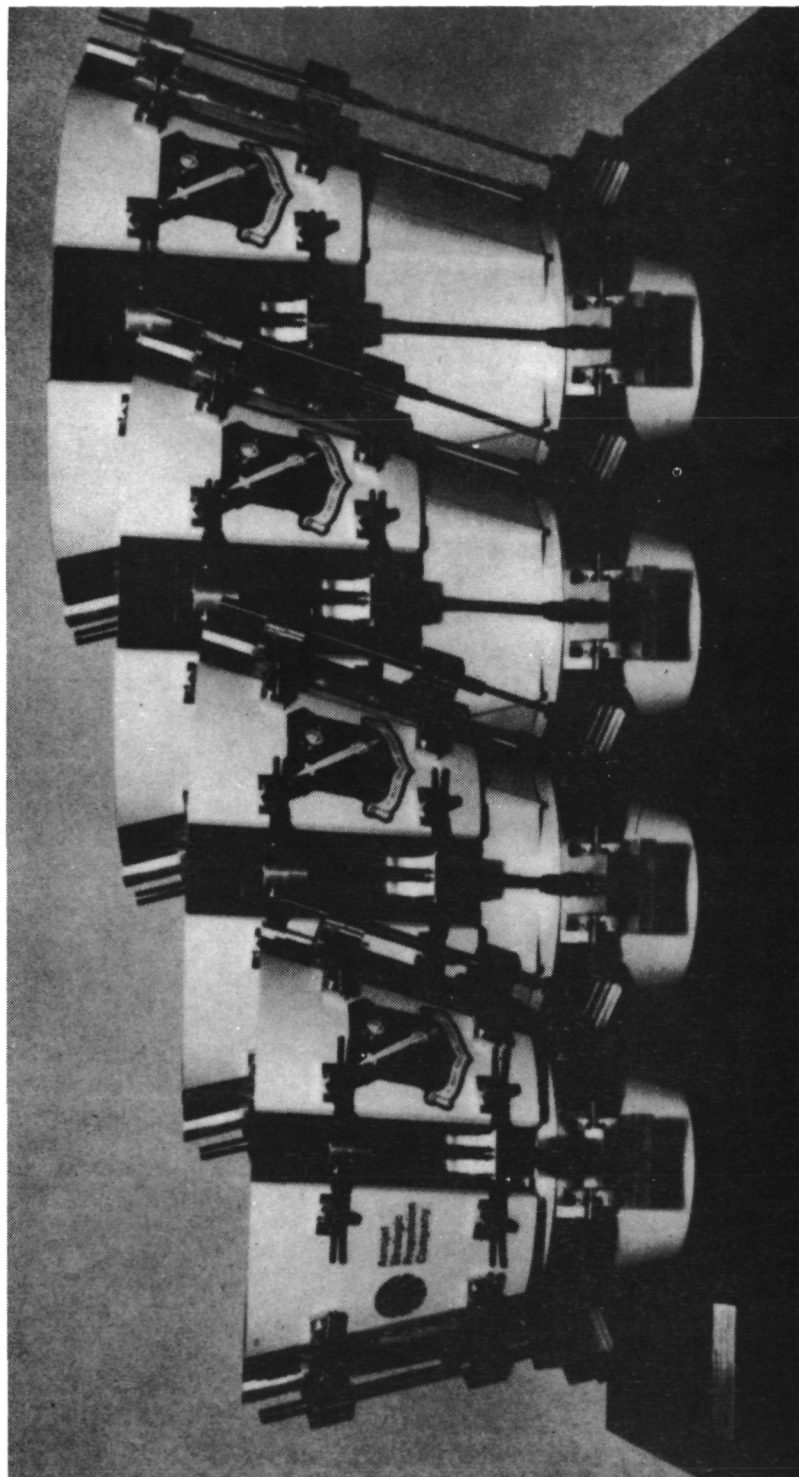
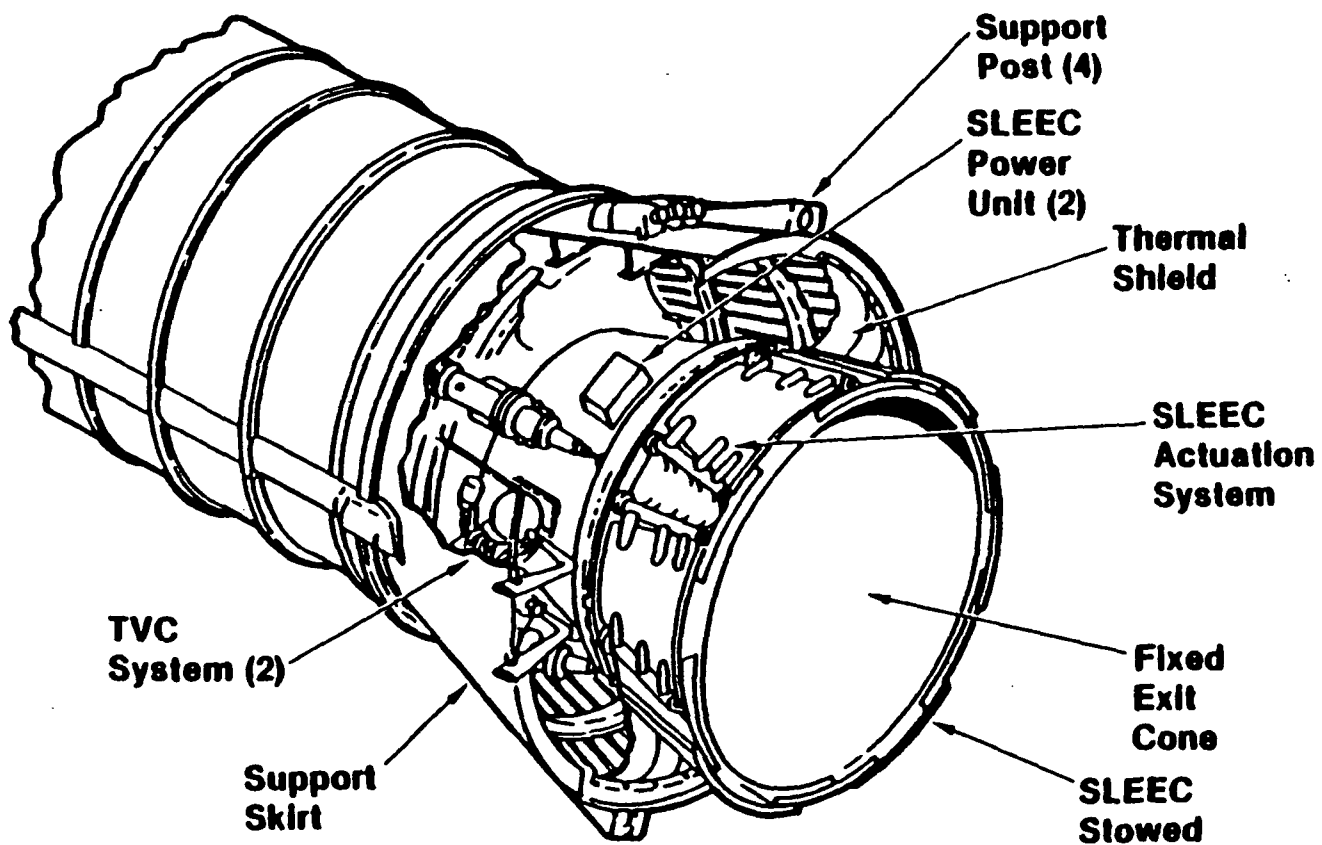


Figure 1.0-2 SLEEC Model Deployment



SRB/SLEEC PERFORMANCE AND COSTS (1)

	<u>STUDY RESULTS</u>
TEST RANGE	WESTERN
SLEEC EXTENSION LENGTH, IN	60
SLEEC EXPANSION RATIO, EXTENDED	10.59
SLEEC HALF ANGLE, DEG	12.0
TIME OF DEPLOYMENT, SEC	44 TO 64
AVERAGE SPECIFIC IMPULSE GAIN, SEC	3.86
ADD-ON WEIGHT (EA OF 2), LBM	4193
WEIGHT LOSS DURING BURN, LBM	300
PREDICTED PAYLOAD GAIN TO LEO, LBM	2471
COST PER SLEEC ASSEMBLY, \$K	1140 (1)

(1) 2 SLEEC ASSEMBLIES PER FLIGHT. ROM COSTS
 BASED ON 1986 DOLLARS, 100 UNIT MINIMUM
 INCLUDES DEVELOPMENT ENGINEERING COSTS

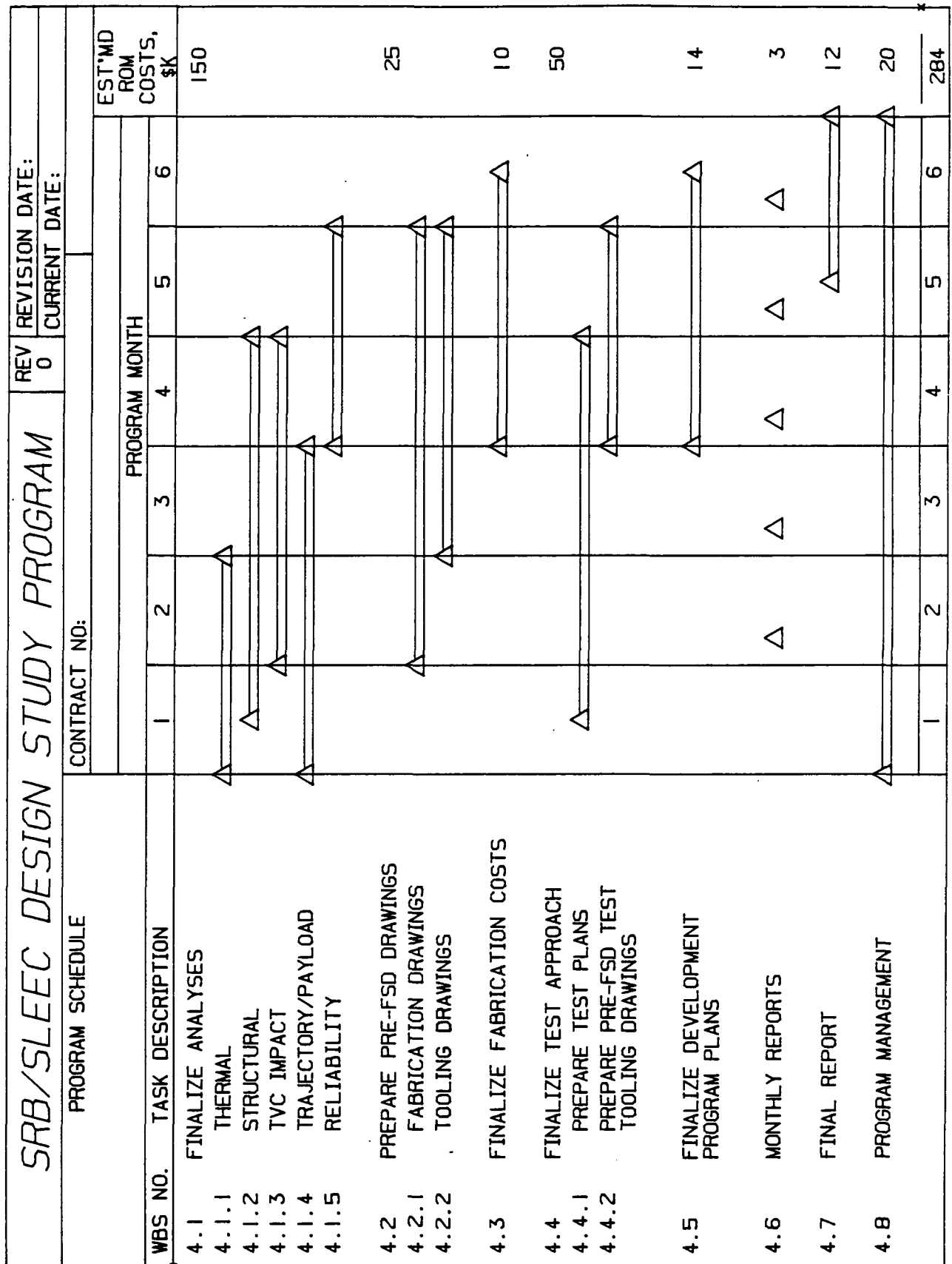


Figure 1.0-5 Suggested Schedule for Follow-On Study Effort

ORIGINAL PAGE IS
OF POOR QUALITY

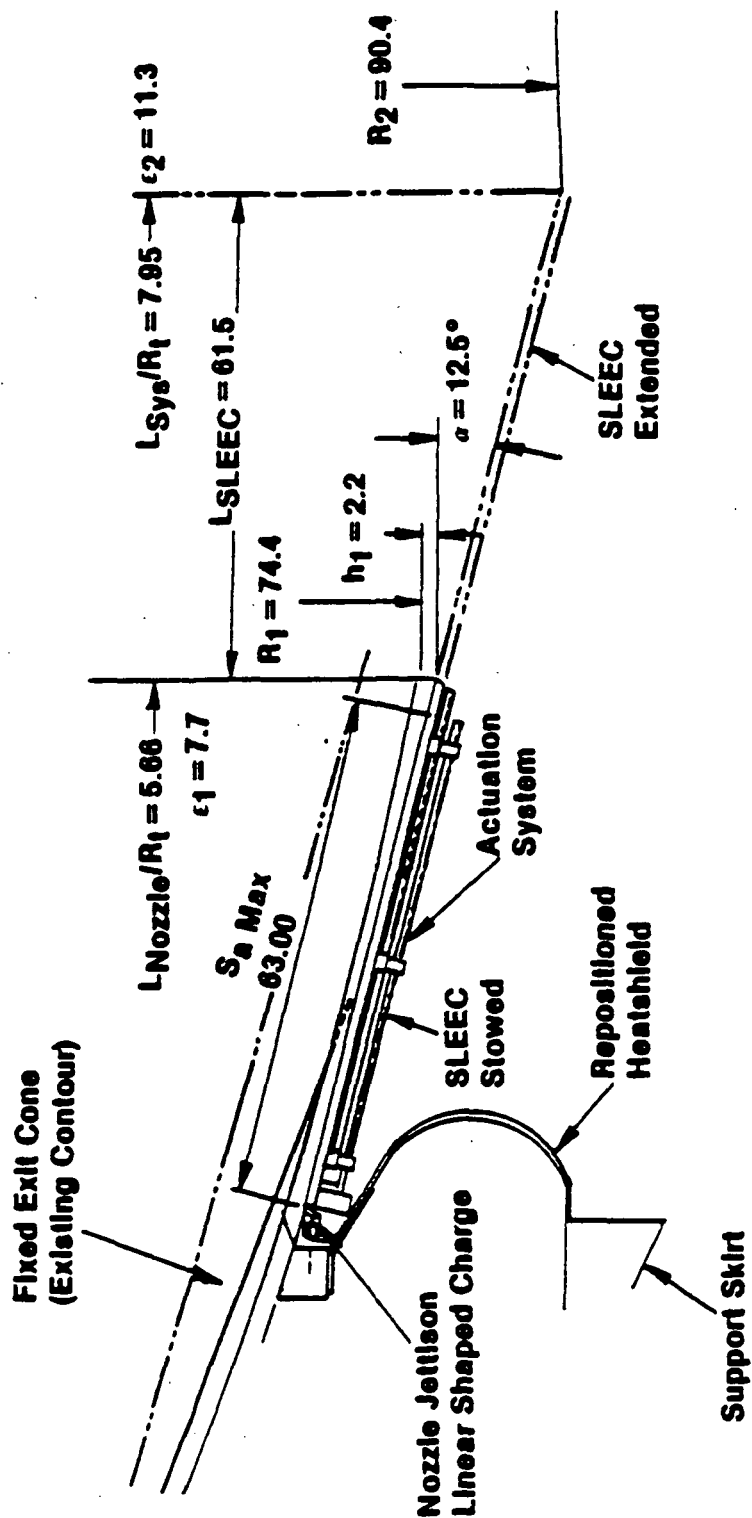


Figure 1.0-6 1981 Preliminary Layout of SLEEC on SRB High Performance Nozzle

ORIGINAL PAGE IS
OF POOR QUALITY



Figure 1.0-7 SLEEC Tested December 1983

ORIGINAL PAGE IS
OF POOR QUALITY

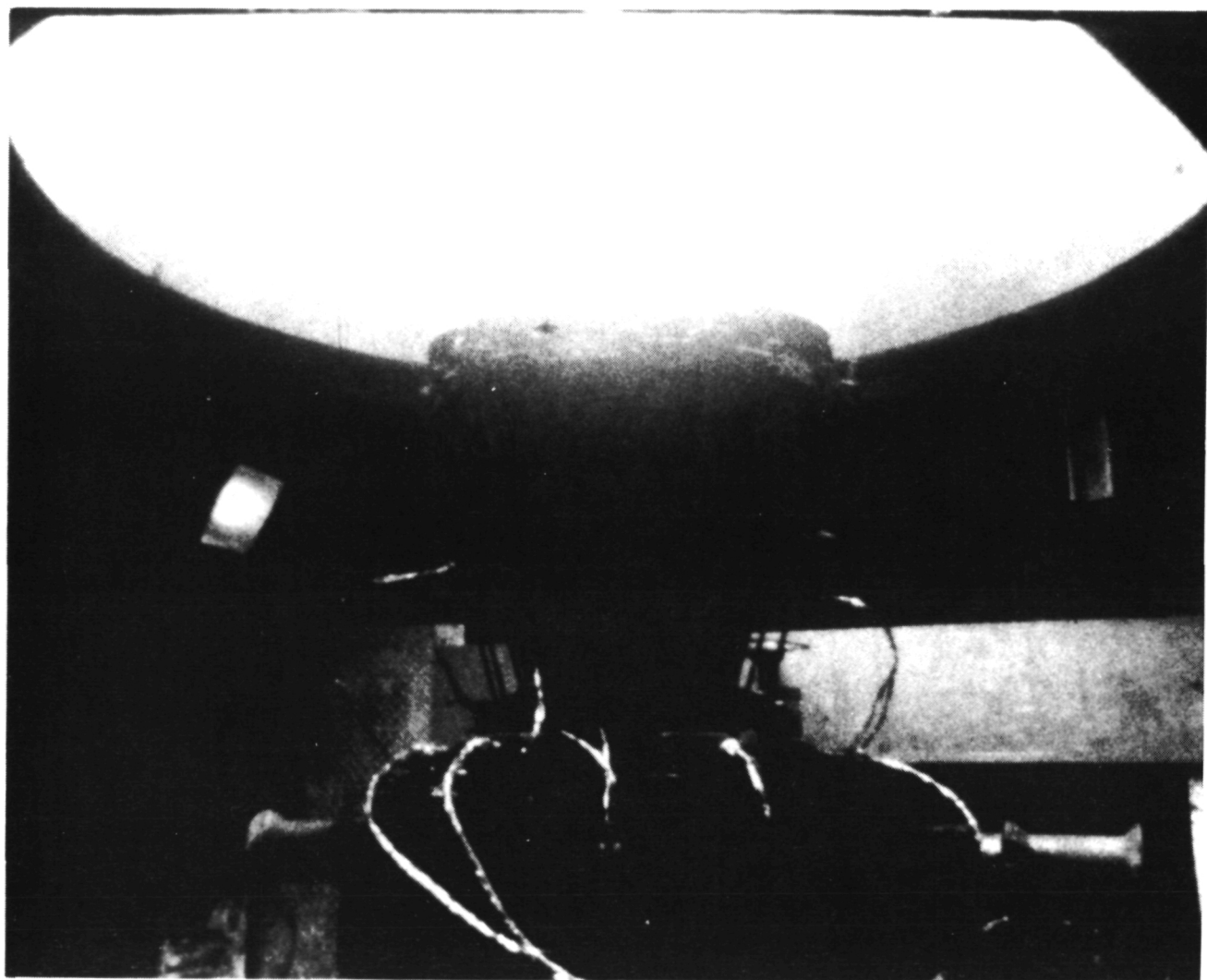


Figure 1.0-8 SLEEC Deploying During Static Test

2.0 OBJECTIVE

The objective of this program was to study the feasibility of increasing Shuttle payload capability through the incorporation of a Shingle Lap Extendible Exit Cone on the Solid Rocket Boosters. It was intended that this feasibility would be determined for all aspects of design, analysis, fabrication and test.

A secondary objective was to define the development program required to successfully accomplish this incorporation.

3.0 SCOPE

The general scope of the technical work accomplished in the study is described in this section and in the schedule of Figure 3.0-1.

3.1 DESIGN STUDIES

A series of design studies were conducted to ensure Aerojet's awareness of all NASA imposed requirements and that these requirements would be fully met by the preliminary SRB/SLEEC development/demonstration design. In addition to the formulation of design requirements, preliminary design layouts were prepared and system integration studies were conducted.

3.2 SUPPORTING ANALYSES

In conjunction with the design studies, a series of supporting analyses were performed to assure the validity and feasibility of performance, fabrication, cost, and reliability for the selected design.

3.3 TEST FEASIBILITY

The feasibility and required amounts of bench, static firing, and flight tests considered necessary for the successful incorporation of SLEEC on the Shuttle SRBs were determined. Each test series received sufficient preliminary planning to permit an assessment of the feasibility and validity of results.

3.4 DEVELOPMENT PROGRAM DEFINITION

This task produced a preliminary plan defining a follow-on development/demonstration effort.

4.0 WORK ACCOMPLISHED

4.1 DESIGN STUDIES

The first portion of the program consisted of a period of design studies. After a brief parametric study, a preliminary design was selected for use in the remaining program tasks.

4.1.1 Establish Design Requirements

In this task, Aerojet worked closely with MSFC to establish those NASA requirements, restrictions and envelopes which might effect the SLEEC design. Additionally, Aerojet generated self-imposed requirements which it deemed necessary for successful incorporation. NASA and Aerojet then agreed on the combined requirements to be imposed on the remaining program tasks.

Aerojet's past experience with other EEC's indicated that most of these requirements and restrictions are envelope/interface related and are primarily associated with the retrofit of an EEC to an existing system. Generally, there is reluctance to change or modify any item in a present system to incorporate new components; therefore, some basic issues had to be clarified to facilitate the SLEEC feasibility study:

Some examples of issues requiring resolution were:

1. Is the flame shield inviolate or can it be penetrated or else repositioned?
2. What is the "free" envelope available between the nozzle and skirt?
3. What are the latest "drift" and "twang" envelope requirements?
4. With regard to cost projections, would NASA supply fixed nozzle aft exit cone assemblies upon which Aerojet could place the SLEEC assembly?

The answers to these questions and the assessment of other known factors would ultimately influence SLEEC design, costs, and resulting performance.

A program kick-off meeting was held on 5 November 1985 at MSFC. A brief overview of the nature and objective of the program was given by Aerojet. Subsequent discussions were held with personnel responsible for various disciplines. The major observations and action items for the meeting are summarized below:

TVC

Aerojet would determine:

- 1) Aerodynamic loads due to SLEEC (nominal and worst case)
- 2) Inertia of SLEEC

3) Maximum power required to extend SLEEC

NASA/MSFC, based on the data provided by Aerojet, would determine:

- 1) Effect of increased loads and inertia on TVC
- 2) If there is enough excess TVC power to operate SLEEC

PERFORMANCE

Aerojet would reconfirm calculations of Isp and reach agreement with NASA/MSFC as to method of calculation.

ENVELOPE

NASA provided a launch "drift" envelope. Aerojet to contact Rockwell for interpretation of data and any additional required information.

The general tone of the meeting appeared to be that Aerojet should make whatever reasonable assumptions necessary to carry out the study and NASA/MSFC would eventually consider their practicality.

4.1.2 Preliminary Design Layouts

4.1.2.1 Prepare Design Layouts

A number of preliminary SLEEC design layouts were made sufficient to ensure that the imposed requirements were met and that performance of the system was maximized. As detailed in Reference 2 and illustrated in Figure 4.1-1, the length and effective half angle of the existing nozzle exit cone essentially fixes the available geometry for the SLEEC installation.

The Aerojet-derived SRB/SLEEC design (Figure 1.0-6) was used as a point of departure (POD) design in preparing the additional preliminary layouts. cursory analyses were made for each layout of interest using the techniques developed in Reference 3. Iterative trades were then made balancing estimated shingle thicknesses versus available envelope until an optimum preliminary design layout was obtained. With NASA agreement, a preliminary design was then selected to be used as the basis for the the remaining studies and analyses.

Figure 4.1-2 depicts the existing High Performance Nozzle (HPN), aft SRB heat (or flame) shield, compliance ring, and linear shaped charge with its covers. Also shown is a low density carbon phenolic build-up which is added to the exterior of the existing HPN structural shell under the 63 in. long shingle. The actuation system is not shown nor is the Fiberform® heat shield protecting the SLEEC exterior. The SLEEC "build" envelope contour which limits the SLEEC structure around each of the four support posts is shown. The derivation of this contour, which accounts for worst case twang and drift and includes a self-imposed 4 in. clearance envelope around each post, is presented in Section 4.1.3.1, Launch Systems.

Based on the results of previous studies, if the shingles are much shorter than 63 in., the shuttle performance gain can be diminished to the point where the feasibility of the installation is questionable. From Figure 4.1-2, it is evident that:

1. The shingles cannot extend past the end of the fixed cone because the build envelope limits four of the outer shingles in this regard.
2. The envelope available for placement of the actuator gear head on the fixed exit cone between the shingle and the linear shaped charge (LSC) is extremely limited by the location of the SRB heat shield as well as the LSC blast shield/covers.

To alleviate this length constraint, Aerojet incorporated two changes to the existing HPN configuration which it considers to be of minimal impact, assuming that these changes would be acceptable to NASA/MSFC. The first suggested change is shown in Figure 4.1-3 which illustrates a relocated torroidal SRB heat or flame shield using an insulated stand-off mounted to the compliance ring. Figure 4.1-3 also shows the overall view of the nozzle as Aerojet understands it, with the SRB heat shield change incorporated.

Figure 4.1-4 shows the detail of the existing LSC with its cork insulation and elastomeric blast shield and stand-off. Aerojet's second suggested modification is shown in Figure 4.1-5 and consists of re-configuring the insulators to provide approximately 5 in. of length along the exit cone shell for positioning the SLEEC actuator gear heads.

Figure 4.1-6 shows the design recommended by Aerojet with the modified heat shield and LSC covers illustrated. If SLEEC were incorporated on the SRB, it is assumed that an actuator mounting ring could be bonded and pinned to the nozzle shell prior to installation of the LSC and the compliance ring adapter. The SLEEC actuator gear head is mounted on this ring and axial loads are reacted by an adjustable support bearing against the compliance ring. Since the SLEEC actuation system is not otherwise attached to the compliance ring or nozzle shell, the entire SLEEC assembly is separated with the exit cone upon LSC initiation.

Figure 4.1-7 is a view of the entire HPN aft cone with SLEEC in place. Figure 4.1-8 defines the geometry of an inner shingle in relationship to the fixed cone, and Figure 4.1-9 details the geometry in the "lapped" area between shingles and fixed cone. Also shown in Figure 4.1-9 are the O-Ring seals formed by bonding 0.275 in.-dia O-Ring stock in grooves routed in the shingle and other mating surfaces.

Each shingle consists of an aft liner of low density carbon phenolic and a forward liner of standard density carbon phenolic, all co-cured with a graphite phenolic structural shell. The ply orientation along any face of the shingle is 12° to the shingle surface and therefore parallel to nozzle centerline since all shingles are oriented 12° to centerline around the fixed nozzle.

The low density material is used in the higher expansion ratio portion of the shingles to minimize weight while the standard density carbon phenolic is used for erosion resistance in the area where the flow reattaches to the shingle from the fixed exit cone for the longest period of time. The preliminary thermal analysis of Section 4.1.2.2 indicates that the entire liner may possibly be made of the low density material, resulting in weight and fabrication savings.

Figures 4.1-10 and 4.1-11 are drawings of an inner and outer shingle, respectively. The basic thicknesses are constant for the entire 63 in. length of the shingles.

Figure 4.1-12 is a view looking aft at the nozzle exit cone with the machined low density carbon phenolic build-up in place. The "tracks" from which the shingles deploy are evident in the build up. It is also evident that, as the shingles extend axially aft, each one extends radially outward in this view.

Figure 4.1-13 is a view looking aft showing the shingles in place around the nozzle. The left side of the Figure 4.1-13 shows the inner and outer shingles "nested" in slots in the build up around the existing nozzle structural shell. The right side shows the shingles "extended" aft down the slots until they overlap the fixed cone by 3 in.-- i.e., a 60 in. extension. Figure 4.1-14 presents the same configuration, only looking forward into the nozzle.

Figure 4.1-15 shows the detail of the "steps" from the ID of the fixed exit cone liner out to the various shingle surfaces. The step heights vary from about 1.62 to 3.17 inches in the radially outward direction.

Figure 4.1-16 is an isometric of a complete system (again minus actuation system) with a quarter-section removed for clarity, and Figure 4.1-17 is an enlargement which shows the detail of shingles, fixed exit cone and build-up, as well as the compliance ring and linear shaped charge. Figures 4.1-18 and 4.1-19 are two additional isometric views depicting the full SLEEC system (less actuation) in both stowed and extended positions.

Figure 4.1-20 illustrates the clip and guide which is used to react axial loads and control axial motion between the inner and outer shingles. As the inner shingle extends or retracts, the load is transmitted to the outer shingle by means of the guide which slides along its forward edge. The clip permits reaction of retraction loads.

Figure 4.1-21 is a view looking aft with the actuation system installed. The design of the actuation system is discussed in Section 4.1.2.4. Figure 4.1-22 is a view looking aft of the overlapping insulative shields which would cover the entire exterior of SLEEC (except for separately insulated axial drive gear heads and ballscrews) and which would extend with it during deployment, thus offering complete thermal protection and a smooth surface to external airflow. These shields would be fabricated from a rigidized, carbon fiber filled foam called Fiberform[®], and would attach to the exterior surfaces of the shingles and actuation system. The estimated weight of these shields is 180 lb. The design of the shields would have to be

finalized in a future effort when Aerojet would be fully knowledgeable of the thermal environment at the base of the SRB during flight.

4.1.2.2 Analyze Designs

Cursory analyses were conducted for the SLEEC design described in Section 4.1.2.1 above in order to verify design feasibility and to establish preliminary thermal and structural margins of safety.

A. THERMAL ANALYSIS

1) Introduction

Thermal analysis of the nozzle exit region requires knowledge of propellant properties, flow field parameters, and the heat transfer coefficient distribution throughout the nozzle. The selection of a conduction model is based on the material's response mechanisms and the configuration in the region of interest. Surface thermochemistry conditions are evaluated considering diffusion rates of reactive species and, when applicable, the kinetically controlled heterogeneous reactions at the surface. Finally, the conduction models are combined with the appropriate boundary conditions and material properties to provide surface regression, in-depth pyrolysis for charring materials, and the associated temperature distribution within the materials.

2) Methods

The overall thermal modeling system can be divided into three sub-groups. These sub-groups are illustrated in Figure 4.1-23. The sub-groups are conduction models, surface thermochemistry models, and supporting analysis for propellant thermochemistry and boundary conditions. Prominent among the conduction and thermochemical regression models is a group of computer codes developed by the Aerotherm company for prediction of thermal response of charring materials such as carbon-carbon, where surface reaction kinetics, as well as diffusion rates, control surface reaction rates. Brief descriptions of the codes used in the analysis of SRB/SLEEC follow:

(a) Surface Thermochemistry Codes

The conduction models utilized for calculating the thermal response of chemically-reacting wall materials require input data relating boundary layer edge conditions to the boundary layer surface interface considering surface reaction rate. There are two basic reaction phenomena modeled by the computer codes. Typically, carbon-carbon materials require a model based on kinetically controlled surface reactions in addition to diffusion rates of reactant and product gases. For carbon phenolic materials, surface reaction rates are usually considered to be rapid and are represented by a heterogeneous equilibrium chemistry model. The resins in these materials decompose creating a gas which percolates through the material and mixes with the other species at the surface.

The particular computer codes used by Aerojet for surface thermochemistry analysis of carbon phenolics are ACE and EST codes developed by Aerotherm. The basic assumption in using these codes is that surface erosion results from chemical reactions of the propellant combustion products with the surface material.

The ACE computer code is a general equilibrium thermochemistry code which provides the thermochemical state of the propellant combustion products attendant with isentropic expansion to the specified local static pressure. The surface regression rate and diffusion thermo-effects are evaluated in a non-dimensional form considering the chemical reactions of the local propellant gas with condensed phase surface material. The state of the fluid adjacent to the surface is considered to be in chemical equilibrium with the surface, and thus the regression rate is controlled by the diffusion rate of the reactants and products in the boundary layer. The reactants considered in the evaluation of the energy associated with reactions include not only the surface material, but also the pyrolysis gases evolved by the in-depth charring process. The EST computer code options are similar to those of the ACE computer code and the selection of which code to use is determined by convenience and the available input to define the state of the free stream.

(b) Thermal Conduction

The use of the conduction model completes the sequence of operations for performance of thermal analysis for one particular location or for a two-dimensional grid network. Once the basic thermochemical properties of the propellant exhaust products have been established, the boundary layer results (heat transfer coefficients), non-dimensional regression rates and the associated energy terms from ACE or EST are combined to form the set of boundary conditions necessary to complete the conduction input data.

A detailed thermal analysis of chemically ablating and charring materials requires a complex thermochemical and heat conduction model to account for surface chemical reactions of exhaust gases and surface materials as well as in-depth thermal degradation. For charring ablators, the one-dimensional CMA conduction computer code is used in conjunction with either ACE or EST. The CMA code can consider surface materials as well as back-up materials that may pyrolyze. It can accept general back-wall boundary conditions, a time-varying heat transfer coefficient, pressure, recovery enthalpy, and radiation heat flux. Material thermal properties are input as functions of temperature and char state. The program accepts virgin and char properties separately and internally combines these properties based on the degree of material pyrolyzed. Non-charring back-up material properties can also be functions of temperature.

The solution to the one-dimensional conduction equation constitutes an implicit finite difference approach which includes the effect of the non-homogeneous materials which may decompose in-depth. Internal decomposition is controlled by kinetics of pyrolysis which are described by an Arrhenius expression for each component—one for the reinforcement and two for the resin.

Boundary conditions may include the full thermochemical reaction calculation which generates transient ablation rates at the surface, in-depth and surface temperatures, and in-depth material decomposition for charring ablators.

3) Analysis

The methodology described above was used to predict char and erosion depths and key interface temperatures for the SRB/SLEEC. A series of one-dimensional cuts were made at representative locations using the transient conduction program (CMA-III) to calculate regression, char depths and in-depth temperatures. Major regions of interest were the reattachment region downstream of the step from the fixed cone to the shingle surface. Analyses were also conducted for the less severe downstream region fore and aft of the standard density/ low density phenolic transition, and at a maximum duration exposure point near the exit plane.

The analyses were based on a 122 sec burn time with an average chamber pressure of 615 psia. The initiation of deployment was assumed to occur at 45 sec after ignition with full deployment completed at 64 sec. The propellant considered in the analysis was the booster propellant with 16 percent Aluminum and a theoretical flame temperature of 6116 R at 681 psia. Ambient backside temperatures were assumed since heat shields will be employed to protect the SLEEC and its actuation system.

Heat transfer coefficients were calculated along the exit cone using method of characteristics (DIVERGENCE) and turbulent boundary layer (TBL) programs. The calculated heat transfer coefficients were amplified 100% where the flow reattaches downstream from the step. The empirical amplification factor was based on past experience with steps in the Aerojet MX ADP ENEC.

During the analysis, the post-fire data available for DM4 was reviewed to determine the general material response in the aft region of the exit cone. Those post-fire results show a nearly constant erosion depth throughout the aft cone. Since results of performance analyses have indicated particle impact in this region, these post-fire results are not considered directly applicable in evaluating SLEEC thermal response. Performance analyses have also indicated that particle impact downstream of the fixed cone are not expected to be significant. Accordingly,, negligible erosion due to particles was assumed in the SLEEC analyses.

4) Results

The predicted erosion and char depth are shown in Figure 4.1-24. The maximum predicted erosion and char depth at end of burn are 0.05 in. and 0.43 in. (relative to initial surface), respectively, at a station immediately downstream of the flow reattach point. The resulting temperatures and char depths are essentially identical for the inner and outer shingles.

The predicted surface regression and char depths at the end of burn for selected SLEEC locations are

summarized in Figure 4.1-25. The char line corresponds to a temperature of 750 °F. Bond line temperatures at the locations are also presented.

The results indicate that the bond line temperatures are within acceptable limits and that the thickness of the virgin material remaining (0.47 in.) is greater than the char depth at the most severe location.

B. STRUCTURAL ANALYSIS

The structural analyses conducted for the SRB/SLEEC are quite extensive and verify the basic structural integrity of the system. The structural analysis for the actuation system is contained in Appendix A, the complete design study description prepared under sub-contract by Garrett Pneumatic Systems Division of Garrett Corporation, Tempe, Arizona.

Aerojet's analysis effort was oriented toward establishing a NASTRAN model of the total system. Using this model, 2 of 6 possible analysis conditions were examined in detail— symmetrical plume load and asymmetrical 1 g transverse, no plume load (as in horizontal deployment check-out). The Aerojet stress analysis of SLEEC is contained in this report as Appendix B.

4.1.2.3 Determine Actuation Loads

Using the shingle geometry, an internal pressure distribution versus extended length can be generated for SLEEC for the SRB operating conditions. The typical shape of this distribution is shown in Figure 4.1-26. This internal pressure varies not only as a function of length along the shingle, but also as a function of step height. The pressure distribution for the SRB/SLEEC is presented in Section 4.2.1, Trajectory/ Payload, along with the methodology describing its derivation.

Once the pressure distribution has been determined, the resulting SLEEC actuation loads are calculated using the geometry and relationships of Figure 4.1-27. Then the actuation system can be preliminarily designed and weighed.

Originally, Aerojet had intended to calculate the actuation loads and supply them to the actuation system subcontractor, Garrett Pneumatic Systems Division of Garrett Corporation, Tempe, Arizona. It became obvious early on that Garrett should calculate the loads unique to their design given the shingle geometry and the internal pressure of the system as calculated by Aerojet. Therefore this task was incorporated into the actuation system design effort.

4.1.2.4 Design Actuation System

The actuation system subcontract kick-off meeting was held at Garrett on 3 Dec 1985. The complete results of the Garrett design subcontract are included as Volume 2, (Appendix A) of this final report. A basic discussion and summary of the design are presented here.

As SLEEC is deployed, each shingle must follow a pre-determined trajectory which is canted 12° outward from the nozzle centerline as was shown in Figures 4.1-12 and 4.1-13. From the moment that SLEEC was conceived, it was apparent that any actuation system must react the exhaust plume radial and axial loads while permitting each shingle to exactly follow its trajectory and that this was best accomplished by using a two-part system—one part which would extend the shingles axially while resisting axial or thrust loads, and one part which would allow the shingles to expand radially as a controlled function of the axial expansion while resisting radial pressure loads.

For a given half angle and number of shingles (12° and 12 shingles in this case), the rate of outer-to-inner shingle motion, or the cross-drive radial extension speed (or distance), can be expressed as an exact function of the axial extension speed (or distance). For the SRB/SLEEC installation, the cross-drives extend at a rate equal to 0.107623 times the axial extension rate, or about 1/10 as fast.

The originally conceived actuation system for SLEEC was shown in Figure 1.0-1, and clearly illustrated the mechanical actuation system of axial and radial drives geared together. Next, a model was built to illustrate shingle motion and permit better understanding of the interaction of the radial and cross drive systems. Model extension was shown in Figure 1.0-2. A subscale SLEEC was built (Figure 1.9-4) and successfully tested on a Super BATES motor at altitude conditions. The actuation system of that unit closely resembled that of the model, but was designed to carry predicted loads.

It was originally thought that a similar system would be suitable for the SRB/SLEEC, i.e., 6 worm screw axial drives which, through geared housings, would in turn mechanically power 3 screw cross drive bands. At least 3 cross drives were thought necessary to better support radial loads and to minimize axial deflections in the shingles which had a much smaller thickness-to-diameter ratio than the model or the subscale unit.

In the current contract, Garrett's initial design for SRB/SLEEC utilized 2 radial cross drives. The weight for the system was determined to be excessive and the anticipated weight for the 3 cross drive system required to minimize shingle deflections would be prohibitive. Alternatively, the weight increase associated with axial stiffening of the shingles to limit deflections would also be prohibitive. Therefore, Garrett embarked on the design of a simple, cable supported cross drive system to replace the heavier geared/shaft system.

This cable cross drive system, based on commercial aviation cable design practices, offers a weight savings of approximately 600 lb over even the 2 drive gear/shaft system, uniformly supports all shingles axially to minimize shingle deflections and weights, and presents a minimum external envelope which can be easily insulated as well as streamlined against external aerodynamic loads. Since cables can only carry tensile loads, a system of passive, commercially available, gas-charged struts (similar to those which support hatch back trunk lids and hoods on many passenger cars) can be used to provide a simulated internal pressure load for special purposes such as bench test or non-operating no-load deployment.

The system consists of two counter-rotating cross-drive "drums" and one axial ball screw located on the back of each inner shingle structural shell. A series of 36 cables are attached to and "unwound" from each drum in synchronization with the SLEEC axial extension resulting from ball screw rotation.

A side view of the cable system is shown in Figure 4.1-28, which also depicts drive gear heads and intermediate drum/cable supports called saddles. A preliminary drawing of the two-piece cast aluminum saddle is presented in Figure 4.1-29 and shows the journals which support the two drums and the central ball screw.

Figure 4.1-30 is a one-sixth end view of the cables which extend from the drums on the inner shingle to "T" brackets on the back of the outer shingle structural shells. Not shown are the gas struts which can be mounted between each saddle bracket and edge of the adjacent outer shingle. The left side shows the system in the stowed position and the right side, the system extended.

Figure 4.1-31 illustrates how the cables are terminated by means of turnbuckles at the "T" bar located on the middle of the back of each outer shingle. Each turnbuckle serves a dual purpose, providing for both the tensioning of a cable set and the positioning of each cable set relative to shingle centerline. Each outer shingle is uniformly supported in the radial direction along its entire length by the 36 cable sets. Each of the cable sets contact each outer shingle at 5 locations across the back of the structural shell (including the "T" bar), thereby providing uniform support against radial loads at 5 locations including the "T" bar.

The six actuator assemblies are redundantly powered by two electric DC motor/brake assemblies, either one capable of deploying or braking SLEEC. The motors are located 180° apart and are connected to the six actuators by full loop of drive cables, thereby making the total drive system to the actuators redundant.

The motor power requirement of 0.2 HP is determined by the loads encountered in accomplishing a ground check-out deployment in a 20 sec period. In flight, SLEEC is unique among extendible systems in that, based on the system coefficients of friction assumed, internal pressure and longitudinal acceleration back drive the system, and only braking loads are encountered. In theory, you merely "let go" of the system to start deployment, and then control the rate of deployment by braking. No latches are required. By agreement with NASA/MSFC, the retraction capability of SLEEC was not pursued during this study since the power requirements (and resulting actuation system weights) necessary to overcome these naturally available deployment loads are quite high.

The actuation system has a calculated weight of 1118 lbs and a predicted reliability of 0.99999941 as derived in the study of Appendix A.

4.1.3 System Integration Studies

System studies were conducted to ascertain that the selected SLEEC design could be successfully integrated with other Shuttle components, launch, and flight systems. An investigation with regard to support post interference during launch was accomplished in order to determine the envelope available for SLEEC around the HPN exit cone.

Also included in this task was the calculation of the inertia and aerodynamic loads information required for NASA/MSFC to examine the effect of SLEEC on the basic nozzle structure and on the thrust vector control system, including the resulting influence on vector response time and natural frequency.

4.1.3.1 Launch Systems

Rockwell International was contacted for launch drift profile information. They provided a drift plot for the Western Test Range (WTR) relative to a "smooth" post (see VC72700020, Sheet 3) which will be used for all launches at the WTR. Rockwell noted that all Eastern Test Range (ETR) launches would also eventually utilize the "smooth" post. Based on this information, the study utilized only "smooth" post dimensions. The drift profile provided by NASA for the ETR at the 5 Nov 86 meeting (ICD-2- 0A002) and the profile provided by Rockwell were both considered and are shown in Figure 4.1-32.

Maximum allowable SLEEC "build" contours were constructed for both WTR and ETR drift profiles in the manner shown in Figure 4.1-33. These profiles depict the maximum allowable SLEEC diameter (Y) vs longitudinal station (X) that can be used without violating a self-imposed 4 inch exclusion zone around the post. The "X" and "Y" coordinates for the most restrictive profile (WTR) are shown in Figure 4.1-34.

Aerojet made the assumption that the SRB/SLEEC system can be rotated relative to the SRB such that four of the outer shingles are directly in-line with the four posts. If the outer shingles, of a basic 0.9 in. thick liner and 0.3 in. thick shell construction at shingle centerline, extend to the end of the present HPN exit cone, this self-imposed envelope just "nips" the end of those four shingles to the depth of the structural shell as shown in Figures 4.1-2 and 4.1-35. Also, the "T" bars and heat shields slightly penetrate the self-imposed envelope. This artificial interference is assumed by Aerojet to be negligible in its impact and Aerojet recommends it be ignored. If not, a slight scallop, as shown in Figure 4.1-35, will eliminate the interference with the outer shingle structure, and the end of the "T" bar and heat shield would require minor redesign.

4.1.3.2 SRB Nozzle

The definition of the basic nozzle as regards integration with SLEEC was shown in Figure 4.1-7. Aerojet has assumed, contingent on subsequent NASA/MSFC structural analysis, that it can utilize the existing design of the HPN liner and structural shell as the foundation for a low density carbon phenolic build-up in which the shingles are stowed and from which they are deployed.

This analysis will determine if the basic nozzle structure, reinforced by the build-up, is sufficient to react the inertial and operational loads which SLEEC imposes. The ability of the SRB/SLEEC system to withstand ignition and flight vibrational loads will also be determined.

A description of how Aerojet would utilize the aft exit cone of the HPN as the basis for the SLEEC build-up and assembly is given in Section 4.2.2, Fabrication Feasibility and Cost.

4.1.3.3 SRB TVC System

The SRB/SLEEC system was modeled by Aerojet using Geomod, a comprehensive 3-D modeling program. One of the benefits of Geomod is the program's ability to calculate the physical properties of components individually as well as complicated assemblies made from those components. This is accomplished by assigning a density to each component. The weights and moments of inertia associated with the shingles and actuation system of SLEEC, in both the stowed and extended positions, were determined using Geomod and are tabulated in Figures 4.1-36 and 4.1-37 so that NASA/MSFC may examine the effect of SLEEC on booster CG and TVC response and power requirements as agreed upon in the program kick-off meeting. The effect on power requirements is important not only from the TVC capability standpoint, but also because one of the possible power sources for the SLEEC actuation system might be excess available hydraulic power from the TVC system.

Figure 4.1-36 is an add-on weight listing for the SRB/SLEEC and Figure 4.1-37 is a tabulation of calculated add-on moments of inertia and Center of Gravity (C.G.) locations for both the stowed and extended positions. The information in Figure 4.1-37 is calculated relative to the nozzle flexseal pivot point in the un-pressurized condition. The term "add-on" weight means the approximate weight over and above the existing nozzle weight. "Add-on" inertia implies that these inertia values are additive to that of the present system about the nozzle pivot point. C.G. locations given are for the add-on weights only about the pivot point.

Another important TVC consideration with SLEEC added is the magnitude of the external aerodynamic loads acting on the extended system. These loads must eventually be considered in the structural analyses for SLEEC. The additional external aerodynamic forces acting on the SLEEC become "add-on" vectoring loads which must be reacted by the TVC system.

An analysis was performed which considered that the SRB/SLEEC was fully extended for the entire flight. The external pressure distributions acting along the outer surface of the extended SLEEC were then determined for the nozzle in both the null and 8° vectored positions. Figure 4.1-38 illustrates the geometrical model used in this method of characteristics analysis.

Figures 4.1-39 through 4.1-41 show the resulting external surface pressure acting along the surface as a function of Mach No., altitude and TVC angle for various flight times. A limiting angle of 8° TVC was used for the study and the resulting pressure distributions along the system can be interpreted as being roughly linear from 0 to 8°.

Each figure shows the pressure distribution along the nozzle/SLEEC at 0° (null) as well as the distributions along the side of the system when deflected into the airstream ($+8^\circ$), and deflected away from the airstream (-8°). The 0° distribution exists evenly around the system at any axial location when the nozzle is not vectored. The distribution around the system when the nozzle is vectored 8° varies from one side to the other at any axial location from the $+8^\circ$ value to the -8° value. The integration of these unbalanced pressure distributions result in an asymmetric load to the SRB nozzle/SLEEC system. This load must be reacted by the SLEEC actuation system for SLEEC structural stability and by the TVC system in the form of increased vector loads. The aerodynamic force component, however, effectively provides an added "rudder-like" TVC component to the Shuttle configuration, reducing the amount of actual TVC required.

The internal pressure distribution of a fully deployed SLEEC (derived as described in Section 4.2.1) is also shown in each Figure based on the chamber pressure at that time.

As seen in Figure 4.1-39, the external pressure even at null for 15 and 30 sec varies from 2 or 3 psi higher at the SLEEC attach point to as much as 9 psi at the exit. Such a pressure differential would intuitively cause SLEEC to collapse and, if not, would result in drag loads exceeding any thrust benefit obtained.

In Section 4.2.1, 44 sec is determined as the optimum time to start deploying SLEEC at 3 in/sec from a performance gain standpoint based on ambient pressures. Figure 4.1-40 indicates that SLEEC could be deployed as much as 20 inches at that time (with nozzle at null) without experiencing external compressive loads. For the 60 sec case, with a planned extension of 48 inches, SLEEC would experience some minor compressive loads on the shingle tips. The resulting effect on performance was not determined in this study.

At 74 and 90 sec, Figure 4.1-41 clearly indicates the internal pressures to be well above external pressure values, even at the exit plane. Again, the possible effect of the external pressures shown on SLEEC thrust values was not considered in this program and should be investigated in any future effort.

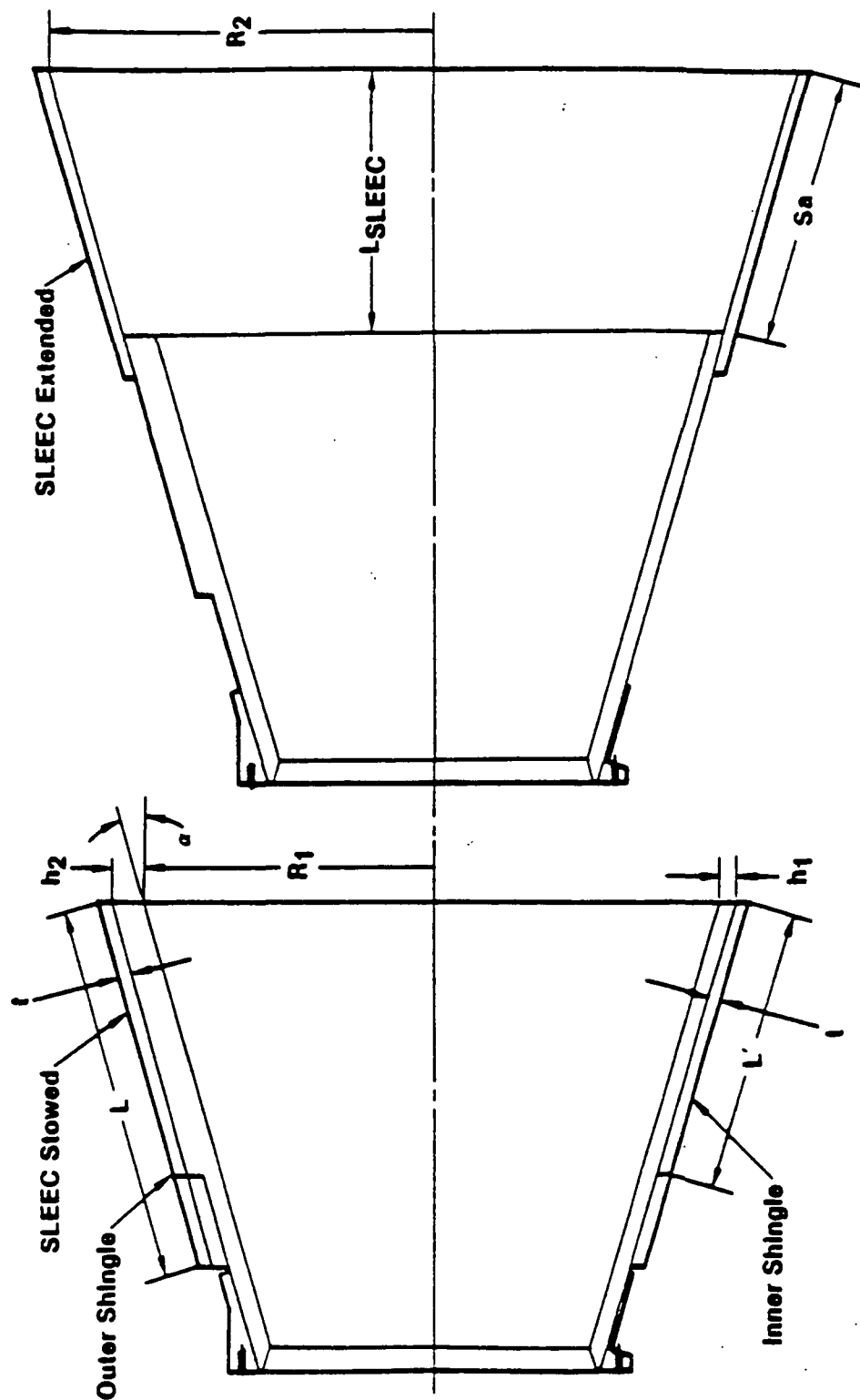


Figure 4.1-1 General SLEEC Geometry Defined

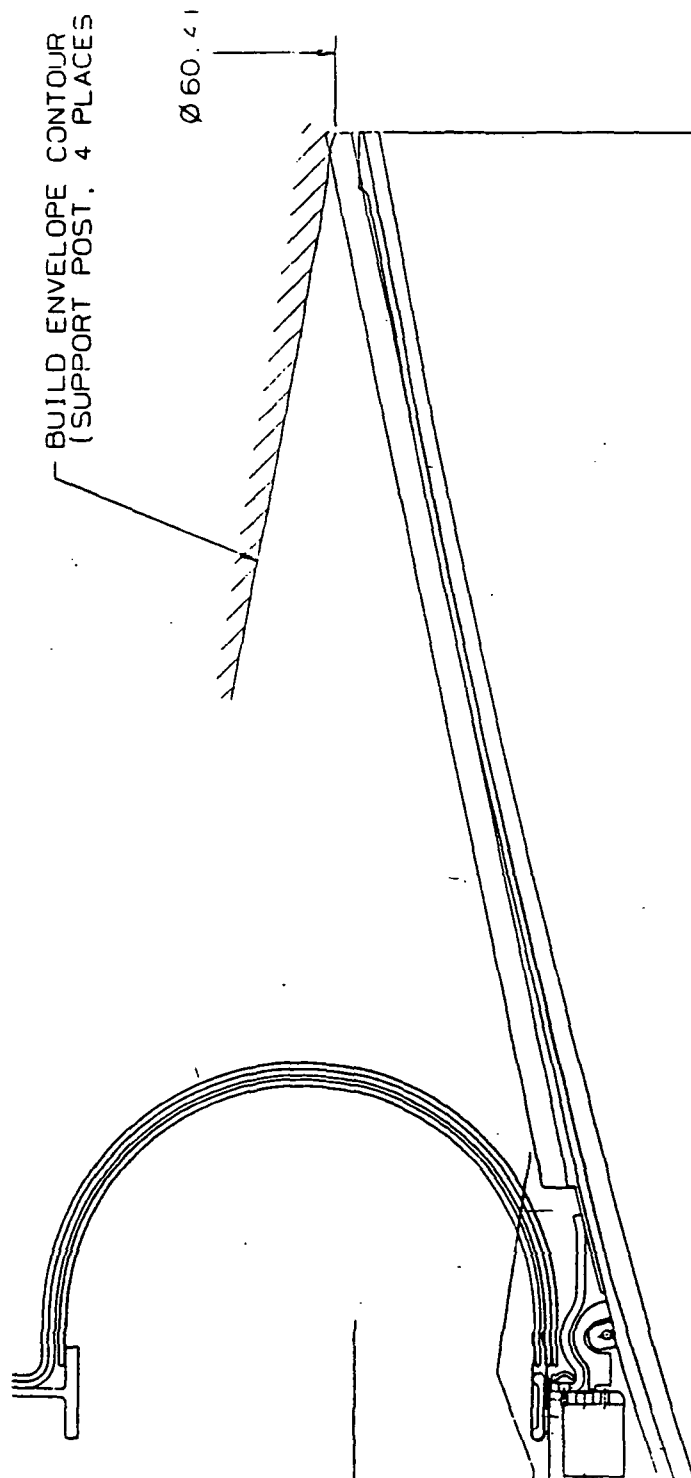


Figure 4.1-2 Existing SRB Configuration Showing Post Envelope and Shingle C/L

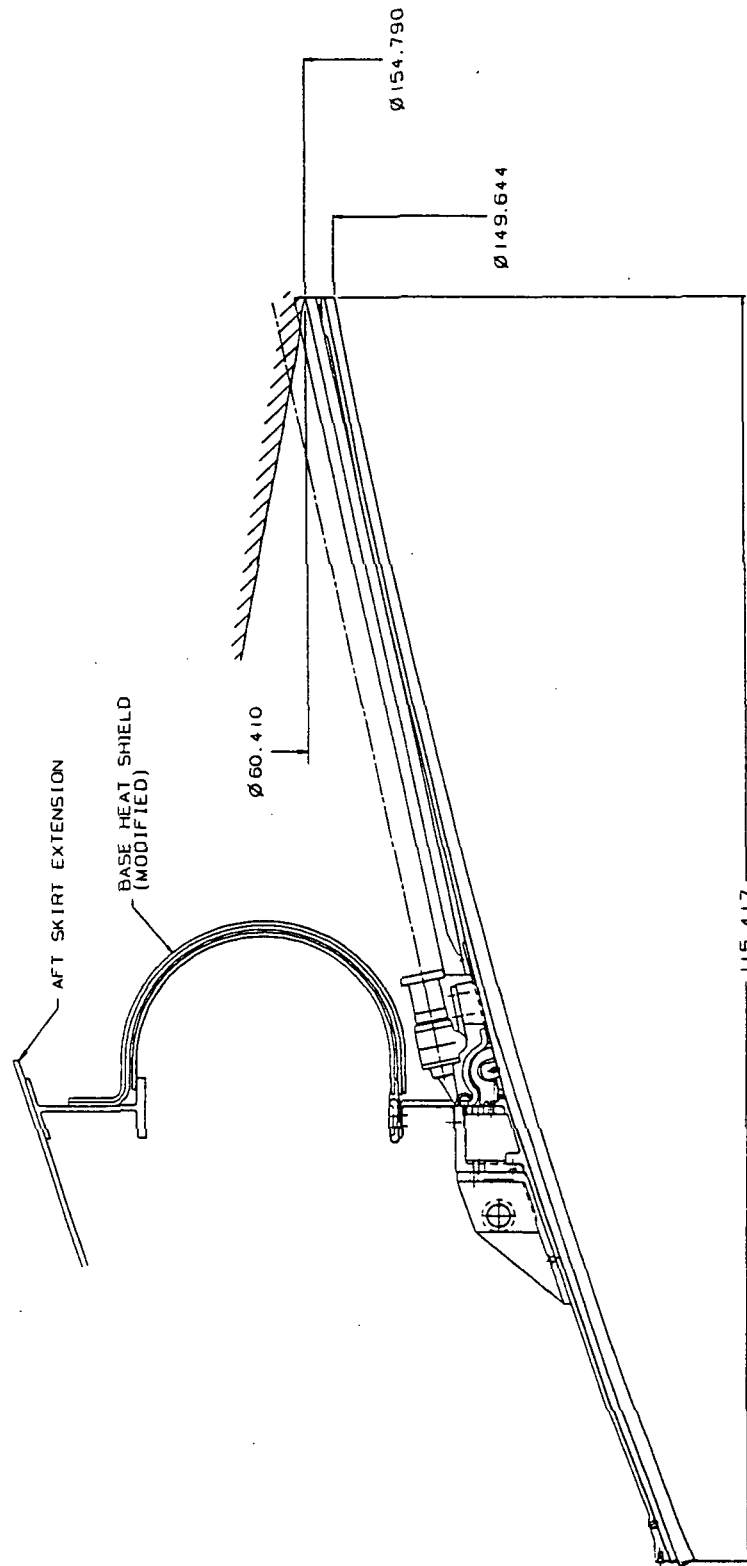


Figure 4.1-3 Overall SRB Configuration Showing Relocated Blast Shield

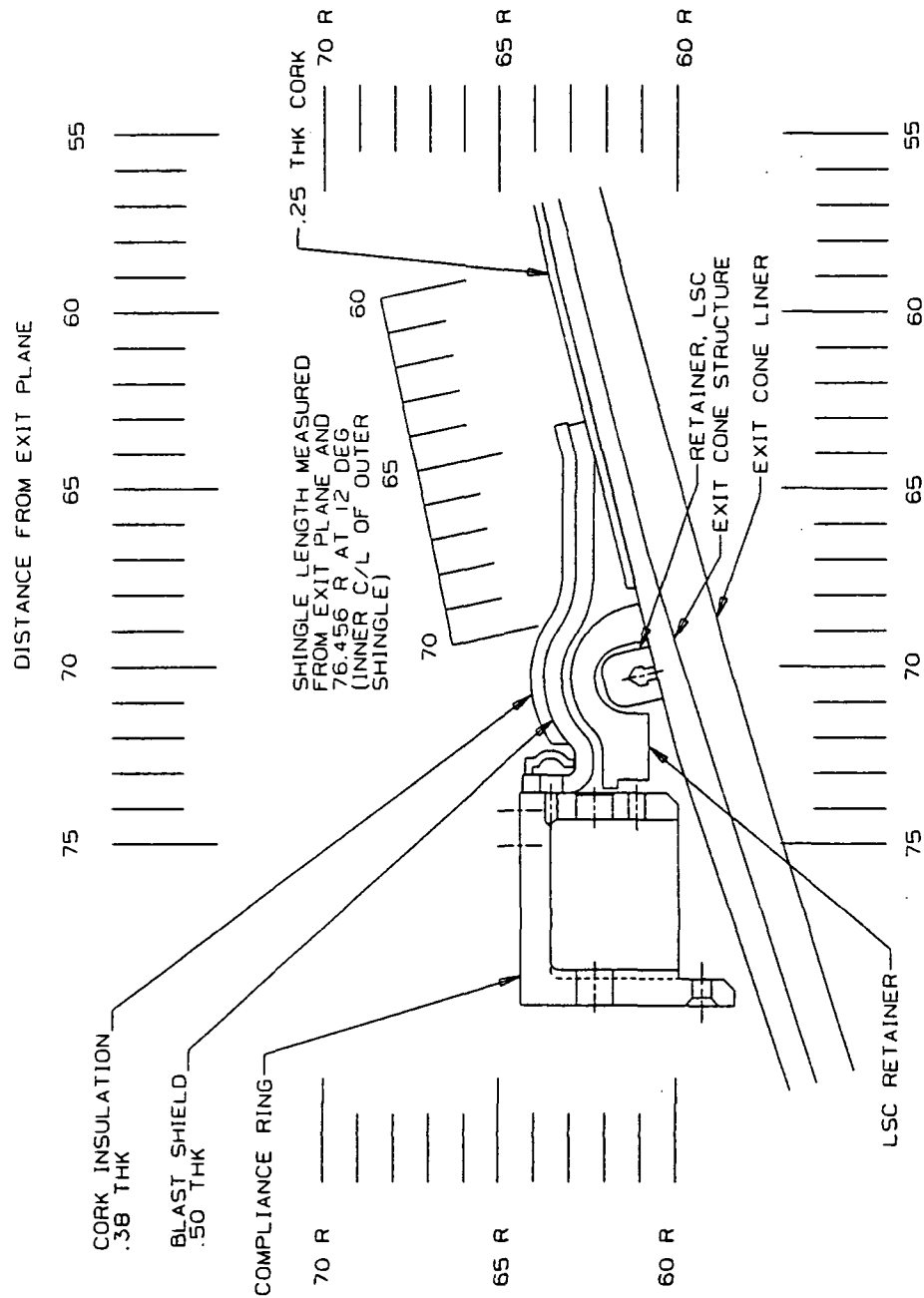


Figure 4.1-4 Existing Exit Cone, Compliance Ring and Linear Shaped Charge

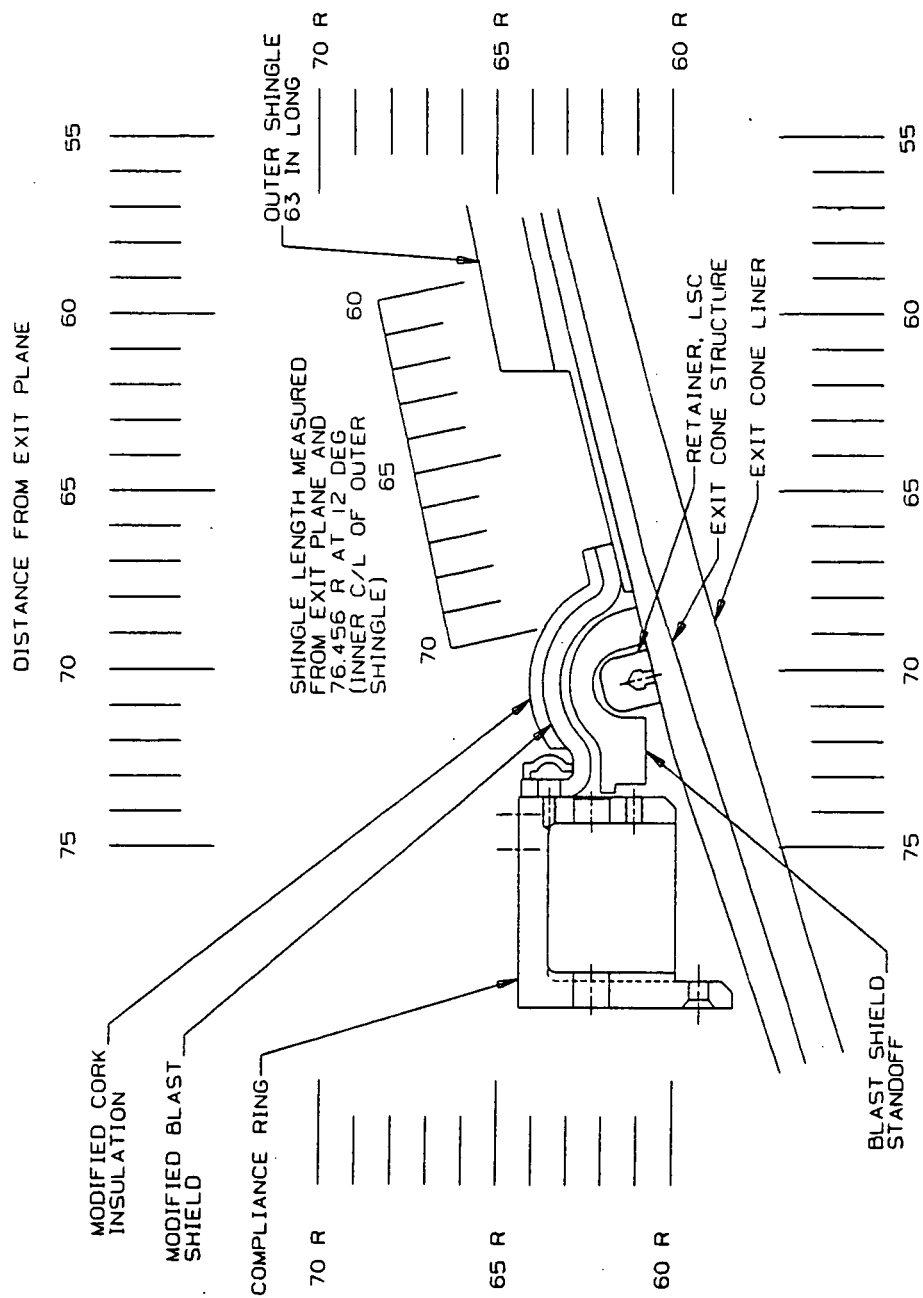


Figure 4.1-5 Suggested Modifications to Linear Shaped Charge Insulators

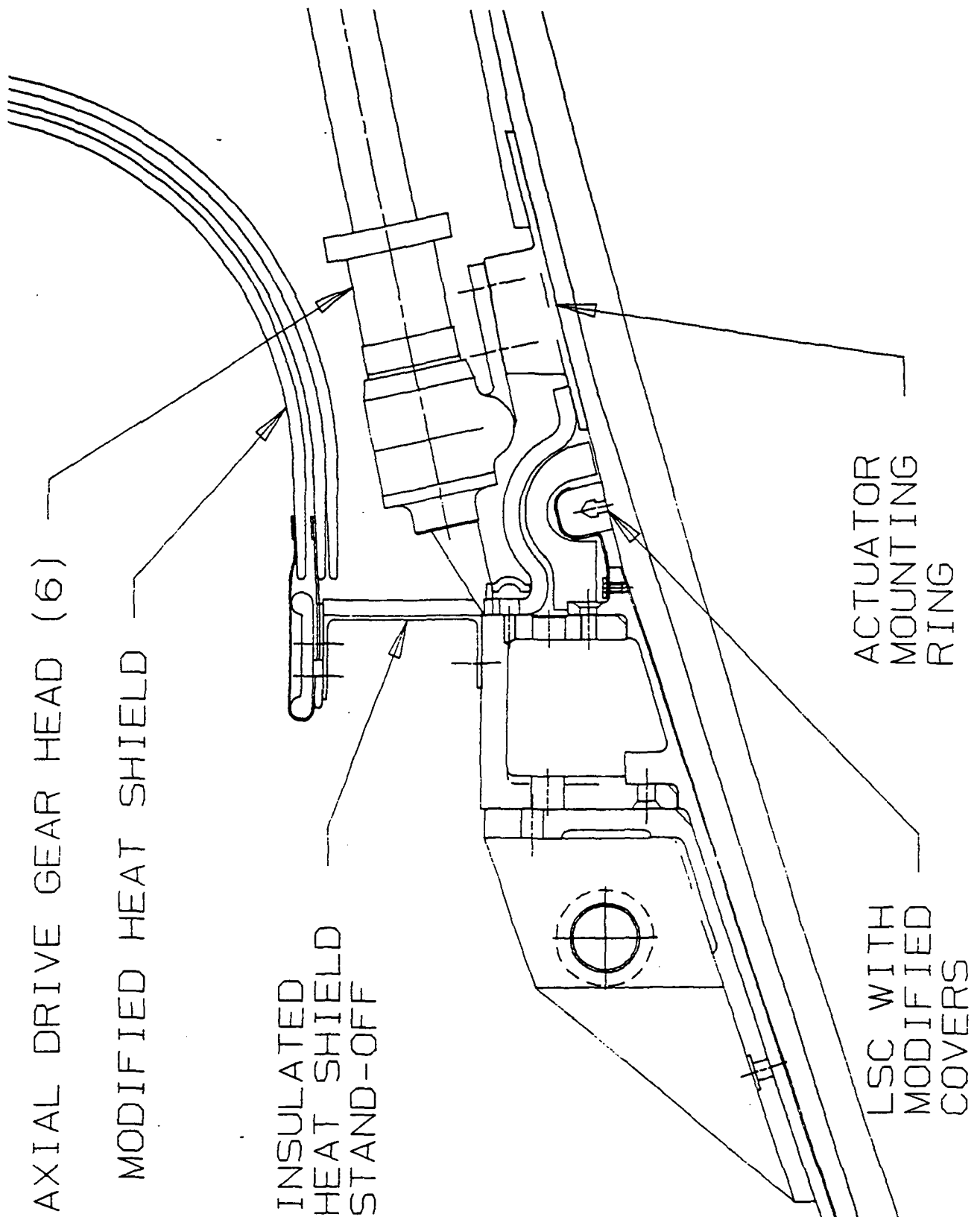


Figure 4.1-6 Recommended Heat Shield and LSC Cover Modifications

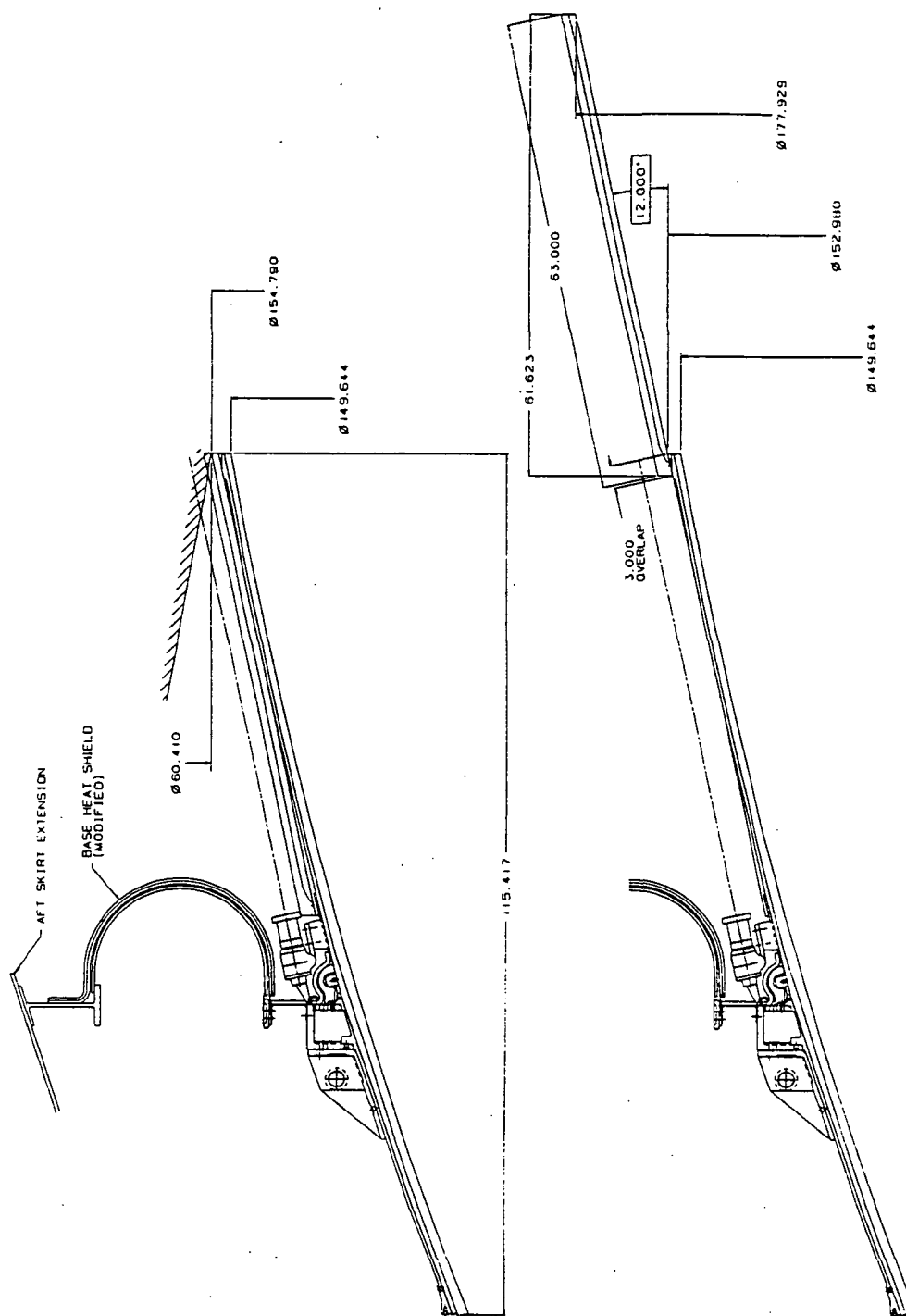


Figure 4.1-7 View of Aft HPN Exit Cone Assembly with SLEEC Installed

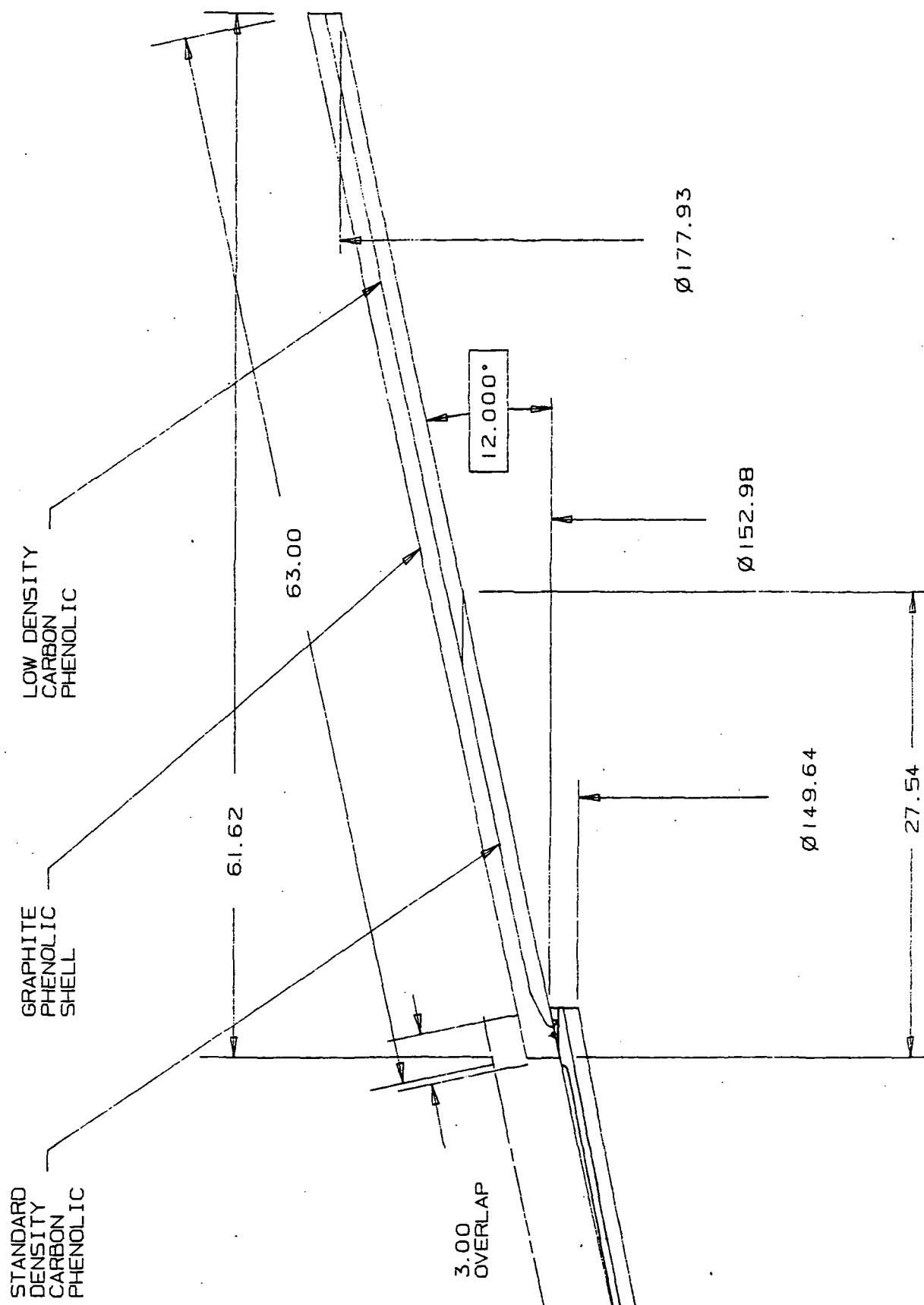


Figure 4.1-8 Shingle-to-Exit Cone Geometry

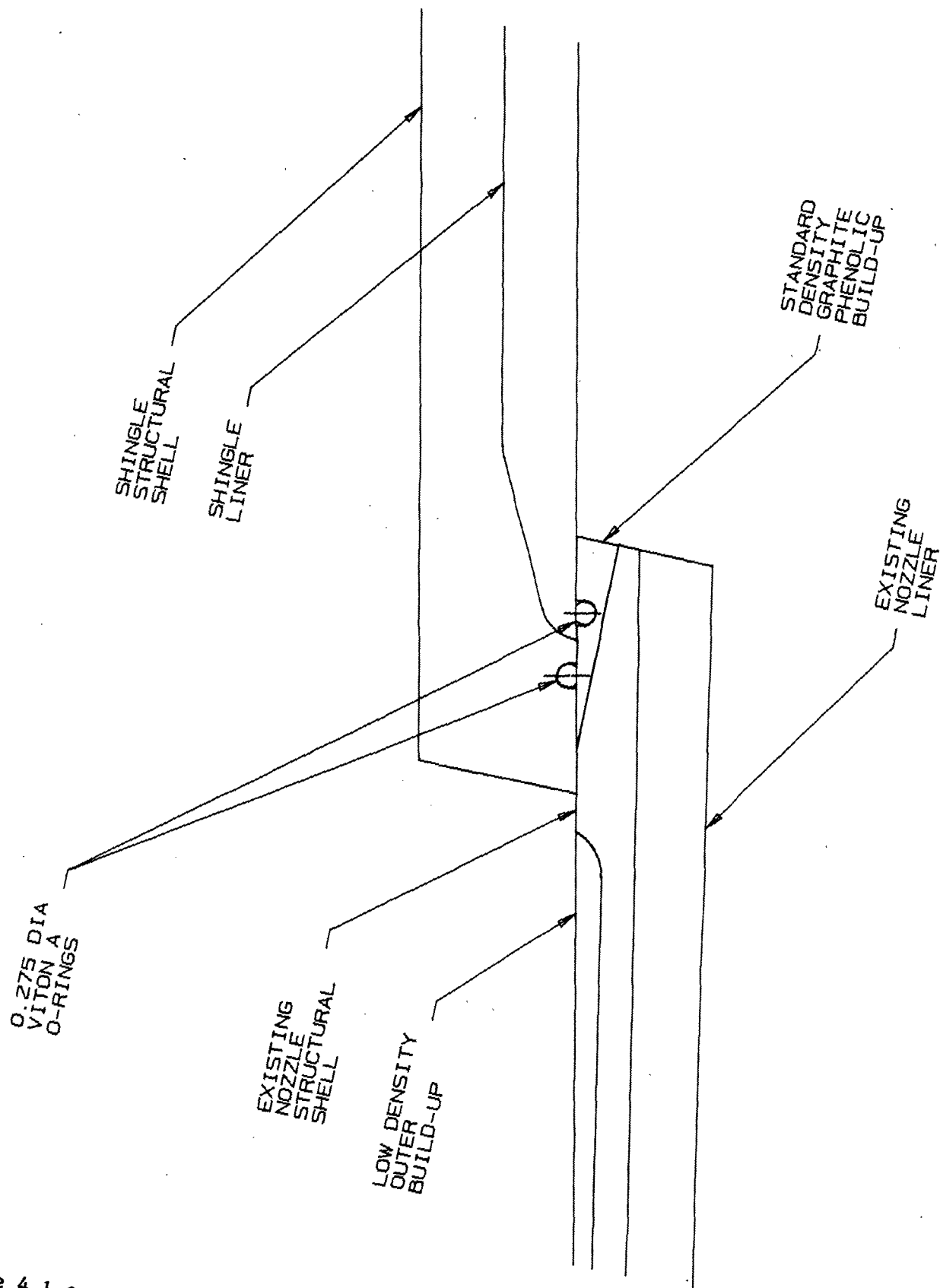


Figure 4.1-9 Detail of Shingle-to-Exit Cone "Lapped" Region

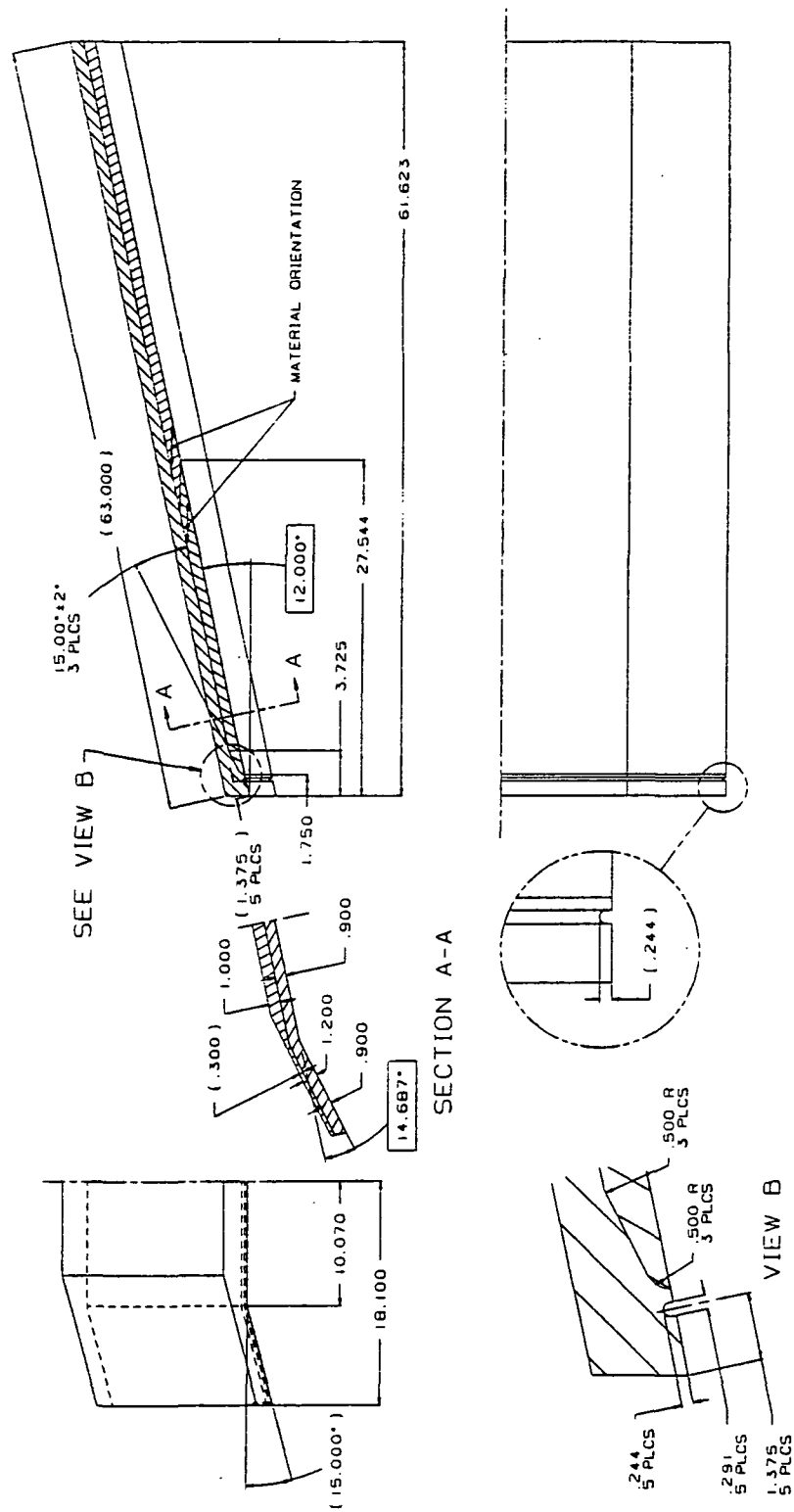


Figure 4.1-10 Inner Shingle Detail

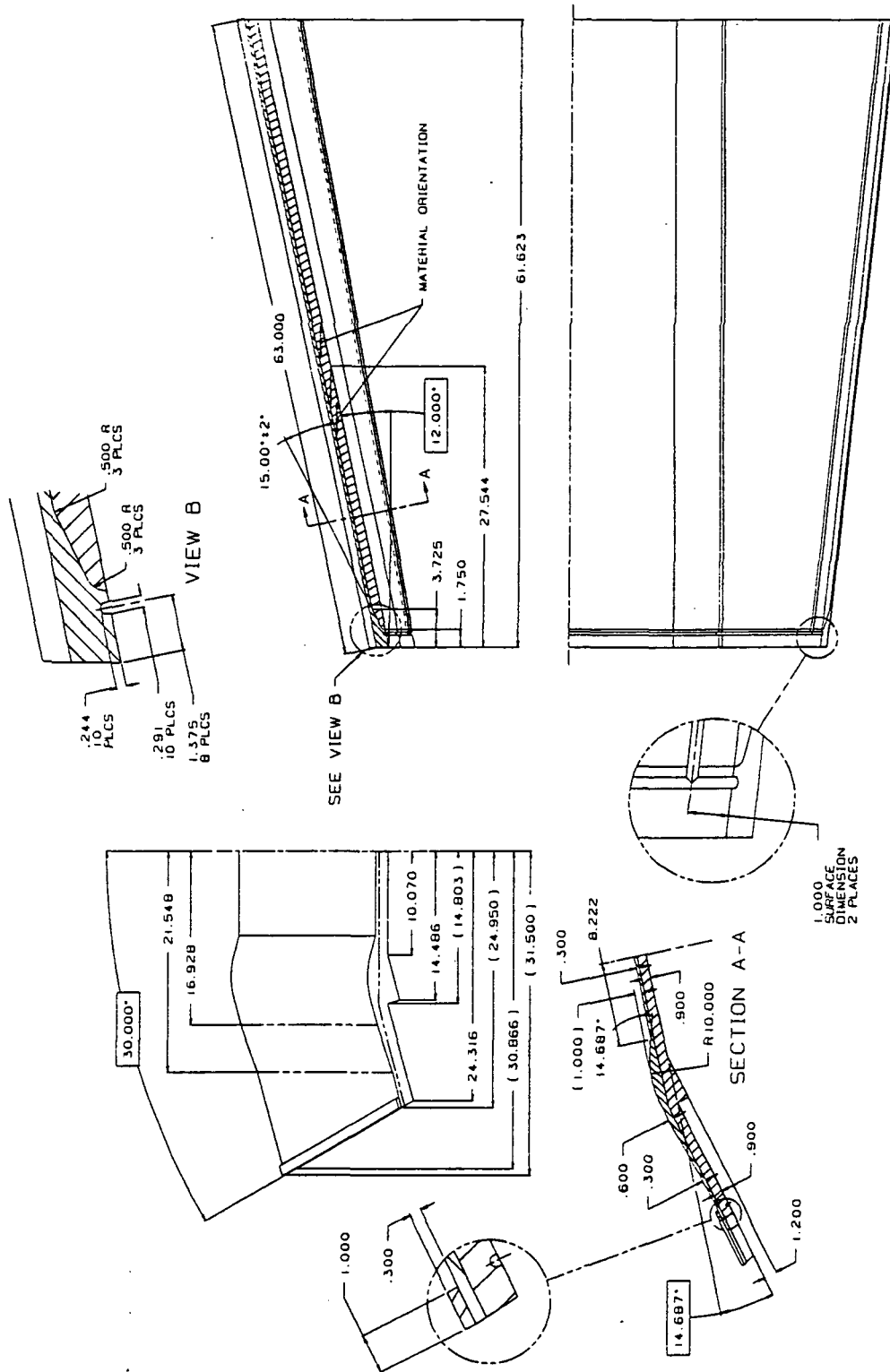


Figure 4.1-11 Outer Shingle Detail

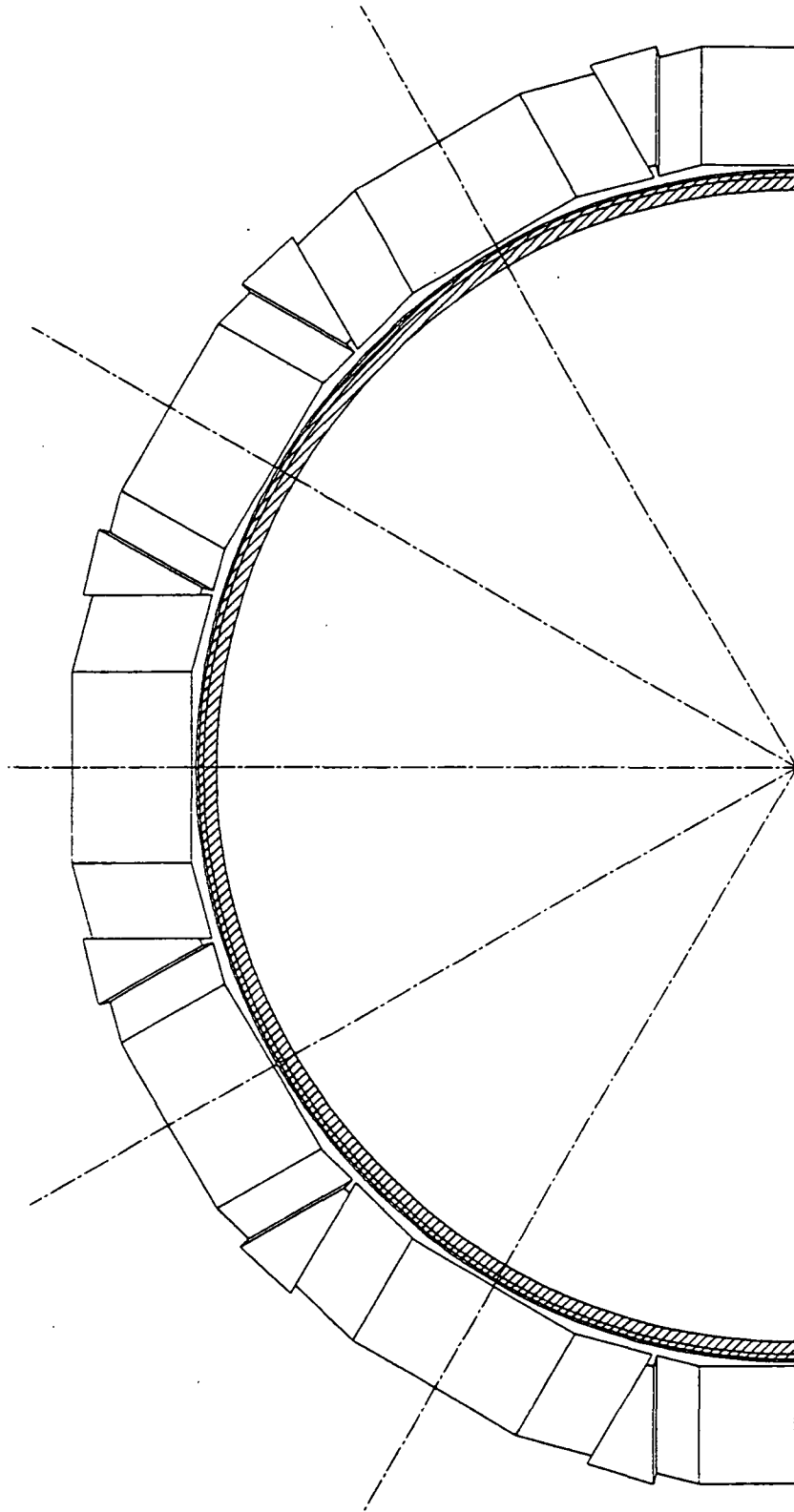


Figure 4.1-12 Machined Build Up on Exit Cone Looking Aft

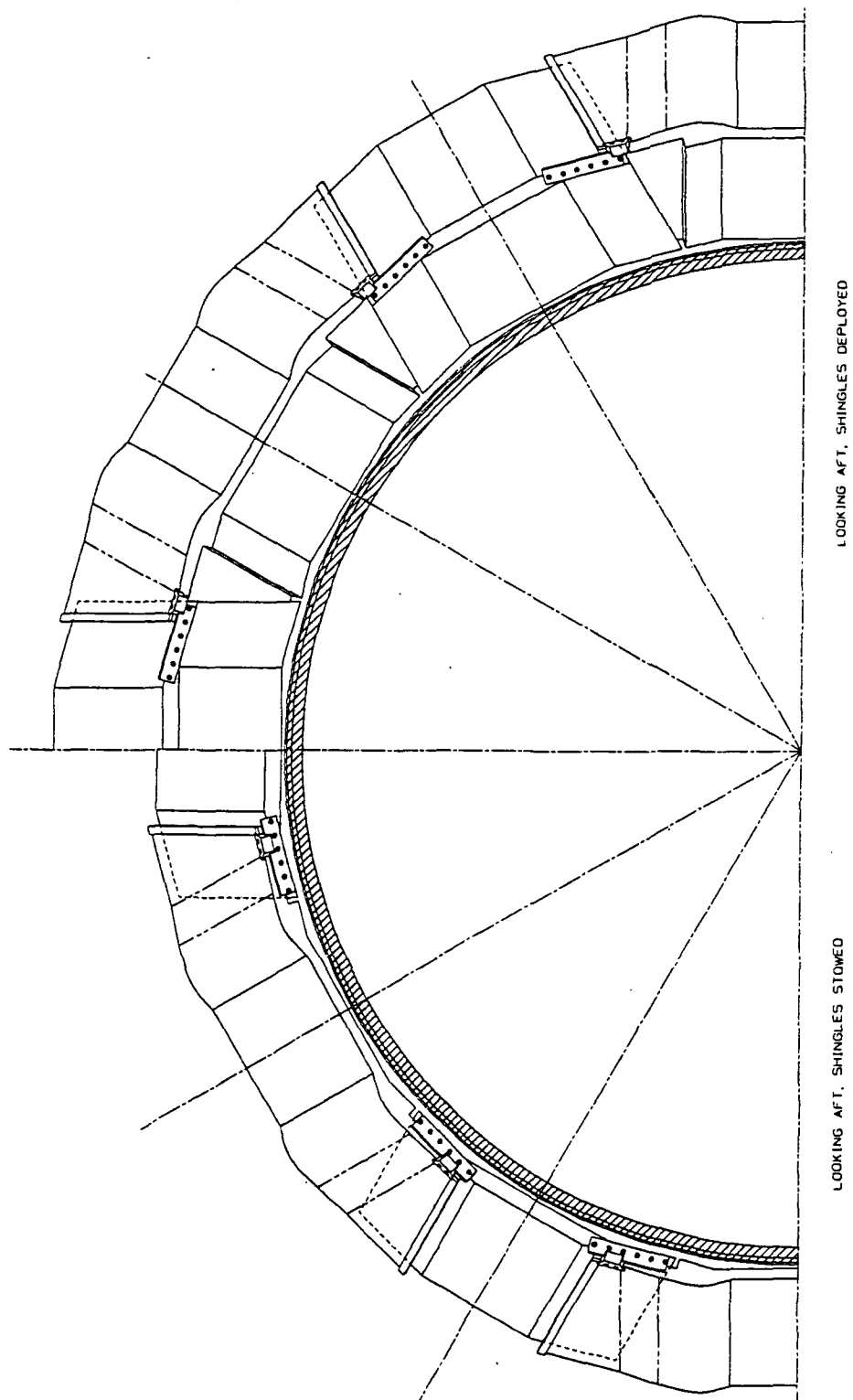


Figure 4.1-13 SRB/SLEEC System Looking Aft

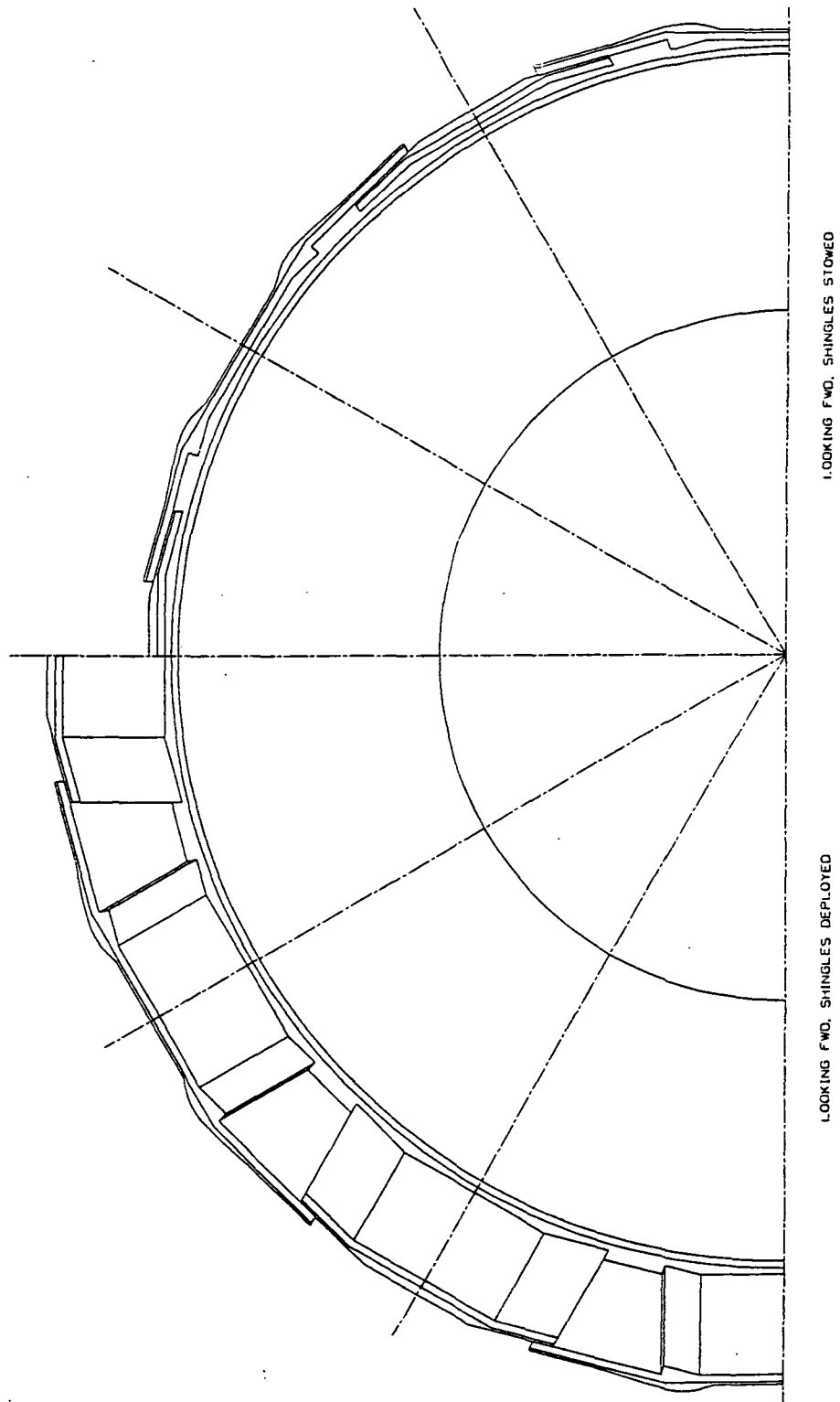


Figure 4.1-14 SRB/SLEEC System Looking Forward

ORIGINAL PAGE IS
OF POOR QUALITY

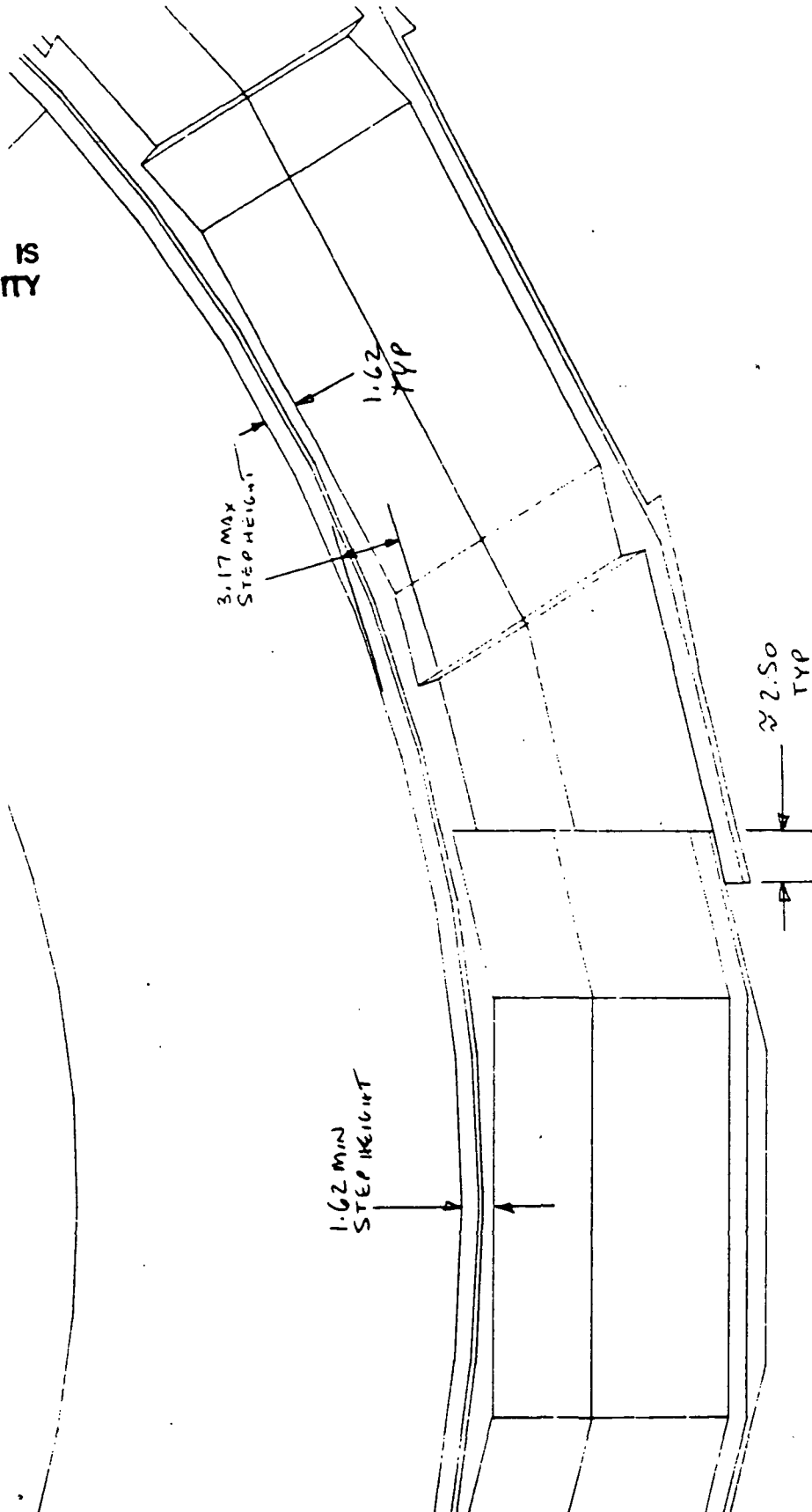


Figure 4.1-15 Detailed View of "Steps"

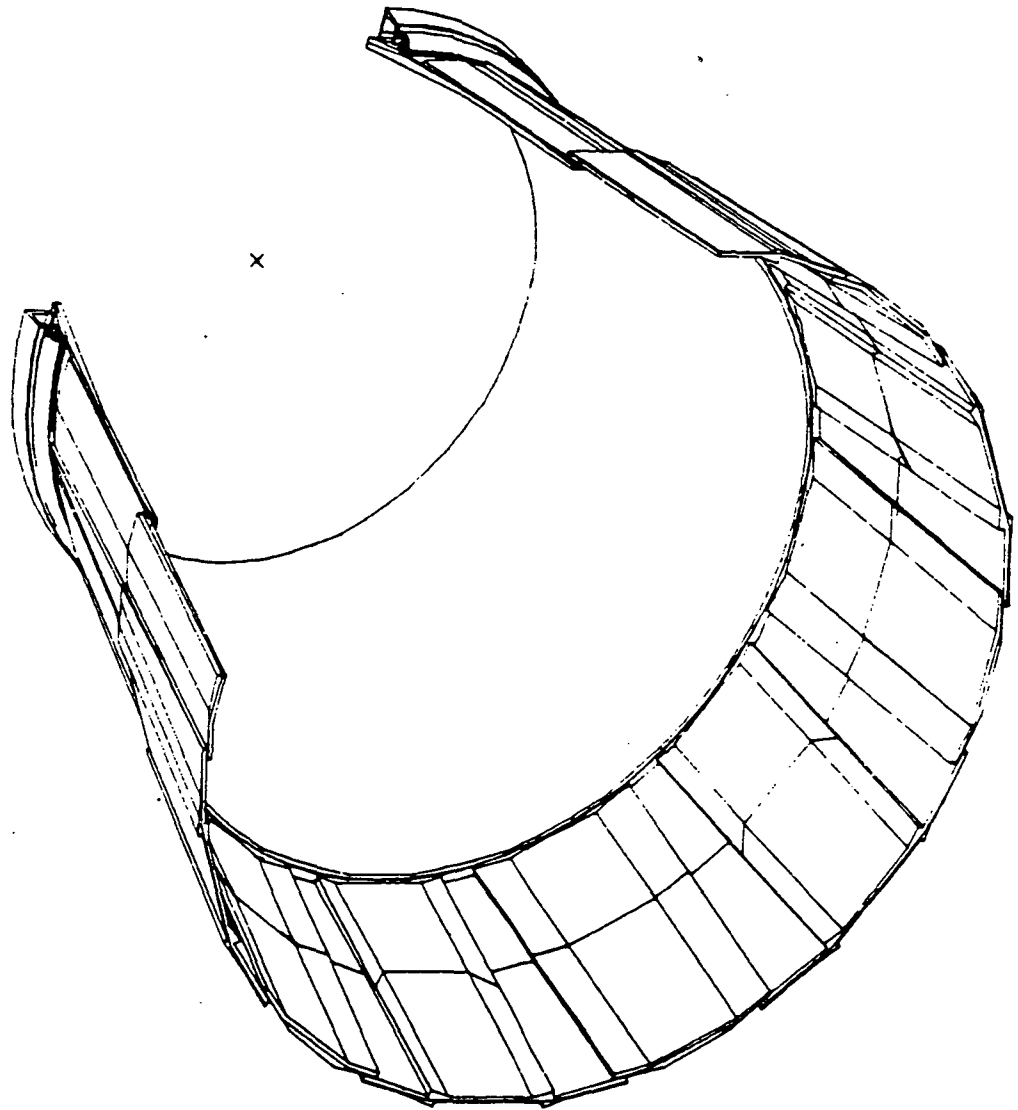


Figure 4.1-16 Cutaway Isometric View of SRB/SLEEC System

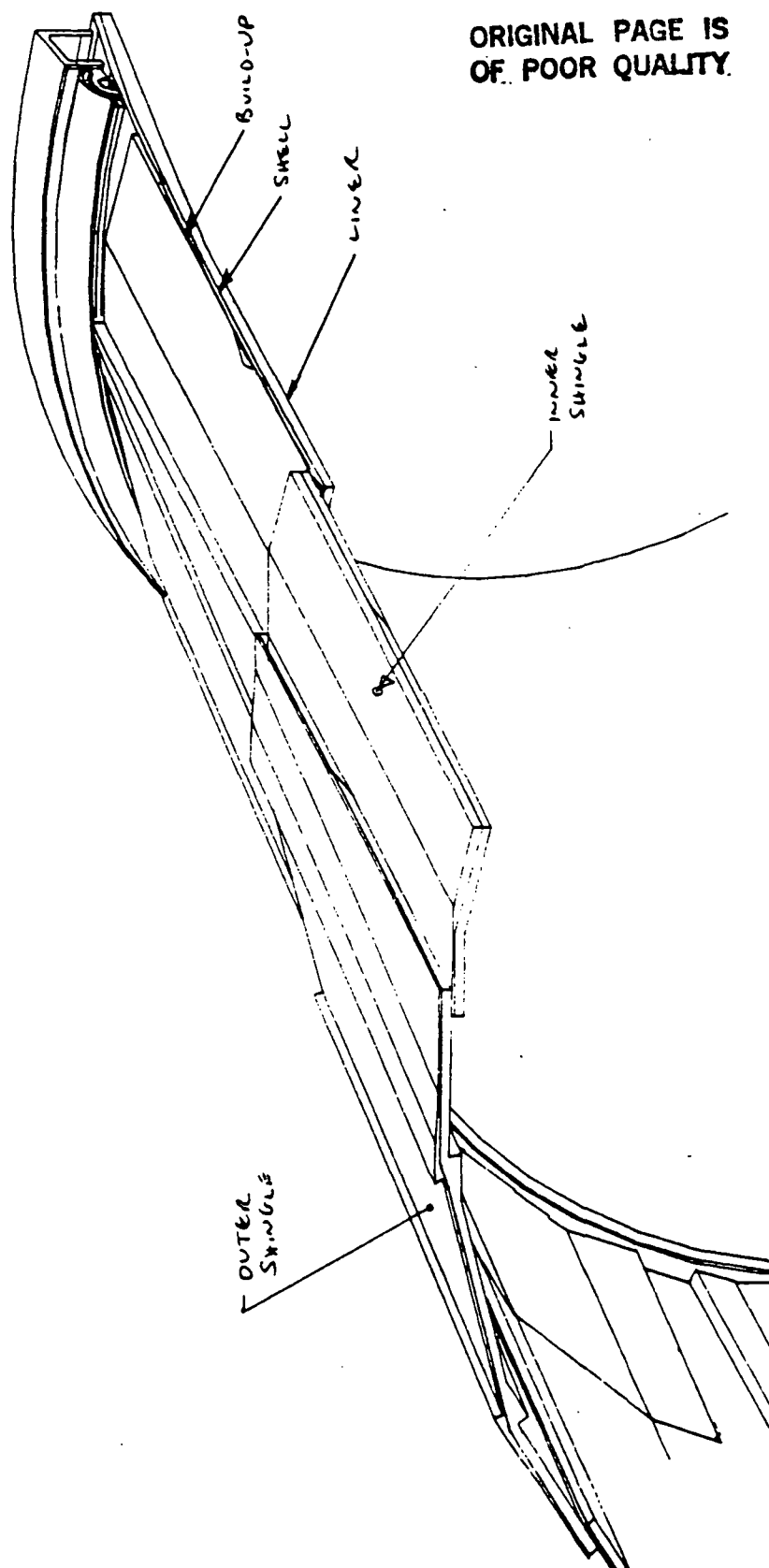


Figure 4.1-17 Enlarged Detail of Cutaway SRB/SLEEC Isometric View

SRB/SLEEC
9/19/86

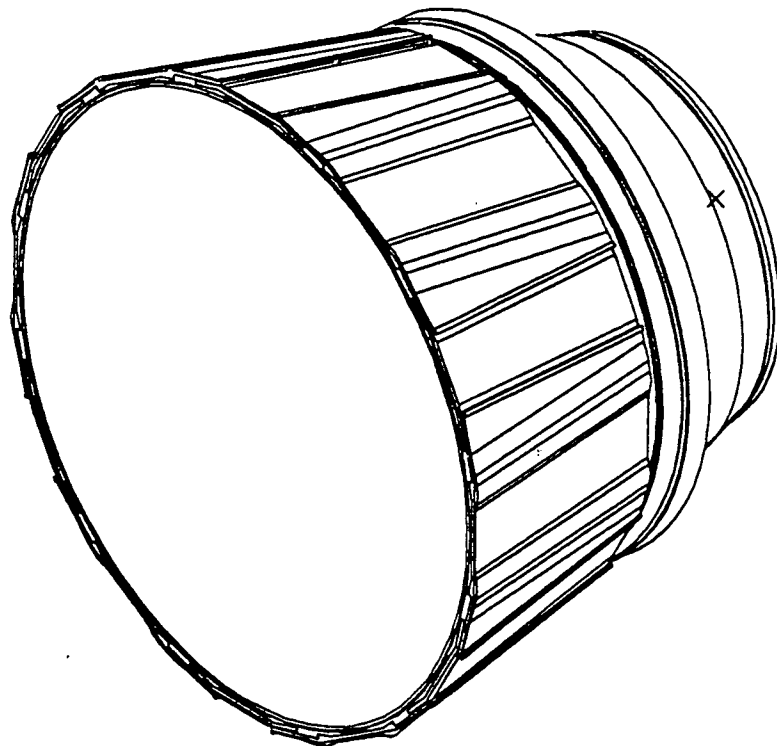


Figure 4.1-18 Full Isometric View of Stowed SRB/SLEEC

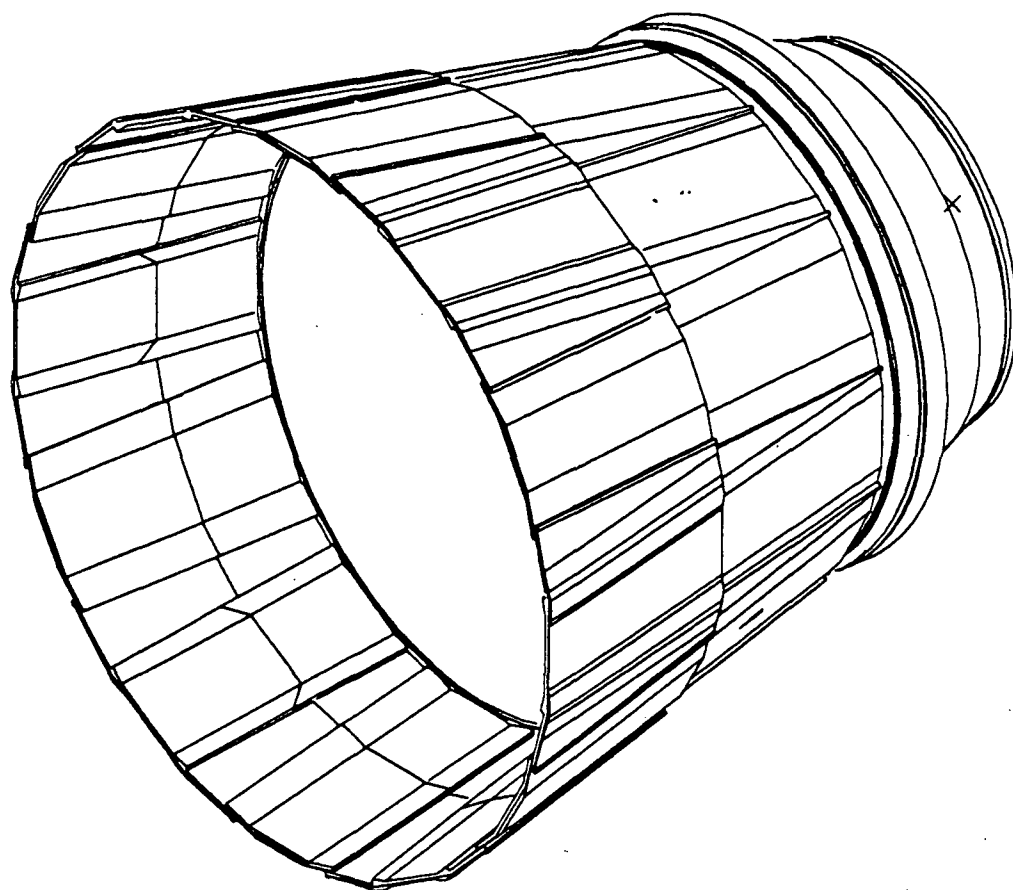


Figure 4.1-19 Full Isometric View of Extended SRB/SLEEC

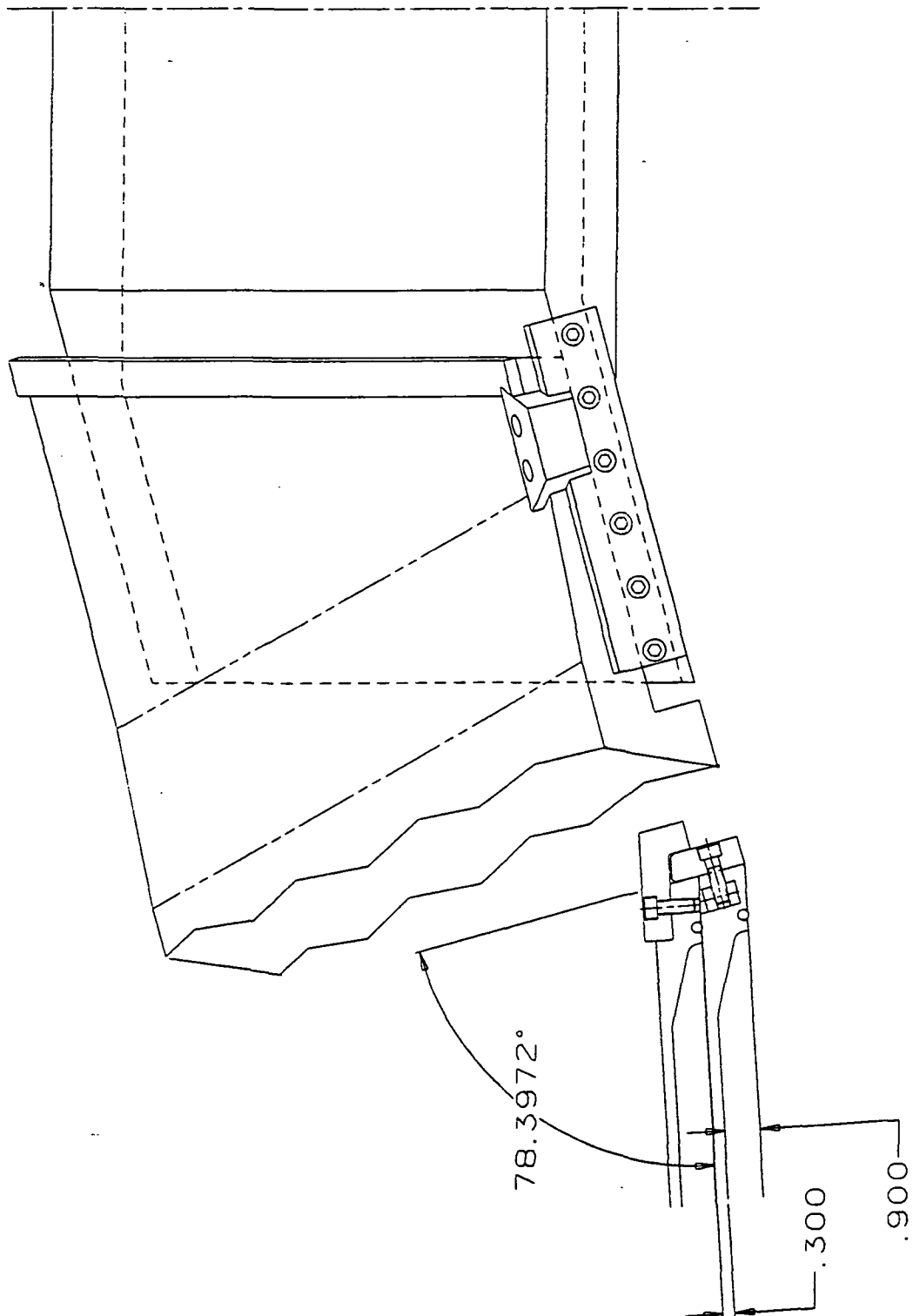


Figure 4.1-20 Details of Shingle Clip and Guide

ORIGINAL PAGE IS
OF POOR QUALITY

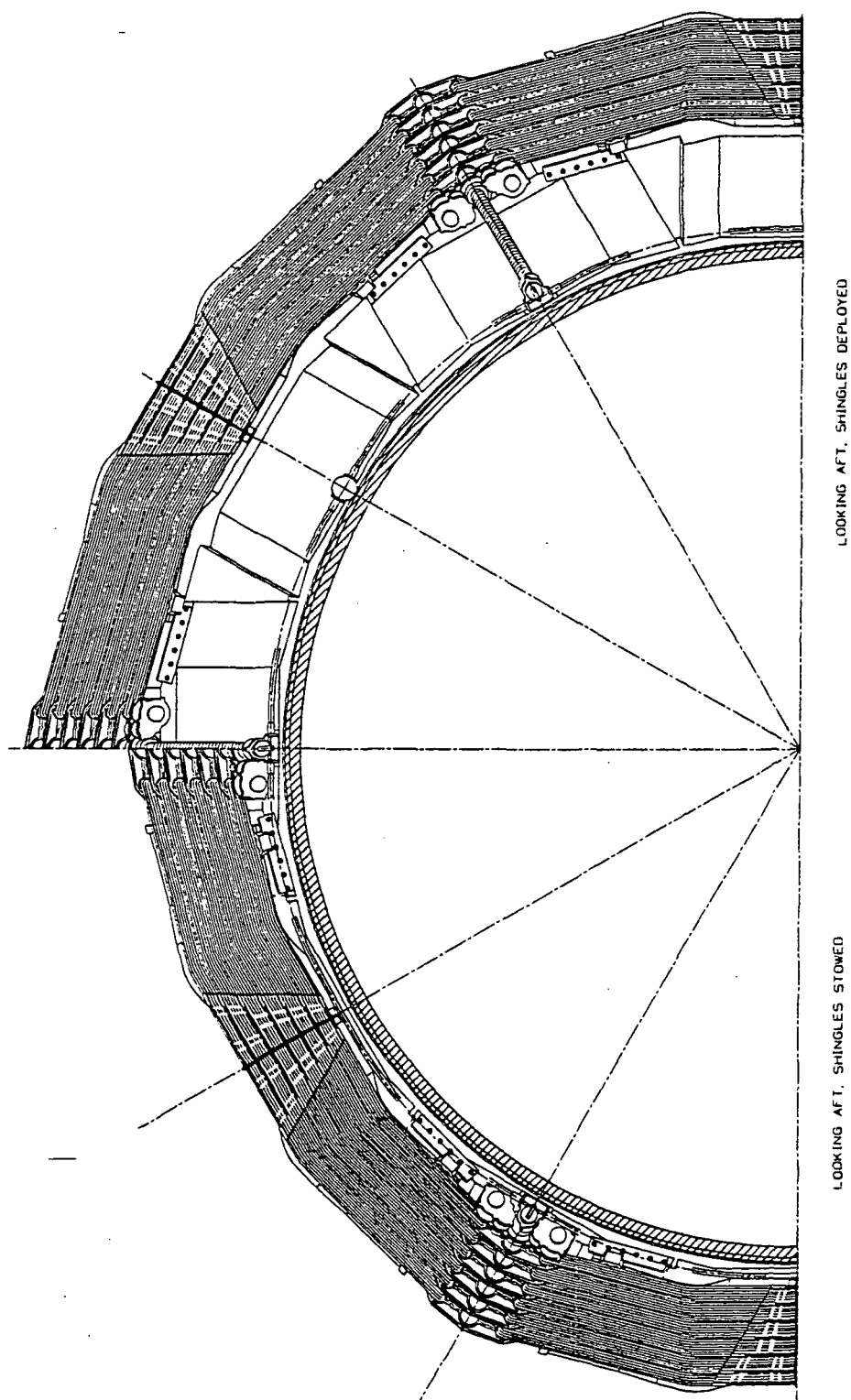


Figure 4.1-21 View of SRB/SLEEC Looking Aft With Actuation System Installed

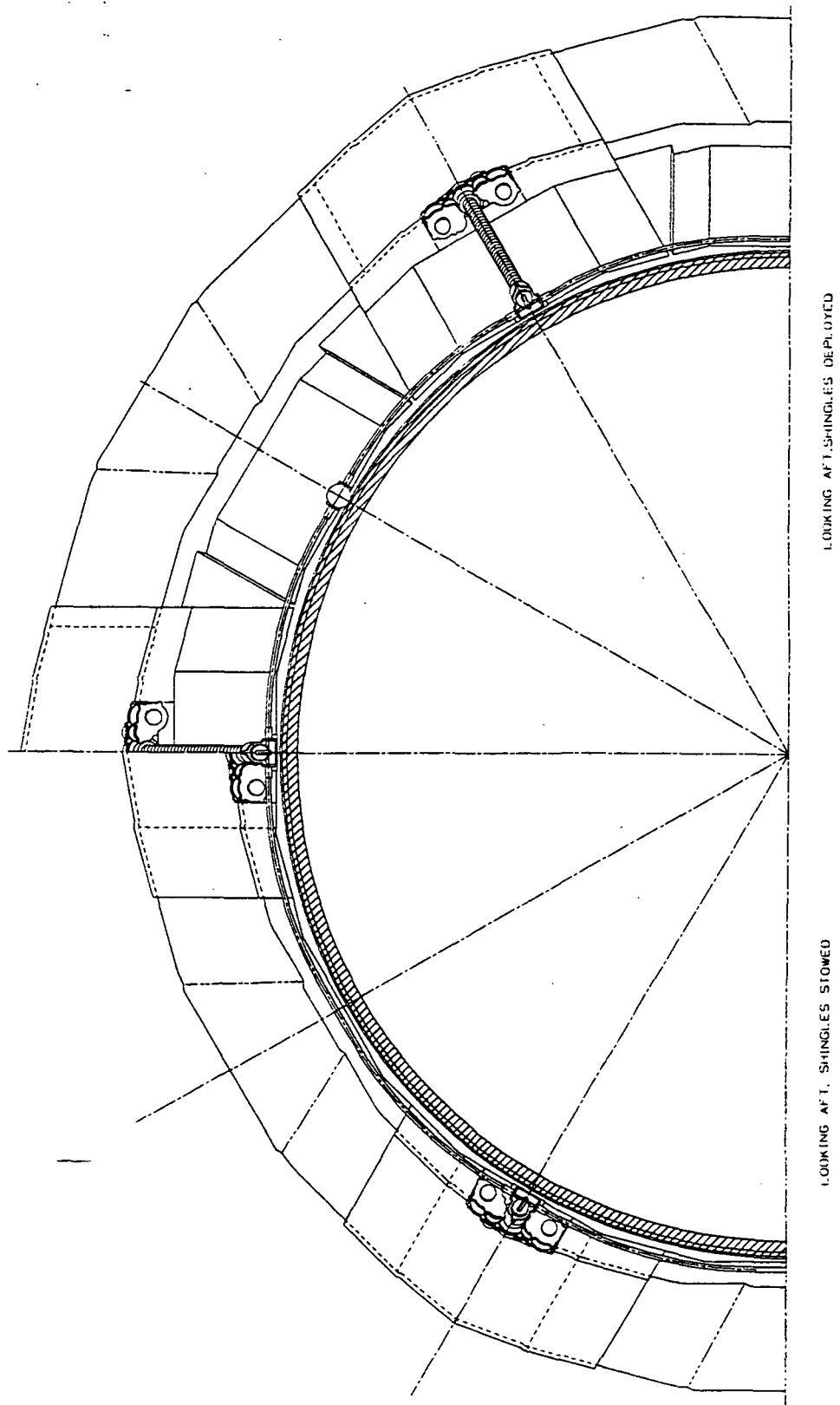


Figure 4.1-22 View of SRB/SLEEC Looking Aft With Protective External Heat Shields Installed

ORIGINAL PAGE IS
OF POOR QUALITY

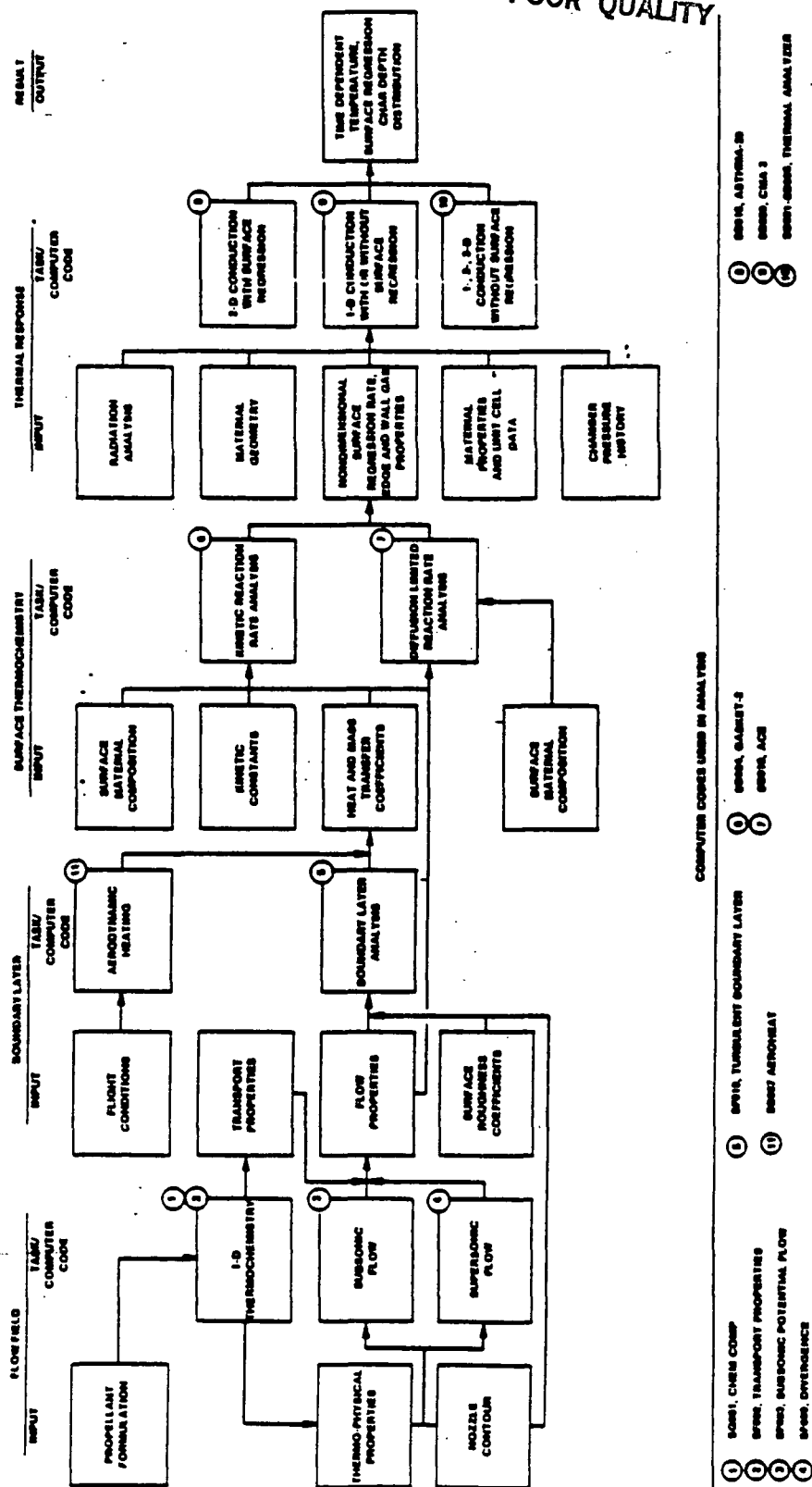


Figure 4.1-23 Thermal Response Prediction Procedures

SURFACE REGRESSION AND CHAR DEVELOPMENT VS TIME FOR SLEEC STATION 1

TIME, SEC	SURFACE REGRESSION, INCHES	CHAR (1) DEPTH, INCHES	CHAR THICKNESS, INCHES
61.5	0.0000	0.00	0.000
65.0	0.0008	0.09	0.089
70.0	0.0053	0.15	0.145
75.0	0.0106	0.19	0.179
80.0	0.0163	0.23	0.214
85.0	0.0219	0.26	0.238
90.0	0.0274	0.29	0.263
95.0	0.0325	0.31	0.278
100.0	0.0375	0.34	0.303
105.0	0.0423	0.36	0.318
110.0	0.0466	0.38	0.333
115.0	0.0500	0.40	0.350
120.0	0.0508	0.42	0.369
122.0	0.0508	0.43	0.379

(1) RELATIVE TO INITIAL SURFACE

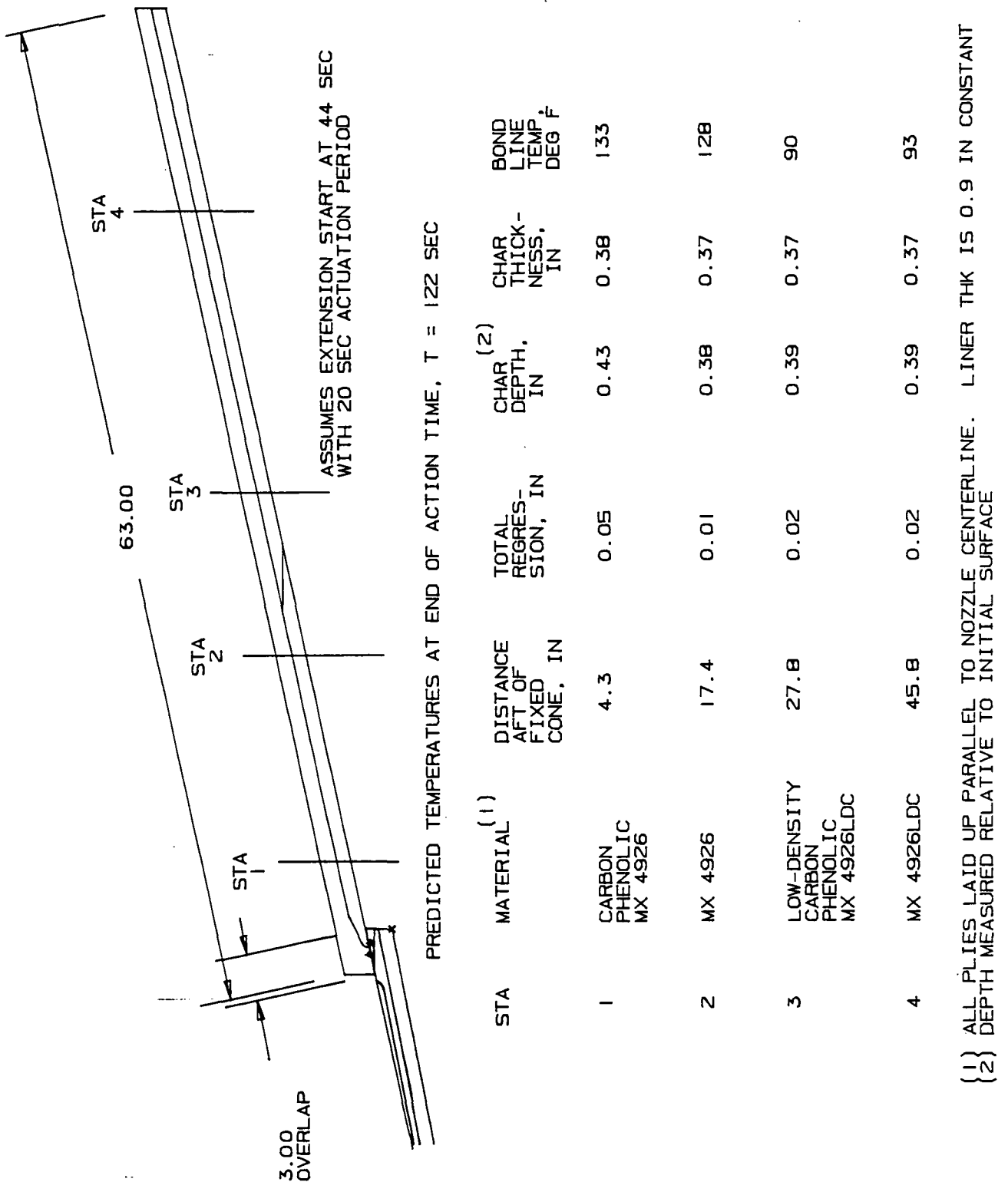


Figure 4.1-25 SLEEC Thermal Analysis Results

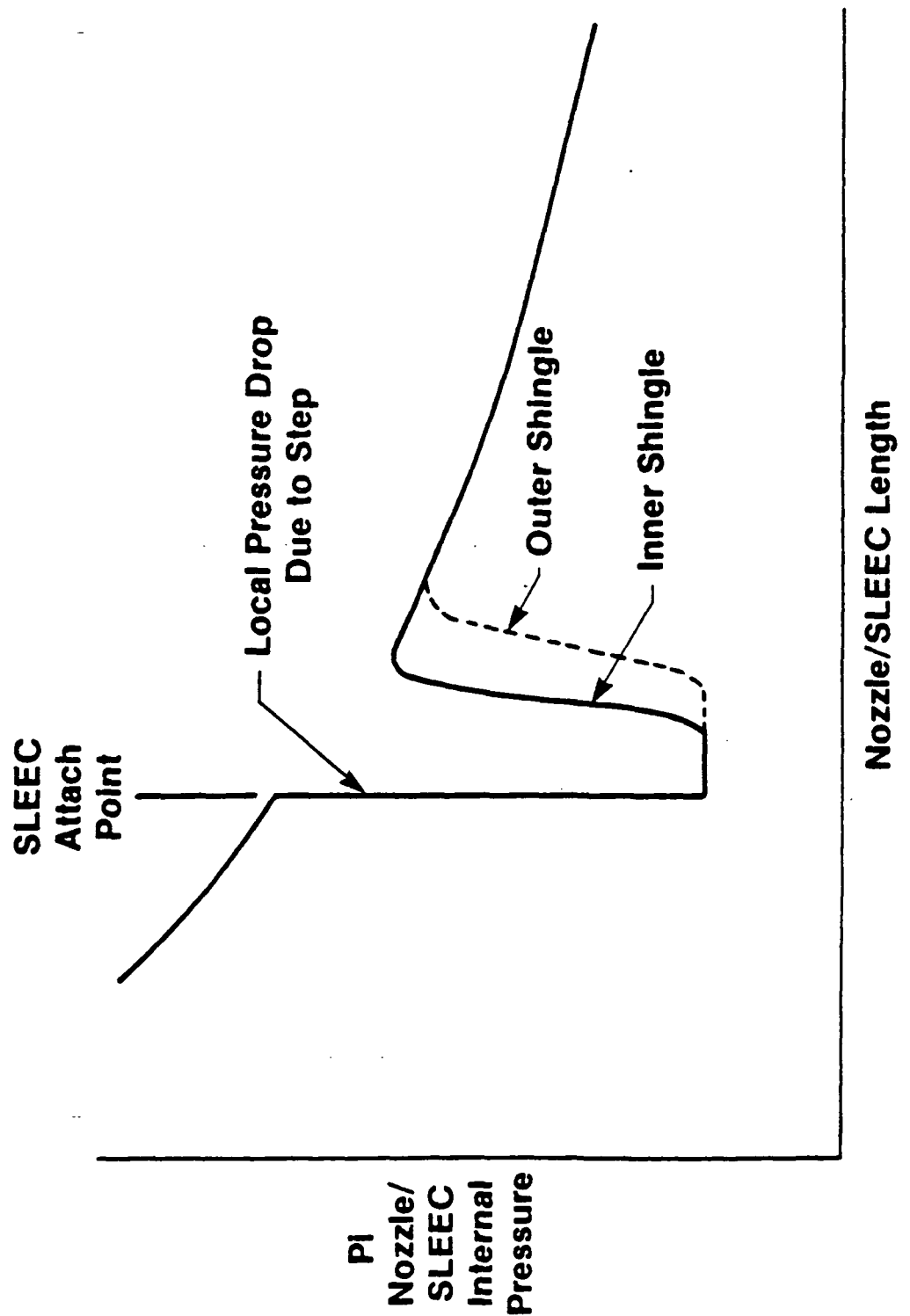


Figure 4.1-26 Typical SLEEC Internal Pressure Distribution

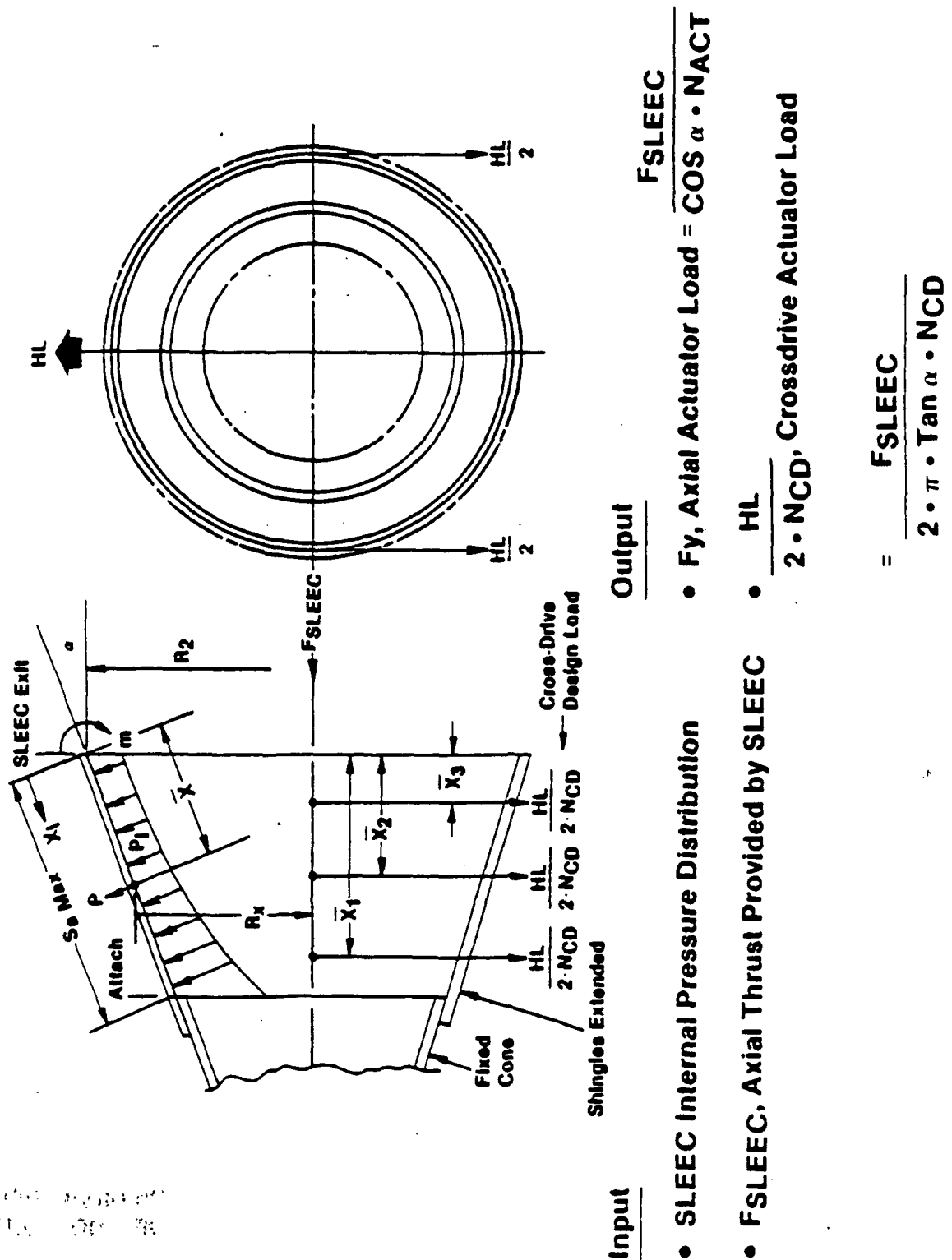
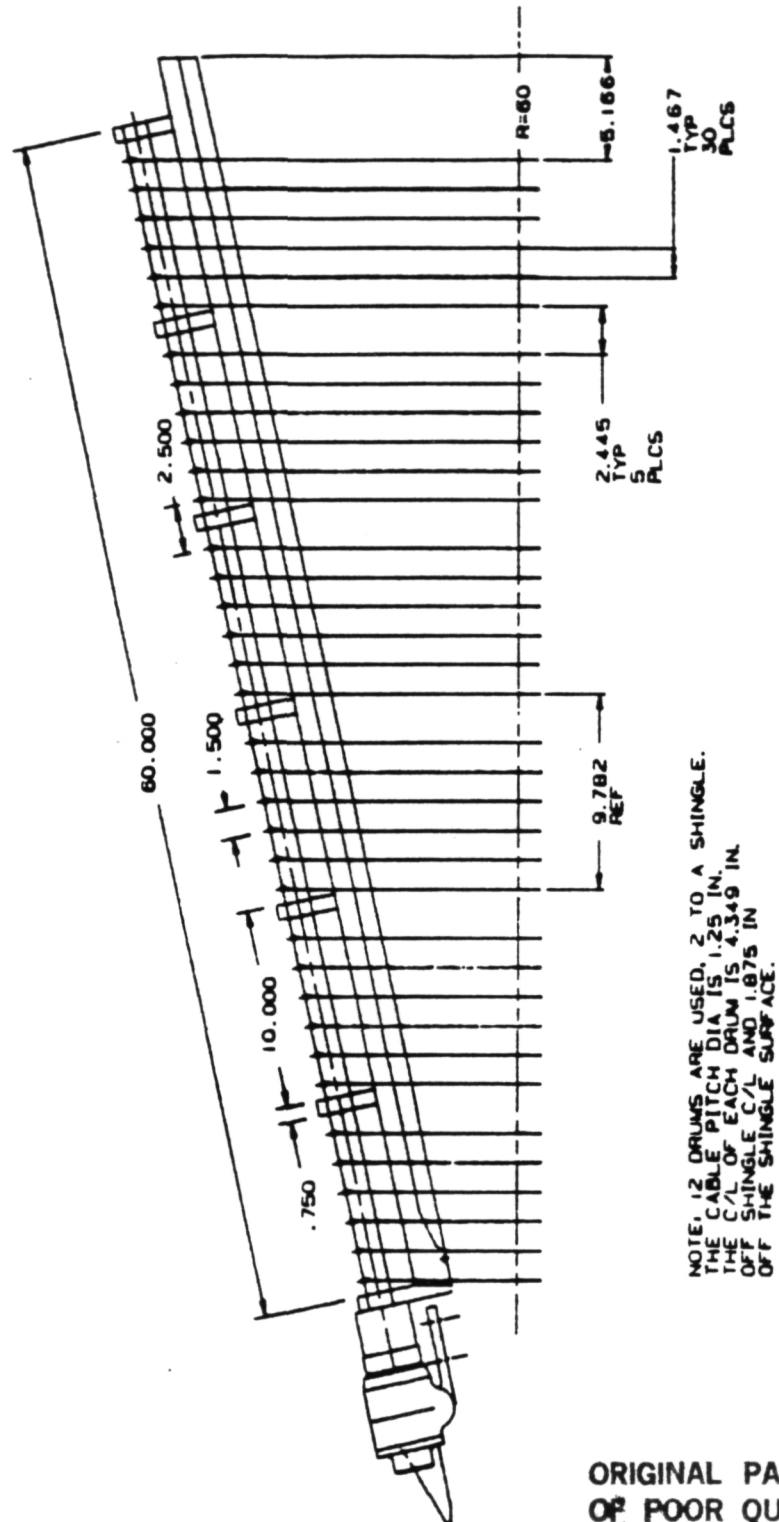


Figure 4.1-27 SLEEC Actuation Loads Defined



ORIGINAL PAGE IS
OF POOR QUALITY

Figure 4.1-28 Side View Layout of Cable Actuation System

ORIGINAL PAGE IS
OF POOR QUALITY

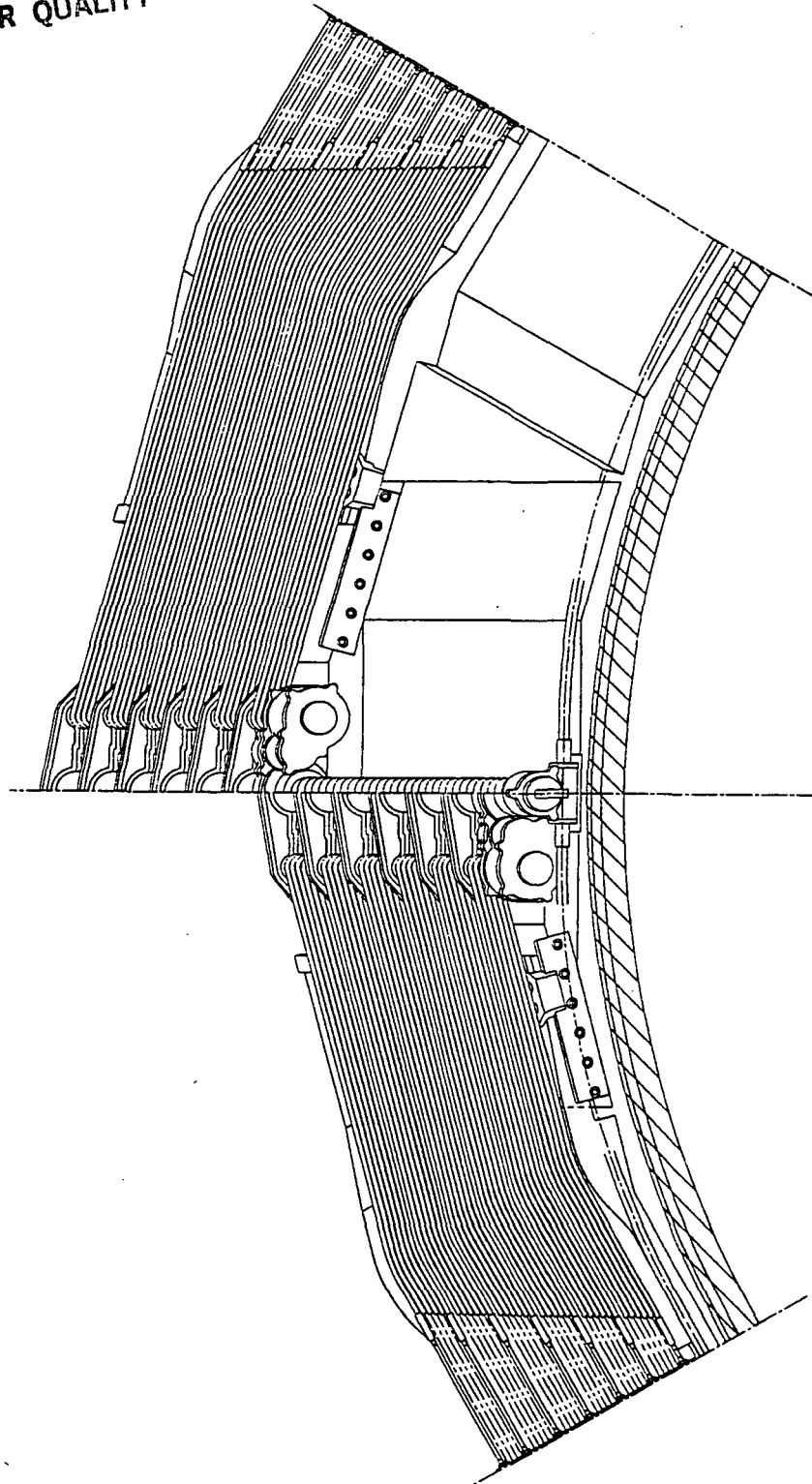


Figure 4.1-30 View Looking Aft, Layout of Cable Actuation System

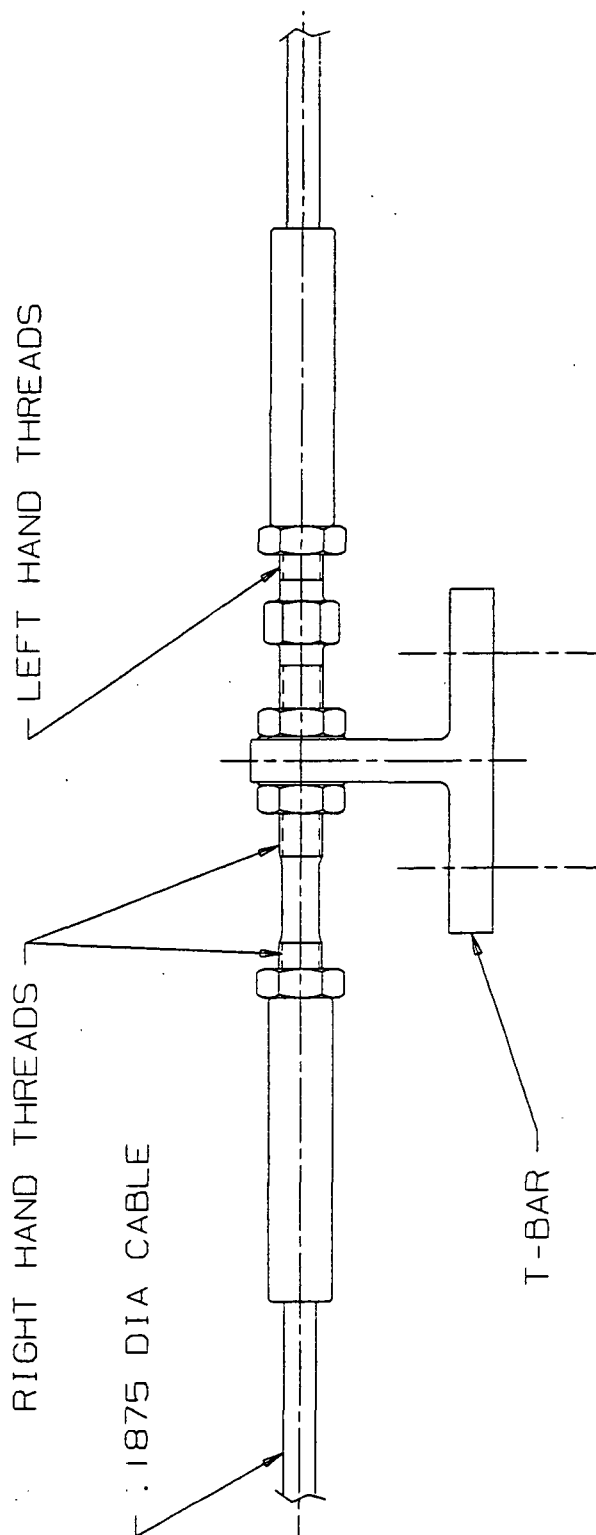


Figure 4.1-31 Turnbuckle and "T" Bar Configuration

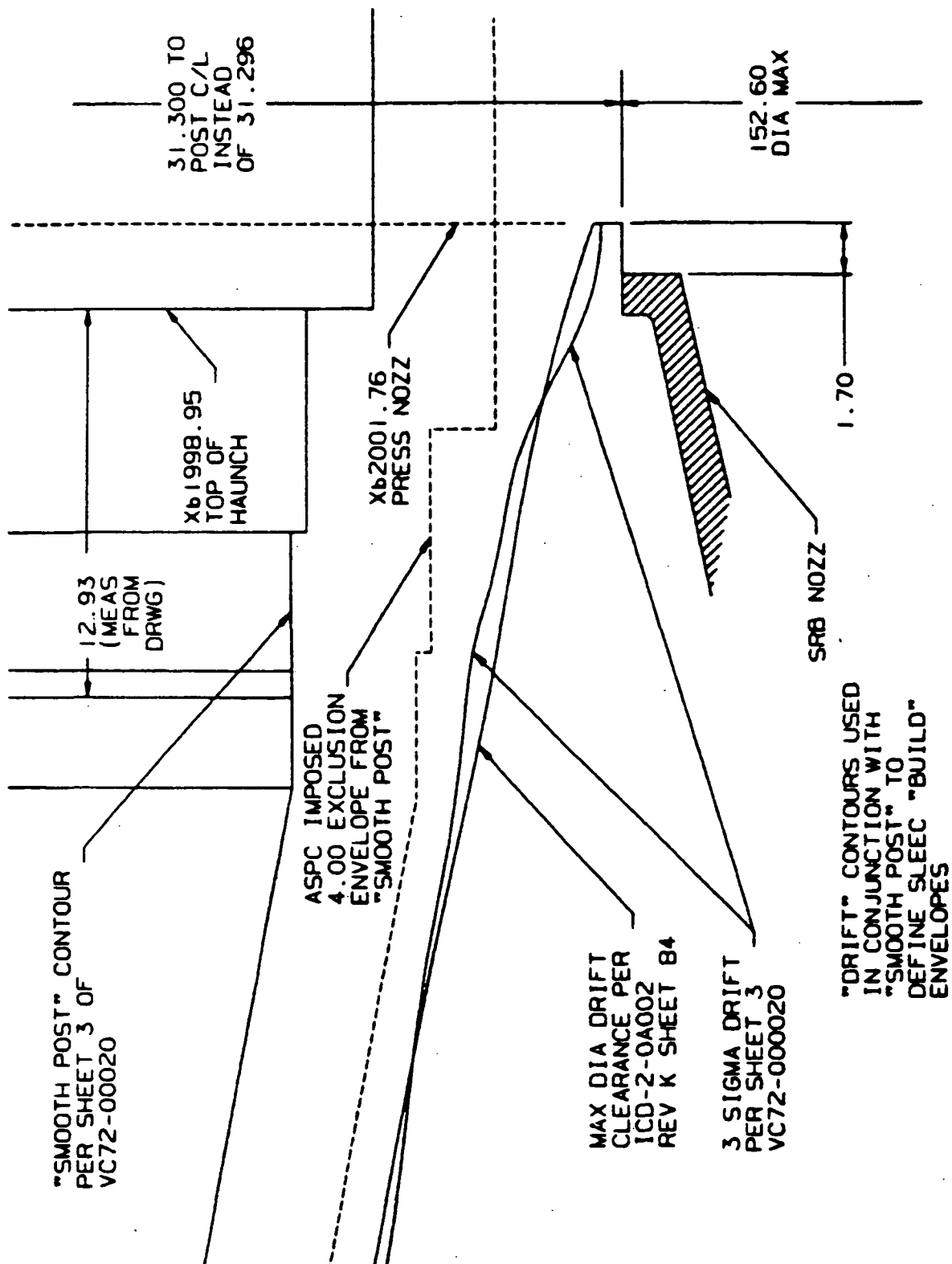


Figure 4.1-32 "Drift" Contours Used in Conjunction with "Smooth Post" to Define SLEEC "Build" Envelopes

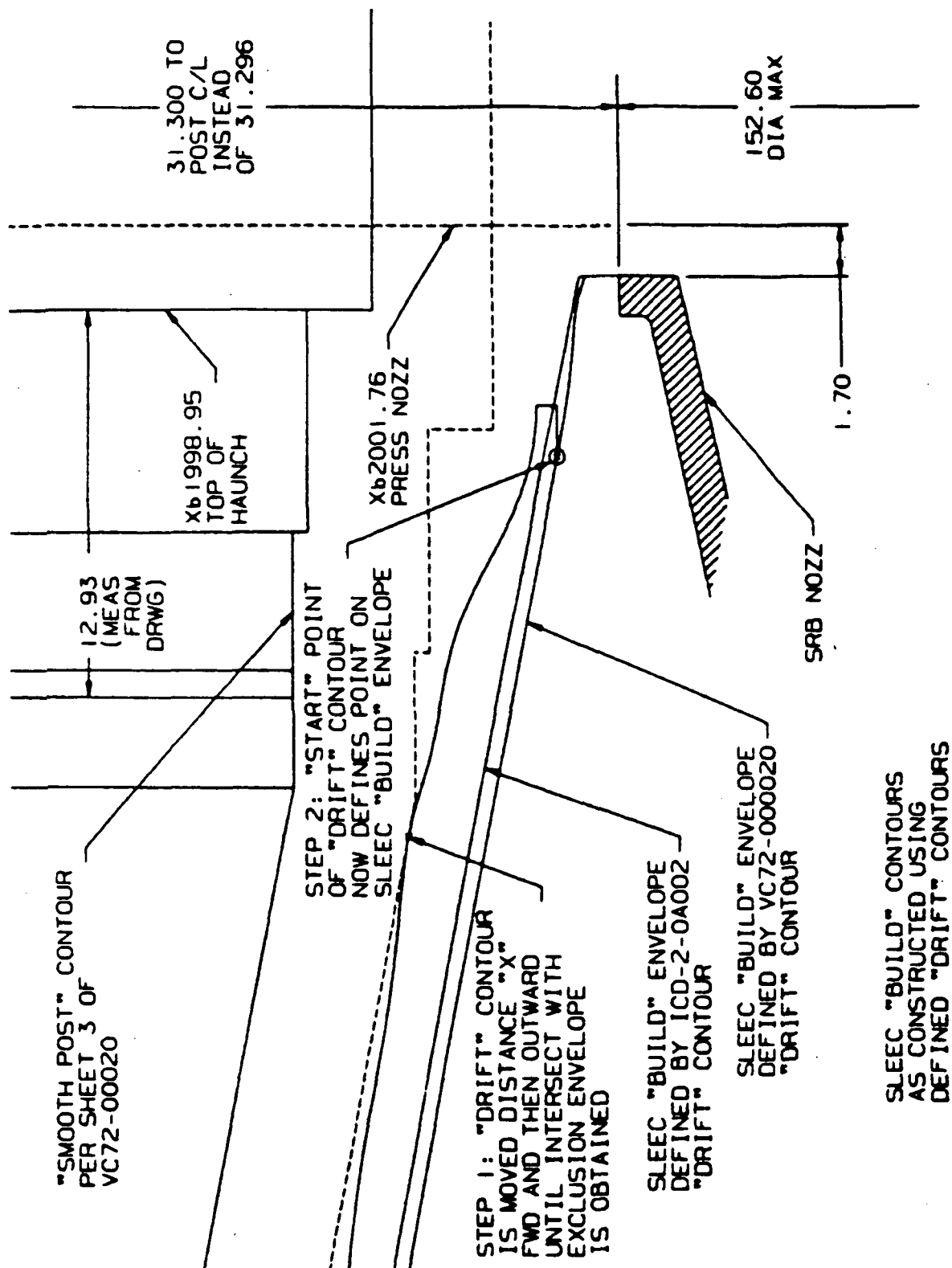
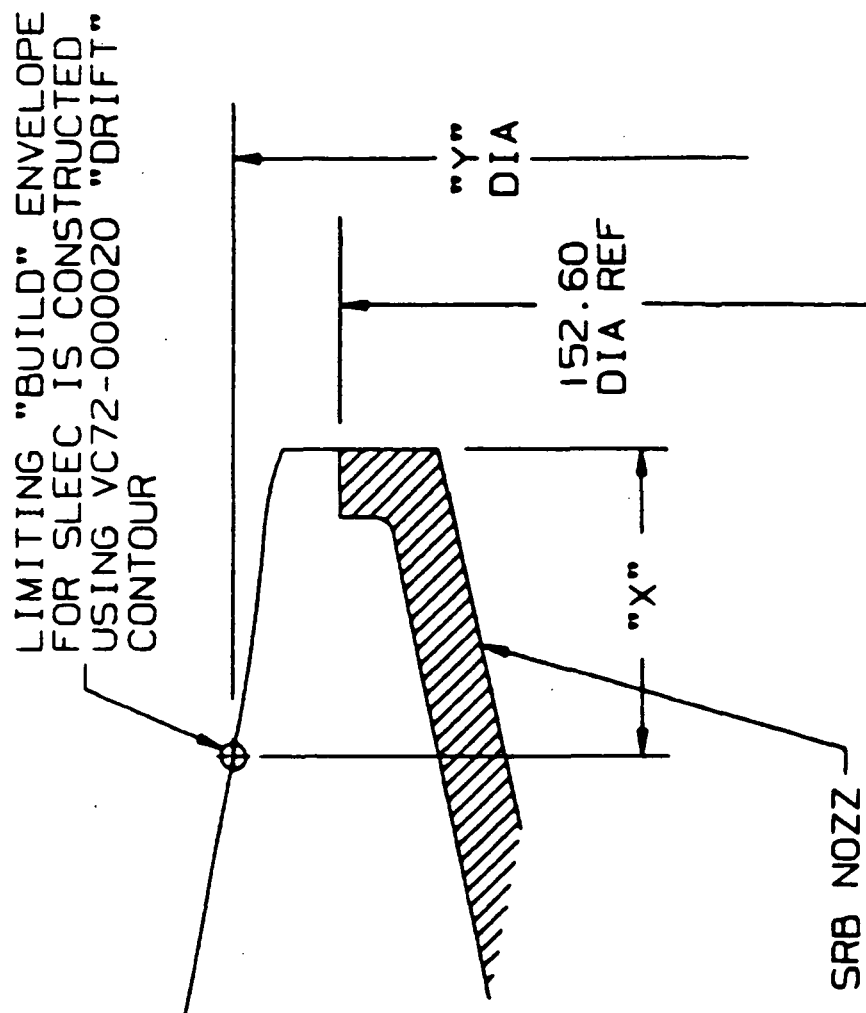


Figure 4.1-33 SLEEC "Build" Contours as Constructed Using Defined "Drift" Contours



"X"	"Y" DIA
0.000	154.790
0.500	155.134
1.000	155.372
1.500	155.507
2.000	155.590
2.500	155.676
3.000	155.777
4.000	156.026
5.000	156.346
6.000	156.710
7.000	157.090
8.000	157.464
9.000	157.827
10.000	158.190
15.000	160.059

Figure 4.1-34 Limiting "Build" Envelope for SLEEC Constructed Using VC72-000020 "Drift" Contour

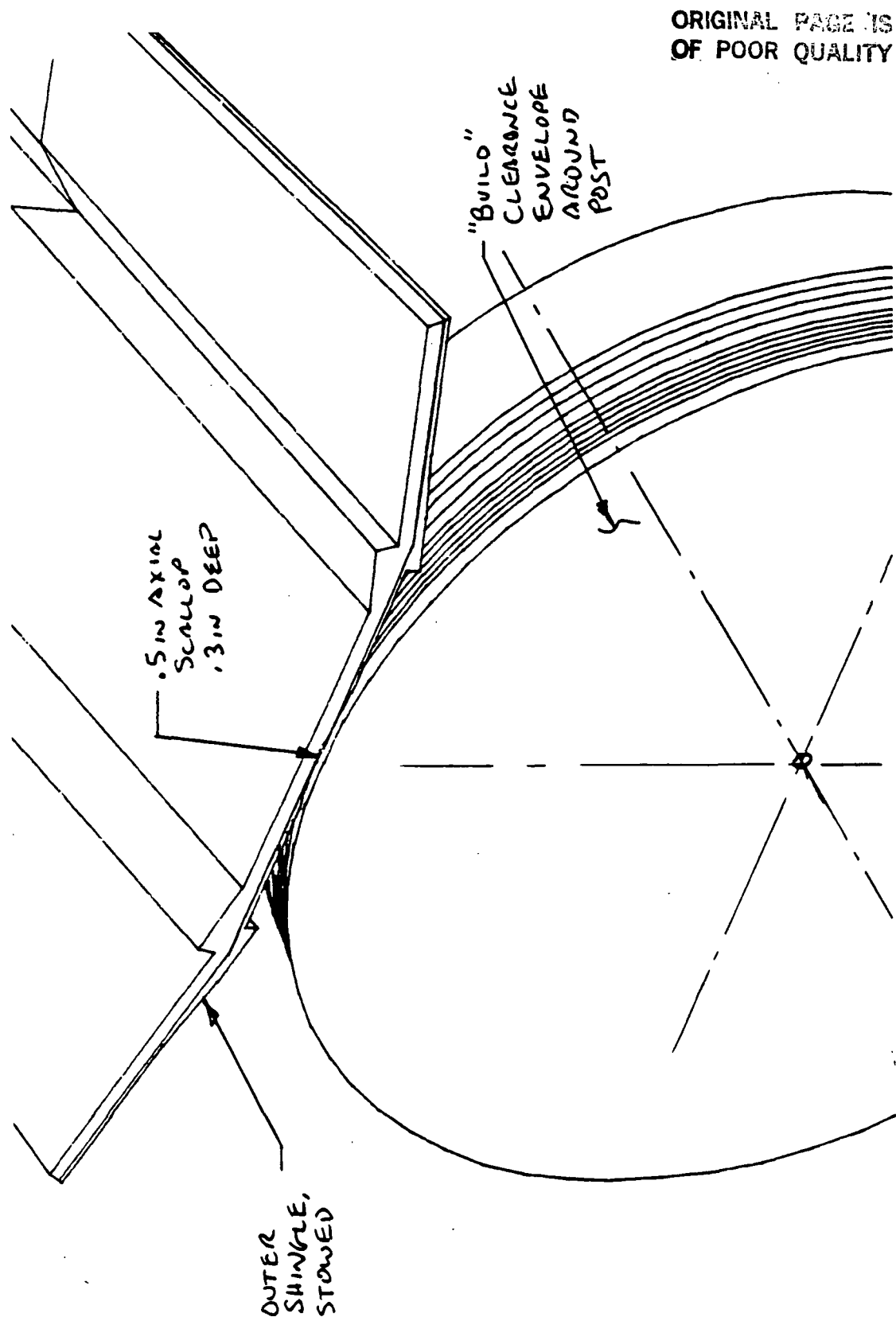


Figure 4.1-35 Intersection of Post Clearance "Build" Envelope and Outer Shingle

CALCULATED SRB/SLEEC ADD-ON WEIGHTS		<u>LBM</u>
FIXED CONE BUILD UP, LOW DENSITY CARBON PHENOLIC		585
OUTER SHINGLES, 6 EA		
STRUCTURAL SHELL, GRAPHITE PHENOLIC	82	
FWD LINER, STD DENSITY CARBON PHENOLIC	72	
AFT LINER, LOW DENSITY CARBON PHENOLIC	<u>65</u>	
	219 X 6 =	1314
INNER SHINGLES, 6 EA		
STRUCTURAL SHELL, GRAPHITE PHENOLIC	84	
FWD LINER, STD DENSITY CARBON PHENOLIC	45	
AFT LINER, LOW DENSITY CARBON PHENOLIC	<u>37</u>	
	166 X 6 =	996
ACTUATION SYSTEM (INCLUDING BRACKETS/SUPPORTS)		
STATIONARY	68	
MOVING	<u>1050</u>	
	SUB-TOTAL	1118
SLEEC HEAT SHIELDS, FIBERFORM [®] OR EQUIV.		
6 EA INNER AT 10 LBM EA	60	
6 EA OUTER AT 20 LBM EA	<u>120</u>	
	SUB-TOTAL	180
SLEEC SYSTEM ADD-ON WEIGHT/ UNIT		<u>4193</u>

Figure 4.1-36 Calculated SRB/SLEEC Add-On Weights

CALCULATED SRB/SLEEC ADD-ON INERTIA		
A. MOMENTS OF INERTIA ABOUT NOZZLE PIVOT POINT, $\text{LBM} \cdot \text{IN}^2 \times 10^{-6}$		
	<u>PITCH OR YAW AXIS</u>	<u>ROLL AXIS</u>
SLEEC STOWED	5.655	2.089
SLEEC EXTENDED	11.404	2.734
B. CENTER OF GRAVITY OF 4193 LBM SYSTEM, INCHES AFT OF PIVOT		
SLEEC STOWED	105.1	
SLEEC EXTENDED	154.9	

Figure 4.1-37 Calculated SRB/SLEEC Add-On Inertia

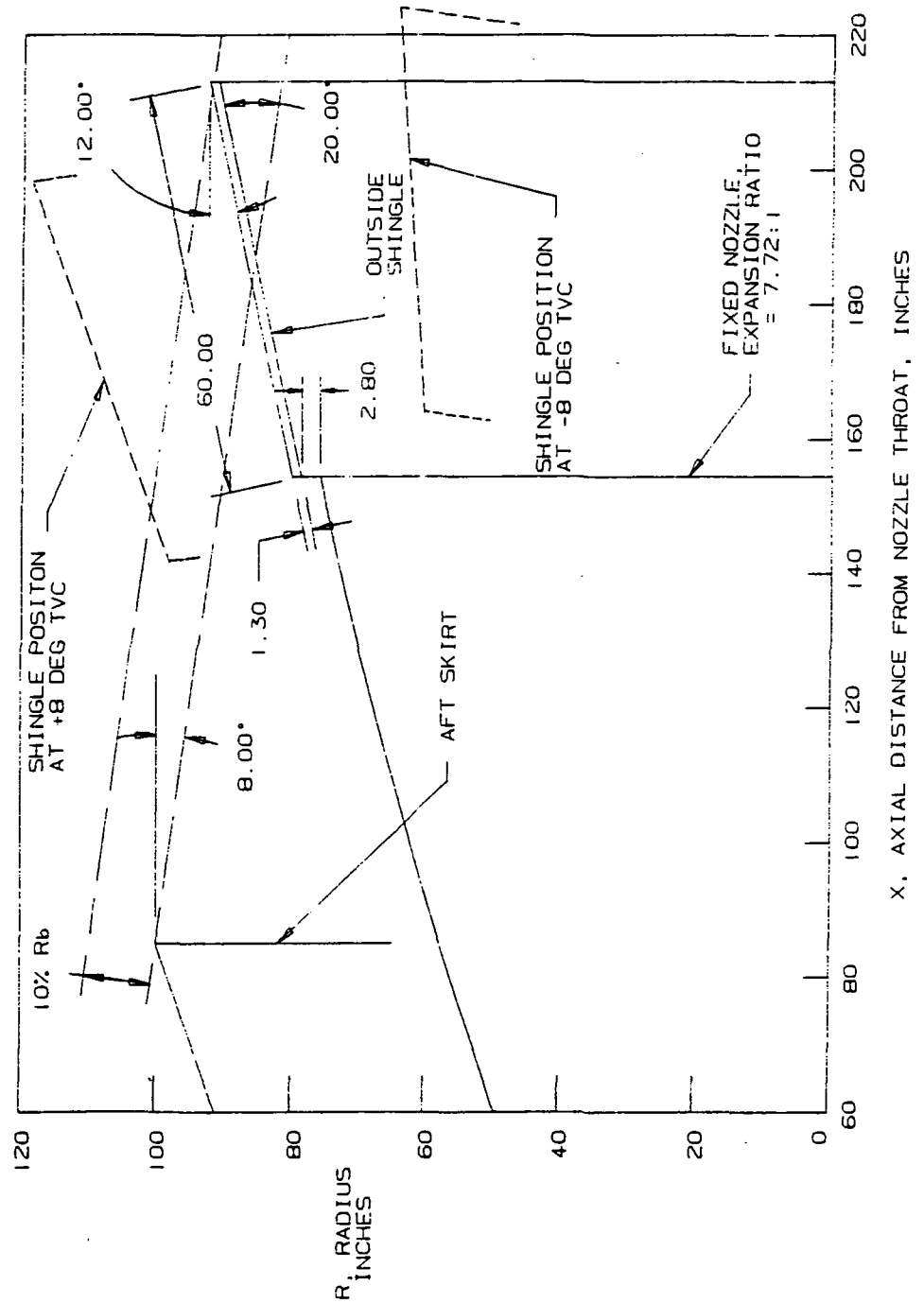


Figure 4.1-38 Model Used for External Aerodynamic Force Studies

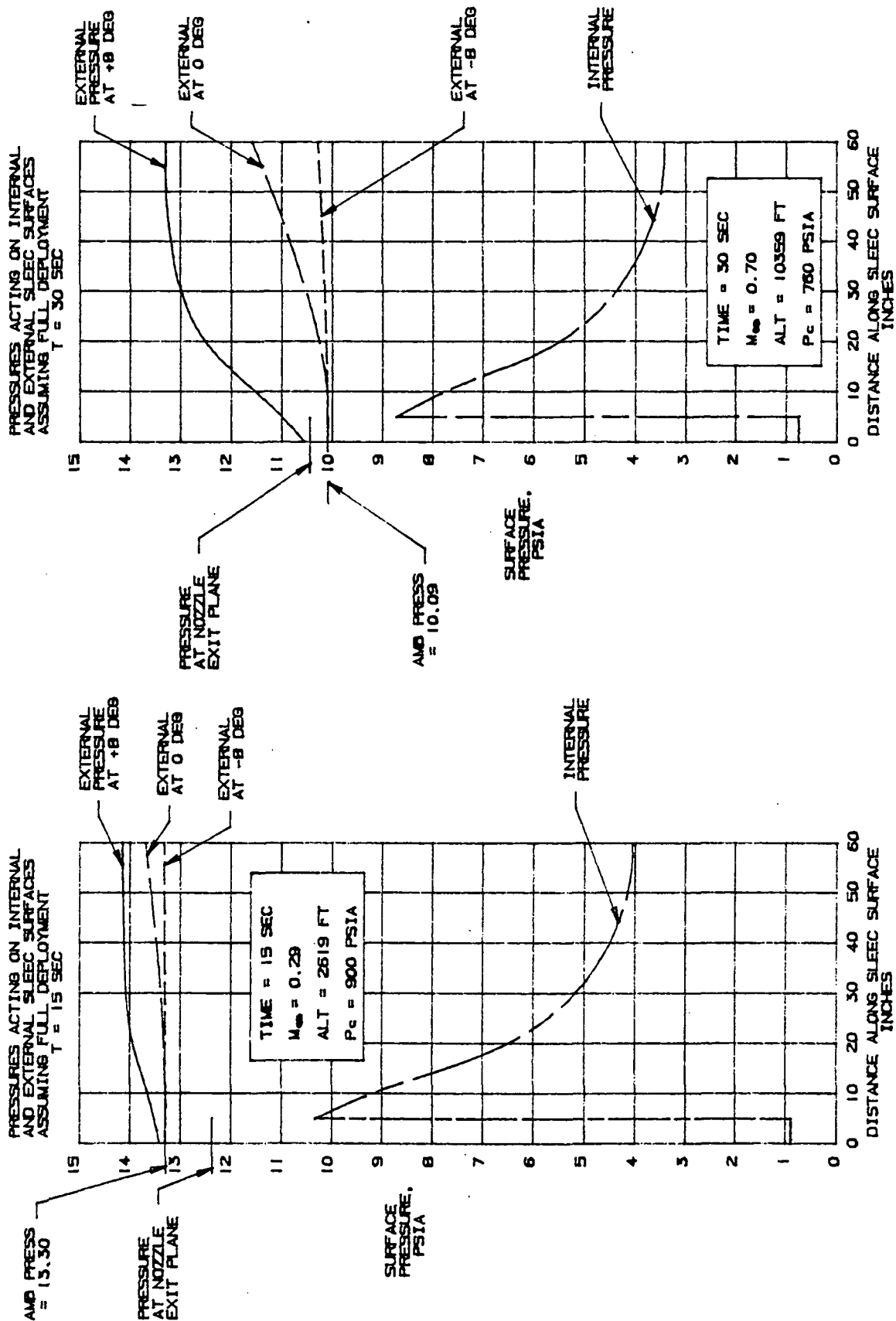


Figure 4.1-39 Axial Pressure Distributions Along SLEEC External Surface at 15 and 30 Seconds

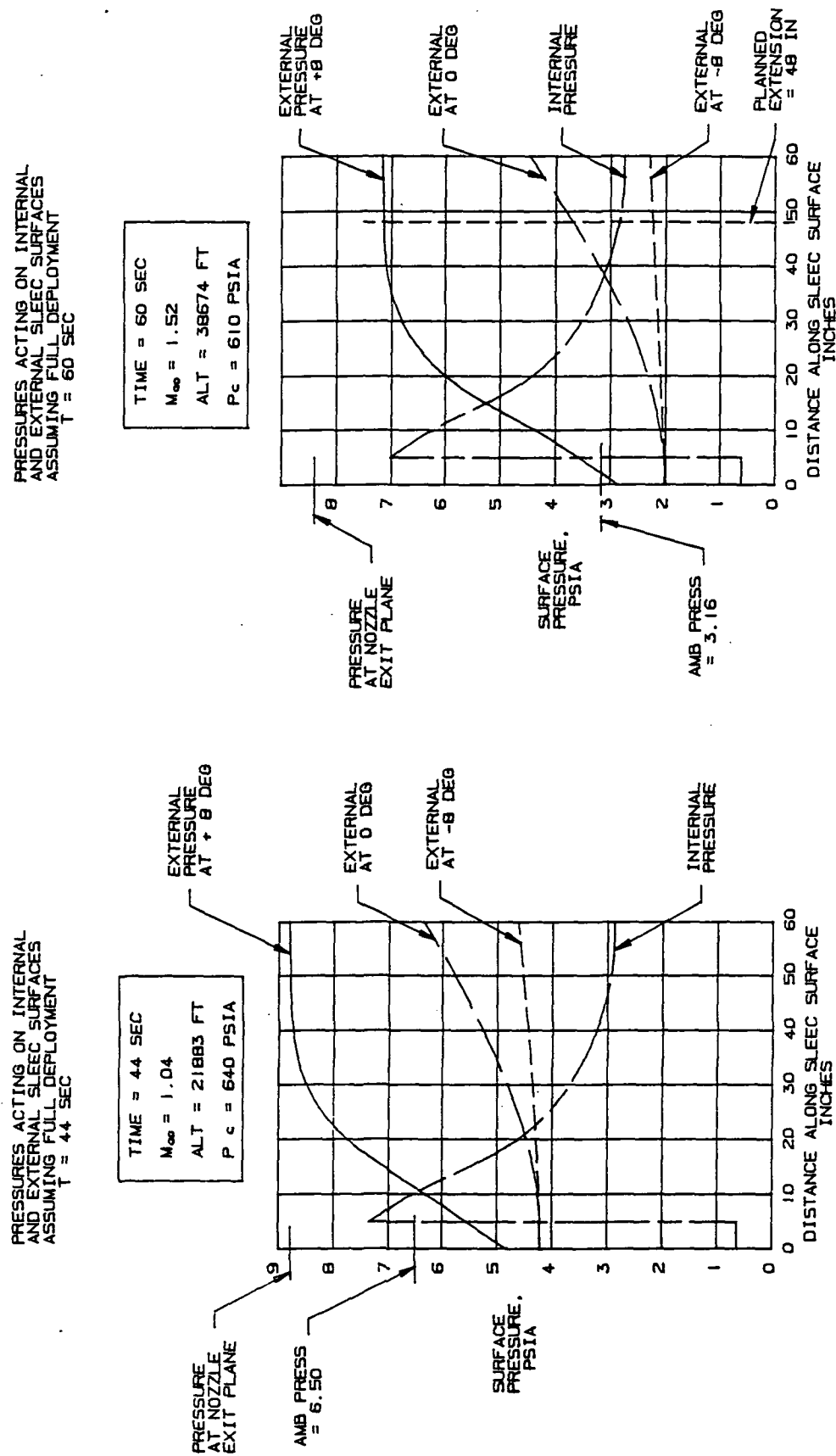
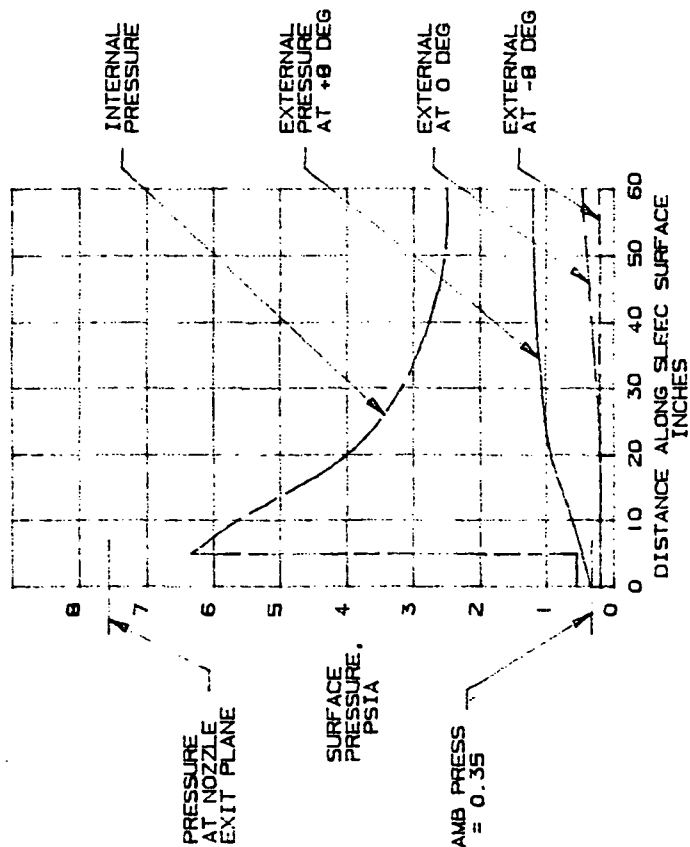


Figure 4.1-40 Axial Pressure Distributions Along SLEEC External Surface at 44 and 60 Seconds

ORIGINAL PAGE IS
OF POOR QUALITY

PRESSURES ACTING ON INTERNAL
AND EXTERNAL SLEEC SURFACES
WHILE FULLY EXTENDED AT
T = 90 SEC

TIME = 90 SEC
 $M_{\infty} = 3.00$
ALT = 84392 FT
 $P_c = 550$ PSIA



PRESSURES ACTING ON INTERNAL
AND EXTERNAL SLEEC SURFACES
WHILE FULLY EXTENDED AT
T = 74 SEC

TIME = 74 SEC
 $M_{\infty} = 2.17$
ALT = 57288 FT
 $P_c = 640$ PSIA

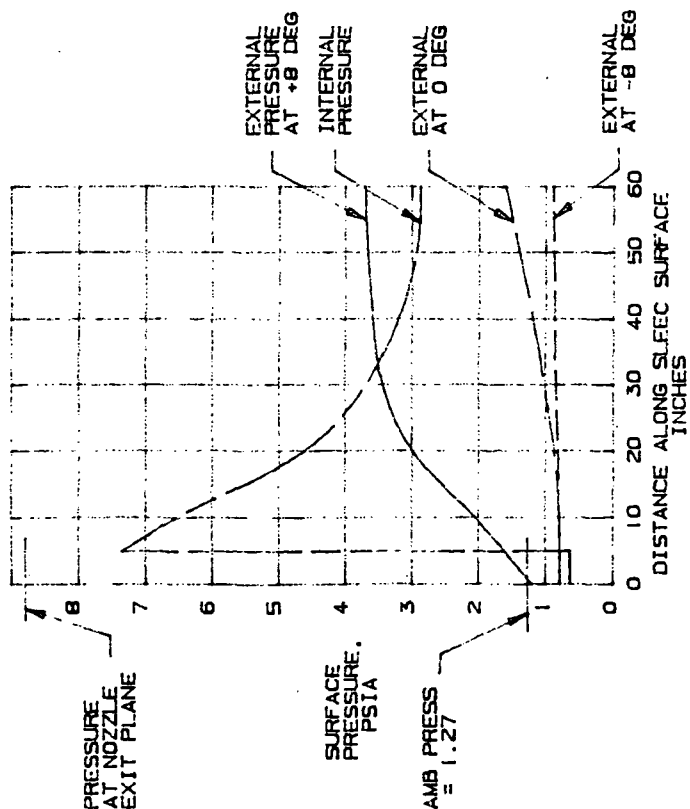


Figure 4.1-41 Axial Pressure Distributions Along SLEEC
External Surface at 74 and 90 Seconds

4.2 SUPPORTING ANALYSES

Supporting analyses were conducted to determine SRB/SLEEC performance/payload benefits, fabrication feasibility and costs, and predicted reliability.

4.2.1 Trajectory/Payload

To derive the potential payload benefit for SLEEC added to the STS SRB, three things must be known; 1), the average delta increase in DELIVERED Isp over that obtained for the SRB alone; 2), the delta (or add-on) weight of SLEEC added to the SRB and 3), the SLEEC inert weight loss during SRB burn. Once these are known, the appropriate Isp and weight performance partials supplied by NASA/MSFC can be used to determine the potential payload increase.

Working closely with the MSFC Trajectory Analysis group, Aerojet performed trajectory/payload analyses in which the Shuttle SRB configuration was "flown" with and without the selected SLEEC design to obtain the delta change in delivered Isp. Reference trajectories for the Western Test Range were used as supplied by NASA/JSC.

First, as described in Section 4.1.2.2, thermal and structural analyses were performed to determine the adequacy of the SRB/ SLEEC design of Figure 4.1-7 and to verify the resulting add-on weights. Figure 4.1-36 showed the add-on weights predicted by Aerojet for the SRB/SLEEC design of Figure 4.1-7. "Add-on" weight refers to the difference in weight between the SRB nozzle with SLEEC installed and the original weight of the nozzle. The total add-on weight for each SLEEC assembly is estimated to be 4193 lbm. The inert weight loss of material ablated during the burn can also be estimated from thermal analyses and is predicted to be approximately 300 lbm for each assembly.

Second, the propellant exhaust properties, plus the geometry of the SRB HPN/SLEEC combination, were used with the Solid Performance Program (SPP) computer code to predict the vacuum delivered specific impulse for the system for different SLEEC extensions as a function of chamber pressure. This was done both for the conditions at start of flight (0 sec) at end of flight (122 sec) using the methodology described below.

Since even the inner shingles slide along the outside of the nozzle exit cone, there is a definite step outward from the inside of cone to the inside surface of the shingle. Thus the expansion ratio achieved by SLEEC is always obtained in a shorter length than that of an optimally contoured nozzle with no step. Theoretically, therefore, SLEEC will always have slightly less performance than an ideal EEC. Also, because of the step, there is an associated "dead-band" through which SLEEC initially deploys without influencing performance.

The procedure for calculating the increase in Isp as a function of extension length is described in detail in Reference 3 and summarized in Figure 4.2-1. Using the SPP, vacuum delivered Isp is first calculated as a function of length for an ideal EEC formed by attaching a conical extension to the fixed nozzle which has the same half angle and expansion ratio as the extended SLEEC. Due to the presence of the "step"

between the inside of the fixed cone and the inside of SLEEC at the exit plane of the fixed nozzle, this ideal EEC or "fictitious nozzle" is always longer than the fully deployed SLEEC configuration and thus a "dead band" is created, defining the extension length required before SLEEC contacts the fixed nozzle exhaust plume. The length of this "dead band", x_0 in Figure 4.2-1, is a function of the step size and the SLEEC half angle, and thrust is assumed to remain unchanged until SLEEC is deployed beyond this length. Since a fully extended SLEEC with a zero step size would deliver about the same performance as the fictitious nozzle, the end points of the SLEEC Isp vs length curve are thus known. Previous experimental data obtained with other EEC configurations, as well as the data obtained from the Super Bates SLEEC static test at AFRPL, indicate an approximate linear relationship between these end points, thus defining the shape of the lower curve of Isp vs length attributed to SLEEC as shown in Figure 4.2-1. In summary, SLEEC incurs two losses which must be accounted for in predicting its performance: (1) a loss due to the step and (2) a loss due to length/expansion ratio mismatch.

The methodology described above was used to derive the vacuum delivered Isp curves versus SLEEC extension of Figures 4.2-2 and 4.2-3.

Next, a method of characteristics solution was used to define the internal pressure inside the extended SRB/SLEEC as a function of extension distance. The pressure is presented for convenience as a ratio of local wall pressure to chamber pressure in Figure 4.2-4. The "dead band" from 0 to 5 inches is obvious in this curve. A dashed line indicates a theoretical blend to the pressure ratio which exists at the end of the fixed nozzle. In this analysis, a changing value of gamma is used for the exhaust gas which matches the local gamma predicted by the SPP program. The value of gamma changes because of two-phase flow losses.

The typical Western Test Range (WTR) trajectory information used in the performance analysis was obtained from NASA/JSC and is presented in the four pages of Figure 4.2-5. Ambient pressure for a given time (and altitude) is the significant parameter listed in Figure 4.2-5. If SLEEC were to be deployed prematurely, the exit plane pressure would be less than the local ambient pressure at altitude and the thrust obtained would be less than optimum. Ideally, the exit plane pressure of SLEEC should just match the ambient pressure at any altitude (and corresponding flight time).

The nominal chamber pressure for the STS HPM is shown in Figure 4.2-6. The ambient pressure for a given flight time can be obtained from the trajectory information of Figure 4.2-5 to obtain the optimum exit plane pressure. When divided by the chamber pressure for that time from Figure 4.2-6, the desired value of the optimum P_{wall}/P_c (or P_{exit}/P_c) is obtained, and the optimum extension distance for SLEEC at that time may be read from Figure 4.2-4. When this was done, it was determined that the optimum time to start deploying SLEEC was 44 sec into the flight and that deployment should occur over an approximate 20 sec period. The extension versus time curve for SRB/SLEEC derived in this manner is presented in Figure 4.2-7. If SLEEC were deployed earlier than shown, less performance would be obtained.

The maximum vacuum delivered Isp that could be obtained with and without SLEEC is presented in Figure 4.2-8. A particular vacuum delivered Isp value for a given time is derived as follows:

1. For a selected flight time, T_f , the amount of SLEEC extension is determined from Figure 4.2-7.
2. Using the extension distance obtained and the chamber pressure for time T_f , the amount of vacuum delivered Isp is determined for both $T=0$ and $T=122$ from Figures 4.2-2 and 4.2-3, respectively.
3. Assuming a linear throat regression rate, the difference between the two Isp values is multiplied by the ratio $T_f/122$ and subtracted from the value of Isp at $t=0$ to give the value of Isp at time T_f .

The values of vacuum delivered Isp versus time can be plotted as shown in Figure 4.2-8. The curve for the HPM without SLEEC is obtained by the above process, considering no SLEEC extension. If the area between the two curves is determined and divided by the total burn time of 122 sec, a value of 4.303 sec average delta Isp increase is obtained with SLEEC, however; this is the difference in theoretical vacuum delivered Isp, not the difference realized when the actual motor delivered values of Isp obtained during STS ascent are considered. Since all internal nozzle/SLEEC losses were accounted for in the SPP program to arrive at the vacuum delivered Isp values of Figures 4.2-2 and 4.2-3, the only additional Isp loss to be considered during ascent is the loss due to ambient pressure rather than vacuum existing at the nozzle exit plane. Therefore, actual delivered values are obtained considering the ratio of delivered to vacuum thrust coefficients (C_f) as follows:

1. For a given gamma, it can be shown that

$$\begin{aligned} \text{Delivered Thrust Coefficient, } C_{f \text{ del}} \\ = C_{f \text{ vac}} - ER \times (P_{\text{amb}} / P_c) \end{aligned}$$

where ER is the expansion ratio of the nozzle/SLEEC configuration at time T_f , P_{amb} is the ambient pressure at altitude at time T_f , and P_c is the chamber pressure at time T_f .

2. Therefore, at any time T_f , the ratio $C_{f \text{ del}} / C_{f \text{ vac}}$ can be determined. Then, at any time T_f ,

$$\begin{aligned} \text{Delivered Specific Impulse, } I_{sp \text{ del}} \\ = (C_{f \text{ del}} / C_{f \text{ vac}}) \times I_{sp \text{ vac}} \end{aligned}$$

The only problem with this procedure is deciding which gamma to use since the SPP program considers a varying gamma depending on local conditions. Therefore, it was decided to determine delivered Isp for 3 different values of gamma which would cover the range of interest; 1.2, 1.4 and 1.6. Figure 4.2-9 shows the approximate expansion ratio of the SRB/SLEEC configuration versus

SLEEC extension. Figure 4.2-10 presents the theoretical values of C_f vac versus expansion ratio for the 3 values of gamma considered.

For a given flight time, the amount of SLEEC extension was used to determine the resulting expansion ratio and then the value of delivered Isp was calculated vs time using the vacuum delivered values shown in Figure 4.2-8. The resulting curves of delivered Isp for the 3 different gamma values are shown in Figure 4.2-11. Again, the curves are given for the ascending SRB with and without SLEEC.

The integral of the area between the curves now produces an average delivered delta Isp due to SLEEC. The values range from 3.844 sec (gamma = 1.6) to 3.881 sec (gamma = 1.2) which are lower than the 4.303 sec vacuum delivered average delta of Figure 4.2-8. Additionally, the difference in the calculated values is quite small over the range of the gammas considered.

The potential STS payload benefit predicted with the addition of SLEEC is determined using the SLEEC add-on weight, the predicted inert weight loss during burn, and the predicted average delivered specific impulse increase as shown in Figure 4.2-11. This is accomplished using a performance equation and flight partials supplied by NASA/MSFC.

The delta payload benefit of the SRB/SLEEC to the STS can be calculated as

Delta Payload Increase

= Average Delta Isp Increase x 830 lbm/sec -

(Add-on weight - (weight loss/2)) x 2/ 11 lbm/lbm

For a gamma of 1.2, the payload increase

= 3.881 x 830 - (4193-300/2) x 2/ 11

= 3221 - 735

= 2486 lbm

For a gamma of 1.6, the lowest considered, the payload increase is 2456 lbm.

In 1981, as discussed in Section 1.1, Aerojet utilized its AIDE II computer program to "fly" SLEEC on the STS. AIDE II is a computer code which uses scaling functions and general approximations of parameters to simulate the flight of a given missile/vehicle configuration. For essentially the same conditions, AIDE II predicted a payload increase to the STS of about 3750 lbm. NASA/MSFC studied the results independently and verified a 3000 to 3250 lbm gain. The significant parameters resulting from the 1981 Aerojet study are compared with the results of the current study program in Figure 4.2-12. Due to some concerns about the accuracy of the AIDE II results, the payload gains for the current program were calculated by hand. The current effort indicates a nominal payload increase of 2471 lbm. This is considered a

lower limit and the real payload increase capability probably lies between these values and requires that a definitive effort be mounted with NASA/MSFC to reach an equitable and agreeable value of payload capability.

Some features of the current configuration of Figure 4.1-7 versus the 1981 preliminary layout of Figure 1.0-6 which tend to reduce performance are:

The WTR trajectory may be more demanding than the ETR trajectory.

The current SLEEC extension, half angle and expansion ratio have been reduced in order to fit the new "build" envelope.

The current SLEEC weighs 200 lbm more for heat shields.

Current external aerodynamic studies prevent early deployment of SLEEC.

AIDE simulations usually constitute approximations of scaling functions and do not necessarily take into account the changing value of parameters with time (i.e., may use average values instead of time or function-dependent values to evaluate some parameters).

The AIDE simulations tend to gain altitude faster and result in a quicker deployment of SLEEC, hence more delta Isp.

It was mentioned previously that the current study program has probably raised more issues than it has settled. The exact amount of payload gain attributed to SLEEC remains one of those issues.

4.2.2 Fabrication Feasibility and Cost

Once the preliminary SLEEC design was selected, analyses were conducted to assure that the selected design could be successfully fabricated. The analysis covered materials as well as fabrication methods.

The fabrication analyses were used to generate preliminary ROM estimated costs for the manufacture of SLEEC components and systems for development, demonstration and production quantities. The preliminary costs in 1986 dollars are presented in Figure 4.2-13. The estimates assume that NASA will supply nozzle exit cones for use in the SLEEC assemblies and that QA/QC levels experienced by Aerojet for Stage II Peacekeeper will be acceptable.

Actuation System Fabrication

Most of the SLEEC actuation system (shown in Figure 4.2-14) designed by Garrett Pneumatic Systems Division of Garrett Corporation, Tempe, Arizona, is comprised of hardware similar to that currently in use for thrust

reversers and flaps on large passenger aircraft. Little of this hardware is "off-the-shelf" however when applied to unique applications. Garrett's experience runs the gamut from the aircraft systems, to the actuation systems for Peacekeeper Stage I and Stage II TVC and the Stage II ENEC, to turbo systems for automobiles. A complete description of the mechanical design of the actuation system is given in Appendix A. The ROM preliminary fabrication costs for the actuation system presented in Figure 4.2-13 were supplied by Garrett.

Aft HPN Exit Cone Modification

Figure 4.2-15 is an isometric view of the HPN aft exit cone assembly. The fabrication studies assume that NASA would supply these assemblies for SLEEC incorporation. The exit cone can be modified either before or after installation of forward adapter, compliance ring and LSC (Linear Shaped Charge) and modified LSC covers; however, the modification task is greatly simplified if the LSC is installed later, thus facilitating autoclave cure of laid-up composites.

Exit cone modification consists of two parts; 1), addition of the mounting ring for the SLEEC actuation system gearheads, drive motors and flexshafts just aft of the LSC cover, and 2), the tape-wrap and machining of the low density carbon phenolic build-up, in and on which the shingles are stowed and from which they deploy.

If the bare exit cone liner and structural shell are available prior to attach flange and LSC installation, a one-piece aluminum actuator mounting ring can be bonded and pinned to the exit cone shell. If a completed exit cone assembly is provided, a two-piece ring can be first, bolted around the shell and then, bonded and pinned.

Next, the outer structural shell of the HPN aft cone assembly is cleaned and lightly abraded, a light coat of phenolic resin applied, and low density carbon phenolic (LDC) tape wrapped around the shell at a 0° ply pattern, starting just aft of the actuator mounting ring. After wrap, the entire assembly is vacuum bagged, placed in an autoclave and de-bulked, and the LDC overwrap cured. If the LSC has been previously installed, either a suitable, lower cure temperature would have to be agreed on, or a process worked out where local heating blankets could be used for cure.

After cure, the exit cone LSC assembly, attach flange and compliance ring are installed (if the exit cone was not initially a completed assembly). Finally, the entire assembly is mounted aft end down on a holding fixture and placed on the bed of a multi-axis milling machine. The gearhead pads on the mounting ring and the slots and O-ring grooves for the inner shingles only are machined in the LDC relative to centers established from the attach flange and the exit plane diameter. The slots for the outer shingles are not machined at this time.

An isometric view of the modified exit cone assembly is shown in Figure 4.2-16 after machining for both inner and outer shingle interfaces has been accomplished.

Shingle Fabrication

The details of the inner and outer shingles were given in Figures 4.1-10 and 4.1-11, respectively. Since both shingles have constant thickness cross-sections from end-to-end, the fabrication process for either shingle is basically the same, and inner shingle fabrication is used as an example.

First, a tool is prepared that duplicates the desired inside surface of the shingle as much as possible to minimize subsequent machining. Next, because every ply of material in the shingle is laid up at 12° to any shingle surface, a 12° wedge is placed in one end of the tool as shown in Figure 4.2-17. Then, standard density carbon phenolic (CP) bias tape is laid back and forth across the wedge to the appropriate length, vacuum bagged, autoclave de-bulked, and "B" staged but not final cured. To the layman, this means firm, but not hard. This basic shingle lay-up process can be easily automated. The "B" staged CP is shown still in the tool in Figure 4.2-18.

The LDC aft liner of the shingle is then laid up using the same process except the peel ply area of the LDC is used as the 12° tool and a light coat of phenolic resin applied at the interface. After lay-up, the LDC material is also vacuum bagged, autoclave de-bulked, and "B" staged. The "B" staged CP and LDC liners are shown still in the tool in Figure 4.2-19.

Finally, the high modulus graphite phenolic structural shell is laid up on top of the liners. The backside of the liners is rough machined to produce fingers of carbon fibers, a light coat of phenolic resin applied, and the GP laid up as shown in Figure 4.2-20. The lay-up can be either of "shingle lap" or "involute ply" construction. The entire assembly is then vacuum bagged, autoclave de-bulked and final co-cured.

After cure, each shingle is removed from the tool and the edges, flame liner surfaces and O-ring grooves on those surfaces final machined. The fore and aft surfaces of the shingle are left over length and not yet machined. It is estimated that several prototype shingles will have to be fabricated with tool angles being changed before the desired shingle shape is obtained in a stress-free condition after cure.

Final Assembly

With the aft HPN exit cone assembly machined as described above, and still mounted aft end down on the holding fixture of the multi-axis milling machine, final assembly is begun. First, with O-ring stock bonded in the grooves of the mating surfaces, the inner shingles are positioned in the slots of the LDC build up around the exit cone and held in place with tensioned banding straps or cables laid over the extra length stock on the ends. In this condition, the outer surfaces of the inner shingles and the LDC build up can be match machined to provide perfectly level "flats" over which the outer shingles slide and perfectly aligned slots or tracks from which they deploy. At this point, all remaining O-ring grooves are machined, and O-ring stock installed.

Next, the outer shingles are positioned around the assembly and held in place with banding straps or cables. In this condition, the machining of all remaining surfaces (except over-length stock) as well as

actuation system mounting pads and holes takes place, still relative to established system centers, and threaded inserts are bonded into the shingles to mount the actuators. The cable bearing strips are then bonded to the edges of the outer shingles and the banding straps moved into place around the shingles in positions which will not interfere with mounting the actuators. The overstock on fore and aft ends of all shingles is then removed using single machining cuts to establish end planes of the shingle system.

The "T" bars are then mounted to the outer shingles, the clips and guides installed on the forward ends of the shingles, and the six actuator assemblies bolted to the actuator mounting ring and the mounting pads on the backs of the inner shingles. Next, all of the cables are loosely attached to the turnbuckles running through the "T" bars, and all slack is removed from the system. Finally, all of the cables are uniformly pre-tensioned to the desired value(s) using tensiometers, the jam nuts on the "T" bars tightened to retain outer shingle placement, and the temporary banding straps removed.

At this point, flexshaft cables and drive motor/brake assemblies are added and the assembly is ready for acceptance check-out or bench test deployment. Gas struts may be installed between actuator saddles and adjacent outer shingles to maintain cable tension during non-firing deployments if desired. If the system is to be used in flight, the final assembly step is the installation of the insulative shields which protect the SLEEC from aft end heating.

4.2.3 Reliability

The reliability of the selected design was established in cooperation with Garrett. Aerojet's SLEEC design is formulated with the goal of achieving a redundant, man-rated, fail-safe system. Reliabilities of approximately 0.9996 are currently being predicted for State-of-the-Art EEC systems without incorporating redundancy.

The reliability of the SRB/SLEEC is defined as the probability that the actuation system will properly deploy the system and that no leakage will occur through the cone or the O-Ring seals at the shingle interfaces during the mission cycle. The reliability is modeled as follows:

$$R_{\text{SLEEC}} = R_{\text{act}} \times R_{\text{cone}} \times R_{\text{seal}}$$

where:

R_{SLEEC} = Reliability of the SLEEC system
 R_{act} = Reliability of the actuation system
 R_{cone} = Reliability of the deployable shingles
 R_{seal} = Reliability of the seals at the shingle interfaces

Actuation Reliability

Garrett developed the design for the actuation system as detailed in Appendix A. In summary, the actuation system consists of six (6) actuation assemblies, four (4) short flexible drive shafts, four (4) long flexible cable drive shafts, and two (2) drive motor/brake assemblies. Each

actuation assembly is composed of a ballscrew/nut assembly, two (2) differential gearbox assemblies, two (2) cable pay-out drums and aircraft type stainless steel cables. A preliminary reliability analysis of the SLEEC actuation system was prepared by Garrett and is contained in Appendix A. The analysis is based on Garrett's experience for like components in similar applications and a run time of 30 seconds. The results of the analysis are summarized here:

Component	Failure Rate, $\times 10^{-6}$ Hours	Predicted Reliability
Electric Motor	4.28	0.99999996
Brake	30.26	0.99999975
Flex Drive	5.94	0.99999995
Gearbox Drive	4.50	0.99999996
Ballscrew	0.94	0.99999999
Cable Drum	25.21	0.99999979
Aircraft Cable	nil	-----
TOTAL	71.13	0.99999941

Cone Reliability

The extendible system consists of six (6) inner shingles and six (6) outer shingles deployed axially and radially from around a fixed cone. The shingles are fabricated from carbon phenolic materials identical to those used on the Peacekeeper Stg II Extendible Nozzle Exit Cone (ENEC). Based on an analysis of Peacekeeper erosion and char data, the reliability of the fixed and translating cones for that system was calculated as 0.99999999. This same reliability is estimated for the shingles on the SRB/SLEEC system.

Seal (and interface) Reliability

In order to minimize erosion and prevent leakage of exhaust gas, the SLEEC system utilizes O-Ring seal gasket material between the inner and outer shingles and at the shingle/fixed cone interfaces. Based on generic failure rate data contained in Reference 4, the failure rate for a single seal is 65.788×10^{-6} failures per hour. Assuming a nominal 60 sec exposure time during flight, the reliability of the 26 seals is calculated as:

$$R_{\text{seal}} = \text{EXP} [-(65.788 \times 10^{-6} \text{ F/HR})(26)(60 \text{ sec})(1 \text{ HR}/3600 \text{ sec})]$$

$$= 0.99997150$$

Predicted SLEEC Reliability

Substituting the above component reliabilities in the model, the reliability for SRB/SLEEC system is predicted as:

$$R_{\text{SLEEC}} = R_{\text{act}} \times R_{\text{cone}} \times R_{\text{seal}}$$

$$= (0.99999941)(0.99999999)(0.99997150)$$

$$= 0.99997089$$

This prediction is for a mature design of the operational configuration.

$$X_o = h \frac{\sin(70^\circ - \alpha_e) \cdot \cos \alpha_e}{\sin 20^\circ}$$

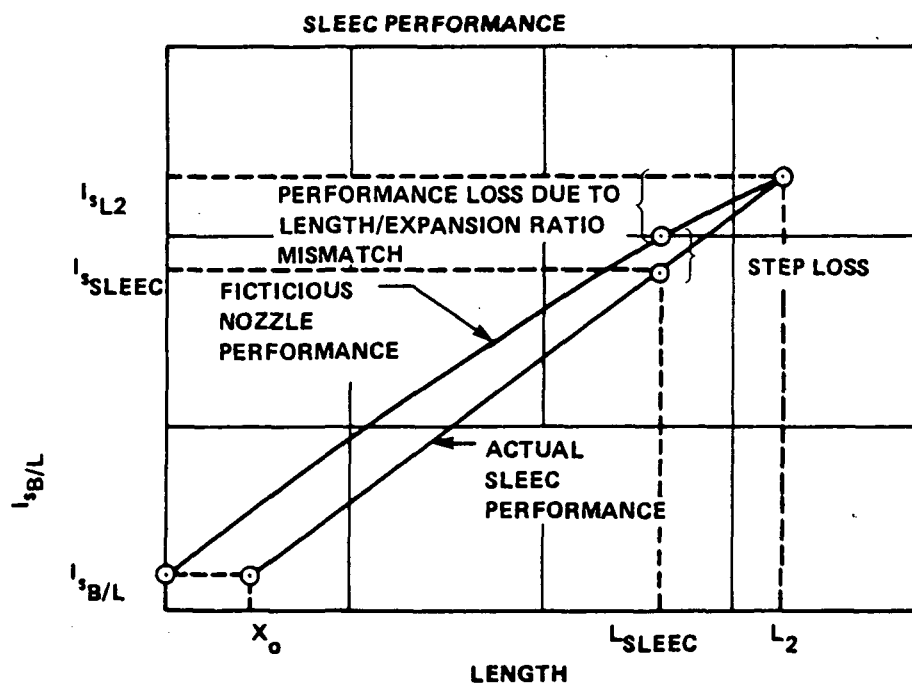
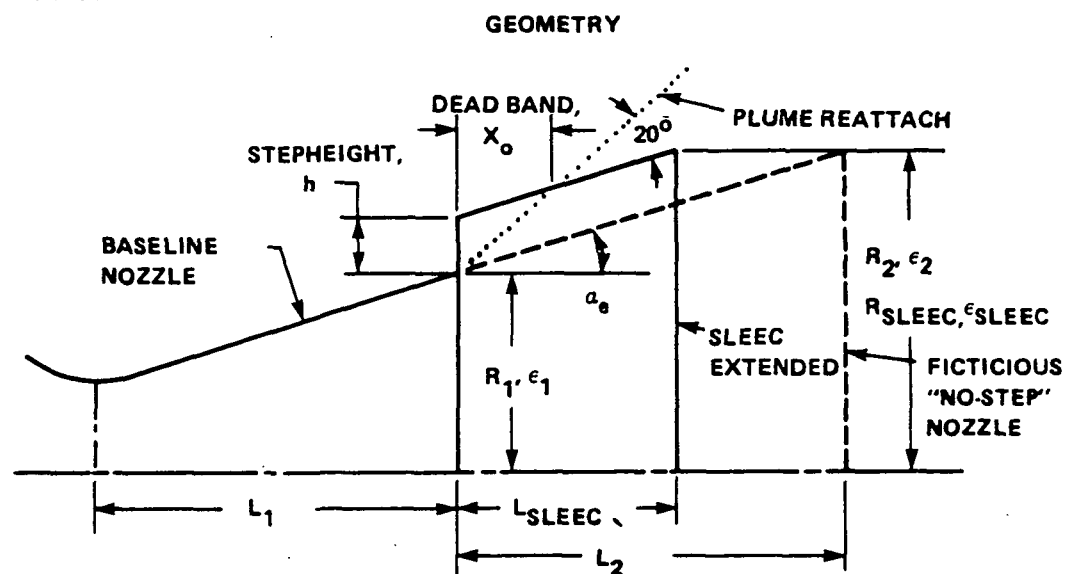


Figure 4.2-1 SLEEC Performance Model

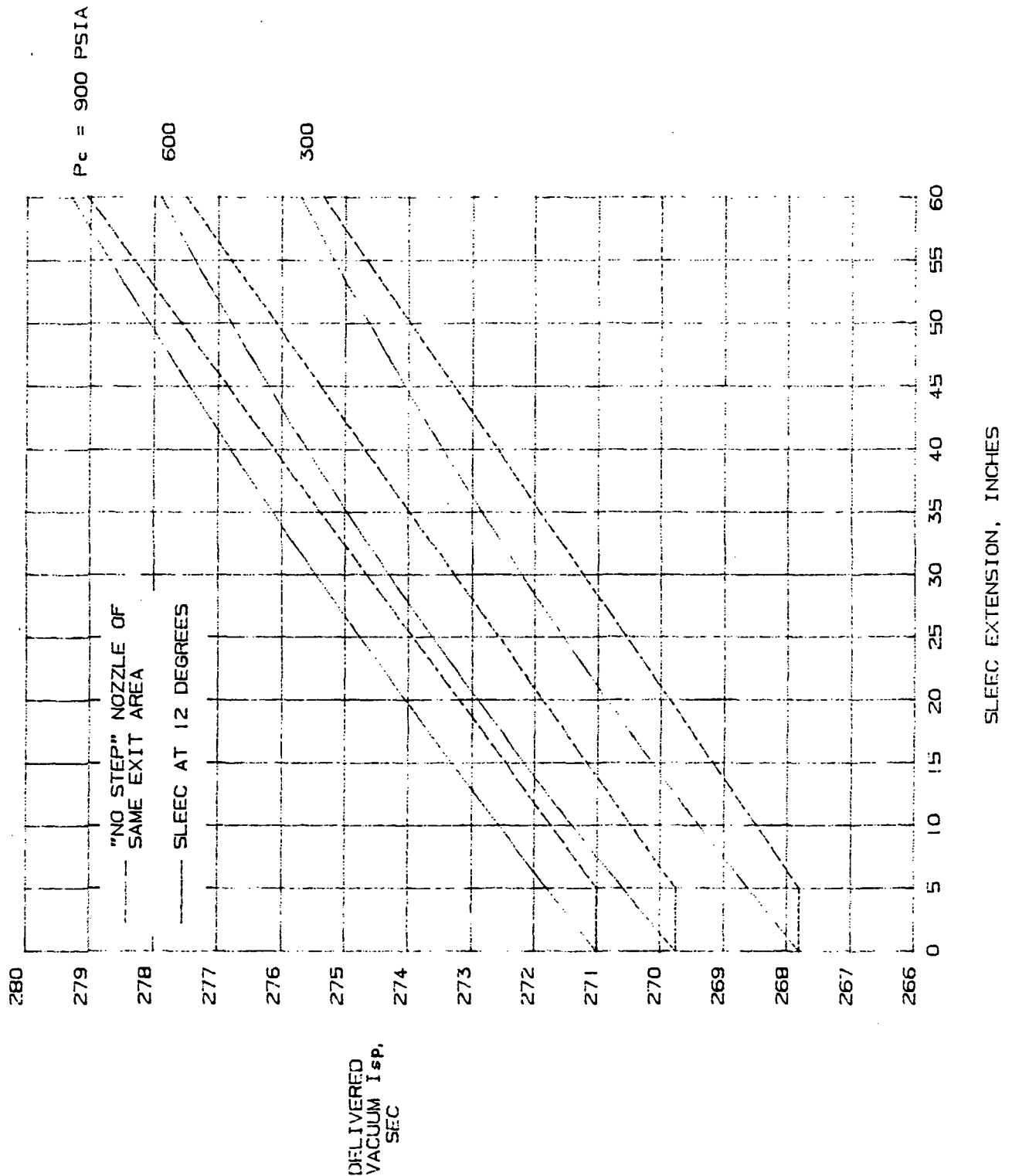


Figure 4.2-2 Predicted Vacuum Delivered Isp vs SLEEC Extension as a Function of Chamber Pressure for Initial Throat Area ($T = 0$ sec)

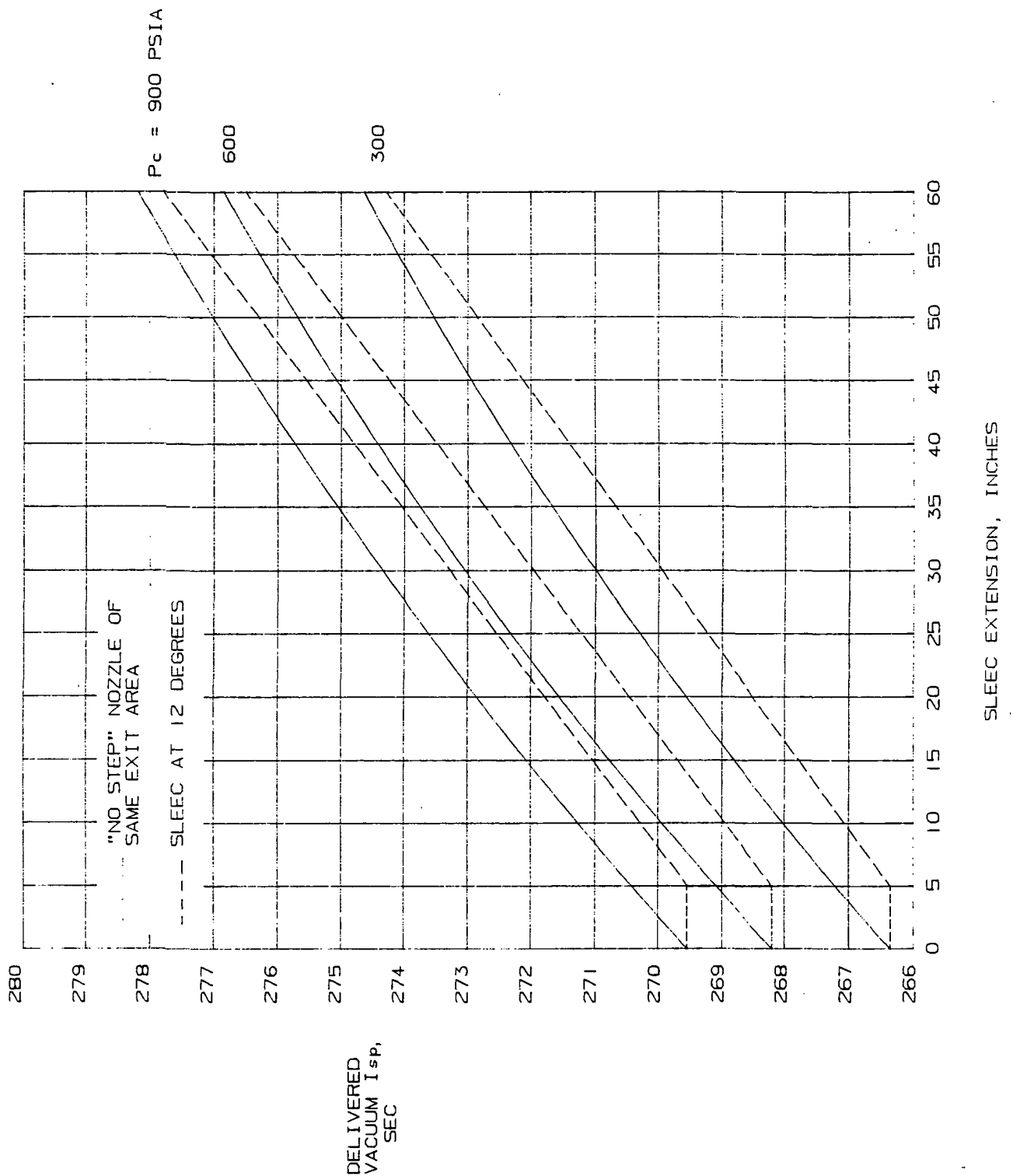


Figure 4.2-3 Predicted Vacuum Delivered I_{sp} vs SLEEC Extension as a Function of Chamber Pressure for Final Throat Area ($T = 122 \text{ sec}$)

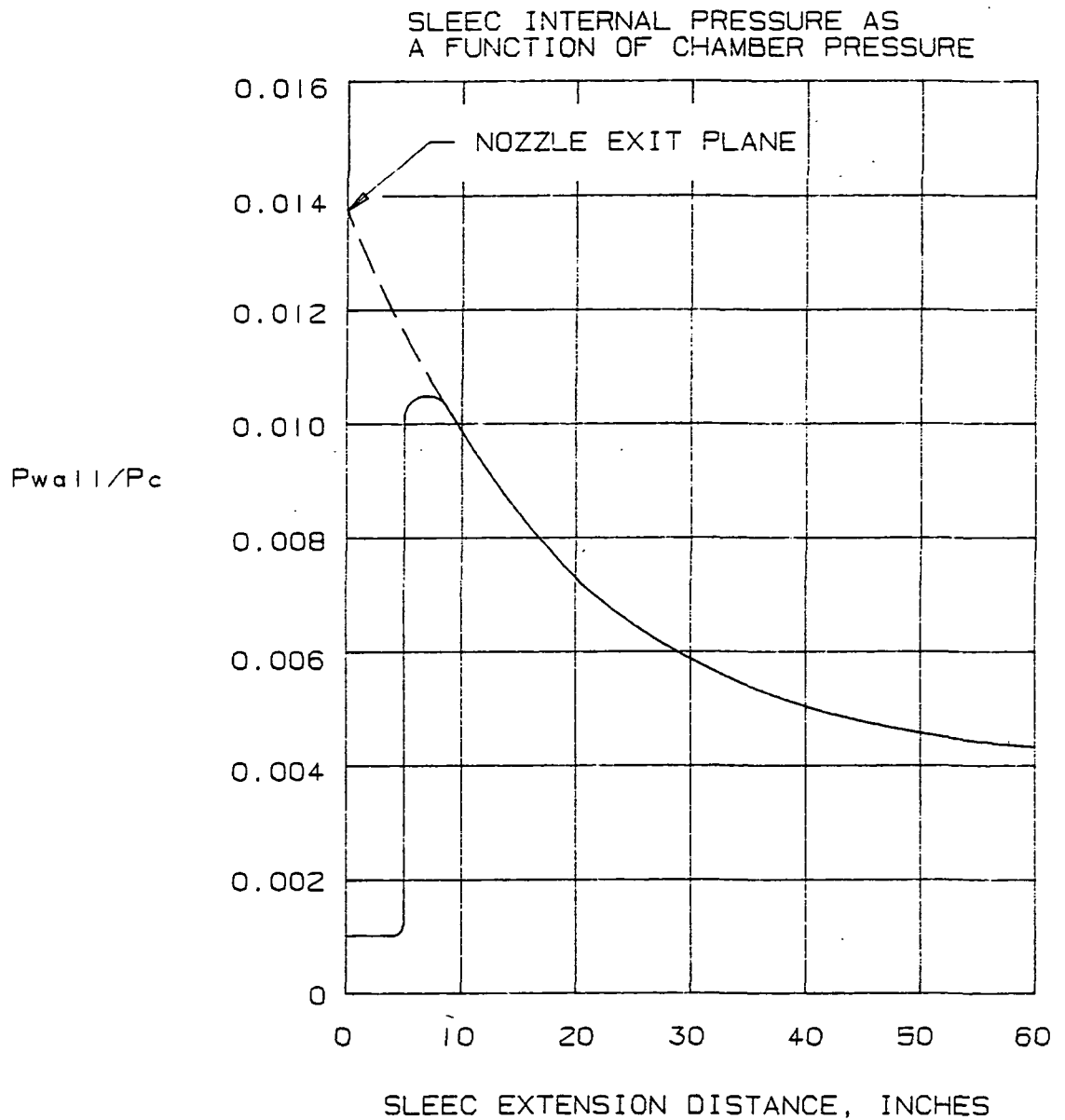


Figure 4.2-4 SLEEC Internal Wall Pressure vs Extension Distance as a Ratio of Chamber Pressure

ORIGINAL PAGE IS
OF POOR QUALITY

PRM4 WTR AUG. LAUNCH, 98 DEG INCLINATION IVBC-3 Q LIMIT
SRM F2B-NOM W/.372 B.R., -.736 FCT THRUST AND ISP
AGT 1 LOAD TRAJECTORY (NOM SRB) RUN213

TIME SEC	MACH	VIRI FPS	ALPHA DEG	PETA DEG	Q-ALPHA PSF-DEG	Q-BETA PSF-DEG	IB.EL DEG	OB.EL DEG	Q PSF	PRES PSF	VRM FPS	VRG FPS	W.AZ. DEG
0.0	.01	0.	-90.00	42.20	-6.3	-3.0	10.0	9.0	0.	2077.12	8.	7.8	312.2
.2	.01	0.	-90.00	42.20	-6.3	-3.0	10.0	9.0	0.	2077.12	8.	7.8	312.2
.2	.01	0.	-90.00	42.20	-6.3	-3.0	10.0	9.0	0.	2077.12	8.	7.8	312.2
.3	.01	0.	-87.90	42.82	-6.1	-3.0	10.0	9.0	0.	2077.12	8.	7.8	312.2
2.0	.03	30.	-3.97	40.41	4.7	-11.2	10.0	9.0	1.	2075.14	32.	7.8	312.5
3.5	.05	61.	1.04	41.93	4.4	-20.9	10.0	9.0	4.	2070.06	61.	7.7	313.2
3.5	.05	61.	1.04	41.93	4.4	-20.9	10.0	9.0	4.	2070.06	61.	7.7	313.2
4.0	.06	71.	1.81	41.23	10.3	-24.2	10.0	9.0	6.	2067.70	70.	7.7	313.6
4.4	.07	79.	2.30	-3.77	16.6	-26.9	10.0	9.0	7.	2065.48	79.	7.7	313.9
4.4	.07	79.	2.30	-3.77	16.6	-26.9	10.0	9.0	7.	2065.48	79.	7.7	313.9
6.0	.10	114.	3.60	-2.59	52.8	-38.0	10.0	9.0	15.	2054.36	113.	7.6	315.5
6.5	.11	124.	3.83	-2.37	66.7	-41.2	10.0	9.0	17.	2050.47	124.	7.6	316.1
6.5	.11	124.	3.83	-2.37	66.7	-41.2	10.0	9.0	17.	2050.47	124.	7.6	316.1
8.0	.14	160.	5.14	-0.88	147.2	-53.6	10.0	9.0	29.	2034.70	159.	7.4	318.6
10.0	.18	207.	9.18	-1.63	437.0	-77.6	10.0	9.0	48.	2008.57	207.	7.3	322.9
12.0	.23	256.	11.79	.94	838.8	-59.5	10.0	9.0	71.	1975.98	256.	7.1	328.6
14.0	.27	306.	10.58	1.56	1051.6	-194.8	10.0	9.0	99.	1937.26	306.	7.0	335.8
15.0	.29	333.	8.74	1.04	1008.1	-119.6	10.0	9.0	115.	1915.78	332.	7.0	339.9
15.0	.29	333.	8.74	1.04	1008.1	-119.6	10.0	9.0	115.	1915.78	332.	7.0	339.9
16.0	.30	360.	6.49	.88	863.5	90.2	10.0	9.0	133.	1892.91	359.	7.0	344.3
16.0	.30	360.	6.49	.88	863.5	90.2	10.0	9.0	133.	1892.91	359.	7.0	344.3
18.0	.37	417.	3.46	.98	602.3	170.5	10.0	9.0	174.	1843.17	415.	5.9	345.5
20.0	.46	476.	1.99	.83	440.4	183.3	10.0	9.0	222.	1788.29	475.	4.4	345.0
22.0	.46	538.	.42	.36	114.7	99.7	10.0	9.0	275.	1728.69	537.	2.7	343.9
24.0	.53	599.	-1.18	.16	-399.8	52.9	10.0	9.0	331.	1664.74	599.	1.1	321.2
26.0	.53	658.	-2.98	-.02	-1159.8	-74.4	10.0	9.0	388.	1596.61	659.	2.1	242.0
28.0	.54	716.	-3.89	-.12	-1723.4	-54.6	10.0	9.0	443.	1525.85	717.	4.4	226.9
28.0	.54	716.	-3.89	-.12	-1723.4	-54.6	10.0	9.0	443.	1525.85	717.	4.4	226.9
30.0	.54	716.	-3.89	-.12	-1724.8	-54.6	10.0	9.0	443.	1525.30	718.	4.4	226.8
30.0	.54	716.	-3.89	-.12	-1724.8	-54.6	10.0	9.0	443.	1525.30	718.	4.4	226.8
30.0	.70	771.	-3.85	-.02	-1800.8	-12.3	10.0	9.0	494.	1452.30	773.	6.3	222.3
31.9	.74	818.	-3.63	.04	-1942.9	20.6	10.0	9.0	535.	1380.42	821.	7.8	220.1
31.9	.74	818.	-3.63	.04	-1942.9	20.6	10.0	9.0	535.	1380.42	821.	7.8	220.1
34.0	.75	820.	-3.64	.04	-1950.4	21.5	10.0	9.0	536.	1377.25	823.	7.9	220.0
34.0	.79	867.	-3.77	.06	-2162.8	32.0	10.0	9.0	574.	1302.13	870.	9.3	219.7
36.0	.94	913.	-3.82	.05	-2322.2	30.9	10.0	9.0	607.	1226.80	917.	10.3	223.0
38.0	.89	959.	-3.86	.04	-2463.0	25.7	10.0	9.0	638.	1152.55	963.	11.5	226.3
40.0	.94	1004.	-3.97	.05	-2636.9	32.3	10.0	9.0	664.	1078.98	1009.	13.3	230.7
42.0	.99	1049.	-4.05	.09	-2781.9	60.0	10.0	9.0	686.	1006.85	1055.	15.3	233.8
44.0	1.04	1093.	-4.14	.12	-2912.3	86.3	10.0	9.0	704.	935.68	1100.	17.7	235.6
46.0	1.09	1137.	-4.24	.10	-3041.9	72.6	10.0	9.0	718.	866.73	1145.	20.5	236.6
48.0	1.14	1181.	-4.20	.07	-3059.9	50.7	10.0	9.0	728.	800.38	1190.	23.6	237.2
50.0	1.20	1225.	-4.16	.13	-3057.9	98.5	10.0	8.5	735.	735.66	1235.	27.4	237.0
52.0	1.26	1269.	-4.14	.15	-3056.1	109.2	10.0	6.5	739.	674.01	1281.	31.3	236.5
54.0	1.31	1315.	-4.13	.12	-3057.9	88.1	10.0	4.5	741.	615.12	1329.	35.1	235.6
56.0	1.38	1364.	-4.17	.06	-3089.1	41.5	10.0	2.3	741.	558.77	1380.	39.0	234.9
58.0	1.45	1416.	-4.18	.02	-3088.3	12.4	10.0	.3	739.	505.34	1435.	42.8	234.2
58.5	1.50	1458.	-4.17	.01	-3068.1	10.9	10.0	-1.2	735.	465.79	1479.	44.9	233.6
58.5	1.50	1458.	-4.17	.01	-3068.1	10.9	10.0	-1.2	735.	465.79	1479.	44.9	233.6
60.0	1.52	1472.	-4.17	0.00	-3061.1	0.0	10.0	-1.7	734.	454.36	1493.	45.5	233.4
62.0	1.60	1537.	-3.84	.03	-2801.9	23.0	10.0	-3.9	729.	406.43	1558.	44.6	231.1
63.4	1.67	1589.	-3.50	-.01	-2544.1	-8.8	10.0	-5.0	727.	373.91	1610.	43.3	229.7
63.4	1.67	1589.	-3.50	-.01	-2544.1	-8.8	10.0	-5.0	727.	373.91	1610.	43.3	229.7
64.0	1.69	1611.	-3.29	-.04	-2383.0	-26.6	10.0	-5.0	725.	361.47	1632.	42.8	230.1
66.0	1.79	1690.	-2.64	-.04	-1891.3	-31.4	10.0	-5.0	716.	319.35	1710.	40.2	231.5
68.0	1.89	1775.	-2.15	0.00	-1504.8	0.0	8.9	-5.0	700.	280.03	1782.	32.9	229.4
70.0	1.99	1864.	-1.64	.01	-1105.1	6.7	7.7	-5.0	675.	244.06	1876.	22.8	223.3
72.0	2.08	1958.	-1.04	-.03	-666.4	-19.4	6.4	-5.0	641.	211.53	1966.	13.0	203.4
74.0	2.17	2056.	-.40	-.07	-243.7	-35.9	5.0	-5.0	603.	182.51	2061.	9.1	149.9
76.0	2.27	2160.	.36	-.05	204.4	-28.7	3.5	-5.0	564.	156.89	2162.	13.7	111.0

Figure 4.2-5A Western Test Range Trajectory Used in Study
(Sheet 1 of 4)

ORIGINAL PAGE IS
OF POOR QUALITY

PRM WTR AUG. LAUNCH. 98 DEG INCLINATION IVBC-3 Q LIMIT
SRM F28MNM W/.372 B.R., -.736 FCT THRUST AND ISP
AGT I LOAD TRAJECTORY (NM SRB) RUNE13

TIME SEC	MACH	V(R) FPS	ALPHA DEG	BETA DEG	Q-ALPHA PSF-DEG	Q-BETA PSF-DEG	IB.EL DEG	OB.EL DEG	Q PSF	PRES PSF	VRW FPS	VRG FPS	W.AZ. DEG
78.0	2.36	2269.	1.16	-.03	610.2	-16.7	2.0	-5.0	526.	134.44	2268.	20.0	98.8
80.0	2.47	2380.	1.92	0.00	937.3	0.0	.5	-3.4	489.	114.92	2378.	25.4	94.1
82.0	2.57	2494.	1.96	.01	868.5	3.8	0.0	-.8	453.	97.93	2490.	30.4	91.5
84.0	2.68	2609.	1.92	0.00	799.5	0.0	0.0	0.0	417.	83.17	2604.	35.8	90.3
86.0	2.78	2725.	1.90	-.04	725.6	-13.7	0.0	0.0	382.	70.46	2720.	40.0	90.3
88.0	2.89	2842.	1.92	-.06	670.0	-22.2	0.0	0.0	348.	59.55	2837.	44.0	90.2
90.0	3.00	2960.	1.88	-.09	593.0	-29.1	0.0	0.0	316.	50.21	2954.	46.8	89.9
92.0	3.11	3080.	1.88	-.13	536.6	-36.8	0.0	0.0	286.	42.29	3073.	49.1	89.6
94.0	3.22	3203.	1.92	-.11	493.8	-28.7	0.0	0.0	257.	35.48	3195.	54.8	90.0
96.0	3.33	3325.	1.96	-.17	452.3	-39.0	0.0	0.0	230.	29.73	3318.	56.9	90.8
98.0	3.43	3448.	1.99	-.19	409.3	-39.6	0.0	0.0	206.	24.92	3442.	59.5	92.3
100.0	3.54	3573.	2.03	-.21	371.4	-39.3	0.0	0.0	183.	20.89	3568.	61.9	94.2
102.0	3.64	3697.	2.02	-.26	328.6	-41.7	0.0	0.0	163.	17.46	3694.	63.6	96.0
104.0	3.75	3822.	2.01	-.28	289.2	-40.0	0.0	0.0	144.	14.57	3817.	62.7	94.6
106.0	3.85	3945.	2.01	-.21	253.7	-26.2	0.0	0.0	126.	12.17	3938.	64.5	93.0
108.0	3.94	4068.	2.04	-.15	225.6	-17.1	0.0	0.0	111.	10.16	4059.	69.5	91.2
110.0	4.03	4189.	2.02	-.16	195.6	-15.0	0.0	0.0	97.	8.47	4179.	75.2	90.1
112.0	4.11	4297.	2.10	-.14	175.6	-12.1	0.0	0.0	84.	7.08	4286.	80.4	90.5
114.0	4.15	4377.	2.34	-.14	168.1	-9.7	0.0	0.0	72.	5.93	4365.	86.5	90.7
116.0	4.18	4435.	2.73	-.11	166.4	-6.9	0.0	0.0	61.	4.97	4420.	95.6	89.6
118.0	4.20	4480.	2.98	-.08	154.5	-4.0	0.0	0.0	52.	4.19	4467.	103.8	90.8
120.0	4.22	4517.	2.73	-.08	120.6	-3.7	0.0	0.0	44.	3.54	4506.	110.1	92.8
122.0	4.24	4548.	2.46	-.14	93.2	-5.3	0.0	0.0	38.	3.00	4539.	115.7	94.3
124.0	4.27	4575.	2.37	-.24	77.2	-7.9	0.0	0.0	33.	2.55	4569.	118.6	95.8
125.6	4.29	4596.	2.16	-.28	62.6	-8.2	0.0	0.0	29.	2.24	4592.	121.1	97.2

C-2

Figure 4.2-5B Western Test Range Trajectory Used in Study
(Sheet 2 of 4)

ORIGINAL PAGE IS
OF POOR QUALITY

PRFM WTR AUG. LAUNCH, 98 DEG INCLINATION IVBC-3 0 LIMIT
SRM FEEDNOM W/ 372 B.R., - .736 PCT THRUST AND ISP
AGT 1 LOAD TRAJECTORY (NOM SRB) RUNE13

TIME SEC	WEIGHT LBS	XCG IN.	YCG IN.	ZCG IN.	V(R) FPS	V(I) FPS	ALTITUDE FT	GAM(R) DEG	GAM(I) DEG	MACH	SSME PERCENT	RANGE N.M.	TLF GYS	THETA DEG
0.0	4452242.	1408.3	.218	418.1	0.	1258.	335.7	0.000	0.000	.007	100.0	0.	.26	90.0
.2	4450750.	1408.4	.219	418.2	0.	1258.	335.7	0.000	0.000	.007	100.0	0.	1.00	90.0
.2	4450750.	1408.4	.219	418.2	0.	1258.	335.7	0.000	0.000	.007	100.0	0.	1.00	90.0
.3	4449825.	1408.4	.219	418.2	0.	1258.	335.7	67.492	.010	.007	100.0	0.	1.25	90.0
2.0	4403181.	1408.2	.219	418.3	32.	1262.	362.7	83.417	1.436	.029	100.0	0.	1.59	89.8
3.5	4362307.	1408.0	.219	418.5	61.	1266.	431.9	83.504	2.737	.054	100.0	0.	1.61	89.8
3.5	4362307.	1408.0	.219	418.5	61.	1266.	431.9	83.504	2.737	.054	100.0	0.	1.61	89.8
4.0	4348852.	1407.9	.220	418.6	71.	1268.	464.1	83.557	3.178	.063	104.9	0.	1.63	89.9
4.4	4337705.	1407.9	.221	418.6	79.	1269.	494.4	83.585	3.554	.071	105.0	0.	1.65	89.9
4.4	4337705.	1407.9	.221	418.6	79.	1269.	494.4	83.585	3.554	.071	105.0	0.	1.65	89.9
6.0	4293570.	1407.7	.223	418.8	114.	1275.	646.9	83.675	5.088	.101	109.0	0.	1.69	89.9
6.5	4280930.	1407.6	.223	418.9	124.	1277.	700.4	83.713	5.538	.110	109.0	0.	1.70	89.9
6.5	4280930.	1407.6	.223	418.9	124.	1277.	700.4	83.713	5.538	.110	109.0	0.	1.70	89.9
8.0	4237542.	1407.4	.233	419.1	160.	1285.	918.4	83.806	7.099	.142	109.0	0.	1.73	89.2
10.0	4181170.	1406.9	.238	419.3	207.	1292.	1283.4	85.124	9.201	.184	109.0	0.	1.76	84.1
12.0	4124484.	1406.4	.244	419.6	256.	1292.	1745.4	86.189	11.407	.227	109.0	0.	1.79	76.8
14.0	4067630.	1405.8	.231	419.8	306.	1293.	2304.2	81.831	13.564	.271	109.0	0.	1.82	72.1
15.0	4033221.	1405.4	.227	420.0	333.	1297.	2619.0	79.434	14.604	.294	109.0	0.	1.83	71.5
15.0	4033221.	1405.4	.227	420.0	333.	1297.	2619.0	79.434	14.604	.294	109.0	0.	1.83	71.5
16.0	4010773.	1405.0	.232	420.1	360.	1303.	2958.2	77.426	15.648	.317	109.0	0.	1.84	71.8
16.0	4010773.	1405.0	.232	420.1	360.	1303.	2958.2	77.426	15.648	.317	109.0	0.	1.84	71.8
18.0	3953841.	1404.2	.250	420.4	417.	1314.	3710.3	74.487	17.798	.368	109.0	0.	1.87	71.7
20.0	3896787.	1403.3	.250	420.7	476.	1327.	4564.1	72.046	19.966	.421	109.0	0.	1.89	70.4
22.0	3833777.	1402.1	.250	421.1	538.	1344.	5521.5	69.952	22.089	.478	109.0	0.	1.90	69.6
24.0	3783984.	1400.7	.254	421.4	599.	1364.	6582.5	68.267	24.079	.534	109.0	0.	1.87	69.3
26.0	3729778.	1399.3	.258	421.7	658.	1386.	7743.9	67.037	26.929	.589	109.0	0.	1.84	69.7
28.0	3676978.	1397.7	.260	422.1	716.	1411.	9003.8	66.250	27.686	.645	109.0	0.	1.82	69.7
28.0	3676978.	1397.7	.260	422.1	716.	1411.	9014.0	66.244	27.699	.645	109.0	0.	1.82	69.7
28.0	3676978.	1397.7	.260	422.1	716.	1411.	9014.0	66.244	27.699	.645	109.0	0.	1.82	69.7
30.0	3625956.	1395.6	.265	422.4	771.	1435.	10359.2	65.433	29.239	.697	89.2	0.	1.73	68.6
31.9	3579233.	1393.4	.268	422.7	818.	1456.	11736.3	64.503	30.459	.744	70.0	1.	1.84	67.5
31.9	3579233.	1393.4	.268	422.7	818.	1456.	11736.3	64.503	30.459	.744	70.0	1.	1.84	67.5
32.0	3577218.	1393.3	.268	422.7	820.	1457.	11798.7	64.460	30.508	.746	70.0	1.	1.84	67.5
34.0	3530043.	1390.5	.271	423.0	867.	1479.	13311.5	63.454	31.606	.794	70.0	1.	1.63	66.6
36.0	3463807.	1387.5	.275	423.3	913.	1502.	14894.3	62.501	32.625	.841	70.0	1.	1.62	65.7
38.0	3438473.	1384.4	.278	423.7	959.	1526.	16544.9	61.574	33.561	.889	70.0	1.	1.61	64.8
40.0	3393990.	1381.1	.281	424.0	1004.	1550.	18261.4	60.688	34.419	.938	70.0	1.	1.59	64.0
42.0	3360279.	1377.5	.283	424.3	1049.	1574.	20041.5	59.844	35.200	.987	70.0	1.	1.57	63.2
44.0	3327225.	1373.9	.285	424.7	1093.	1598.	21882.9	59.033	35.910	1.037	70.0	2.	1.56	62.4
46.0	3284709.	1370.1	.294	425.0	1137.	1623.	23783.8	58.246	36.557	1.088	70.0	2.	1.55	61.7
48.0	3222665.	1366.1	.296	425.3	1181.	1649.	25742.9	57.481	37.149	1.140	70.0	2.	1.55	60.9
50.0	3181145.	1362.1	.297	425.7	1225.	1675.	27758.4	56.681	37.675	1.195	70.0	2.	1.54	59.9
52.0	3140342.	1358.0	.301	426.0	1269.	1701.	29828.2	55.864	38.128	1.252	70.0	2.	1.54	59.0
54.0	3099700.	1353.9	.305	426.4	1315.	1729.	31951.4	55.050	38.550	1.312	70.0	3.	1.58	58.1
56.0	3058782.	1349.6	.310	426.7	1364.	1760.	34130.8	54.250	38.963	1.376	70.0	3.	1.62	57.3
58.0	3017516.	1345.2	.316	427.1	1416.	1794.	36370.3	53.473	39.369	1.445	70.0	3.	1.67	56.5
59.5	2985559.	1341.6	.320	427.4	1459.	1822.	38135.7	52.878	39.671	1.502	70.0	3.	1.71	55.9
59.5	2985559.	1341.6	.320	427.4	1459.	1822.	38135.7	52.878	39.671	1.502	70.0	3.	1.71	55.9
60.0	2975887.	1340.5	.321	427.5	1472.	1831.	38673.7	52.703	39.763	1.519	74.6	3.	1.74	55.7
62.0	2933030.	1335.9	.331	427.9	1537.	1875.	41048.7	51.978	40.209	1.601	94.6	4.	1.89	54.7
63.4	2901248.	1332.6	.329	428.2	1589.	1912.	42808.3	51.492	40.566	1.666	109.0	4.	1.99	53.9
63.4	2901248.	1332.6	.330	428.2	1589.	1912.	42808.3	51.492	40.566	1.666	109.0	4.	1.99	53.9
64.0	2888663.	1331.4	.329	428.3	1611.	1928.	43509.3	51.306	40.706	1.682	109.0	4.	2.01	53.5
66.0	2843704.	1326.8	.336	428.7	1630.	1986.	46065.8	50.581	41.124	1.790	109.0	4.	2.06	52.3
68.0	2798486.	1322.0	.345	429.2	1775.	2048.	48720.3	49.803	41.438	1.889	109.0	5.	2.12	51.1
70.0	2753076.	1317.1	.354	429.6	1864.	2116.	51474.7	48.983	41.644	1.987	109.0	5.	2.18	50.0
72.0	2707478.	1311.8	.359	430.1	1958.	2199.	54330.5	48.116	41.730	2.080	109.0	6.	2.24	48.7
74.0	2661714.	1306.5	.364	430.5	2056.	2269.	57288.4	47.199	41.691	2.172	109.0	6.	2.31	47.3
76.0	2615853.	1300.9	.372	431.0	2160.	2353.	60348.5	46.235	41.525	2.266	109.0	6.	2.37	45.7

Figure 4.2-5C Western Test Range Trajectory Used in Study
(Sheet 3 of 4)

ORIGINAL PAGE IS
OF POOR QUALITYPRM4 WTR AUG. LAUNCH, 98 DEG INCLINATION IVBC-3 Q LIMIT
SRM F28NOM W/.372 B.R. - .736 PCT TRUST AND ISP
AGT 1 LOAD TRAJECTORY (NOM SRB) RUN#13

TIME SEC	HEIGHT LBS	XCG IN.	YCG IN.	ZCG IN.	V(R) FPS	V(I) FPS	ALTITUDE FT	GAM(R) DEG	GAM(I) DEG	MACH	SSME PERCENT	RANGE N.M.	TUF GYS	THETA DEG
78.0	2569981.	1295.3	.378	431.6	2269.	2443.	63509.5	45.218	41.228	2.363	109.0	7.	2.42	43.9
80.0	2564583.	1289.7	.395	432.1	2380.	2537.	66766.4	44.158	40.807	2.465	109.0	8.	2.44	42.1
82.0	2479994.	1284.0	.391	432.7	2494.	2634.	70119.7	43.096	40.297	2.570	109.0	8.	2.46	41.0
84.0	2436213.	1278.5	.396	433.3	2609.	2734.	73560.6	42.080	39.750	2.676	109.0	9.	2.46	40.1
86.0	2393335.	1273.0	.401	433.9	2725.	2837.	77088.5	41.100	39.169	2.784	109.0	9.	2.47	39.1
88.0	2351517.	1267.7	.406	434.5	2842.	2940.	80700.4	40.152	38.558	2.891	109.0	10.	2.45	38.2
90.0	2310726.	1262.6	.412	435.1	2960.	3046.	84392.0	39.238	37.931	2.999	109.0	11.	2.47	37.3
92.0	2270313.	1257.3	.418	435.8	3080.	3155.	88161.5	38.353	37.292	3.107	109.0	12.	2.50	36.4
94.0	2230561.	1252.3	.425	436.4	3203.	3266.	92007.4	37.494	36.643	3.217	109.0	12.	2.50	35.5
96.0	2191845.	1247.2	.432	437.1	3325.	3379.	95825.5	36.660	35.986	3.327	109.0	13.	2.50	34.6
98.0	2153946.	1242.1	.440	437.8	3448.	3493.	99914.9	35.849	35.327	3.435	109.0	14.	2.51	33.8
100.0	2116901.	1237.5	.448	438.4	3573.	3608.	103969.7	35.060	34.666	3.537	109.0	15.	2.50	32.9
102.0	2080771.	1232.8	.455	439.1	3697.	3729.	108087.2	34.293	34.008	3.644	109.0	16.	2.49	32.1
104.0	2045629.	1228.1	.463	439.8	3822.	3841.	112263.8	33.550	33.358	3.749	109.0	17.	2.47	31.4
106.0	2011747.	1223.9	.473	440.5	3945.	3957.	116495.0	32.831	32.716	3.849	109.0	18.	2.45	30.7
108.0	1978657.	1219.8	.482	441.2	4068.	4074.	120776.9	32.131	32.083	3.944	109.0	19.	2.44	30.0
110.0	1946762.	1216.0	.490	441.9	4189.	4188.	125105.9	31.453	31.462	4.034	109.0	20.	2.34	29.3
112.0	1918507.	1213.3	.498	442.7	4297.	4291.	129472.6	30.806	30.866	4.106	109.0	22.	1.97	28.6
114.0	1897030.	1212.2	.502	443.4	4377.	4366.	133854.1	30.194	30.275	4.154	109.0	23.	1.53	27.8
116.0	1880979.	1212.2	.507	444.1	4435.	4421.	138224.3	29.604	29.706	4.181	109.0	24.	1.28	26.8
118.0	1868053.	1212.9	.511	444.6	4480.	4464.	142566.0	29.024	29.142	4.199	109.0	25.	1.12	26.0
120.0	1857600.	1214.1	.516	445.1	4517.	4498.	146868.7	28.458	28.588	4.220	109.0	27.	1.00	25.6
122.0	1848943.	1215.3	.521	445.5	4548.	4527.	151126.0	27.908	28.048	4.241	109.0	28.	.92	25.3
124.0	1841220.	1216.8	.523	445.8	4575.	4553.	155333.4	27.365	27.513	4.268	109.0	29.	.87	24.9
125.6	1835417.	1218.1	.525	446.0	4596.	4572.	158658.7	26.935	27.089	4.289	109.0	30.	.85	24.6
END OF STAGE 1														
295.2	953210.	1265.4	.981	488.4	10141.	9956.	350359.9	2.048	2.086	9.840	109.0	218.	1.62	8.1
299.7	941635.	1269.4	.519	489.7	10286.	10102.	351797.3	1.870	1.905	9.937	109.0	226.	1.11	20.3
299.7	941635.	1269.4	.521	489.7	10286.	10102.	351797.3	1.870	1.905	9.937	109.0	226.	1.12	20.3
301.2	938086.	1270.6	.509	490.0	10330.	10145.	352250.4	1.813	1.846	9.965	109.0	228.	1.11	20.1
301.2	938086.	1270.6	.509	490.0	10330.	10145.	352250.4	1.813	1.846	9.965	109.0	228.	1.11	20.1
304.0	931394.	1272.9	.514	490.5	10412.	10228.	353071.8	1.704	1.735	10.020	109.0	233.	1.12	19.8
320.0	893749.	1286.0	.546	493.5	10893.	10712.	356819.9	1.160	1.179	10.365	109.0	261.	1.16	18.5
336.0	856103.	1299.8	.563	496.8	11404.	11226.	359203.7	.713	.724	10.775	109.0	290.	1.22	17.2
352.0	818458.	1314.4	.625	500.4	11947.	11772.	360401.6	.358	.363	11.249	109.0	320.	1.27	15.8
366.4	784675.	1328.3	.668	503.8	12464.	12292.	360615.6	.110	.112	11.730	109.0	348.	1.33	14.5
366.4	784675.	1328.3	.669	503.8	12464.	12292.	360615.6	.110	.112	11.730	109.0	348.	1.33	14.5
368.0	780868.	1330.0	.674	504.3	12525.	12353.	360594.4	.086	.087	11.788	109.0	352.	1.33	14.5
384.0	743768.	1347.2	.694	509.4	13142.	12973.	359978.0	-.107	-.108	12.392	109.0	385.	1.40	12.9
400.0	706668.	1365.7	.613	515.1	13801.	13634.	358734.2	-.235	-.238	13.061	109.0	420.	1.47	11.3
416.0	669568.	1385.5	.587	521.3	14505.	14342.	357044.4	-.306	-.310	13.798	109.0	457.	1.56	9.7
432.0	632467.	1407.2	.617	527.7	15261.	15100.	355089.2	-.327	-.331	14.603	109.0	495.	1.65	7.9
448.0	595367.	1430.9	.667	534.7	16073.	15915.	353047.2	-.305	-.308	15.477	109.0	536.	1.75	6.0
464.0	558267.	1457.0	.736	542.6	16949.	16793.	351094.3	-.248	-.250	16.420	109.0	579.	1.87	4.1
480.0	521167.	1486.1	.826	551.5	17896.	17742.	349402.4	-.161	-.162	17.429	109.0	624.	2.00	2.2
496.0	484067.	1518.6	.964	561.5	18924.	18773.	348139.4	-.051	-.051	18.505	109.0	672.	2.15	.2
512.0	446966.	1555.6	1.038	573.7	20043.	19894.	347468.5	.076	.076	19.641	109.0	722.	2.33	-1.8
528.0	409866.	1598.5	1.223	587.5	21268.	21121.	347550.4	.216	.217	20.837	109.0	776.	2.54	-3.7
535.2	393273.	1620.0	1.417	594.0	21855.	21709.	347875.1	.262	.264	21.391	109.0	801.	2.64	-4.6
535.2	393273.	1620.0	1.409	594.0	21855.	21709.	347875.1	.262	.264	21.391	109.0	801.	2.61	-4.5
544.0	373212.	1649.2	1.725	602.9	22606.	22462.	348547.5	.362	.365	22.079	109.0	833.	2.75	-5.5
558.0	341456.	1700.9	2.407	619.2	23886.	23744.	350283.8	.494	.497	23.204	109.0	886.	3.00	-7.0
558.0	341456.	1700.9	2.407	619.2	23886.	23744.	350283.8	.494	.497	23.204	109.0	886.	3.00	-7.0
560.0	336950.	1708.8	2.528	621.7	24078.	23936.	350605.2	.514	.517	23.366	107.5	894.	3.00	-7.2
574.1	306884.	1738.5	.085	635.3	25426.	25286.	353405.4	.638	.642	24.464	97.9	950.	2.99	-8.0
574.1	306884.	1738.5	.085	635.3	25426.	25286.	353405.4	.638	.642	24.464	97.9	950.	3.00	-8.0
575.0	305069.	1735.3	-.235	635.9	25505.	25365.	353854.9	.643	.647	24.506	97.9	958.	.24	-8.0
580.1	304711.	1734.7	-.253	636.2	25516.	25376.	354812.7	.637	.640	24.446	0.0	975.	.00	-8.0
580.1	304711.	1734.7	-.253	636.2	25516.	25376.	354812.7	.637	.640	24.446	0.0	975.	.00	-8.0
580.1	304711.	1734.7	-.253	636.2	25513.	25373.	357109.7	.617	.621	24.275	0.0	1016.	.00	-8.0
END AQ4														

Figure 4.2-5D Western Test Range Trajectory Used in Study
(Sheet 4 of 4)

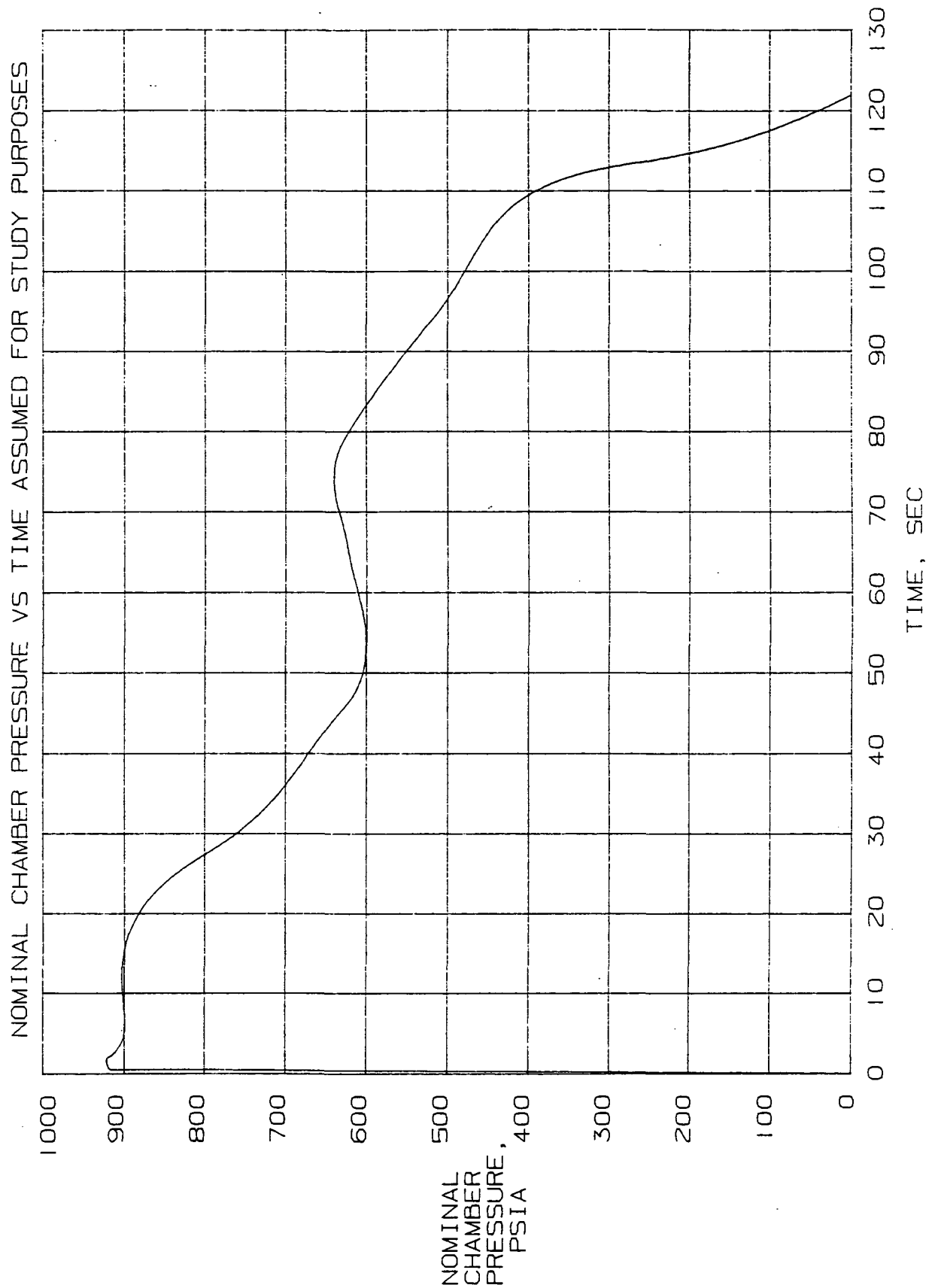


Figure 4.2-6 Nominal Chamber Pressure vs Time

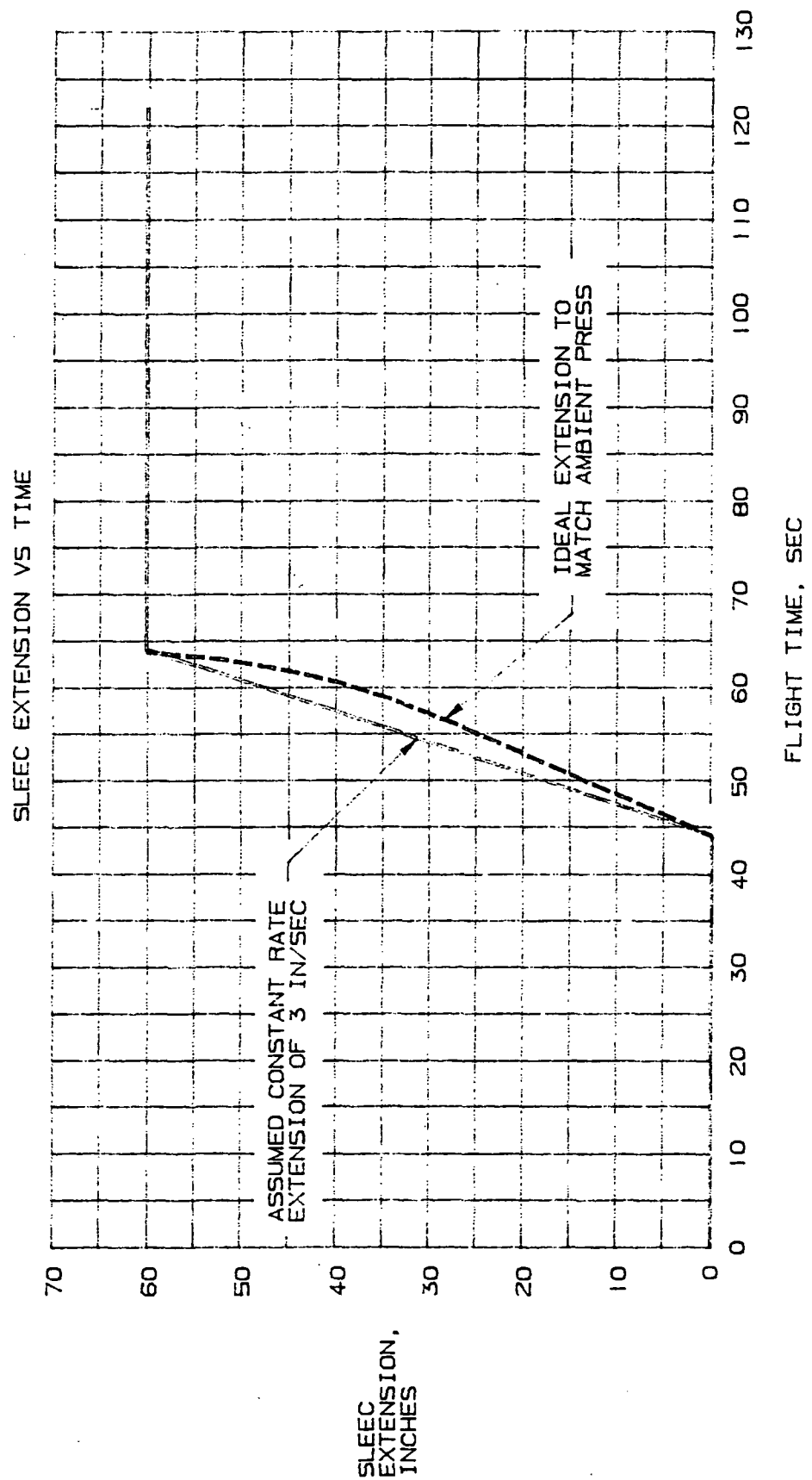
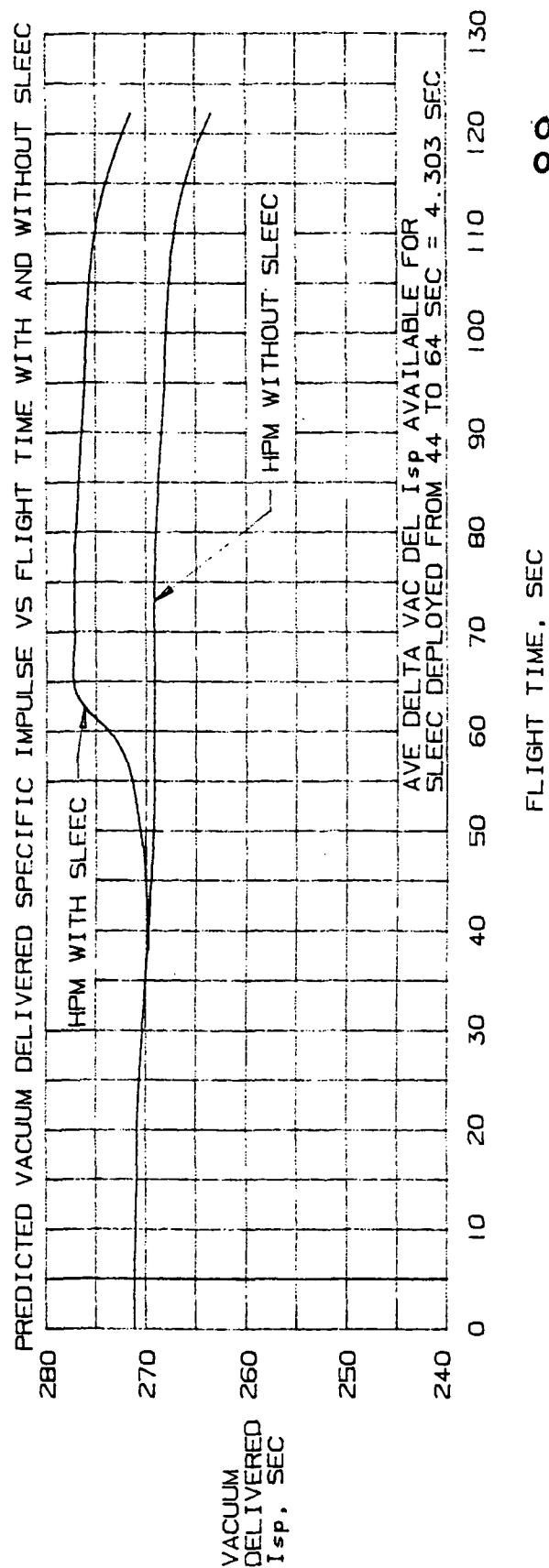


Figure 4.2-7 SLEEC Extension vs Time



ORIGINAL PAGE IS
OF POOR QUALITY

Figure 4.2-8 Vacuum Delivered Specific Impulse vs Time,
With and Without SLEEC

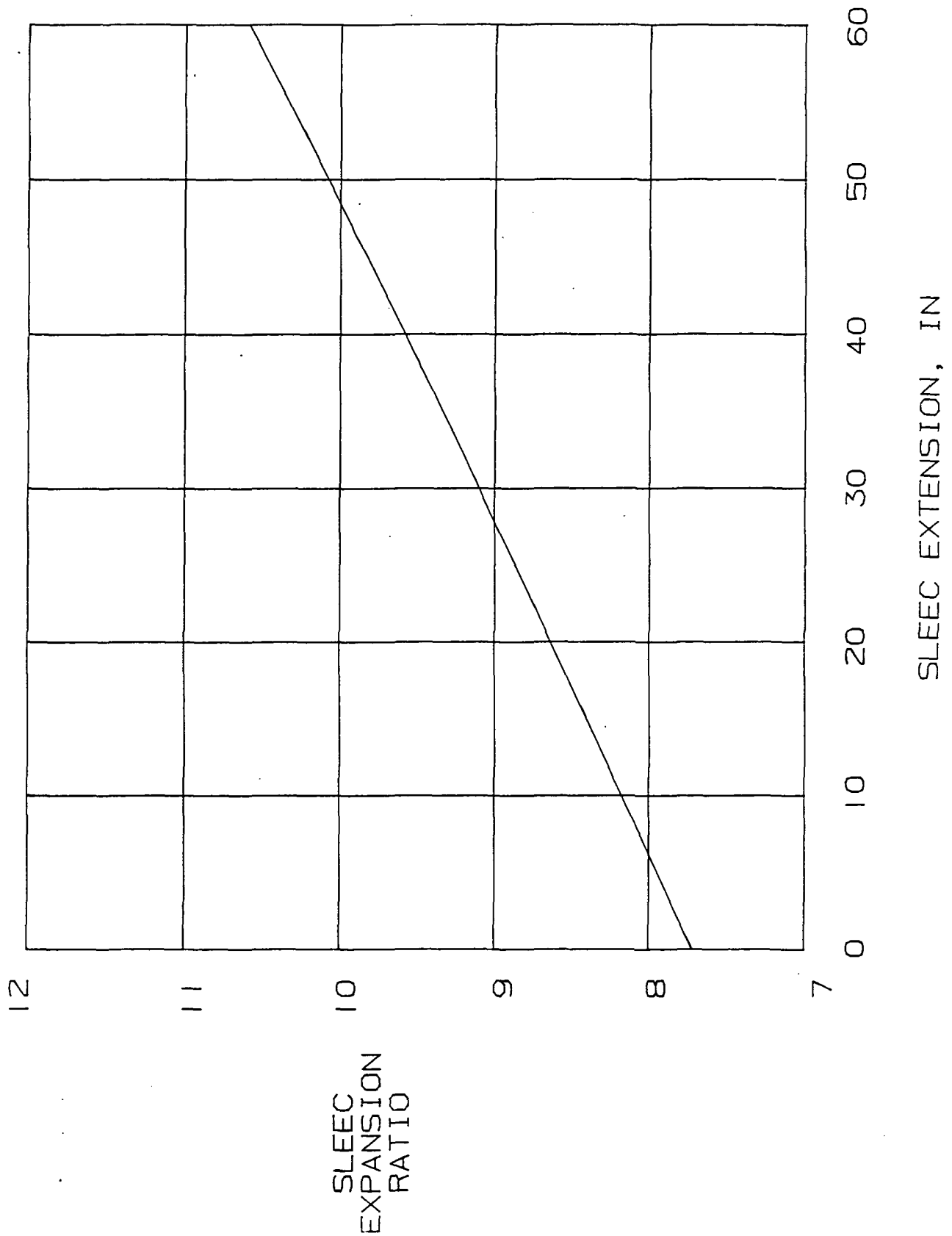


Figure 4.2-9 SRB/SLEEC Expansion Ratio vs Extension Distance

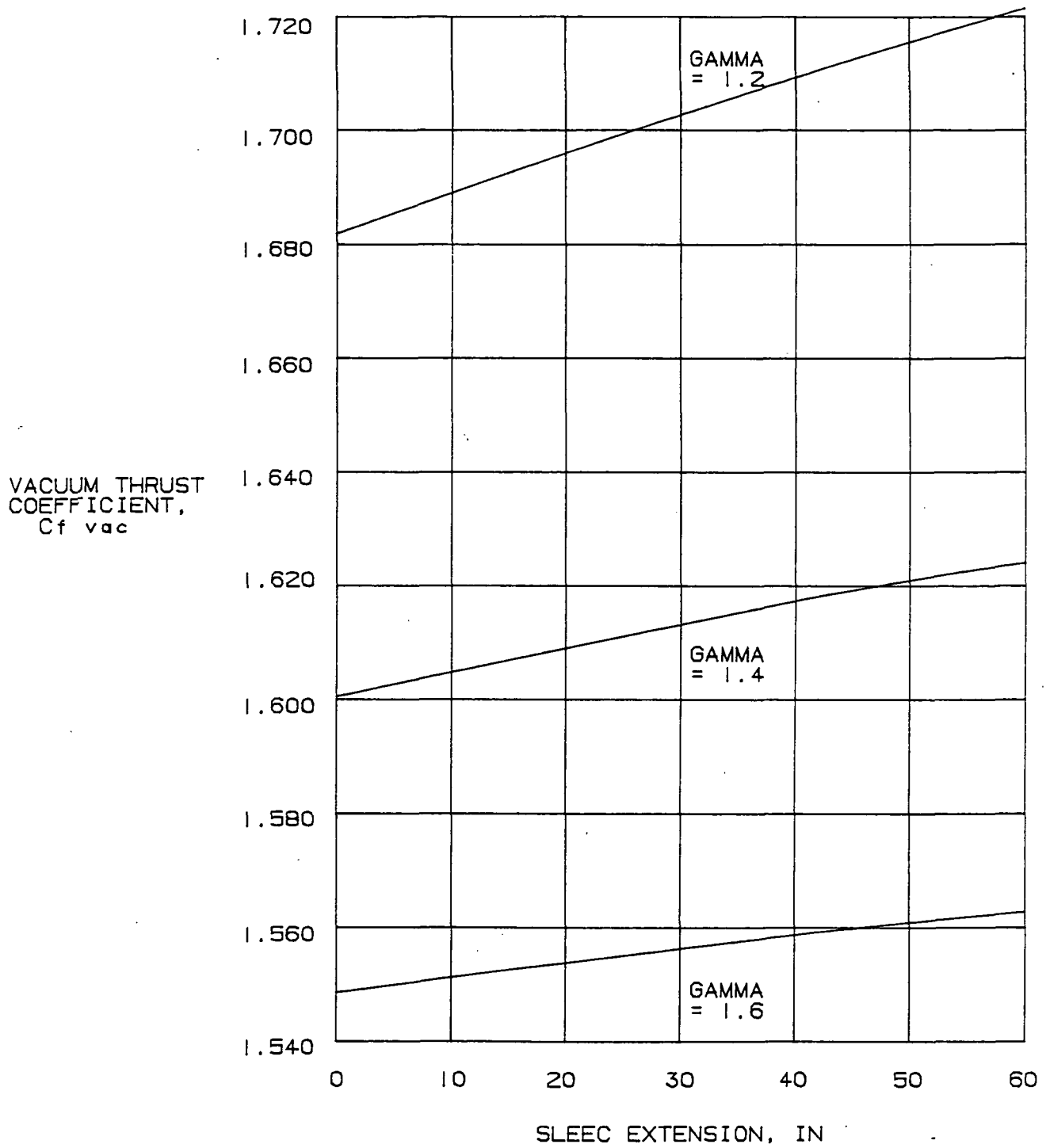


Figure 4.2-10 Vacuum Thrust Coefficient vs Extension Distance

ORIGINAL PAGE IS
OF POOR QUALITY

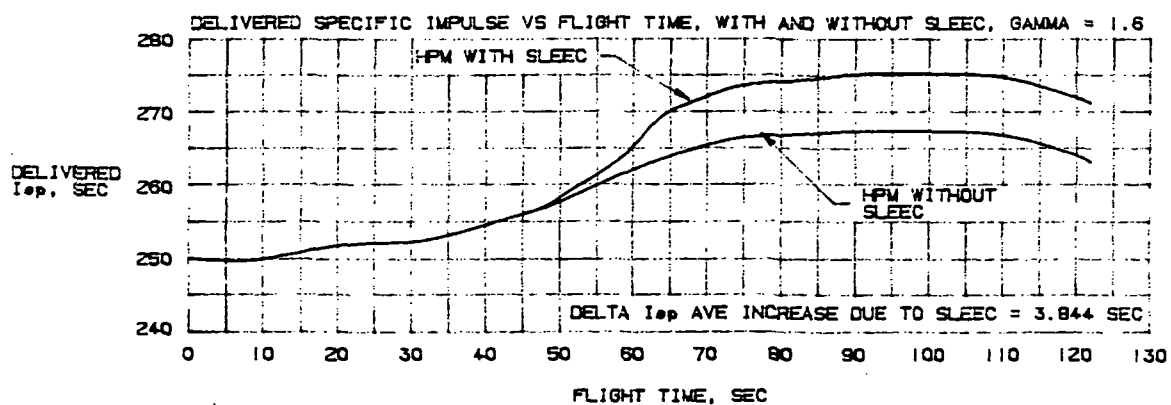
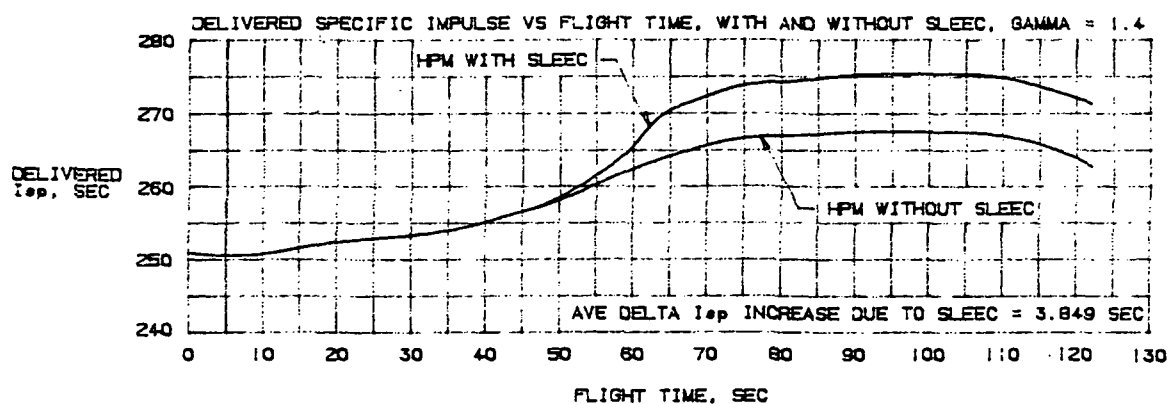
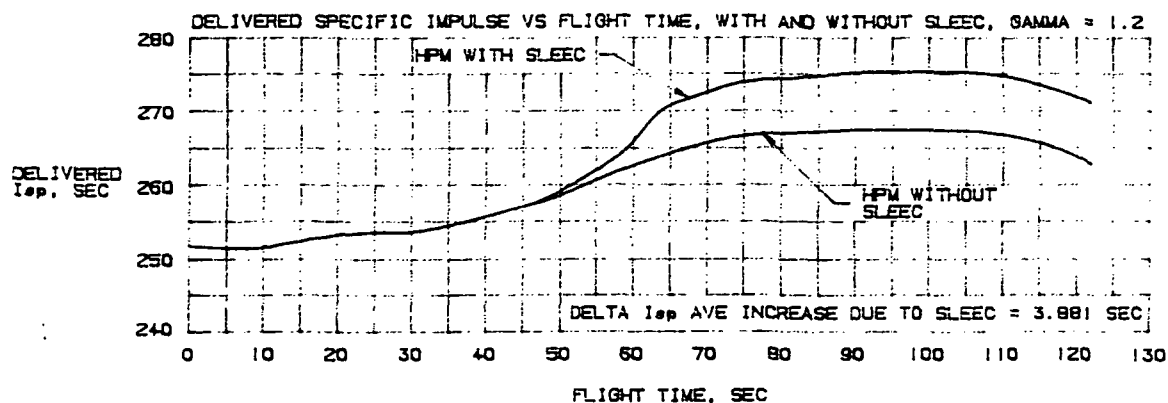


Figure 4.2-11 Delivered Specific Impulse vs Flight Time, With and Without SLEEC

SRB/SLEEC PERFORMANCE COMPARISON		
TEST RANGE	1981	STUDY
	PREDICTIONS	RESULTS
	EASTERN	WESTERN
SLEEC EXTENSION LENGTH, IN	63	60
SLEEC EXPANSION RATIO, EXTENDED	11.35	10.59
SLEEC HALF ANGLE, DEG	12.5	12.0
TIME OF DEPLOYMENT, SEC	3 TO 25	44 TO 64
AVERAGE SPECIFIC IMPULSE GAIN, SEC	6.28	3.86
ADD-ON WEIGHT (EA OF 2), LBM	3990	4193
WEIGHT LOSS DURING BURN, LBM	300	300
PREDICTED PAYLOAD GAIN TO LEO, LBM	3750	2471

Figure 4.2-12 SRB/SLEEC Performance Comparison

PRELIMINARY ROM FABRICATION COSTS

(IN THOUSANDS OF DOLLARS BASED ON 1986 DOLLARS)

	NON-RECURRING COSTS (ENGINEERING, TOOL- ING AND TESTS)	PRODUCTION COST, E BASED ON 100 UNITS
SHINGLES	2,071	460.0
ACTUATION	4,848	132.7
SYSTEM ENG'RG, EXIT CONE MODS, FINAL ASSEMBLY, OTHER	8,500	397.3
	<hr/>	<hr/>
TOTAL COSTS	15,419	990.0
TOTAL COST EA FOR 100 UNITS INCLUDING NON-RECURRING COSTS		1,140.0

Figure 4.2-13 Preliminary ROM Fabrication Costs

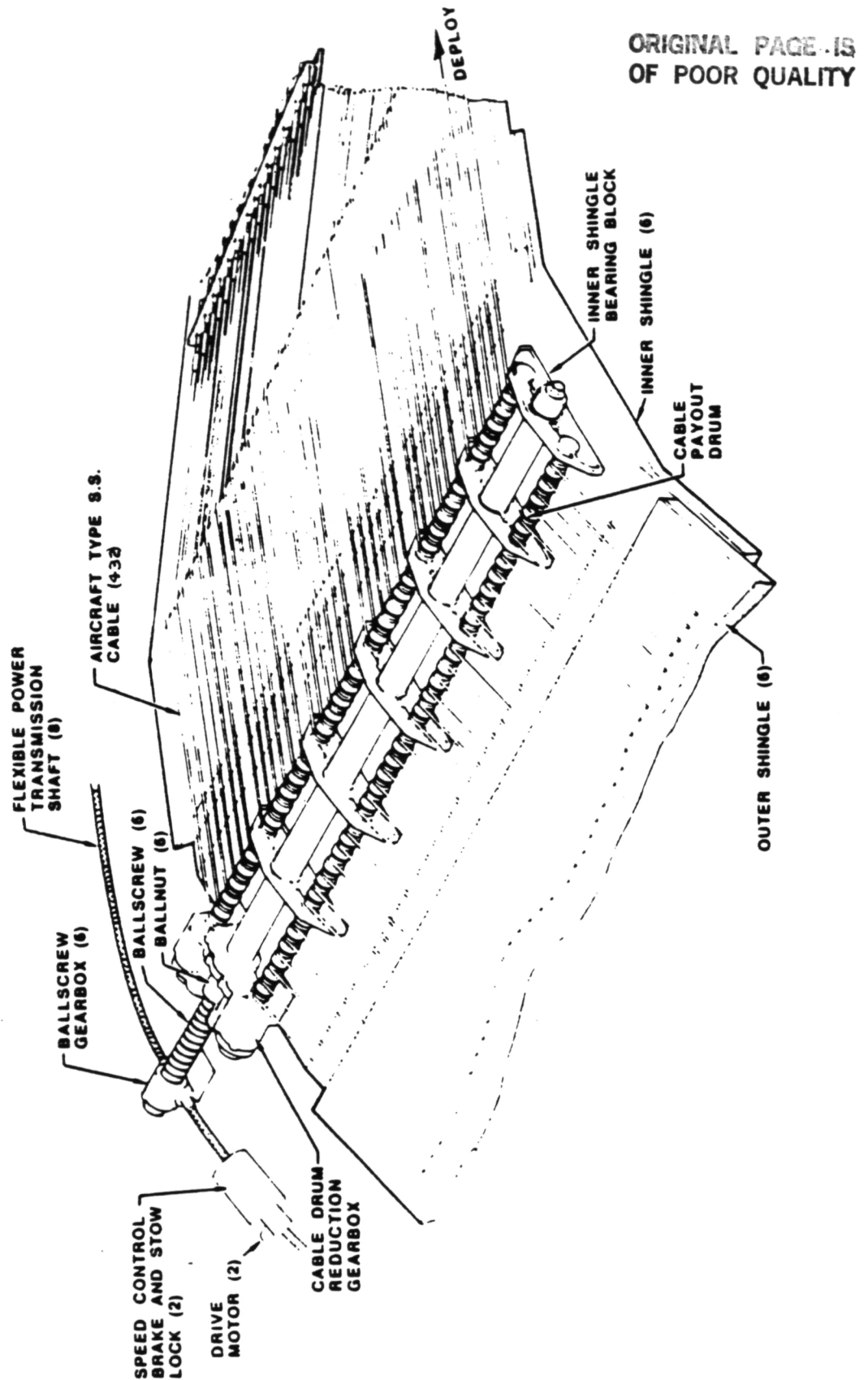


Figure 4.2-14 SLEEC Actuation System Detail

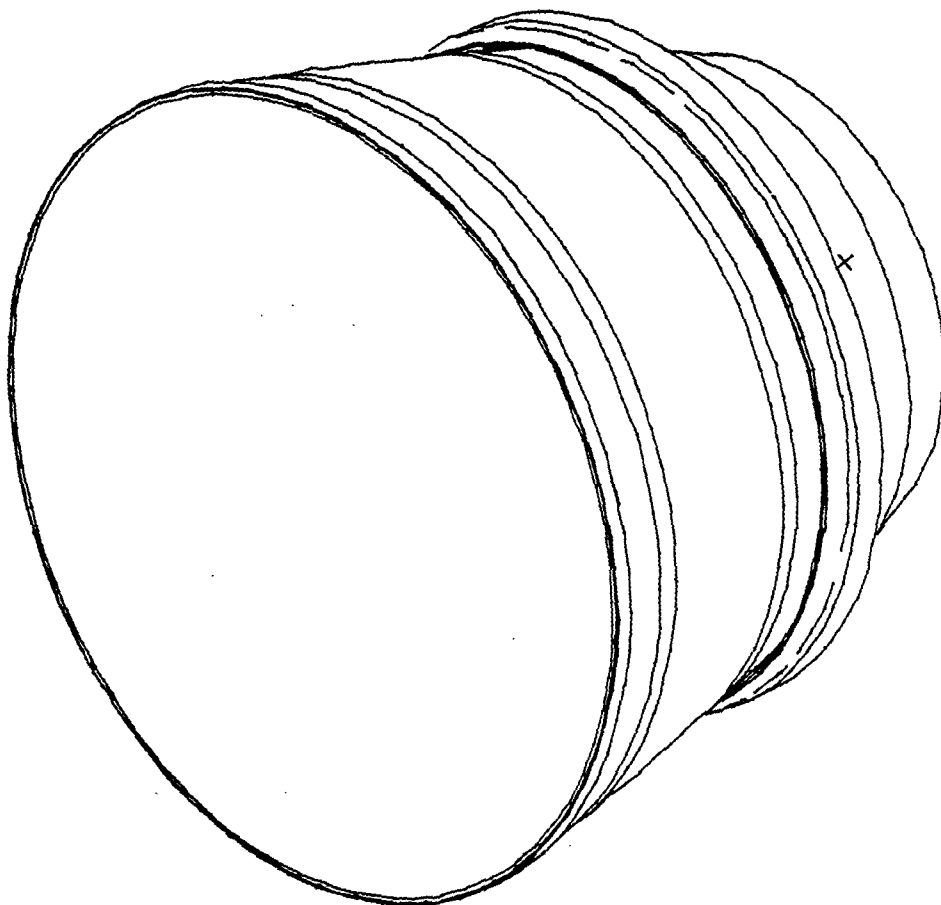


Figure 4.2-15 HPN Aft Exit Cone Assembly Prior to Modification

ORIGINAL PAGE IS
OF POOR QUALITY

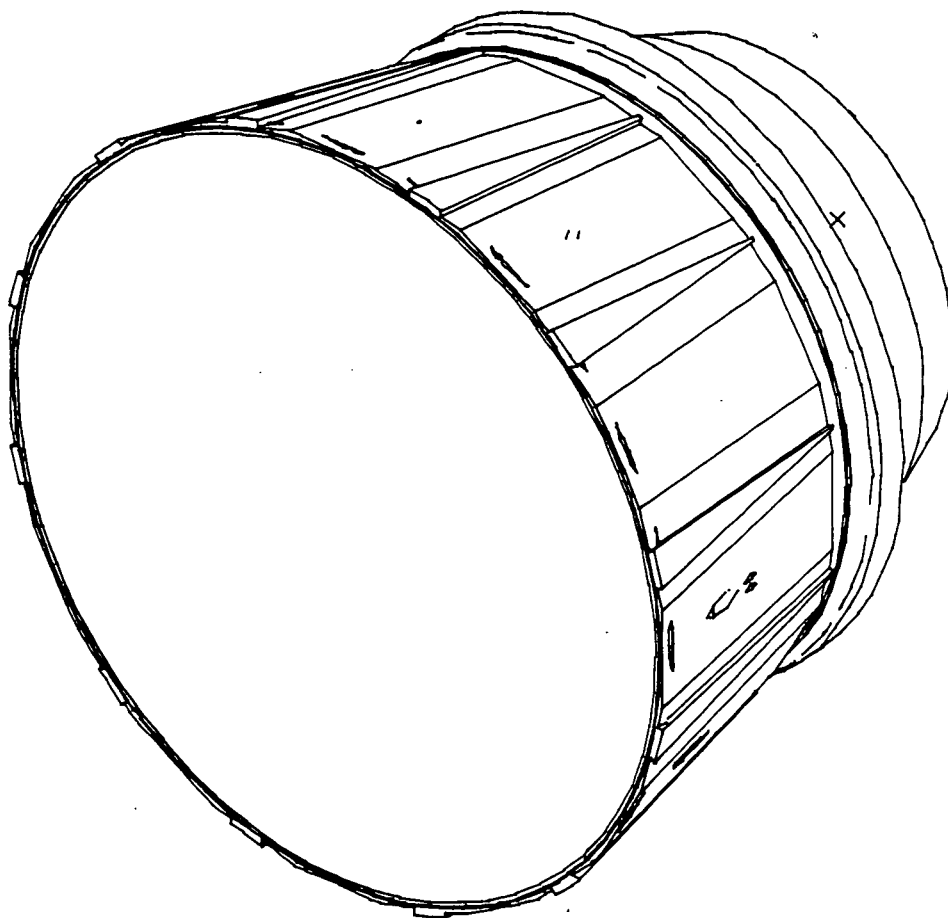


Figure 4.2-16 Modified HPN Aft Cone Assembly

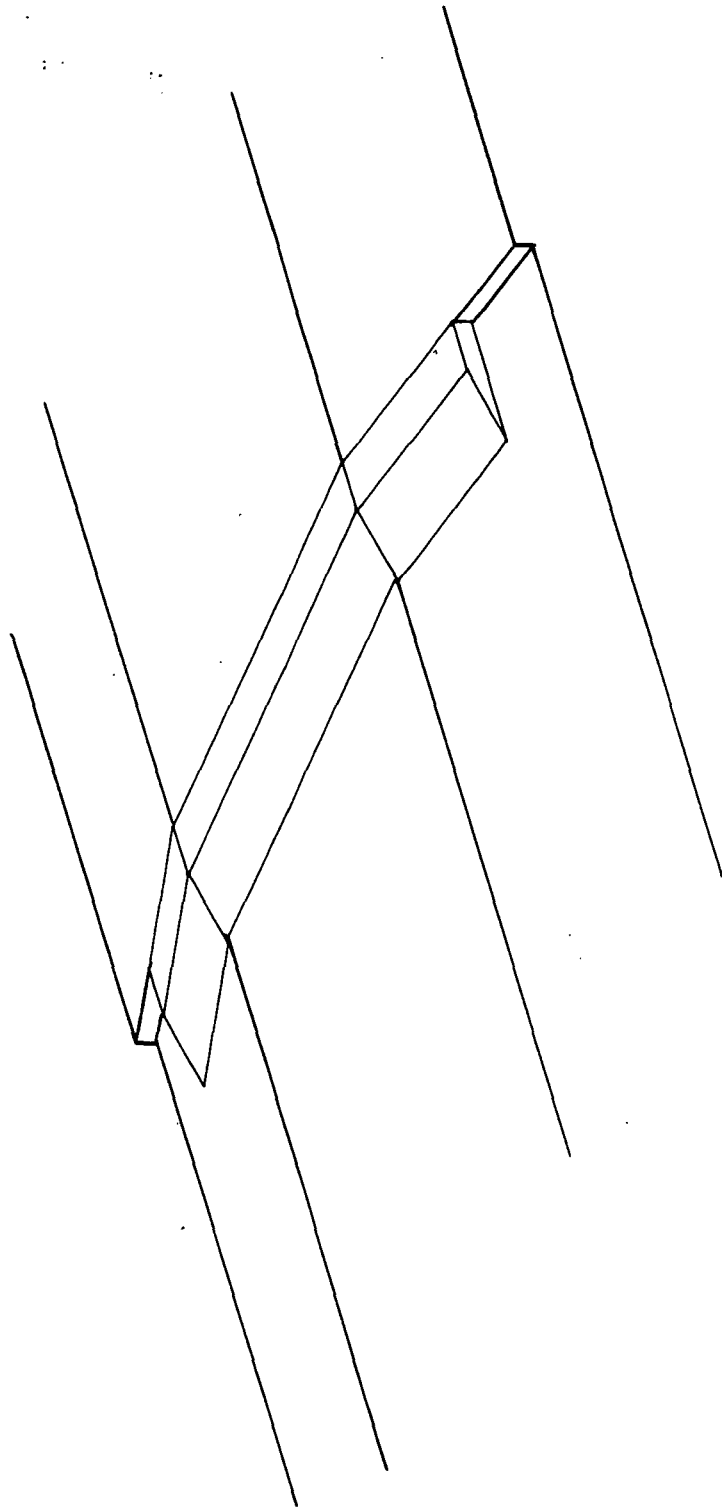


Figure 4.2-17 Shingle Lay-up Tool Surface Showing 12° Wedge

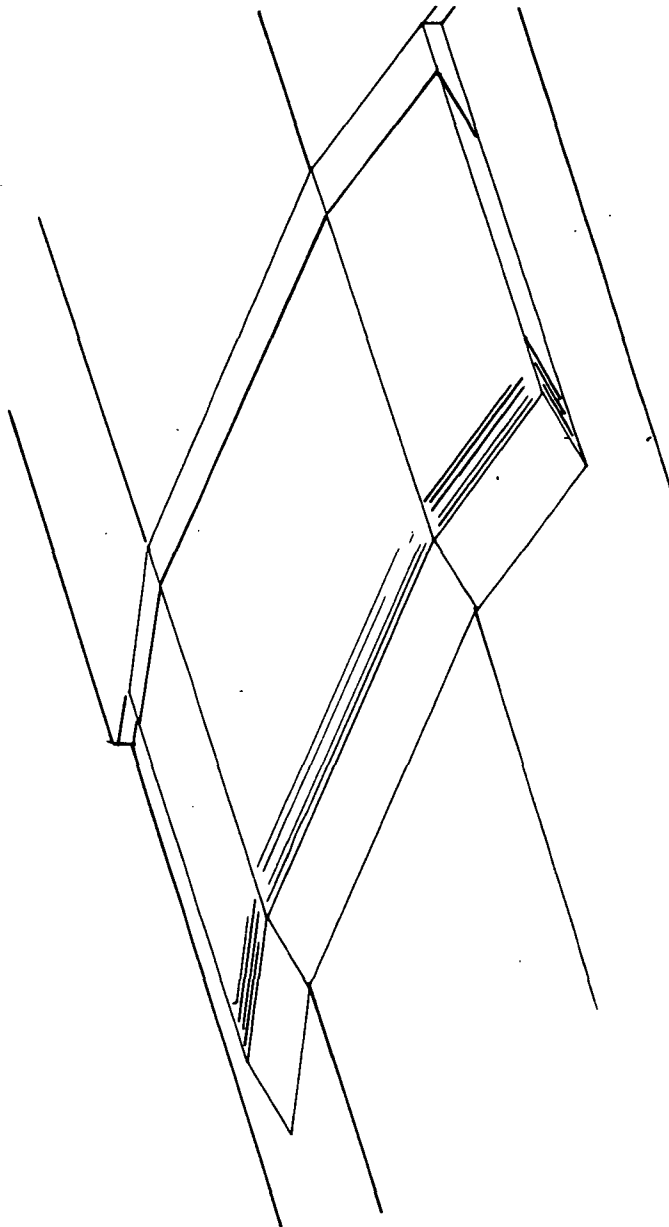


Figure 4.2-18 Shingle "B" Staged Standard Density Carbon Phenolic Liner

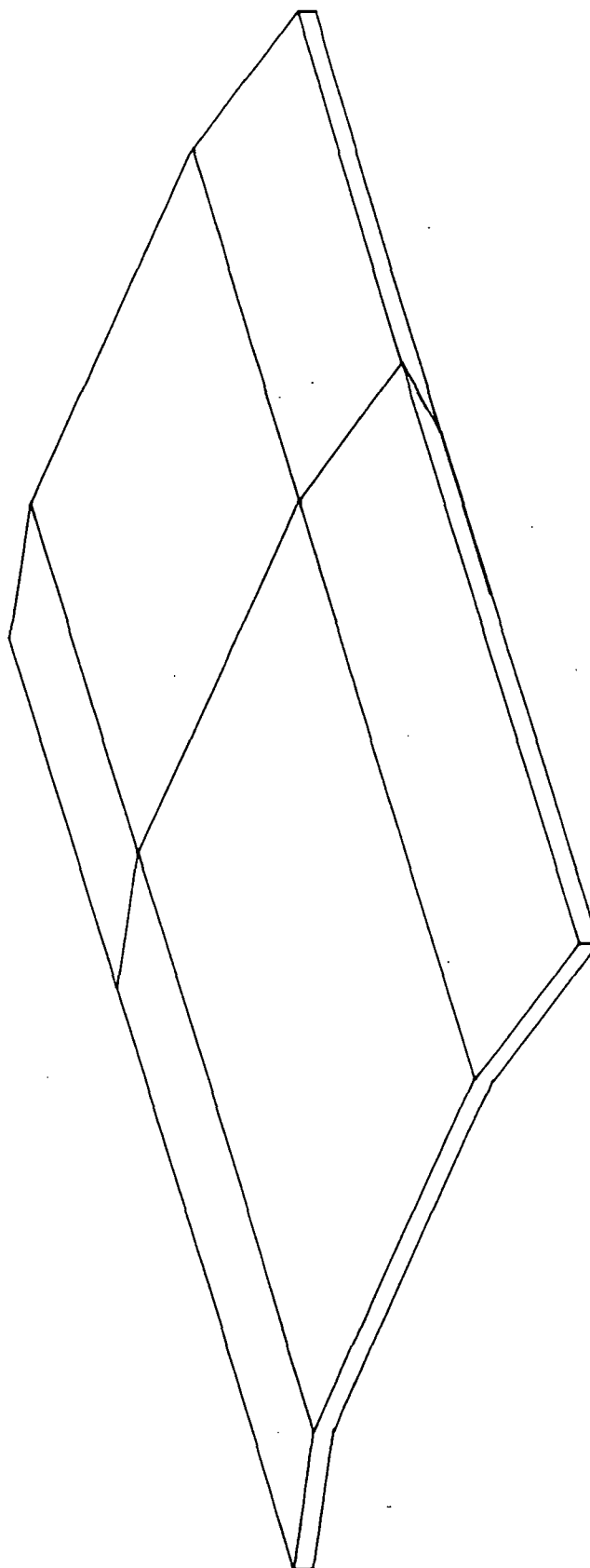


Figure 4.2-19 Shingle "B" Staged Standard and Low Density Carbon Phenolic Liners

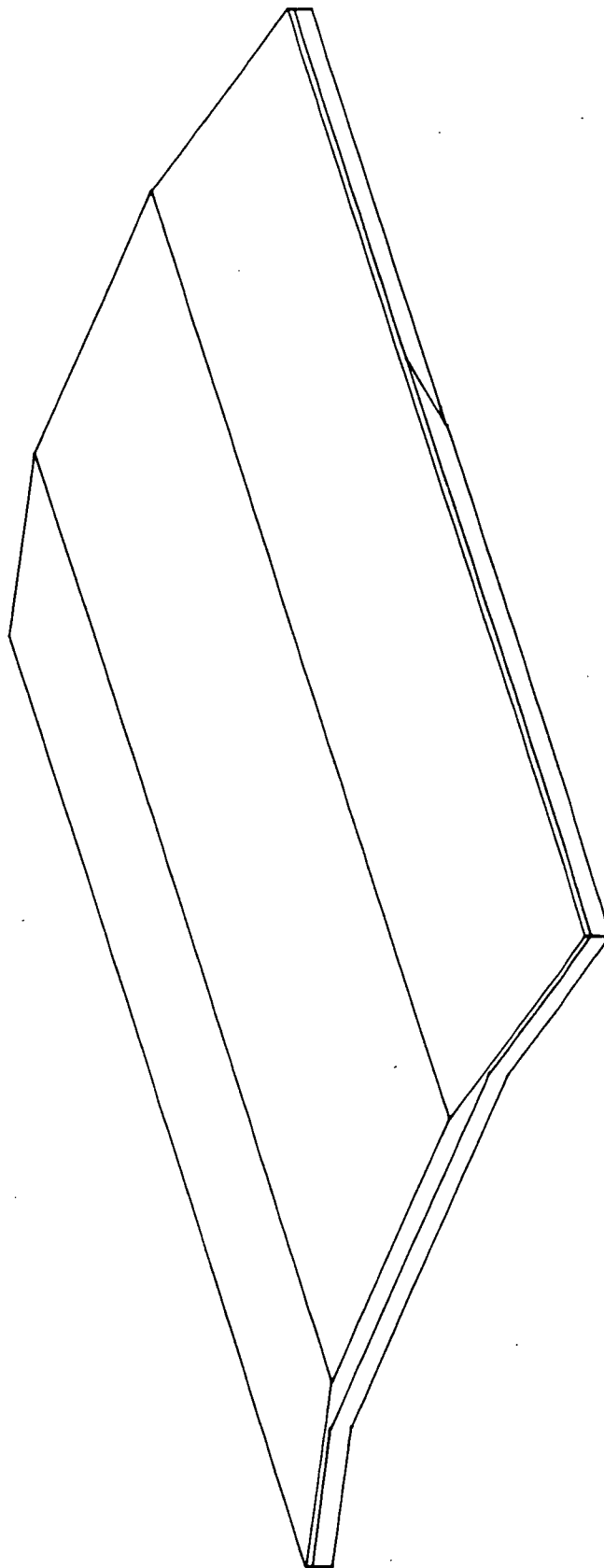


Figure 4.2-20 Shingle with Graphite Phenolic Shell in Place

4.3 TEST FEASIBILITY

4.3.1 Bench Test

In the present program, it was initially considered that bench test merely implied deployment and leak testing. It became apparent that certain other "bench tests" must precede these system tests. Therefore the discussion in this section has been divided into two parts, Bench Tests and Deployment/Load tests.

A. Bench Testing

Initial tests of a single actuator are really bench tests in the literal sense. This testing is described in Appendix A. When six actuators (a shipset) are attached to a shipset of shingles, a system is evolved, ready for deployment load testing.

The other portion of bench testing involves the structural test of single shingles and the preparation of samples cut from shingles to determine their fabricated properties.

B. Deployment Tests

Preliminary planning was accomplished to determine the test set-up and tooling required to verify the ability of SLEEC to deploy under simulated load conditions and to assess the amount and location of possible leakage within the SLEEC system. Figure 4.3-1 outlines the test activity.

SLEEC will be subjected to deployment load testing in a nozzle up position. The deployment tooling consists of a series of load plates hung from the ceiling on supports. As SLEEC is deployed, the extending shingles progressively "lift" a series of plates off supports. The weight of the plate is supported by the shingles through a series of 36 rubber rollers on each plate-- one for the each flat of each shingle. The weights of the plates are varied so as to provide the approximate radial and axial loading to a unit length of SLEEC at that extension distance-- duplicating a changing internal pressure profile. The test set-up is shown in Figure 4.3-2. The load deployment tests will incorporate an Electronic Control Unit (ECU) and other instrumentation (position transducers, etc.) similar to those which will be used as part of the flight deployment system. Motion pictures and video tape will be used to record motion and as a basis for photogrammetry if required.

For leak tests, the SLEEC will be assembled in a vertical nozzle-up attitude. Test tooling will be designed and fabricated to provide a seal at the forward and aft ends of the assembly. An annular centerbody will be employed to reduce free volume within the SLEEC. The centerbody will be designed for use at 50 and 100% extension distances. The SLEEC will be leak tested and proof load tested using this set-up with pressure levels TBD. The leak test will be conducted in proximity to the system using a trace gas at low pressures. The gas load tests will be conducted remotely. The test set-up for leak testing remains essentially the same as originally envisioned in Figure 4.3-3

It does not appear feasible to perform any vibration testing on SLEEC other than that realized during static test. Any vibration test requires that a plume load be applied to SLEEC with out restraining any movement of one component of the system with regard to another. This rules out bladders and other devices which would impart structural rigidity to SLEEC. It is therefore recommended that static test opportunities be utilized to acquire vibrational shock data.

4.3.2 Static Test

One of the major drivers regarding the test of SLEEC on an SRB during static test is the number of tests required to obtain verifiable char and erosion data as well as delivered performance. The number of such tests required for this purpose varies between different government agencies and must be agreed on with NASA/MSFC. Three tests have been considered in formulating the Development Plan of Section 4.4.

The static test firings must be conducted at simulated altitude conditions to obtain correct delivered performance values and not jeopardize the SLEEC system due to flow separation. Therefore, since there is no altitude facility large enough for these tests, the use of a diffuser at a normal static test site must be planned for and costed with NASA/MSFC cooperation.

The SLEEC would be assembled to the SRB nozzle and tested during a static firing of an SRB at the Thiokol T-24 test stand (shown in Figure 4.3-4). As shown in Figure 4.3-5, the HPN/SLEEC would be submerged in the diffuser with an open annulus around the motor. The diffuser pumping action would provide a pressure environment of approximately 7 psia at the SLEEC exit plane when deployed during action time. The diffuser design would have to consider cooling, thrust reaction, instrumentation, photo and other requirements. Motion photo would be the primary measurement requirement to verify SLEEC deployment and survivability during action time and prior to any possible damage caused by "blow back" when the diffuser unloads at end of action time.

Test instrumentation would include diffuser and exit cone pressures, thermocouples and strain gages, and enough system position vs time data to determine simultaneity. Thrust vectoring would be used to obtain TVC inertial and SLEEC vibration data, but would have to limited due diffuser proximity and pressure influence.

4.3.3 Flight Test

Preliminary planning for flight testing was accomplished to recognize and incorporate features in the SLEEC design, hardware or operation which would ensure redundant, fail-safe operation. The first flights can be made essentially risk-free by two methods. First, SLEEC operation can be controlled such that any failure in one unit can be either duplicated in the second unit or so that both units can be simultaneously jettisoned to prevent any overturning moment. Second, SLEEC can compensate for lighter payloads by throttling back the main engines slightly. In case of a SLEEC malfunction, the main engine thrust can be increased to avoid mission failure.

The SLEEC will be installed during SRB final assembly. The actuation system would interface with the Electronic Control Unit (ECU) and would include interfaces for deployment power and braking, command and position feedback, and system instrumentation. The system design would consider the following fail-safe options:

Comparator circuitry that demands deployment simultaneity between both SLEECs within a given tolerance band or else deployment is terminated to preclude an asymmetric overturning moment,

or

Development of a detection and jettison system that would jettison both SLEECs in the event that one suffered catastrophic failure during flight- again to prevent asymmetry.

Flight test instrumentation would include position transducers, accelerometers and thermocouples.

TEST SEQUENCE	TEST TYPE	OBJECTIVE	TEST EQUIPMENT AND INSTRUMENTATION	POSSIBLE PROBLEMS/ FAILURE MODES	CORRECTIVE ACTION
1	FIT	VERIFY DIMENSIONAL INTERFACES AND COMPONENT FIT-UPS	MICROMETERS, CALIPERS, DIAL GAGES, FEELER GAGES, ETC	POOR FIT-UPS	RE-FIT/MACHINE
2	FUNCTION	VERIFY DEPLOYMENT FUNCTION - EEC/ACTUATOR COMPATIBILITY - ACTUATOR CONTROLS	POWER SOURCE, DIAL GAGES, FORCE TRANSDUCERS	BINDING, EXCESSIVE RUN-OUT, INSUFFICIENT ACTUATOR CAPABILITY, STRUCTURAL FAILURE	IDENTIFY AND MODIFY DISCREPANT PARTS - RETEST
3	INTERNAL PRESSURE	DETERMINE LEAK RATES AND LOCATIONS	REGULATED PRESSURE SOURCE, ENTRANCE AND EXIT CONE CAPS, PRESSURE TRANSDUCERS, STRIP RECORDER, LEAK DETECTOR, DIAL GAGES	EXCESSIVE LEAKAGE, SEAL EXPULSION/ DAMAGE, STRUCTURAL FAILURE	REWORK SEALS AND DEFECTIVE PARTS - RETEST
4	DEPLOYMENT LOADS	DETERMINE EFFECT OF PREDICTED THRUST LOADS ON THE DEPLOYMENT FUNCTION - VERIFY ACTUATOR CAPABILITY	POWER SOURCE, DIAL GAGES, FORCE TRANSDUCERS, SPRING LOAD SIMULATORS	BINDING, EXCESSIVE RUN-OUT, INSUFFICIENT ACTUATOR CAPABILITY, STRUCTURAL FAILURE	IDENTIFY AND MODIFY DISCREPANT PARTS - RETEST

Figure 4.3-1

Bench Deployment/Loads Plan

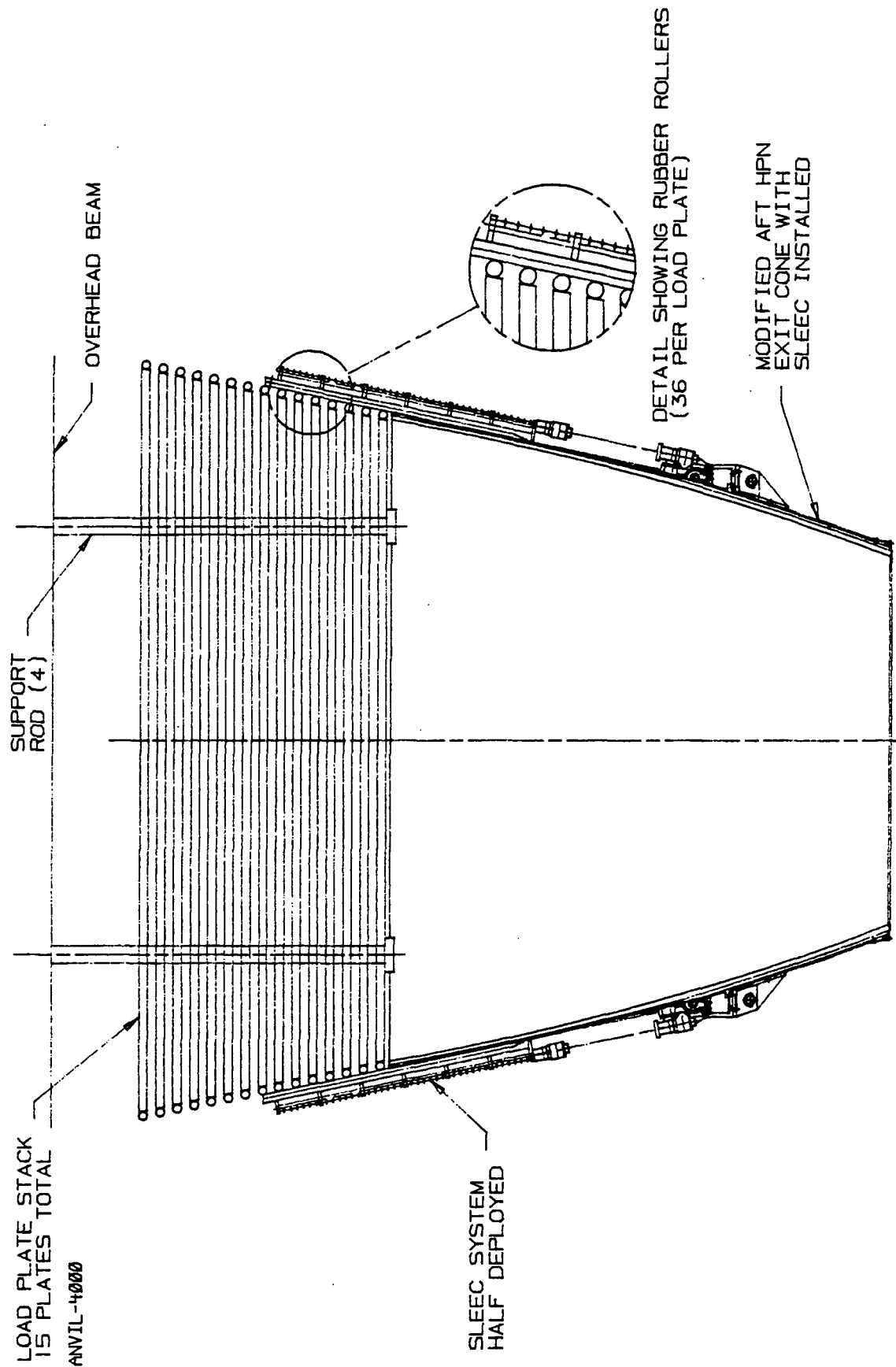


Figure 4.3-2

Deployment Load Test Set-Up

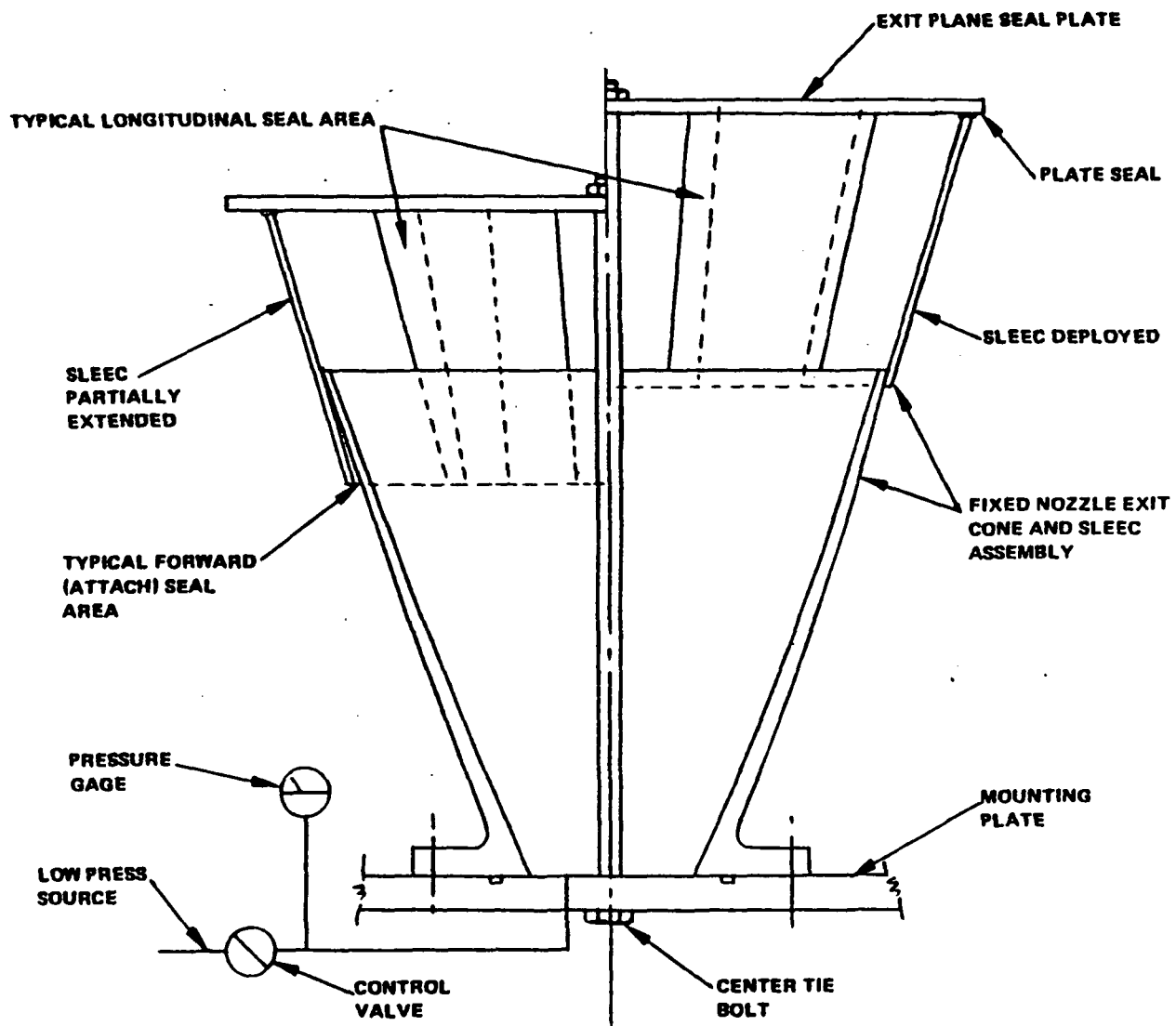


Figure 4.3-3

Leakage Test Set-up

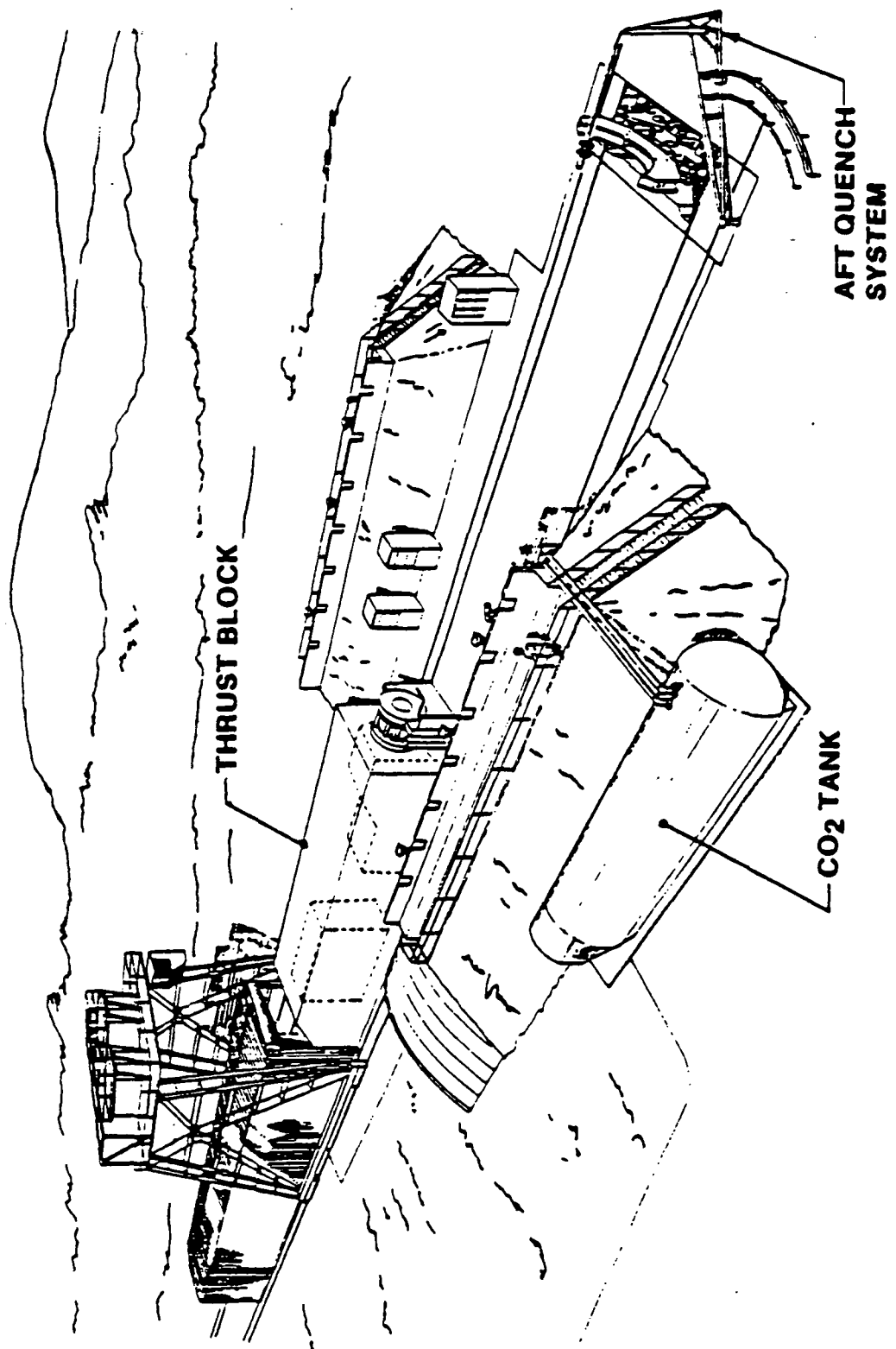


Figure 4.3-4

T-24 SRB Static Test Stand

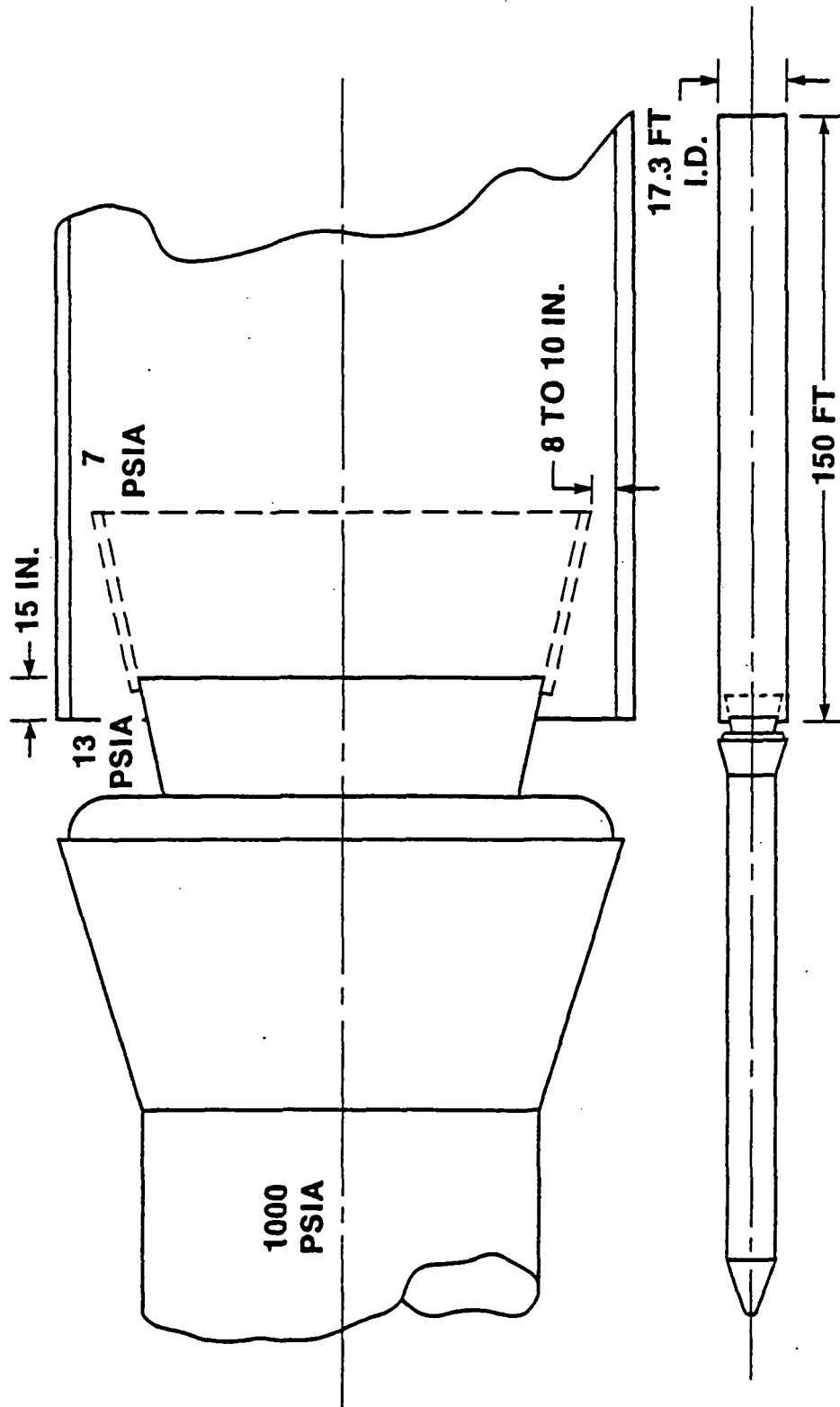


Figure 4.3-5

Jet Pipe Diffuser Schematic

4.4 DEVELOPMENT PROGRAM DEFINITION

On the basis of the feasibility study and the fabrication and test plans considered, Aerojet has defined a development program which will result in the successful incorporation of SLEEC on the Shuttle SRB. This development program, presented in Figure 4.4-1, details all necessary development tasks from initial design and design verification through flight test, and constitutes a 5 year effort with a preliminary ROM value of \$15 million not counting motor test tooling or costs.

Highlights of the plan are as follows:

- A. Phase I is comprised of the design and fabrication of 2 inner and 2 outer shingles, 1 at a time. This will allow mold design changes to account for in-process warpage. The shingles will be structurally tested and as-fabricated properties determined. A single actuator assembly will be bench tested by Garrett.] to verify structural adequacy and performance.
- B. Phase II updates component design and accomplishes the fabrication of 2 shipsets (each shipset is 12 shingles or enough to build 1 SLEEC unit) of shingles, modification of 1 exit cone, and fabrication of an actuator shipset (6 actuators). One assembly will be made and deployment tested in Phase II. After testing, this unit will be used for the first static test in Phase III.
- C. Phase III comprises 3 static tests and 1 Flight test. The static tests require a large diffuser to simulate altitude conditions. Phase III requires the fabrication of 2 SLEEC assemblies for static test and 2 for first flight.

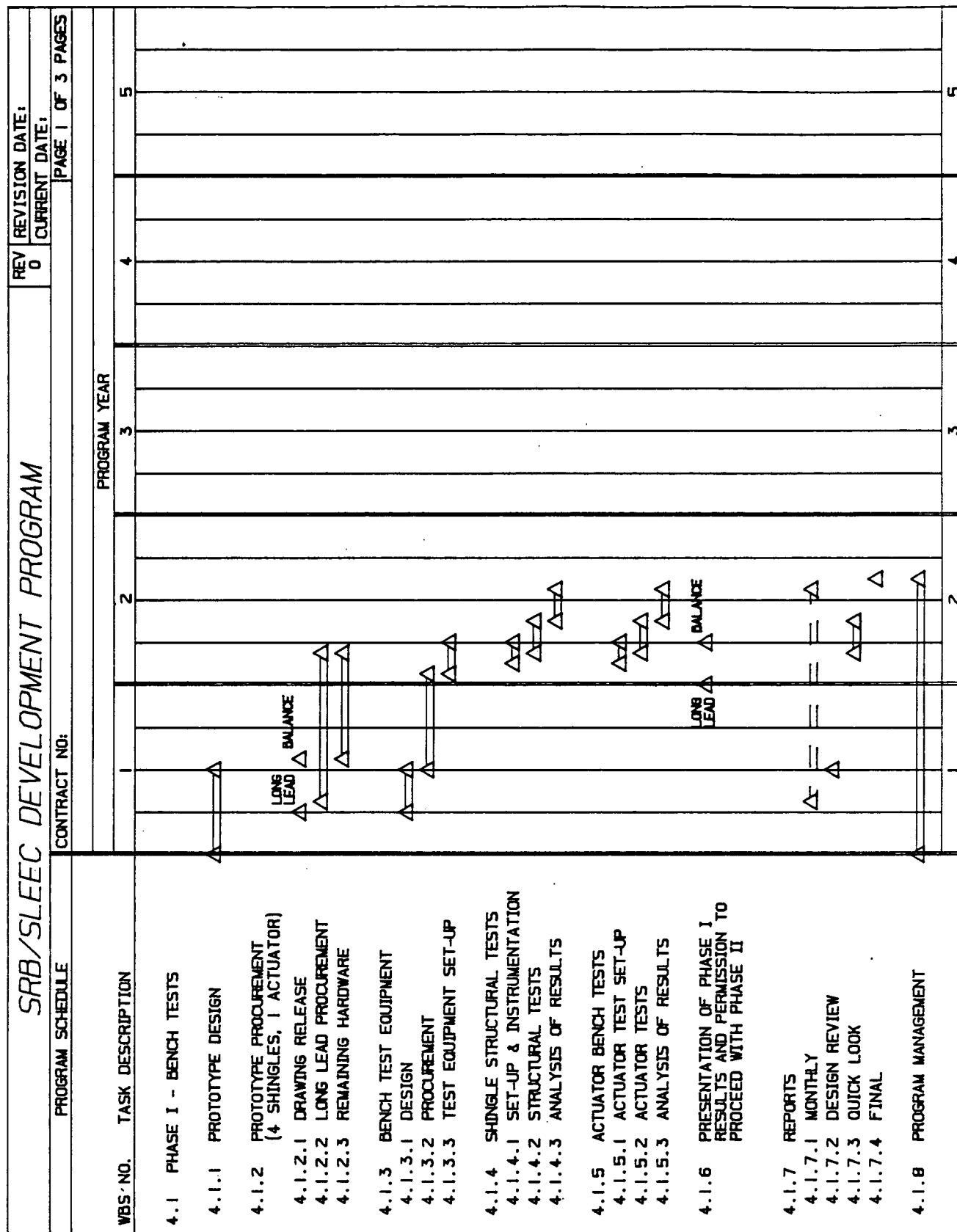


Figure 4.4-1A

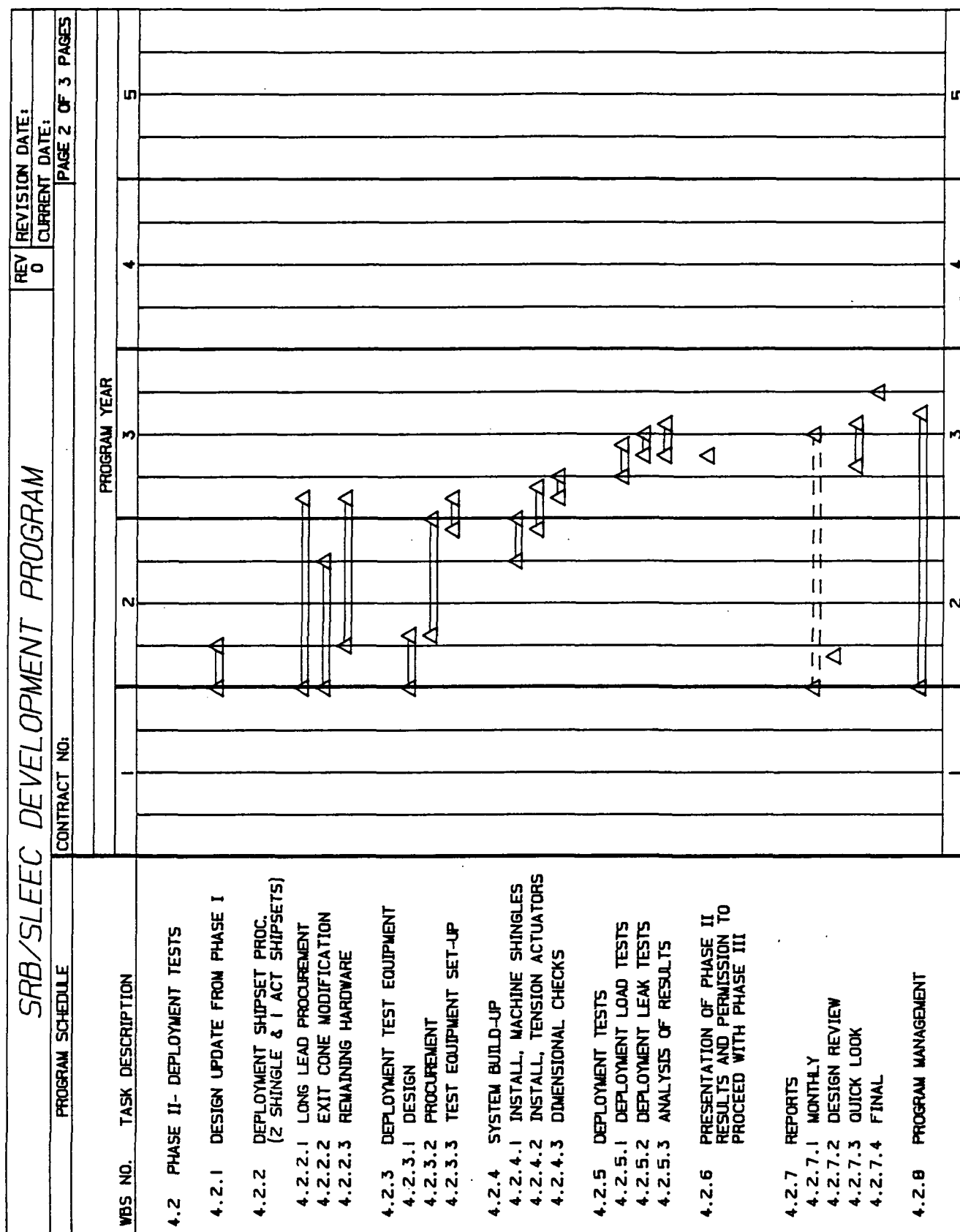


Figure 4.4-1B

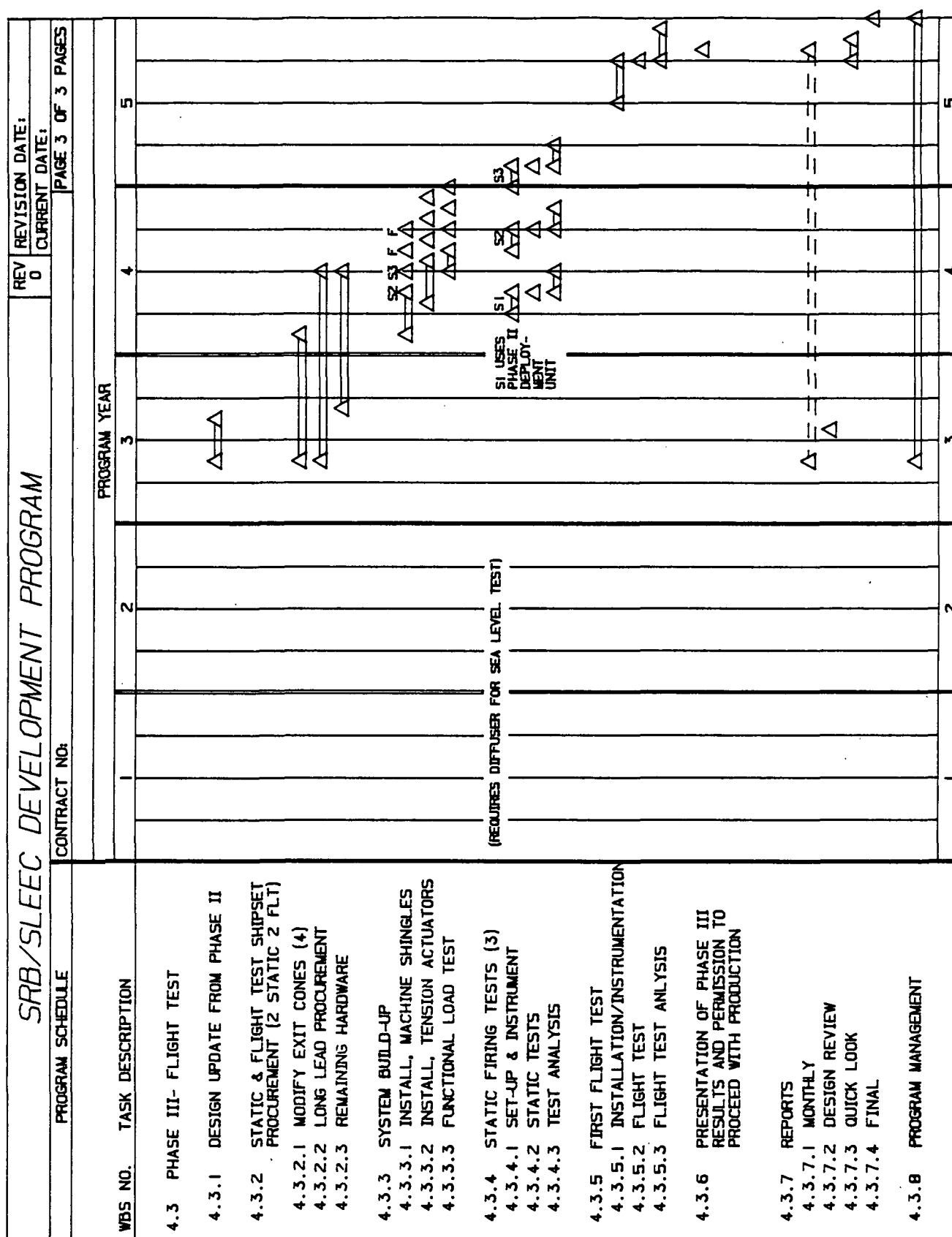


Figure 4.4-1C

4.5 RECOMMENDATIONS

Many events took place during the course of the present program which made a highly coordinated effort between NASA/MSFC and Aerojet somewhat difficult. Additionally, this was a stereotype feasibility study in that it raised many more questions than it answered. Aerojet recommends a strong cooperative effort between NASA/MSFC and itself in order to pursue the study program defined in Figure 1.0-5 so that these questions might be settled.

SRB/SLEEC (SOLID ROCKET BOOSTER/
SHINGLE LAP EXTENDIBLE EXIT CONE)
FEASIBILITY STUDY

APPENDIX B

STRESS ANALYSIS FOR THE SRB/SLEEC

STRESS ANALYSIS OF THE SRB/SLEECTable of Contents

I.	DISCUSSION
1.1	Method of Analysis
1.2	Results Summary
1.3	Additional Analysis Required
II.	DESIGN CRITERIA
2.1	Basic Loads
2.2	Basic Geometry
2.3	Basic Boundry Conditions
2.4	Basic Material Properties
III.	RESULTS
3.1	NASTRAN Grids
3.2	Run 1.0 Internal Pressure
3.3	Run 2.0 One "g" Lateral Load

SECTION I DISCUSSION

1.0

1.1 METHOD OF ANALYSIS

- . Summary of NASTRAN runs
- . Sketch of NASTRAN model
- . Table of NASTRAN element selection

1.2 SUMMARY OF RESULTS

1.3 ADDITIONAL ANALYSIS REQUIRED

- . Analysis to Date
- . Additional Loads
- . Gas Leakage @ Shingle Interface
- . Run Matrix

1.1 METHOD OF ANALYSIS

The loading conditions shown in Table 1.1 were evaluated using a NASTRAN model of the fully deployed SLEEC configuration.

TABLE 1.1
SUMMARY OF NASTRAN RUNS

NASTRAN			
Cond.	Load	SOL	Boundary Conditions
1.0	Internal Pressure 13.5 > p > 3.5 psi	61	. Symmetry @ 0° & 30° edge (2/4/6) . Seals effective @ Shingle Contact surface (RBE2-1)
	1G		
2.0	Lateral Load WT= 3800#	81	. Dihedral Symmetry . 30° Fundamental Region Contact Surface

The nature of the analysis is to confirm weights of the structural components and estimate deflections of the structure.

Figure 1.1 is a "sketch" of the NASTRAN model showing the fundamental region (0°-30°) components and associated code elements. Plate (quad) elements were used on the shingles and gussets. The plate thickness was varied to reflect overwrap pattern. The ablative liner was not modeled which is conservative since it would increase the structure stiffness and reduce deflections.

Rods were chosen for the ball screw since they exhibit only extentional and torsional but no bending stiffness, while bars were

ORIGINAL PAGE IS
OF POOR QUALITY

1.1.2

NASTRAN MODEL - sketch
Fundamental Region

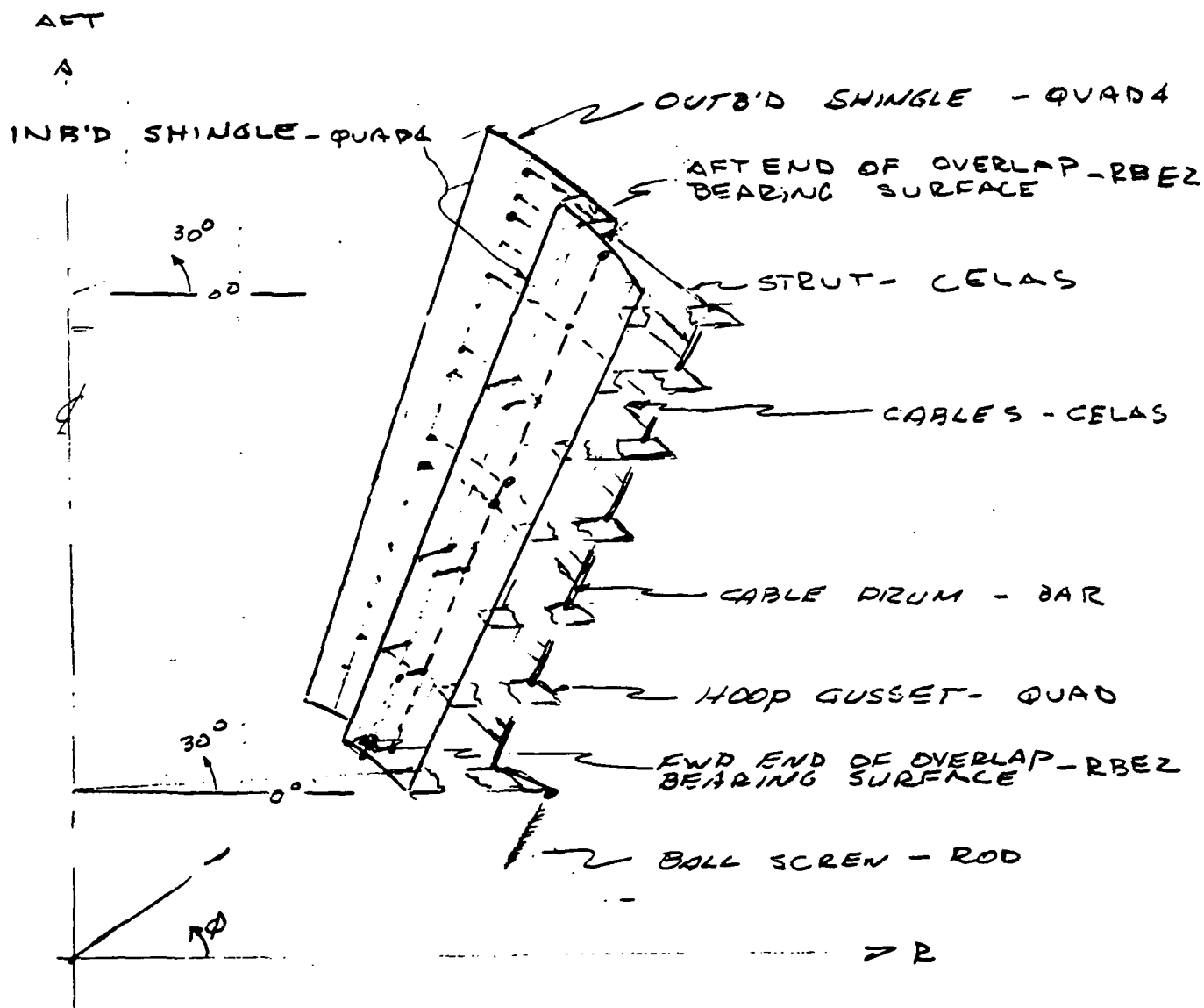


Figure 1.1.1

1.1.3

used to reflect the shear and bending capability of the drum which unwinds the cable. Springs were used to model the strut and cable structure.

Elements (RBE2) were placed at the bearing interface between outboard and inboard shingles (Ref. Fig. 1.1) to let them slide with respect to each other in the hoop and axial direction. They are constrained to move together radially. At the forward edge, an additional constraint in the axial direction transfers thrust in the outboard shingle through a RBE2 element to the inboard shingle which in turn dumps it into the ball screw. There is a fitting at this location which is designed to accomodate this load transfer.

Table 1.2 summarizes some of the data used to define the element properties and constraints and Figure 2.4.2 the shingle structural thickness distribution.

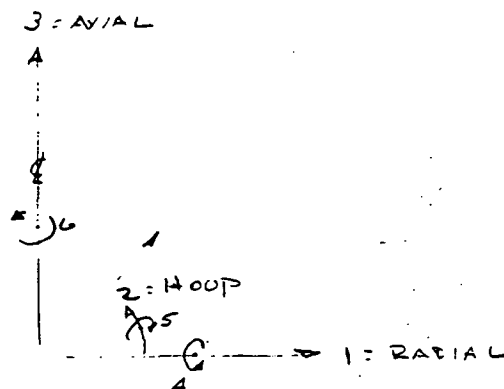
ELEMENT VS COMPONENT SELECTION

TABLE 1.2

COMPONENT	NASTRAN ELEMENT*	COMMENTS
Outboard Shingle	CQUAD4	. Constrained in the 4 direction. . Constrained in the 1 direction @ fwd edge
Inboard Shingle	CQUAD4	. Constrained in the 4 direction . Constrained in the 1 direction @ fwd edge
Overlap Surface between outb'd & inb'd shingle	RBE2	. Constrained in direction 1 . Free to slide in 2 & 3 directions
Strut	CELAS2	. Constrained to move in the 2 direction
Cables	CELAS2	. Constrained to move in the 2 direction
Cable Drum	CBAR	. To follow the gusset motion, CBAR's are constrained in the 1 & 2 directions by RBE2 to the hoop gussets
Hoop Gusset	CQUAD4	. Constrained in directions 4 and 6 where attached to the inboard shingles
Forward End of overlap bearing surface	RBE2	. Constrained in direction 1 & 3 . Transfers thrust from outb'd to inb'd shingle
Ball Screw	CROD	. Constrained in the 1, 2, 4, and 5 directions . Most forward point is constrained in 1, 2, 3, 4, & 5.

*In this Table, CQUAD4=SHELL, RBE2=MPC, CELAS2=SPRING, CBAR=BAR, CROD=ROD.

Fig. 1.1.2



1.2 RESULTS SUMMARY

1.2.0

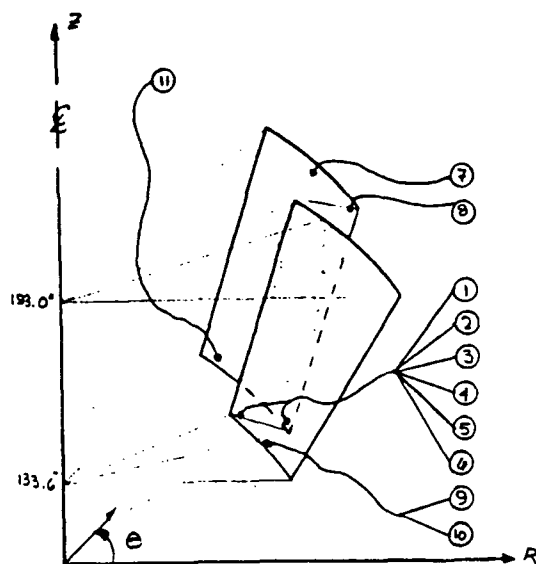


Fig. 1.2.1

TABLE 1.3: TYPICAL MARGINS OF SAFETY

ITEM	SEGMENT NUMBER	LOAD CONDITION	STRESS (PSI)			MARGIN OF SAFETY
			TYPE	PREDICTED	ALLOWABLE	
(1)	1	PRESSURE	MERID.	32,300	70,000	1.2
(2)	1	PRESSURE	MERID.	29,500	70,000	1.4
(3)	1R--3L	1G	MERID.	74,300	70,000	-0.1
(4)	1R--3L	1G	MERID.	72,000	70,000	-0.03
(5)	2R	1G	MERID.	71,900	70,000	-0.03
(6)	2L	1G	MERID.	40,500	70,000	0.7
(7)	1	PRESSURE	HOOP	12,800	70,000	4.5
(8)	1	PRESSURE	HOOP	18,800	70,000	2.7
(9)	1R	1G	HOOP	5,300	70,000	12.2
(10)	3R	1G	HOOP	9,800	70,000	6.1
(11)	2R	1G	HOOP	1,330	70,000	51.6

NOTE: Items 1-6 in TABLE 1.3 are grid points which are RBE2'D together at the interface and thrust transfer point between the inboard and outboard shingles at the forward edge.

1.3 ADDITIONAL ANALYSIS REQUIRED

To date the analysis has used:

- (.) Isotropic material properties
- (.) Assumed contact at bearing surfaces between inboard and outboard shingles
- (.) Neglected the stiffness of the ablative liner

These approximations were made to facilitate reconciliation of NASTRAN results to engineering mechanics. The additional complexity added by the above items to the already complex geometry would make the understanding of the results of a first time study very difficult. There is a tendency to attribute results that appear irrational to the complex material properties or boundary conditions. The additional complexity also adds considerably to debugging error messages and computer time per solution.

Now that solutions have been derived for the (1) symmetrical internal pressure and (2) unsymmetrical lateral side load conditions, the following loading conditions should be examined:

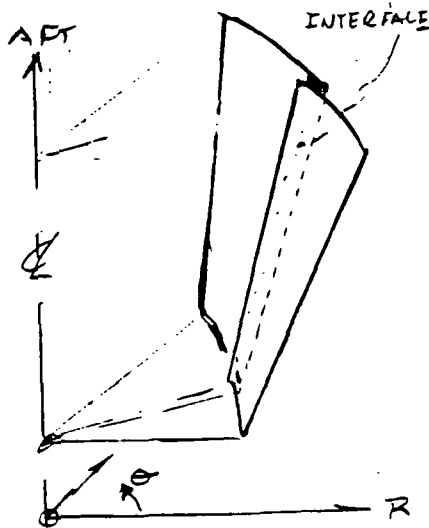
- (.) External aerodynamic loads
- (.) Partially deployed configurations
- (.) Gaps at bearing surface between inboard and outboard shingles by using non-linear springs
- (.) Model the liner geometry and thermal map at discrete time intervals
- (.) Effects of non operating or lagging ball screws

Table 1.3 shows the mix of:

- (.) Pressure and thermal loadings
- (.) Deployed and eroded geometries
- (.) Possible boundary conditions
- (.) Symmetrical, cyclic symmetry, and non-linear solutions

which should be run in NASTRAN.

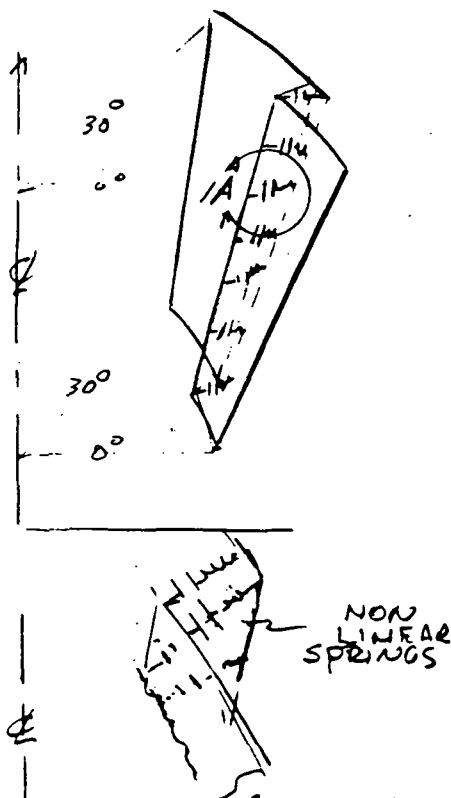
The magnitude of deflections at the shingle bearing interface determines the loadings on each shingle and the extent of gas leakage between shingles.



Using Sol 61, the boundary conditions at the interface are discrete. They are either

- (1) . Free to slide in the hoop (Θ) and axial (Z) direction, but tied together in the radial (R) direction
 - . No internal pressure acts on the interface
- (2) . There is no tie in either the R, Θ , or Z direction
 - . Internal pressure acts on the interface surfaces.

FIGURE 1.3.1



Using Sol 66, a non-linear solution, an initial radial gap is set at the interface and load is not transferred between shingles until the gap closes.

The solution is interactive and the loads are input incrementally until 100% is achieved. At the load level where the gap closes, the additional loads go through the spring. If the gap does not close, its magnitude can be determined.

FIGURE 1.3.2 - VIEW 1A

Axial inertia and internal pressure loads are axysymmetric and the above solutions (61 and 66) use 2/4/6 edge boundary conditions on a fundamental region of 30 degrees of arc. In review, this 2/4/6 edge condition imposes: (Ref: Fig 1.3.3)

- (2) No hoop direction displacement
- (4) No rotation about the radial axis
- (6) No rotation about the axial axis

at the 0° and 30° edges. This makes the deformed geometry axysymmetric.

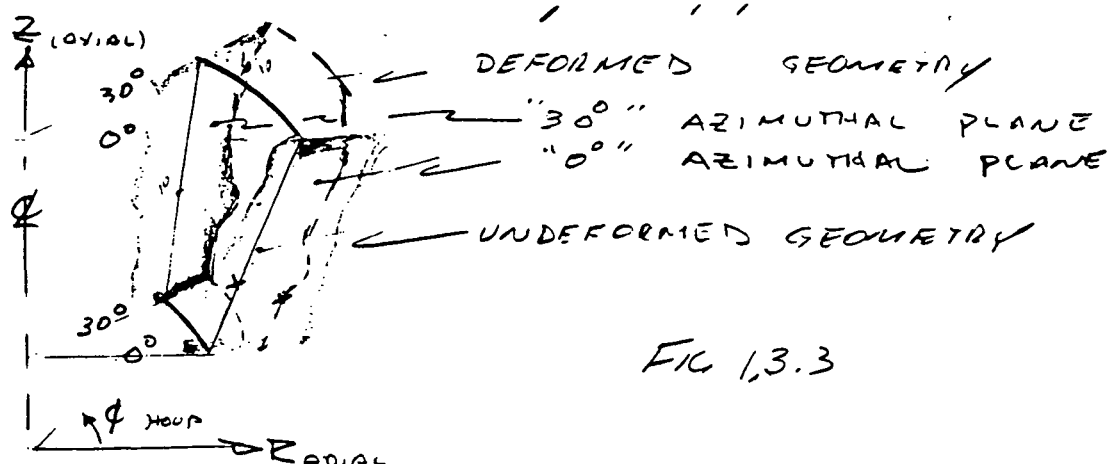


FIG 1.3.3

If the X-sections were initially circular, they may not remain so - grid points on the 0° and 30° azimuthal planes, however, will slide only on those planes while the other grid points can move arbitrarily.

The additional loads on the exit cone are non-axysymmetric. Lateral inertia and external aerodynamic loads tend to arbitrarily deform the initially circular X-sectional geometry.

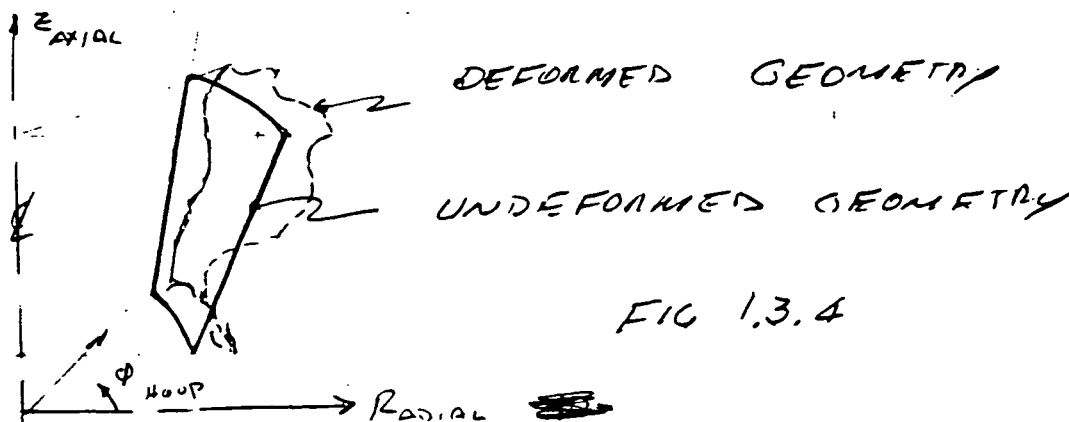


FIG 1.3.4

Solution 66, cyclic symmetry, was used to evaluate these unsymmetrical conditions. A fundamental region of 30° of arc was modeled. It consists of half an:

- (.) Inboard shingle
- (.) Outboard shingle
- (.) Ball screw
- (.) Set of cables, tube & strut

The dihedral option enabled us to "flip" a mirror image of the fundamental region to create 60° of arc or one full set of shingles and support structure.

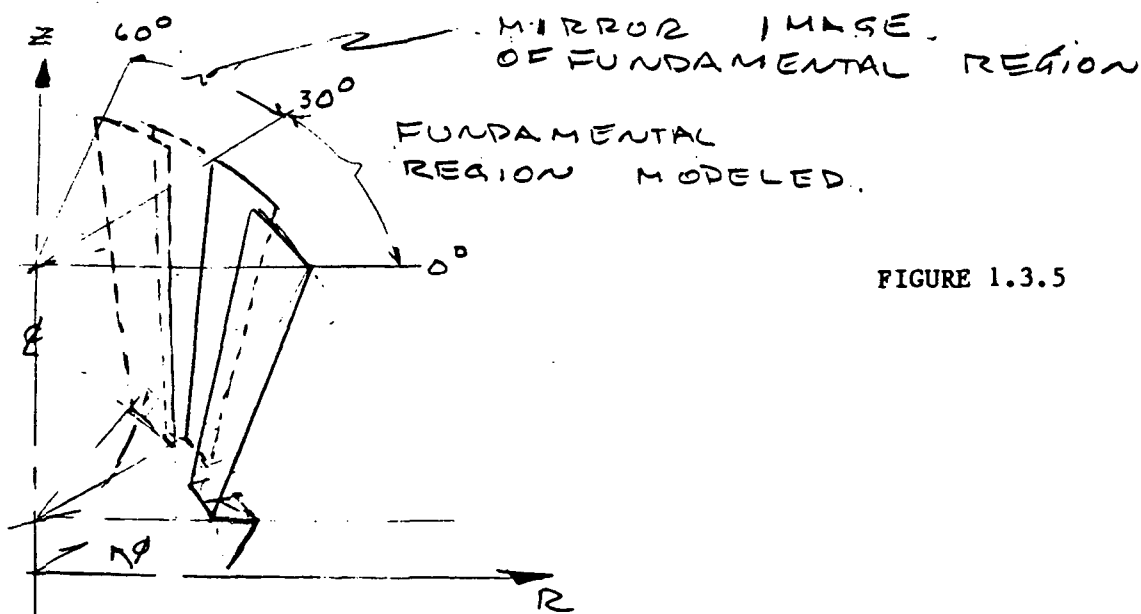


FIGURE 1.3.5

Six sets of the above now make the entire model, where:

- . The initial geometry of each region is identical
- . Each region can be loaded individually
- . Deflections for each region is not identical, but continuity is retained at common edges

1.3.5

Table 1.4 shows the mix of loading conditions and geometries to be investigated and Fig. 1.3.6 is a flow chart of the analysis path.

It should be noted that as the analysis proceeds judgments based on the results at the seal may:

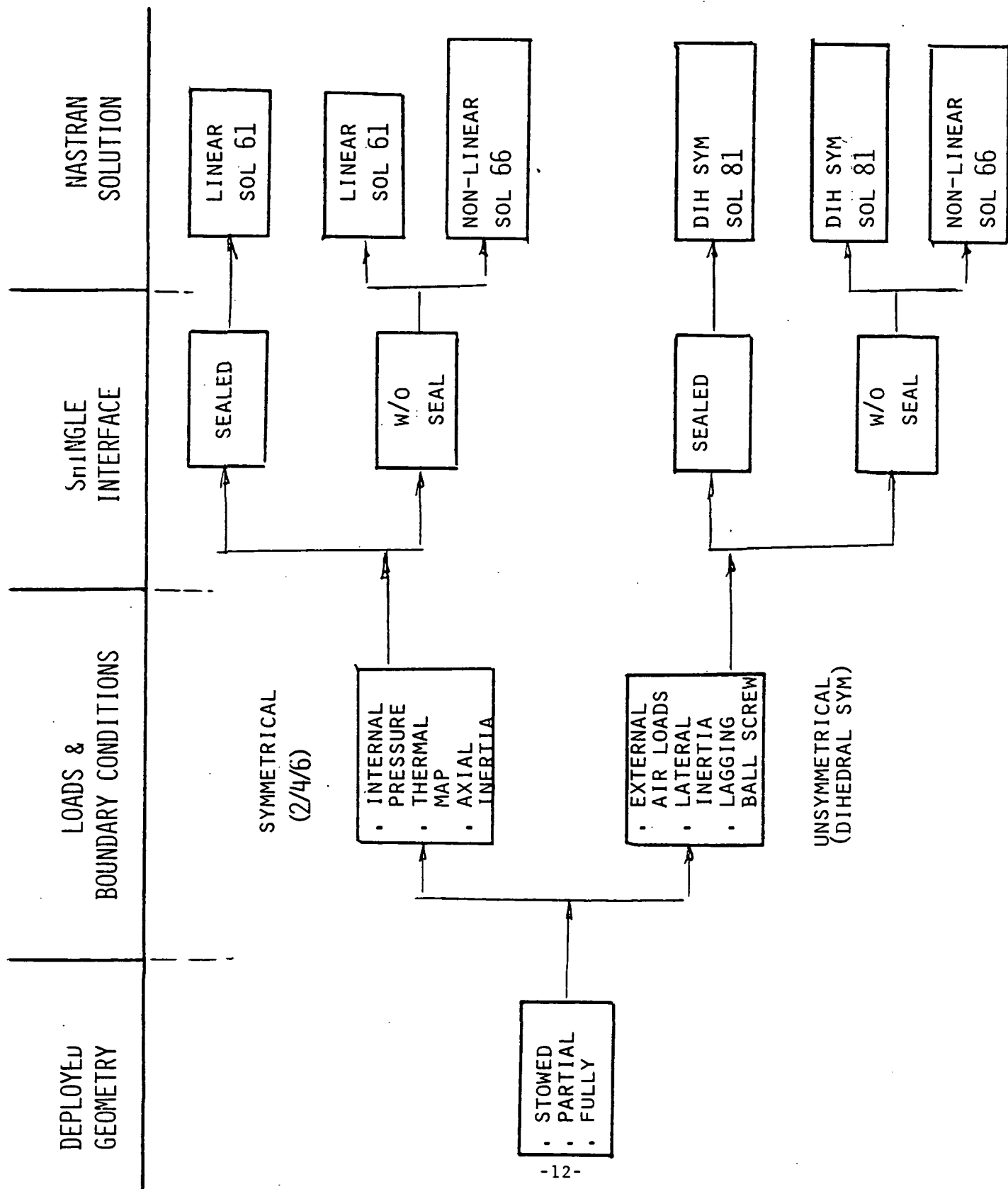
- (.) Eliminate the need for some downstream analysis for symmetric loads.
- (.) Revise the model to a 180° fundamental region for non-axysymmetric loads

This model could then be used to evaluate the following dynamic analyses:

- (.) Normal modes
- (.) Dynamic Response
- (.) Power Spectral Density
- (.) Transient Response

TABLE 1.4

#	Load	Geometry	SOL	Boundary Condition	Comments
1.1.1	Internal pressure	. Fully Deployed	61	246 Sym	Seals assumed effective
1.1.2	"	. Eroded Liner	"	"	Seals assumed not effective
1.1.3	"		66	"	Non-linear springs
2.1.1	"	At start	61	"	Seals assumed effective
2.1.2	"	up	61	"	Seals not effective
2.1.3	"		66	"	Non-linear springs
3.1.1.	"	. 80% Deployed	61	"	Seals effective
3.1.2	"	. Eroded	61	"	Seals not effective
3.1.3	"	Liner	66	"	Non-linear springs
4.1.1	Internal Pressure	. 10% Deployed	61/66	246	As above
4.1.2	Thermal Map	thru	"	"	" "
4.1.3		Fully Deployed	"	"	" "
4.1.4		Eroded liner	"	"	" "
4.1.5			"	"	" "
4.1.6			"	"	" "
4.1.7			"	"	" "
4.1.8			"	"	" "
4.1.9			"	"	" "
5.1.1	Inertia	Fully Deployed	81	Dihedral Symmetry	
5.1.2	& External Aerodynam	Start-up	"		
5.1.3		80% Deploy.	"		
6.1.1	Inertia +	Fully Depl. +	81	Dihedral Sym.	
6.1.2	Aerodynamic +	Eroded			
6.1.3	Int.Press. +	Liner			



ANALYSIS FLOW CHART

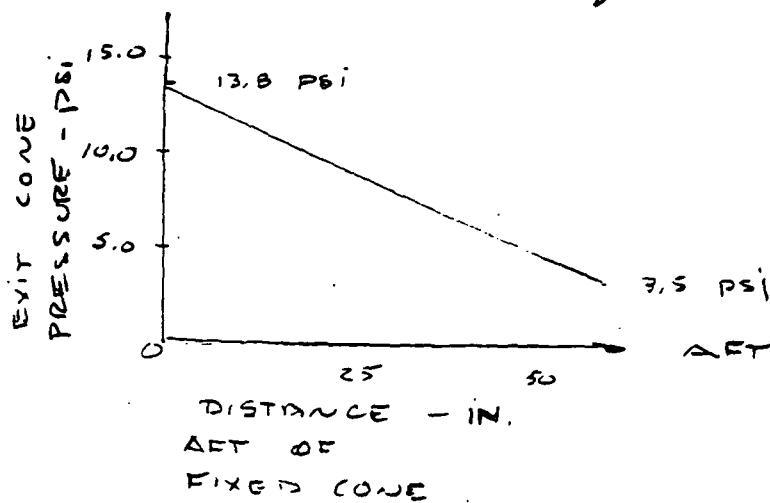
II. DESIGN CRITERIA

2.0

- 2.1 Basic Loads
- 2.2 Basic Geometry
- 2.3 Basic Boundary Conditions
- 2.4 Basic Material Properties and Material Distribution

2.1 BASIC LOADS

c INTERNAL PRESSURE , $p_c = 920$ psi



FIG

WT OF MOVING PARTS - 3800 #

2.2 BASIC GEOMETRY

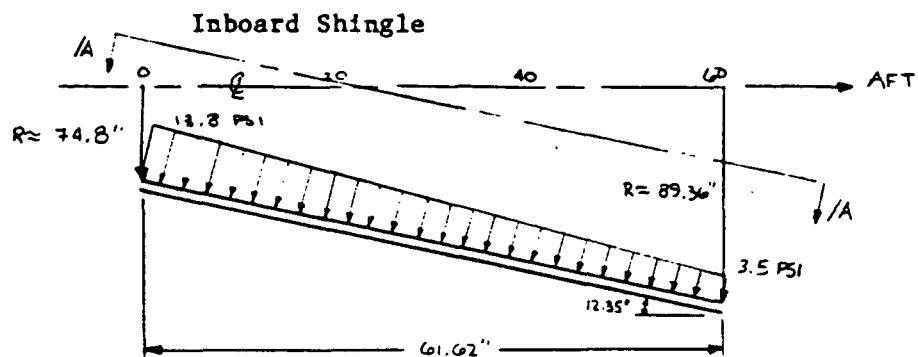


FIG. 2.2.1

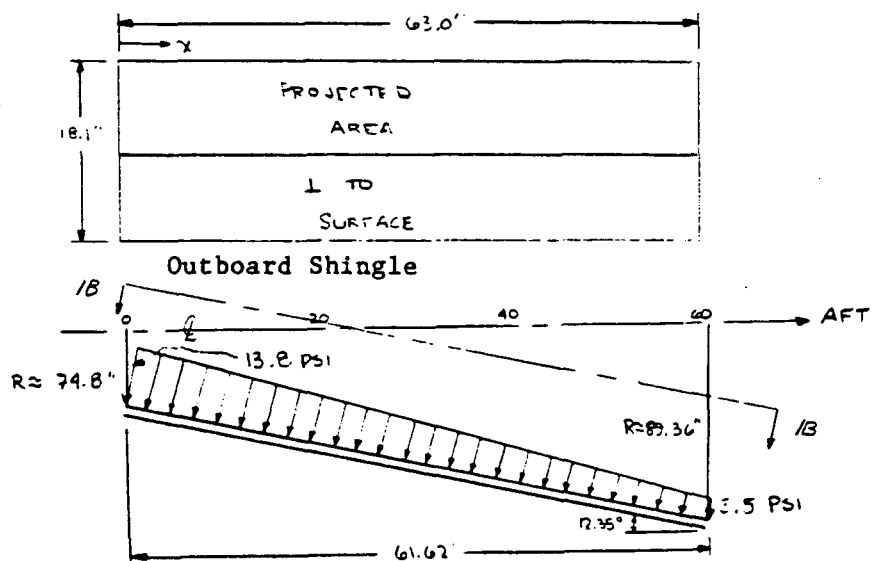
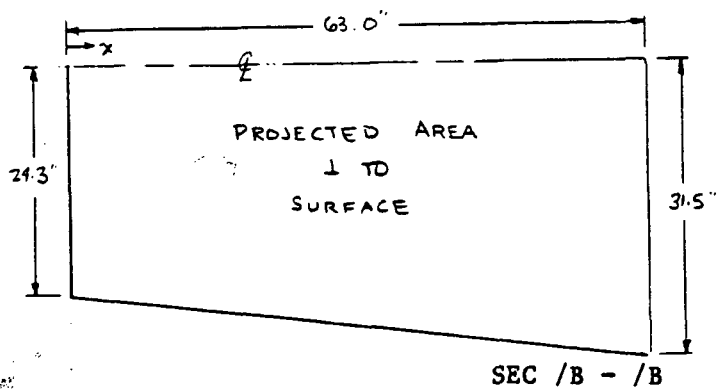
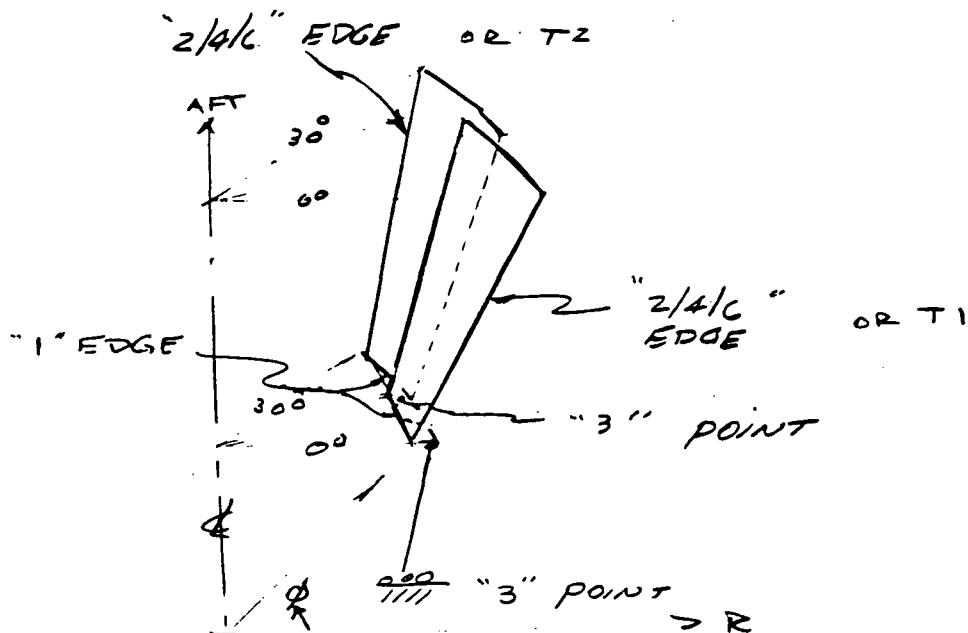


FIG. 2.2.2



2.3 BASIC BOUNDARY CONDITIONS - Fully Deployed

F/S 2.3

SOL 61

- "1" Edge, tied to fixed cone - radially
- "246" Edge, symmetry
- "3" Point, thrust transfer from outboard shingle to inboard shingle
- "3" Point, thrust transfer to fixed cone

SOL 66

TI & T2 Edges for dihedral symmetry, "CYJOIN"

2.4 BASIC MATERIAL PROPERTIES - Isotropic

Shingles - MX 4261

$$E = 10 \times 10^6 \text{ psi}$$

$$G = 3.6 \times 10^6 \text{ psi}$$

$$\nu = .3$$

Actuation Structure

$$E = 30 \times 10^6 \text{ psi}$$

$$G = 11 \times 10^6 \text{ psi}$$

$$\nu = .3$$

Anisotropic material properties for the liner and overwrap as a function of temperature are shown in Figure 2.4.1 and tables 2.4.1 through 2.4.3. These will be used in future analyses.

The allowables used in Figure 2.4.1 were used to compute the margins of safety.

MX 4926 - Bias Molding Tape

TABLE 2.4.1 - Throat Insulation and Exit Cone Liner

(Ref. C-4 Dev Data Per Hercules/Thiokol Rpt. SE025-A2D-C4-Dev-001
and SoRI Preliminary Report dated March 4, 1982)

Temp °F	E_n	E_s	E_t	G	ν_{ns}	ν_{nt}	ν_{st}	α_n	α_s	α_t
	(x10 ⁶ psi)				[10 ⁻⁶ (in./in.)/°F]					
70	1.74	2.55	2.30	.79	.26	.26	.10	8.2	2.0	2.0
350	1.10	2.27	2.00	.67	.26	.26	.10	12.0	3.6	3.6
750	.52	1.78	1.42	.52	.26	.26	.10	36.0	4.2	4.2
1000	.38	1.28	1.02	.38	.26	.26	.10	5.0	1.0	1.0
1500	.08	.30	.30	.08	.26	.26	.10	-16.0	0.6	0.6
3000	.08	.30	.30	.08	.26	.26	.10	-9.5	2.1	2.1
4000	.08	.30	.30	.08	.26	.26	.10	-9.0	5.2	5.2
5200	.08	.30	.30	.08	.26	.26	.10	-12.0	6.1	6.1

Strain Failure Criteria:

$$t_{,s} \text{ (allow)} = 1.20\% \text{ room temp} - 750^\circ$$

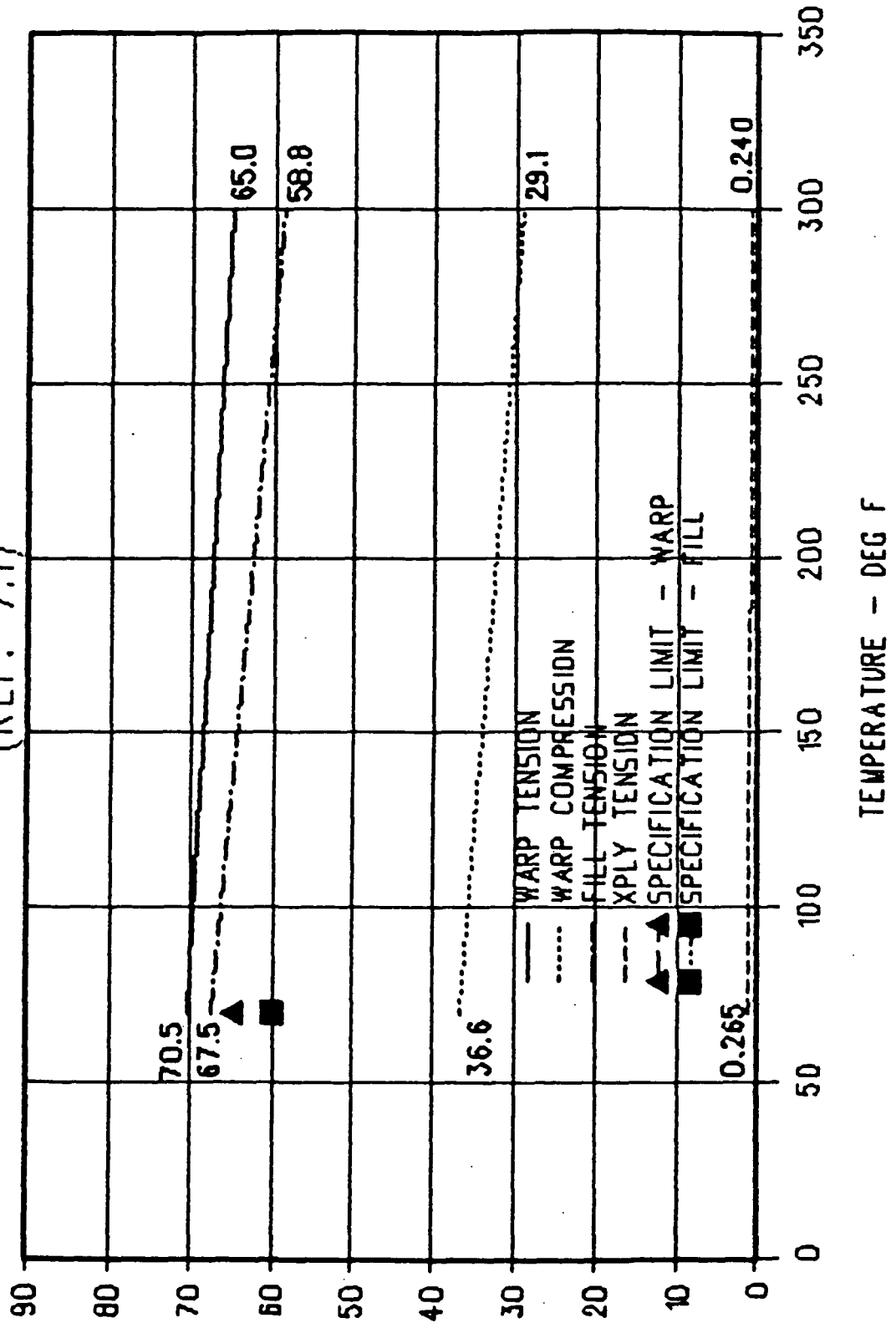
TABLE 2.4.2 - MX 4961 Graphite Phenolic

Exit Cone Overwrap
(Ref SoRI preliminary data report 3-4-82)

Temp °F	E_n	E_s	E_t	G	ν_{ns}	ν_{nt}	ν_{st}	α_n	α_s	α_t
	(x10 ⁶ psi)				[x10 ⁻⁶ (in./in.)/°F]					
70	0.66	9.33	8.49	0.44	.030	.043	.023	16.0	2.0	1.2
300	0.40	8.90	7.59	0.32	.030	.043	.040	12.0	0.22	0.62
600	0.10	1.0	1.0	0.10	.020	.030	.030	-1.90	0.38	0.61

MX 4961 - ALLOWABLE TENSION & COMPRESSION VS TEMP

(REF: 7.1)



2.4.1
Figure 2.4.1 MX 4961 Allowable Tension and Compression vs. Temperature
Average Test Values

ISX - 553815

SOURCE	TENSION			COMPRESSION			SHEAR		
	WARP	FILL	X-PLY	WARP	FILL	X-PLY	WARP	FILL	X-PLY
CDR Report (1)	72,500	67,500	900	---	---	---	2,800	2,900	18,700
SoRI MX 4961 (3)	70,530	67,530	265	36,570	32,470	88,000	3,186	3,350	16,790
FM 5785 (2)	69,940	63,000	870	40,870	---	104,540	2,834	2,988	18,729
SPC-34568A (4)	65,000	60,000	---	43,000	33,000	---	2,500	2,500	---

- 20

(1) Per memo from Armour, dated 9 April 1982

(2) Per Ref. 7.1.

(3) Per Ref. 7.1.

(4) Dated 24 August 1982

TABLE 2.4.3 MX 4961 EXIT CONE OVERWRAP ALLOWABLES AT 70°F

2.4.5

PSHELL COL #	THICKNESS IN	COMPONENT
(1)	1.0	INB'D SHINGLE
(2)	1.0	INB'D SHINGLE
(3)	.4	INB'D SHINGLE
(4)	.3	INB'D SHINGLE
(5)	.5	OUTB'D SHINGLE
(6)	.3	OUTB'D SHINGLE
(7)	.45	OUTB'D SHINGLE
(8)	.55	OUTB'D SHINGLE
(9)	1.0	OUTB'D SHINGLE
(11)	.5	HOOP GUSSET
(16)	.75	TIE TO BALL SCREW

PSHELL DISTRIBUTION
ON THE
SHINGLES

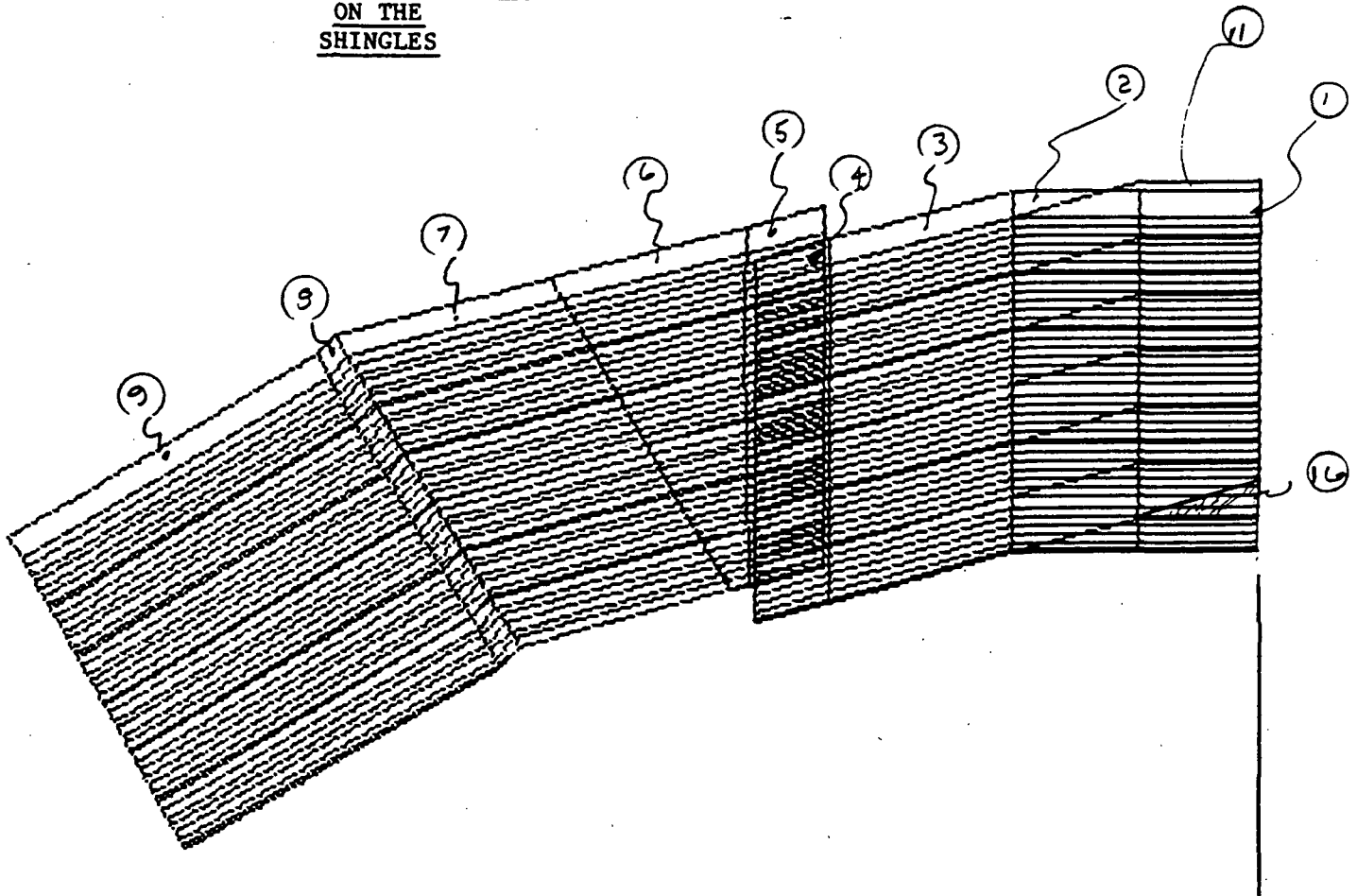
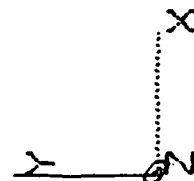


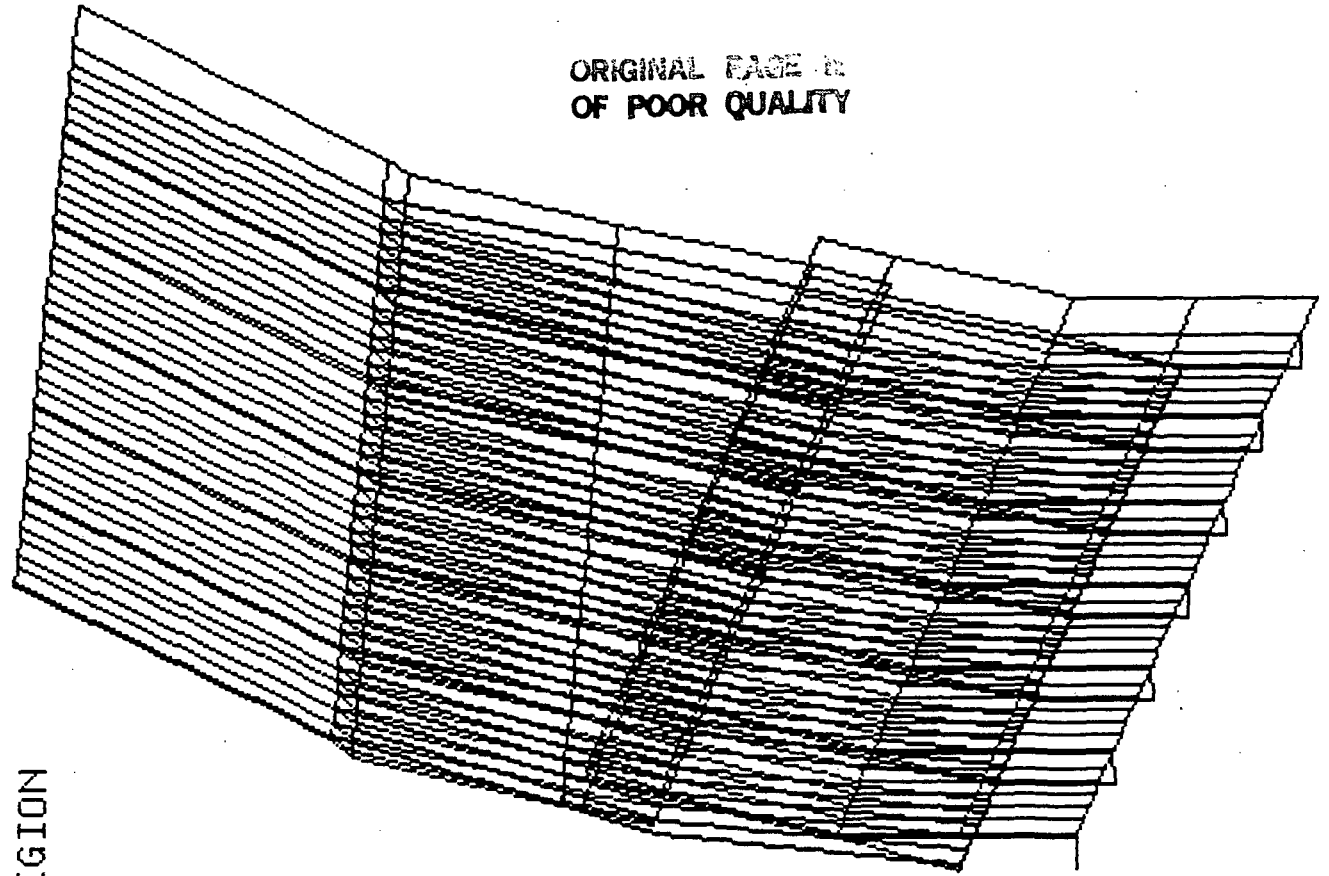
FIGURE 2.4.2



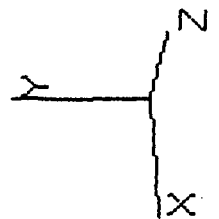
III. RESULTS

3.1	Models	Page
.	Fundamental Region	3.1.1
.	Inboard & Outboard SHINGLES, BALL SCREW, GUSSETS	3.1.2
.	Cables, Struts, and Drum	3.1.3
.	Inboard Shingle - Quad Element Numbers	3.1.4
.	Outboard Shingle - Quad Element Numbers	3.1.5
.	Gussets and Drum - Example Element Numbers	3.1.6
3.2	Run 1.0 - Internal Pressure	
.	Meridional Stress vs θ - Forward Edge	3.2.1
.	Hoop Stress vs θ - Aft Edge	3.2.2
.	Meridional Stress vs Z - Outboard Shingle	3.2.3
.	Hoop Stress vs Z - Outboard Shingle	3.2.4
.	Radial Displacement at Three Axial Positions	3.2.5
3.3	Run 2.0 - 1G Lateral Load	
.	Hoop Stress vs θ - Forward Edge, (-) Fibre Distance	3.3.1
.	Hoop Stress vs θ - Forward Edge, (+) Fibre Distance	3.3.2
.	Meridional Stress vs θ - Forward Edge, (-) Fibre Distance	3.3.3
.	Meridional Stress vs θ - Forward Edge, (+) Fibre Distance	3.3.4
.	Hoop Stress vs θ - Aft Edge, (-) Fibre Distance	3.3.5
.	Hoop Stress vs θ - Aft Edge, (+) Fibre Distance	3.3.6
.	Meridional Stress vs θ - Aft Edge, (-) Fibre Distance	3.3.7
.	Meridional Stress vs θ - Aft Edge, (+) Fibre Distance	3.3.8
.	Meridional Stress vsZ - Outboard Shingle, Segment 1R	3.3.9
.	Meridional Stress vsZ - Outboard Shingle, Segment 1L	3.3.10
.	Meridional Stress vsZ - Outboard Shingle, Segment 2R	3.3.11
.	Meridional Stress vsZ - Outboard Shingle, Segment 2L	3.3.12
.	Meridional Stress vsZ - Outboard Shingle, Segment 3R	3.3.13
.	Meridional Stress vsZ - Outboard Shingle, Segment 3L	3.3.14
.	Hoop Stress vsZ - Outboard Shingle, Segment 1R	3.3.15
.	Hoop Stress vsZ - Outboard Shingle, Segment 1L	3.3.16
.	Hoop Stress vsZ - Outboard Shingle, Segment 2R	3.3.17
.	Hoop Stress vsZ - Outboard Shingle, Segment 2L	3.3.18
.	Hoop Stress vsZ - Outboard Shingle, Segment 3R	3.3.19
.	Hoop Stress vsZ - Outboard Shingle, Segment 3L	3.3.20
.	Radial Displacement vs θ - Aft Edge	3.3.21

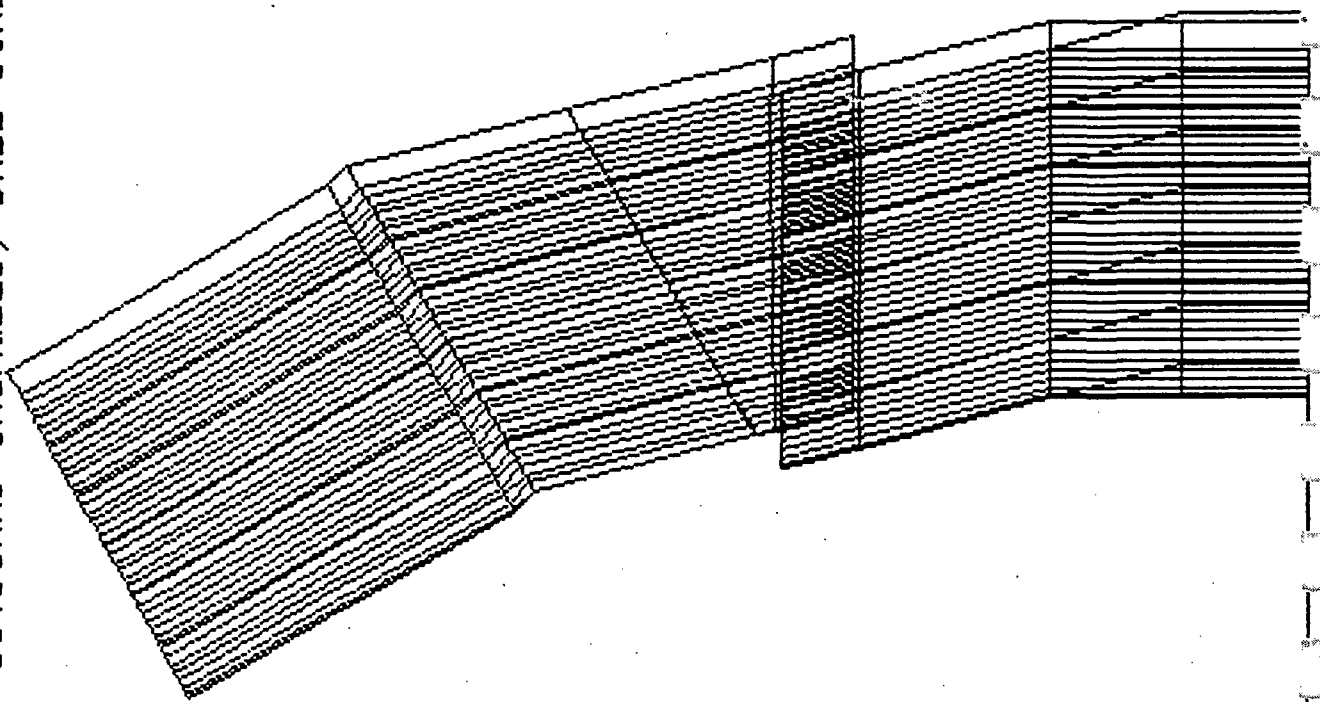
ORIGINAL PAGE IS
OF POOR QUALITY



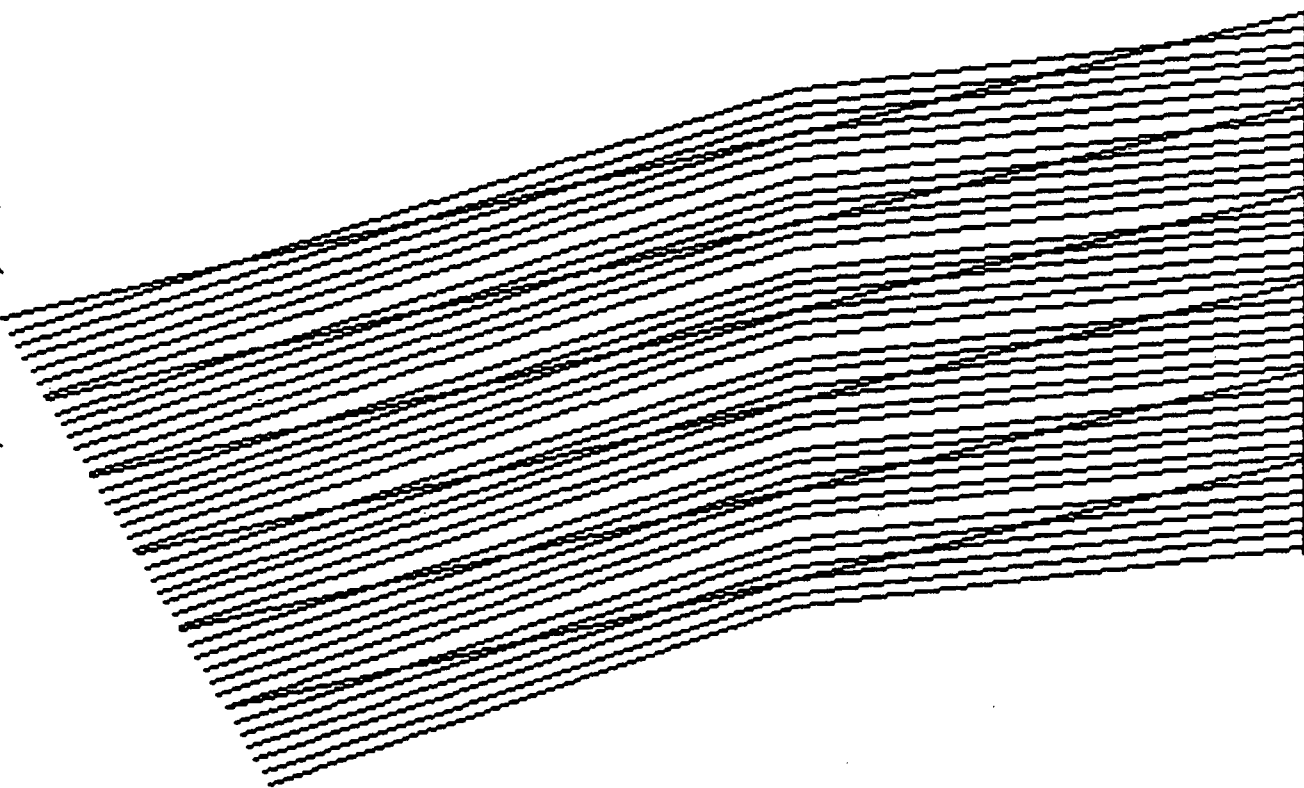
VIEW OF THE FUNDAMENTAL REGION



VIEW OF INBOARD AND OUTBOARD SHINGLES, BALL SCREW AND GUSSETS

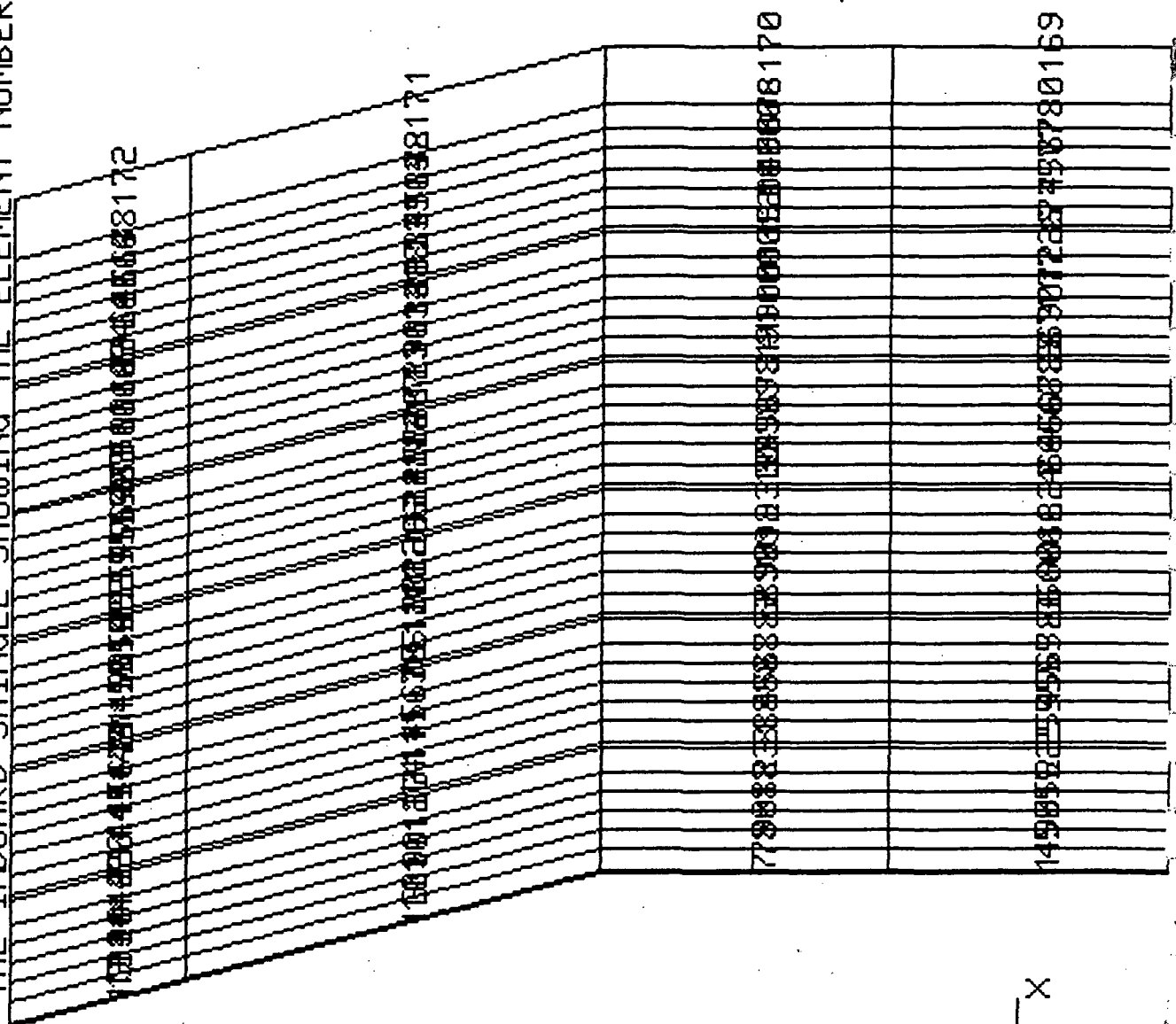


VIEW OF CABLES, STRUTS, AND DRUM



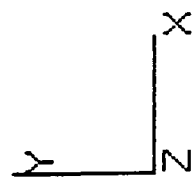
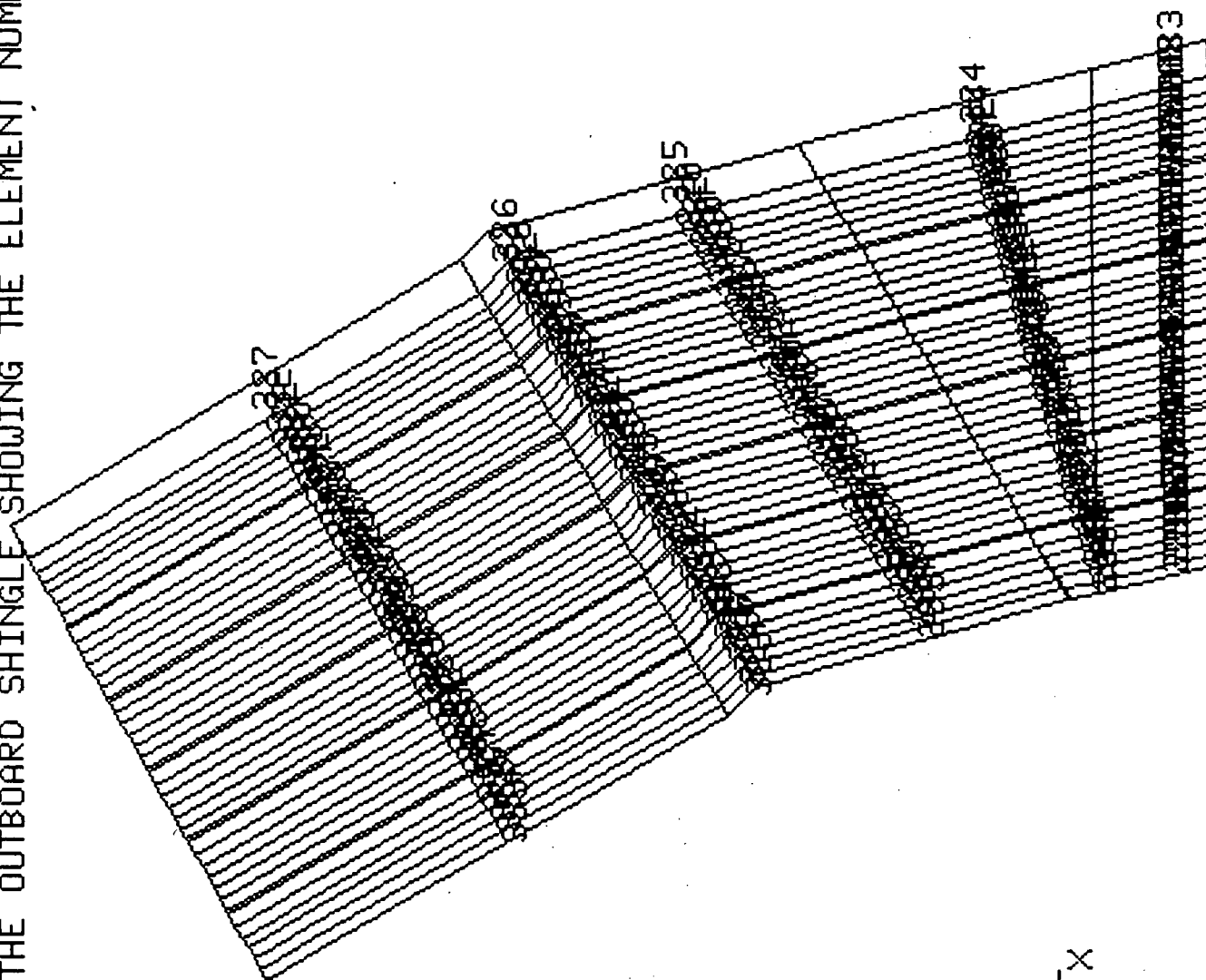
ORIGINAL PAGE IS
OF POOR QUALITY

VIEW OF THE INBOARD SHOWING THE ELEMENT NUMBERS

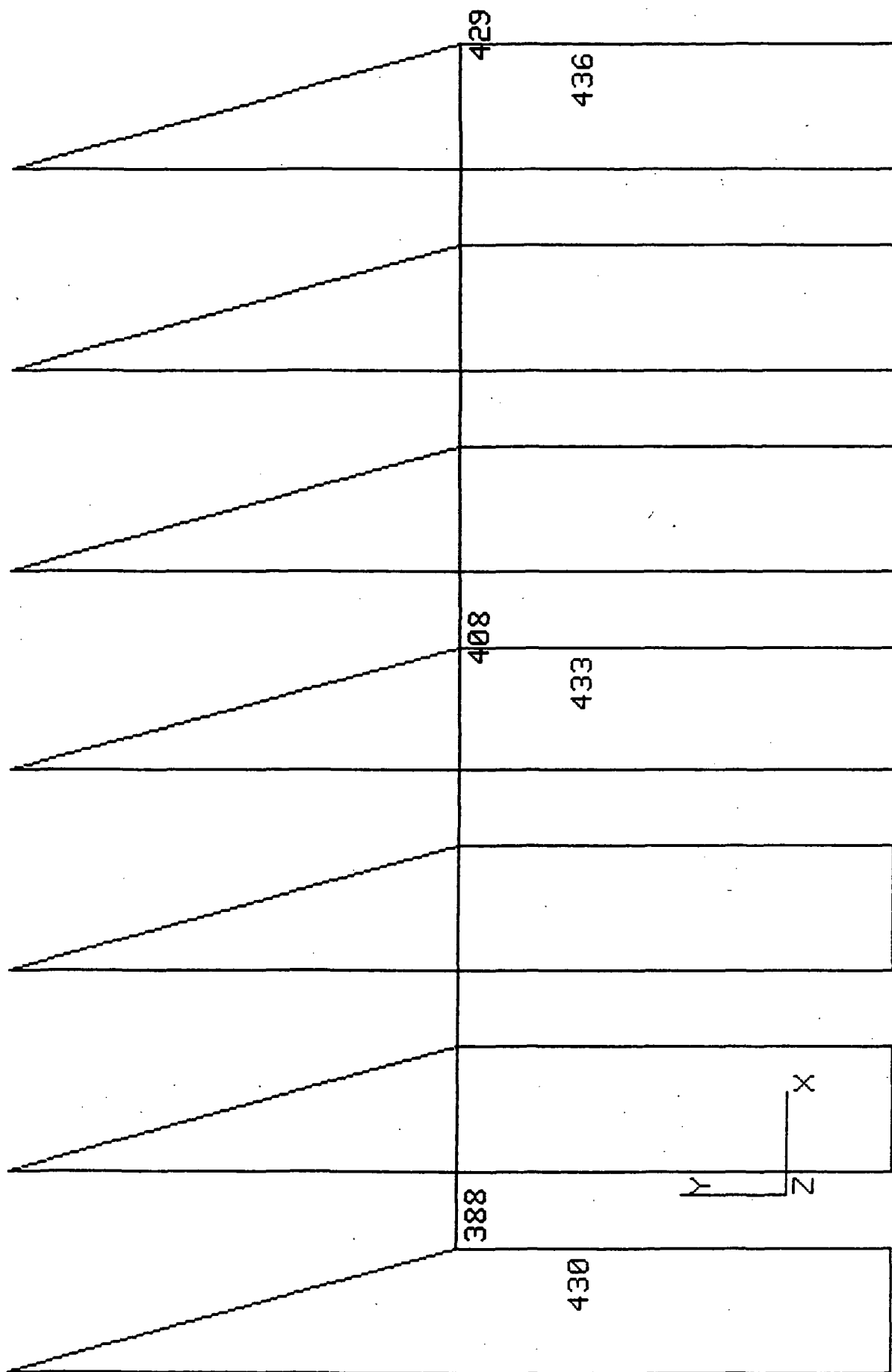


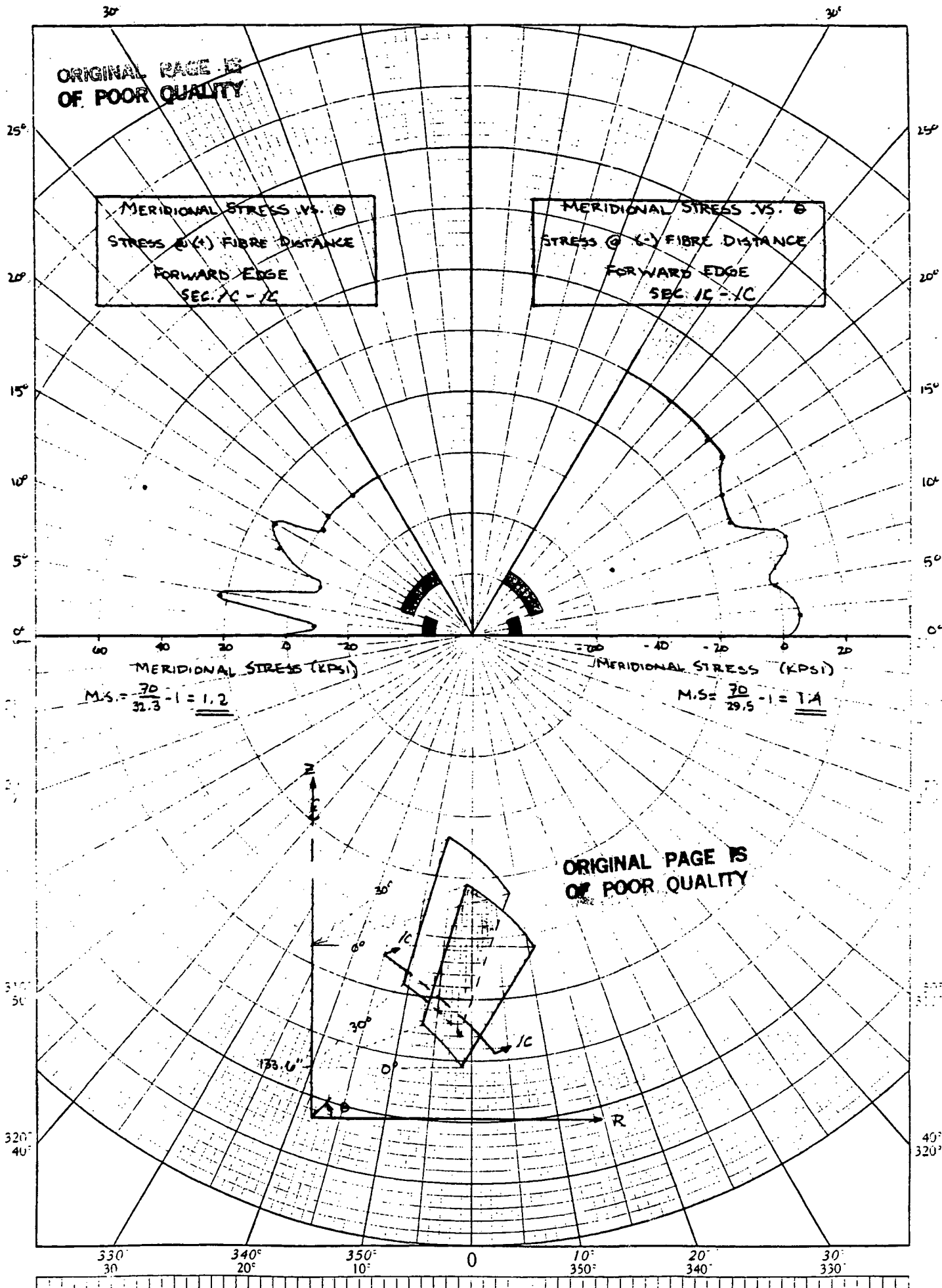
ORIGINAL PAGE IS
OF POOR QUALITY

VIEW OF THE OUTBOARD SHINGLE SHOWING THE ELEMENT NUMBERS



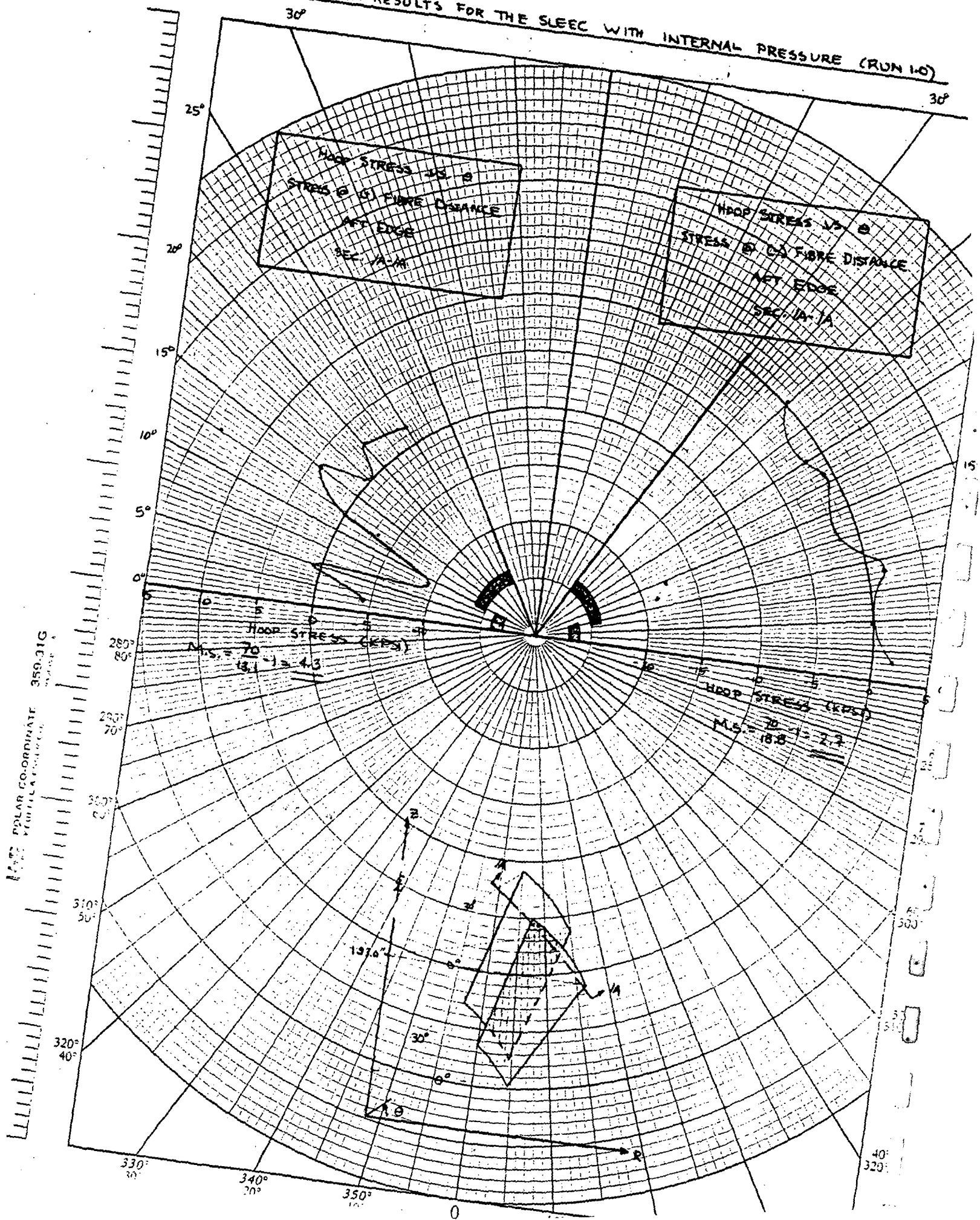
VIEW OF GUSSETS AND DRUM WITH EXAMPLE ELEMENT NUMBERS





VT. POOR QUALITY

NASTRAN RESULTS FOR THE SLEEC WITH INTERNAL PRESSURE (RUN 140)



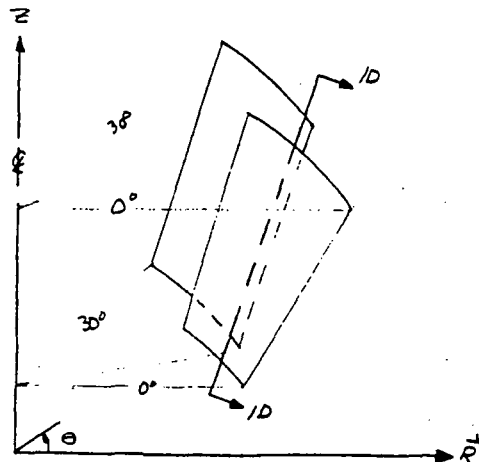
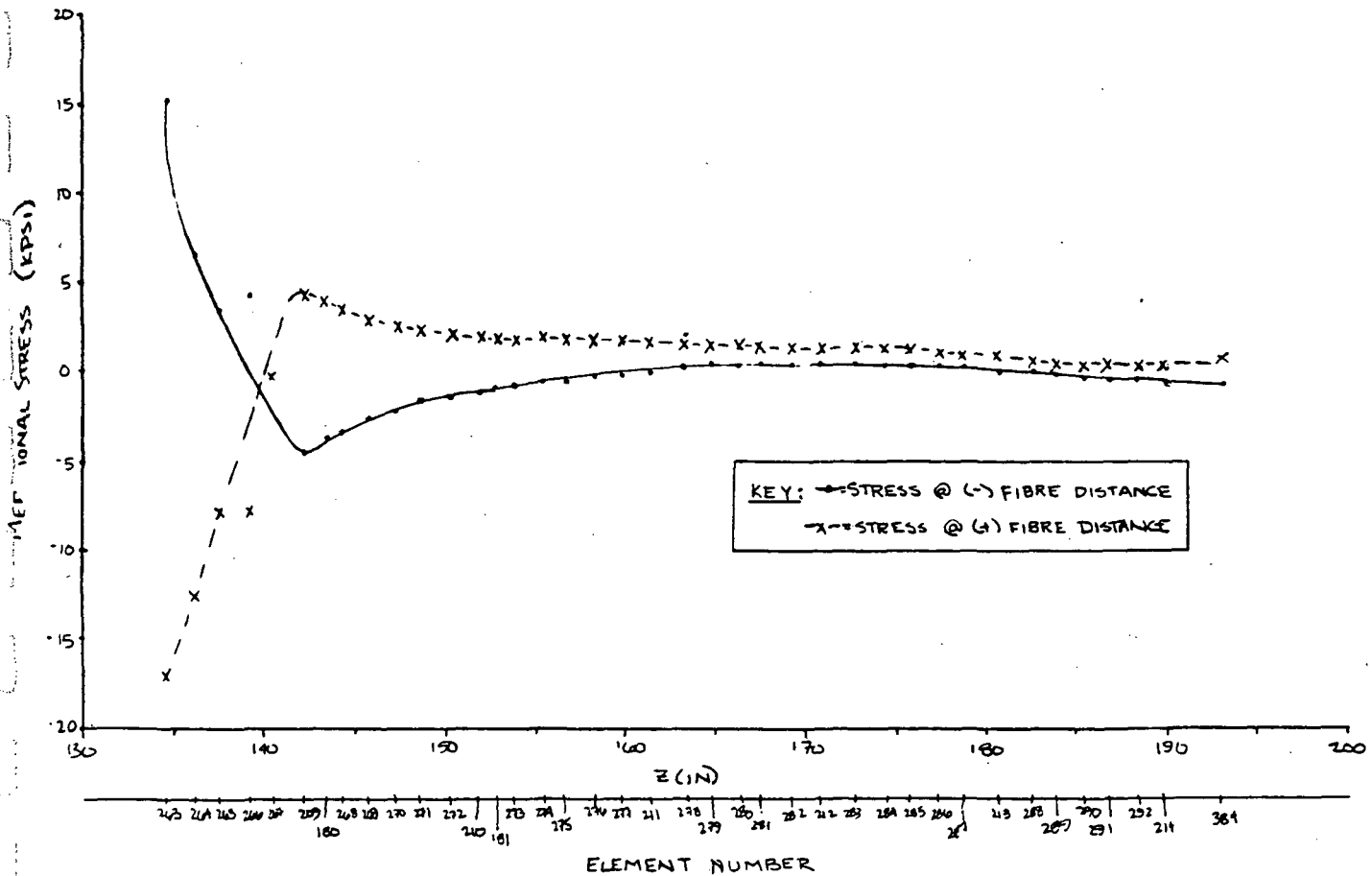
ORIGINAL PAGE IS
OF POOR QUALITY

SUBJECT		REPORT NO.	PAGE OF
NASTRAN RESULTS FOR THE SLEEC WITH INTERNAL PRESSURE (RUN 1.0)		DATE	5 AUGUST 1986
BY		CHK. BY	WORK ORDER
		DATE	

MERIDIONAL STRESS VS. Z

OUTBOARD SHINGLE

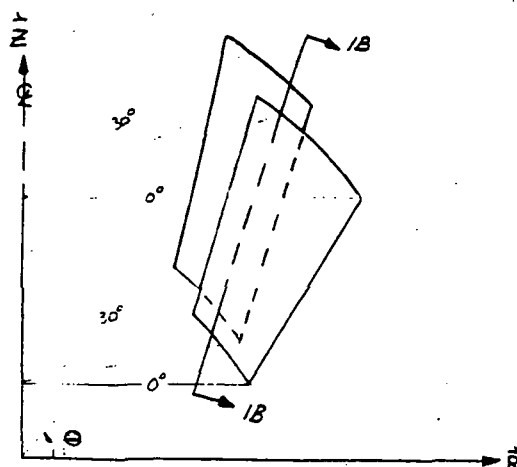
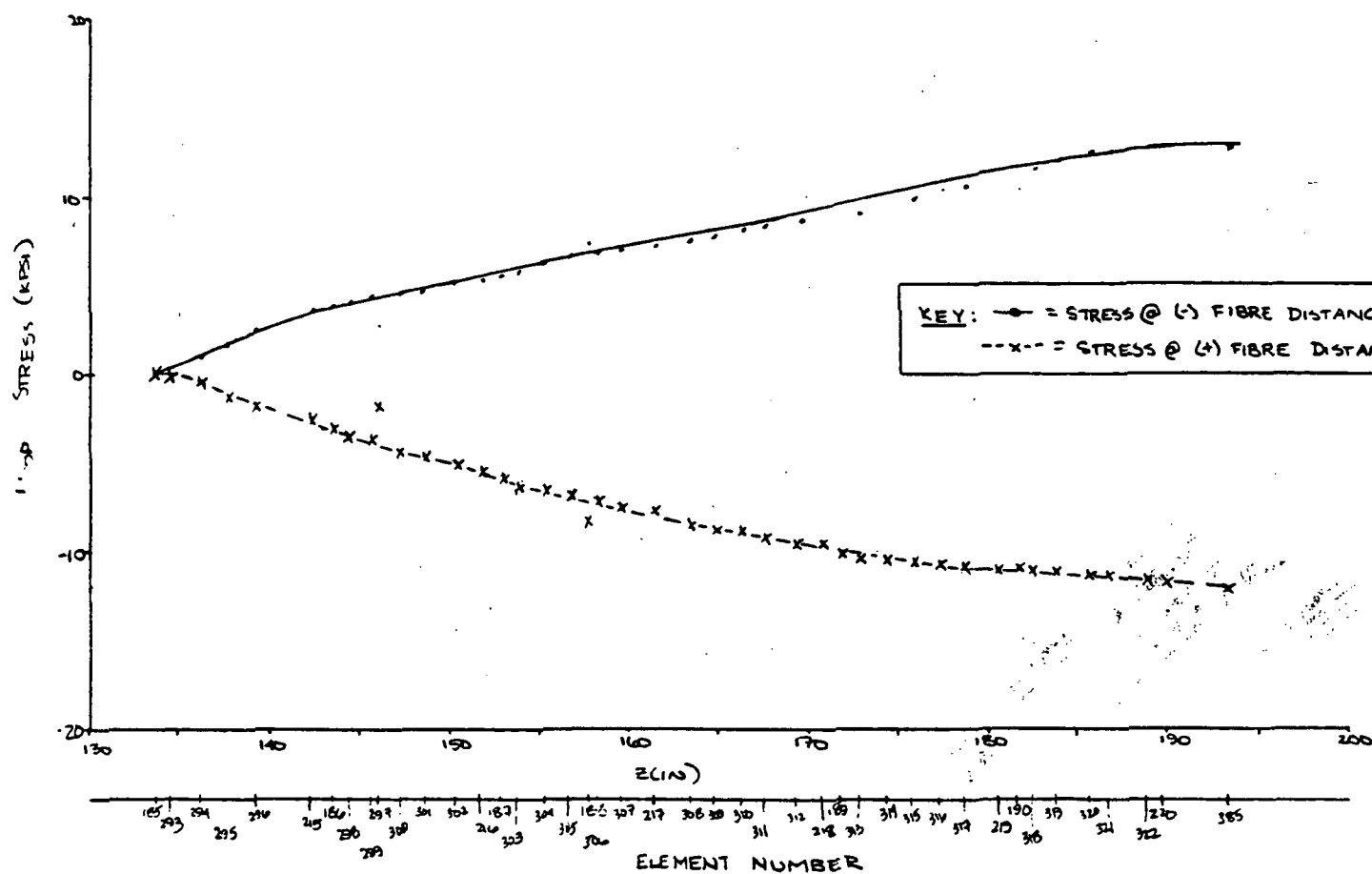
SEC. 10-10



$$M.S. = \frac{70}{17} - 1 = \underline{\underline{3.1}}$$

REPORT NO.		PAGE OF
SUBJECT		DATE
NASTRAN RESULTS FOR THE SLEEC WITH INTERNAL PRESSURE (RUN 1.0)		5 AUGUST 1986
BY		WORK ORDER
CHK. BY		DATE

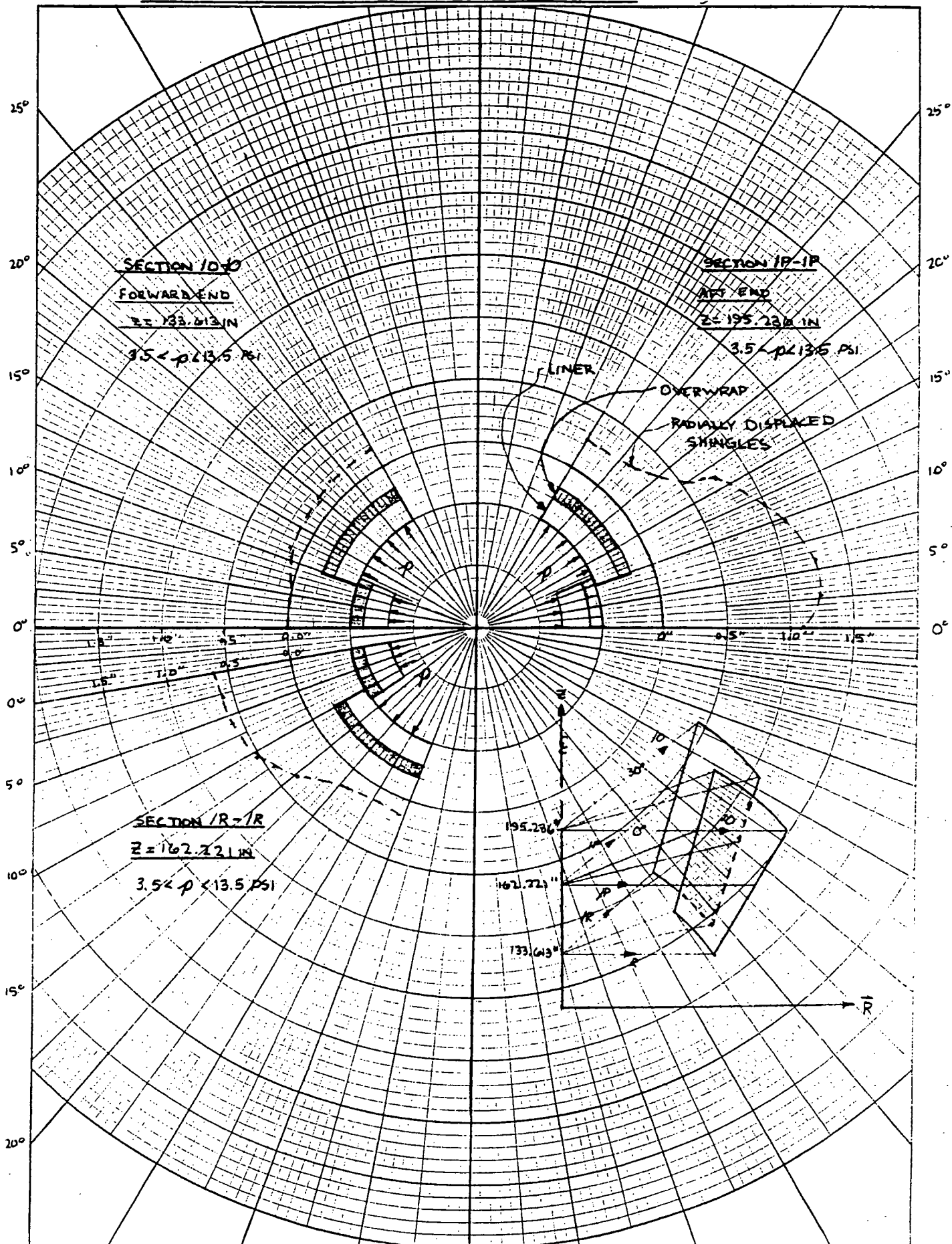
HOOP STRESS VS. Z
OUTBOARD SHINGLE
SEC. /B- /B



RADIAL DISPLACEMENT OF SHINGLES AT THREE AXIAL POSITIONS

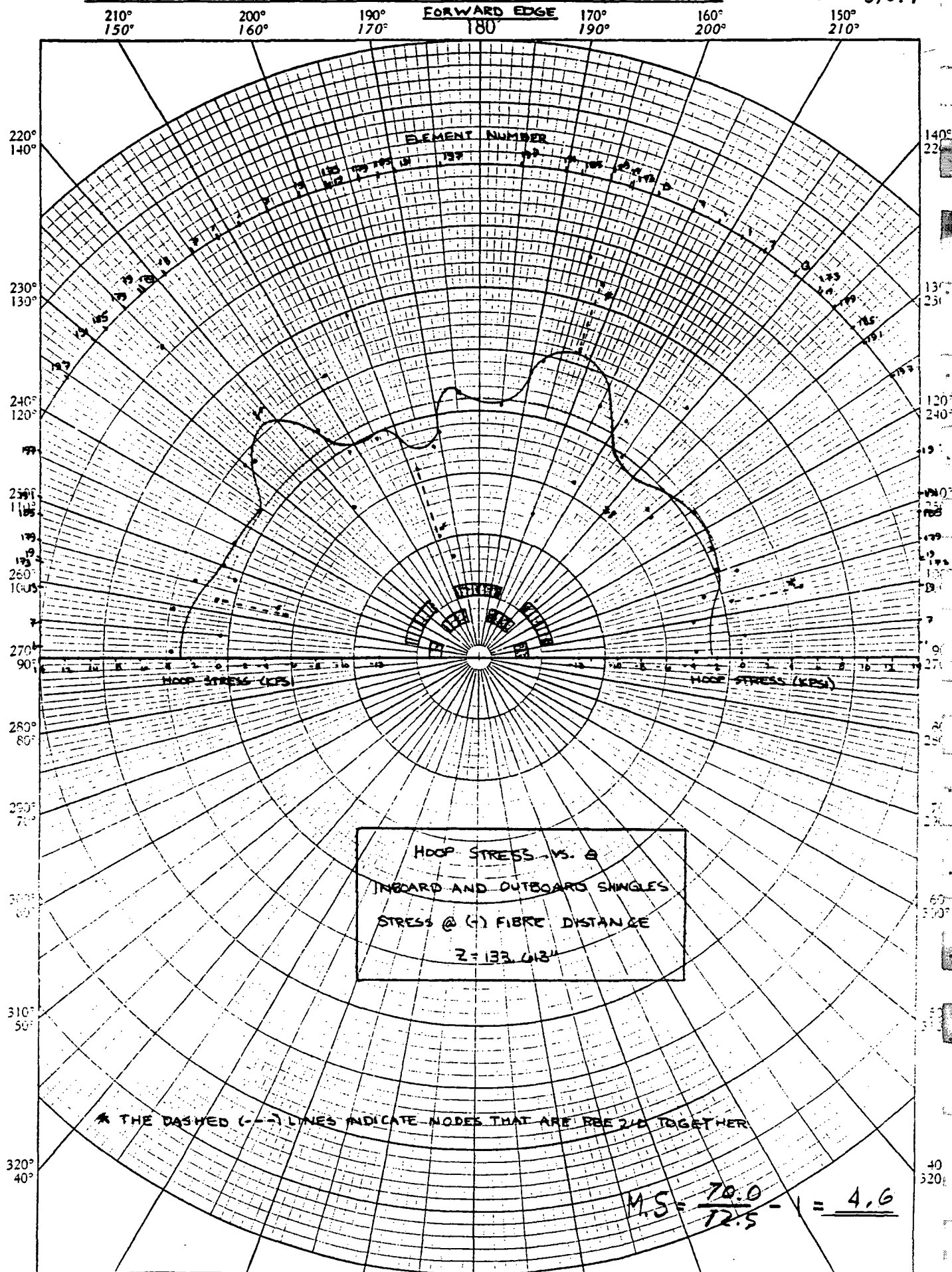
3.2.5

FOR NASTRAN RESULTS OF RUN 1.0 (PRESSURE RUN)



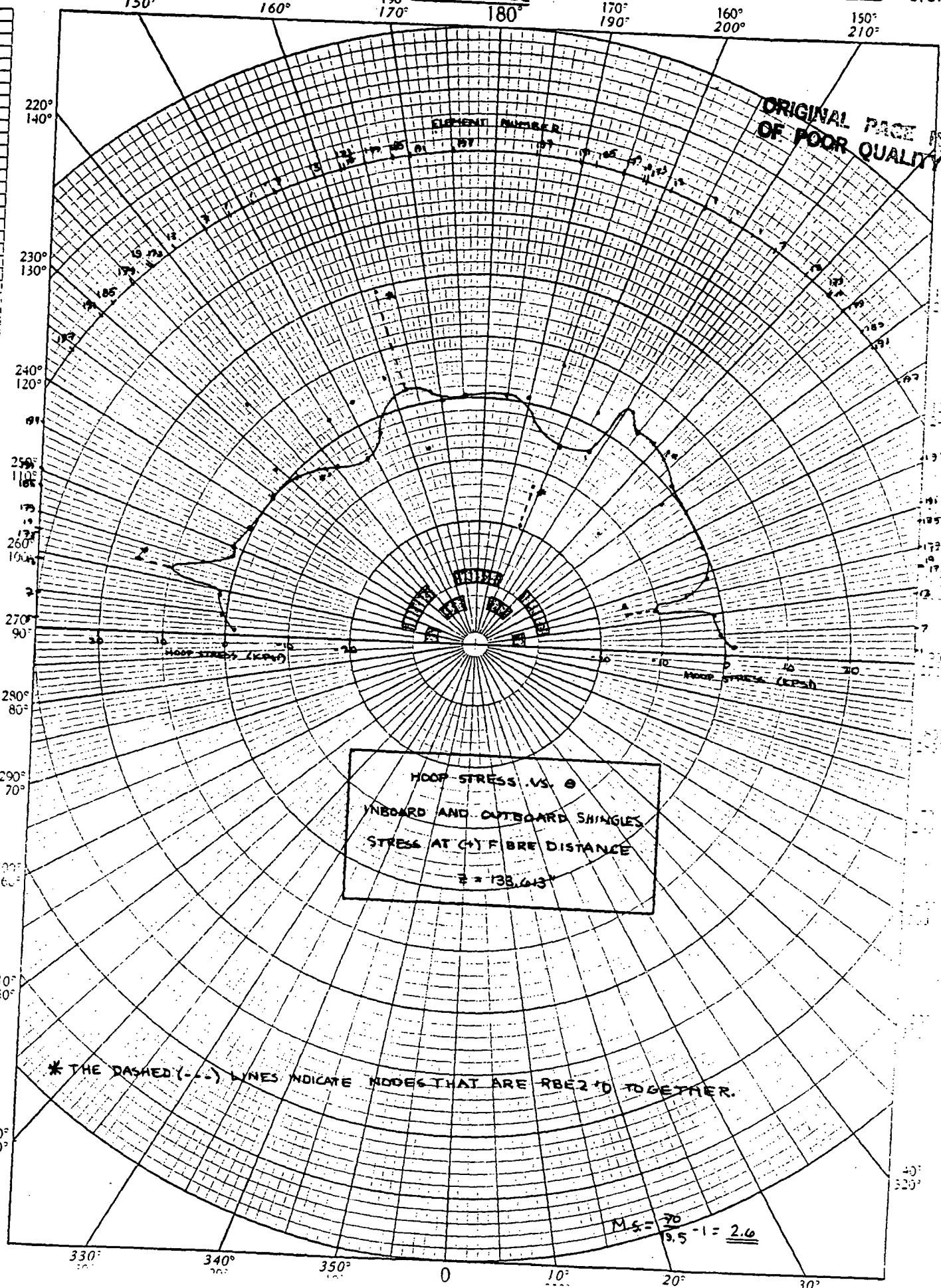
NASTRAN RESULTS FOR THE SLEEVE WITH 1G LATERAL LOAD (RUN 2.0)

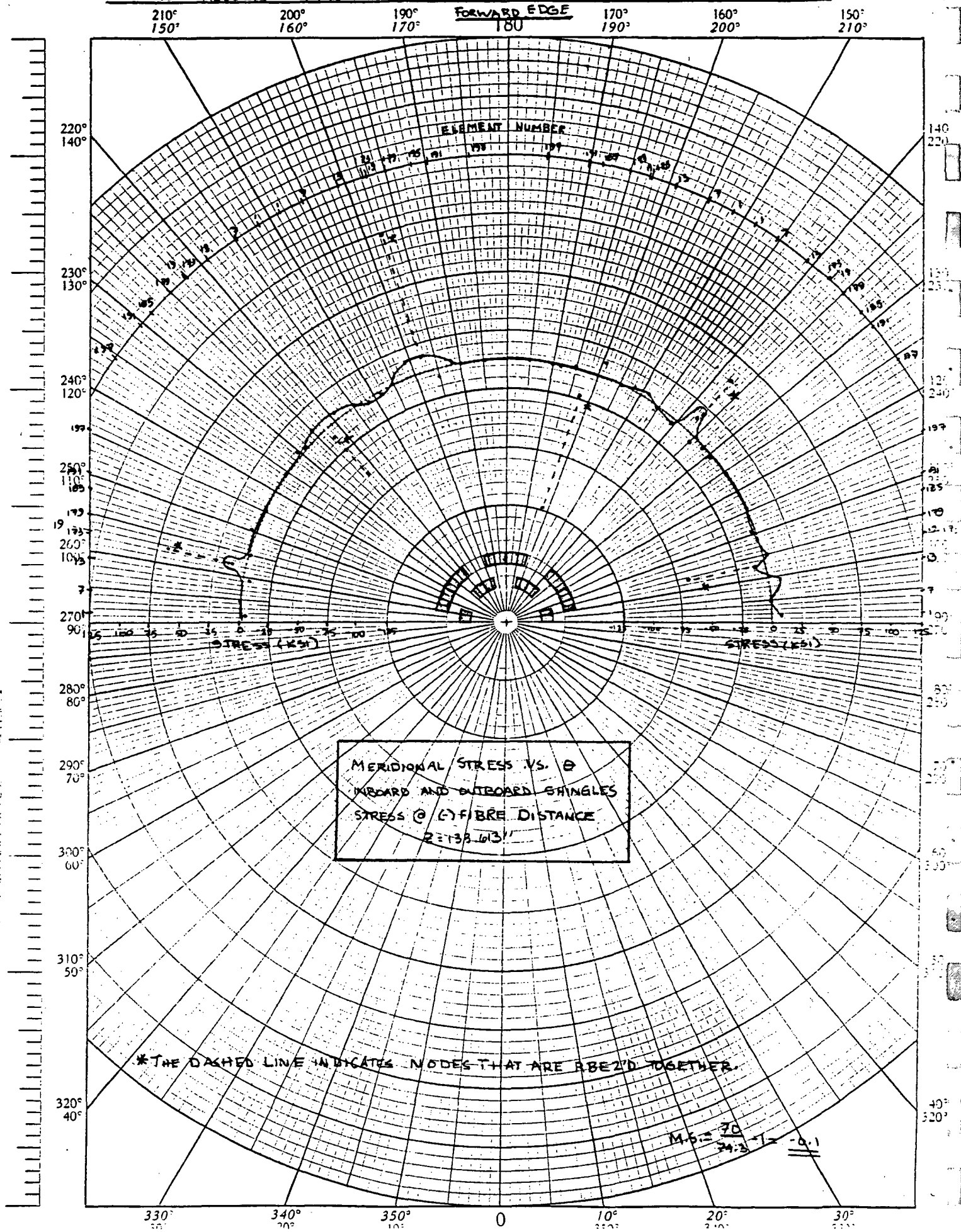
3,3.1

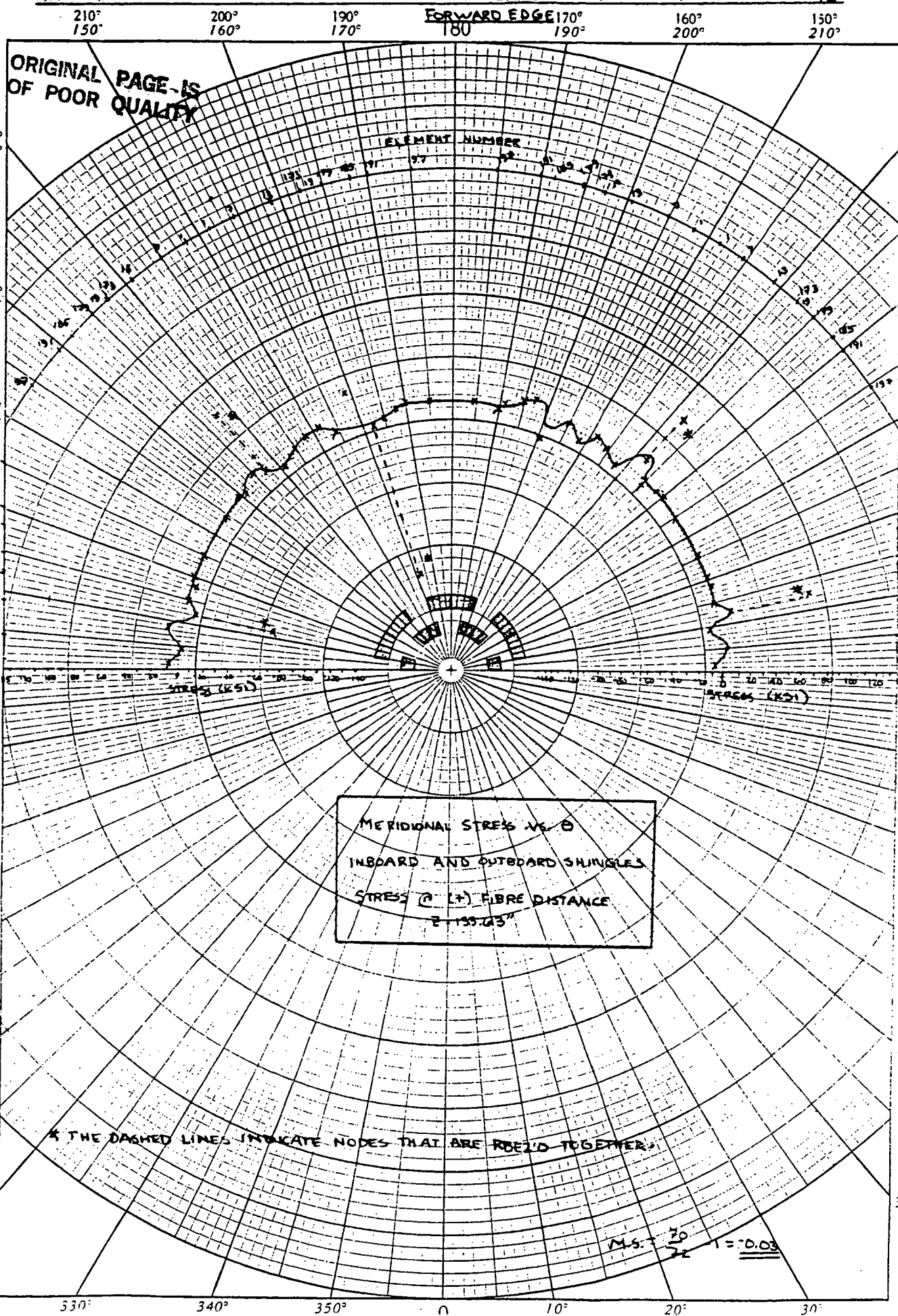


NASTRAN RESULTS FOR THE SLEEVE WITH IG LATERAL LOAD (RUN 2.0) - ALL SEGMENTS

3.3.2







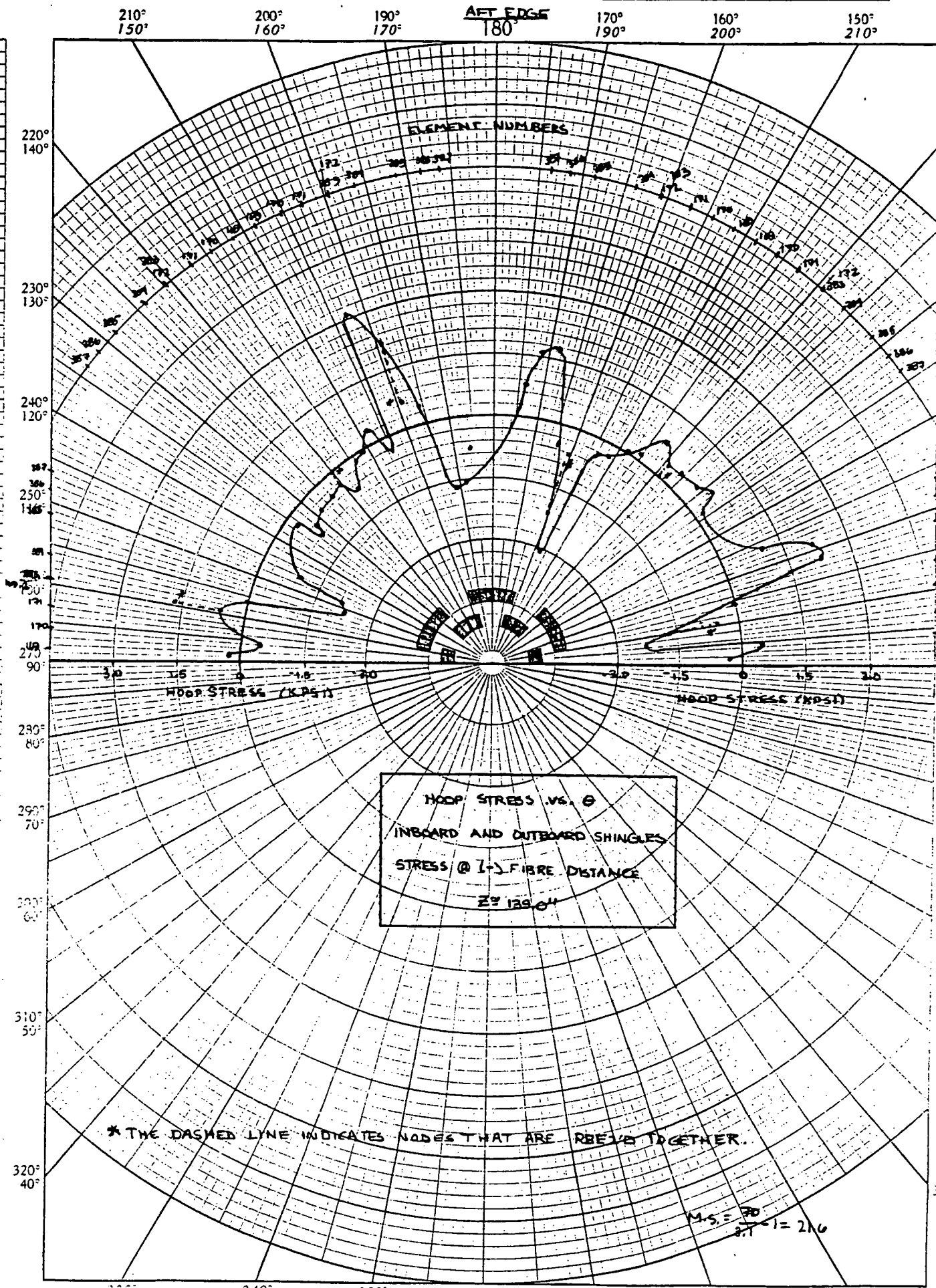
359-31G
POLAR CO-ORDINATE
REFERENCE

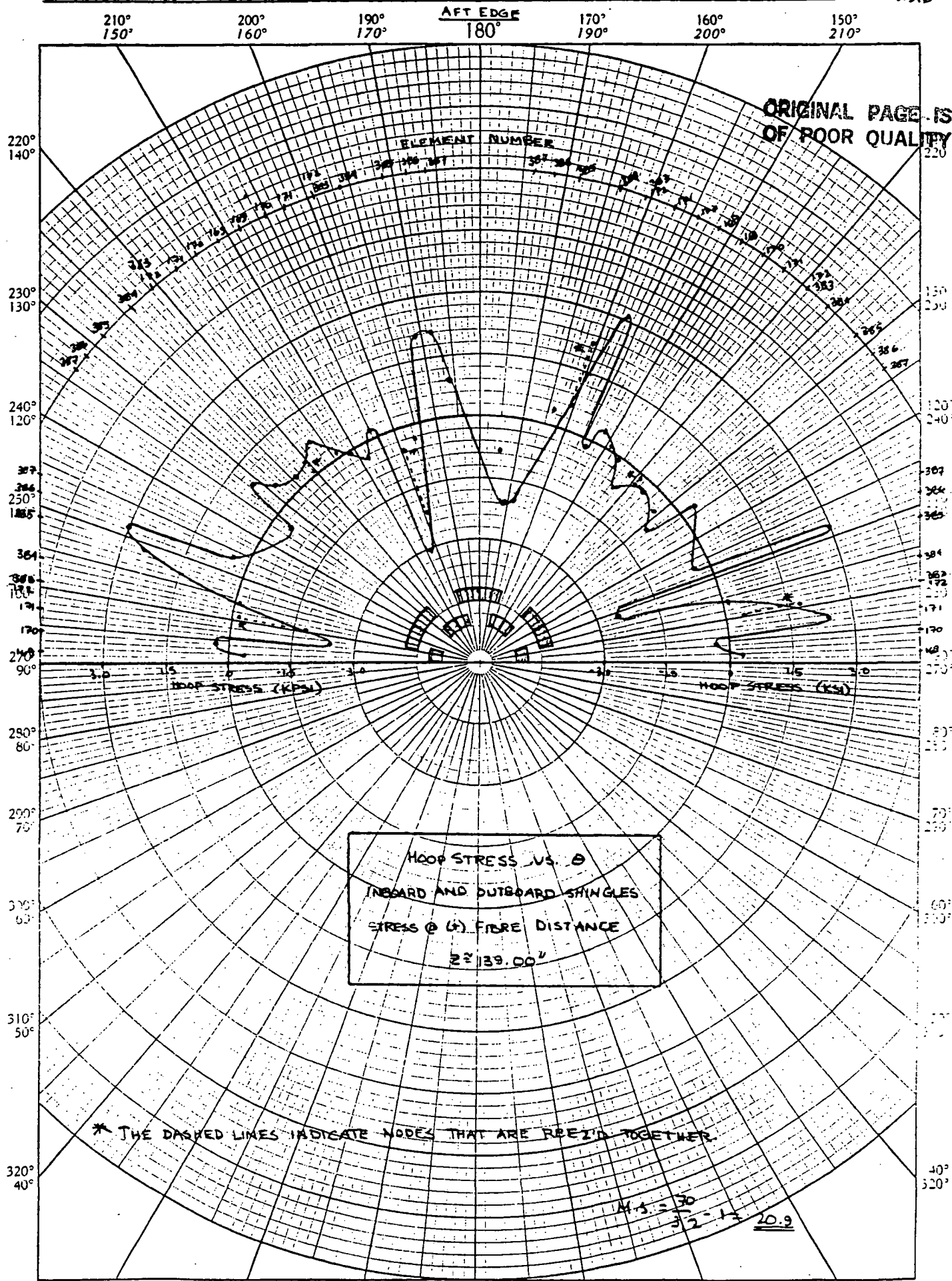
ORIGINAL PAGE IS
OF POOR QUALITY

NASTRAN RESULTS FOR THE SLEEVE WITH 1G LATERAL LOAD (RUN 2.0) - ALL SEGMENTS

3.3.5

15.0 POLAR COORDINATE 350.31G



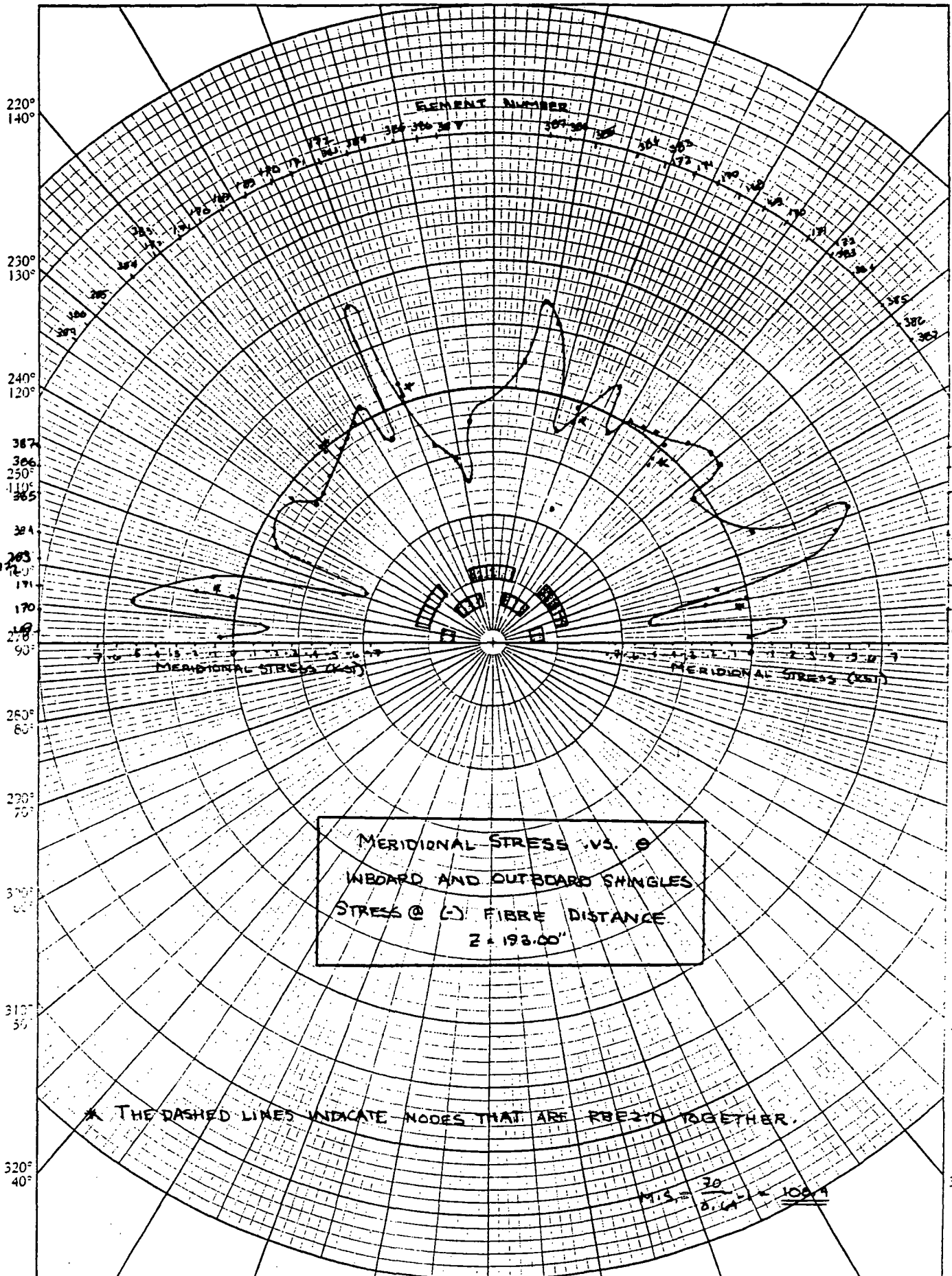


ORIGINAL PAGE 17
OF POOR QUALITY

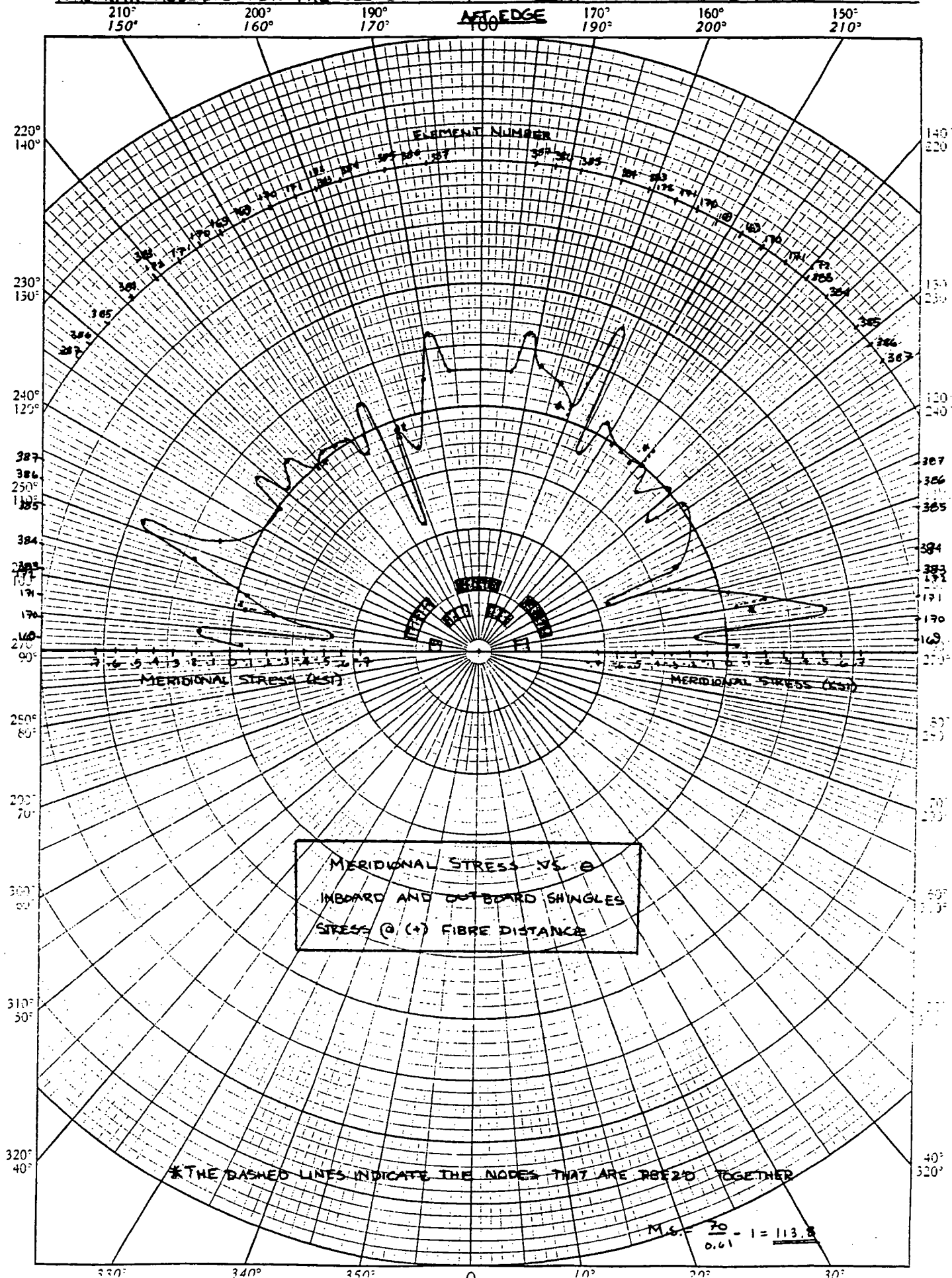
3.3.7

NASTRAN RESULTS FOR THE SLEEVE WITH 1G LATERAL LOAD (RUN 2.0) - ALL SEGMENTS

210° 200° 190° 180° 170° 160° 150°
150° 160° 170° 180° 190° 200° 210°

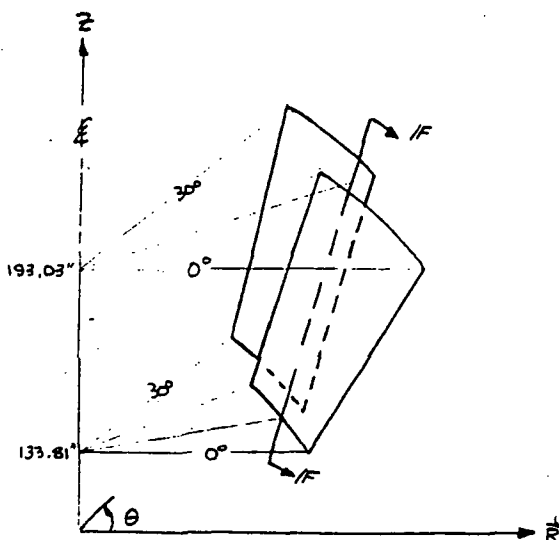
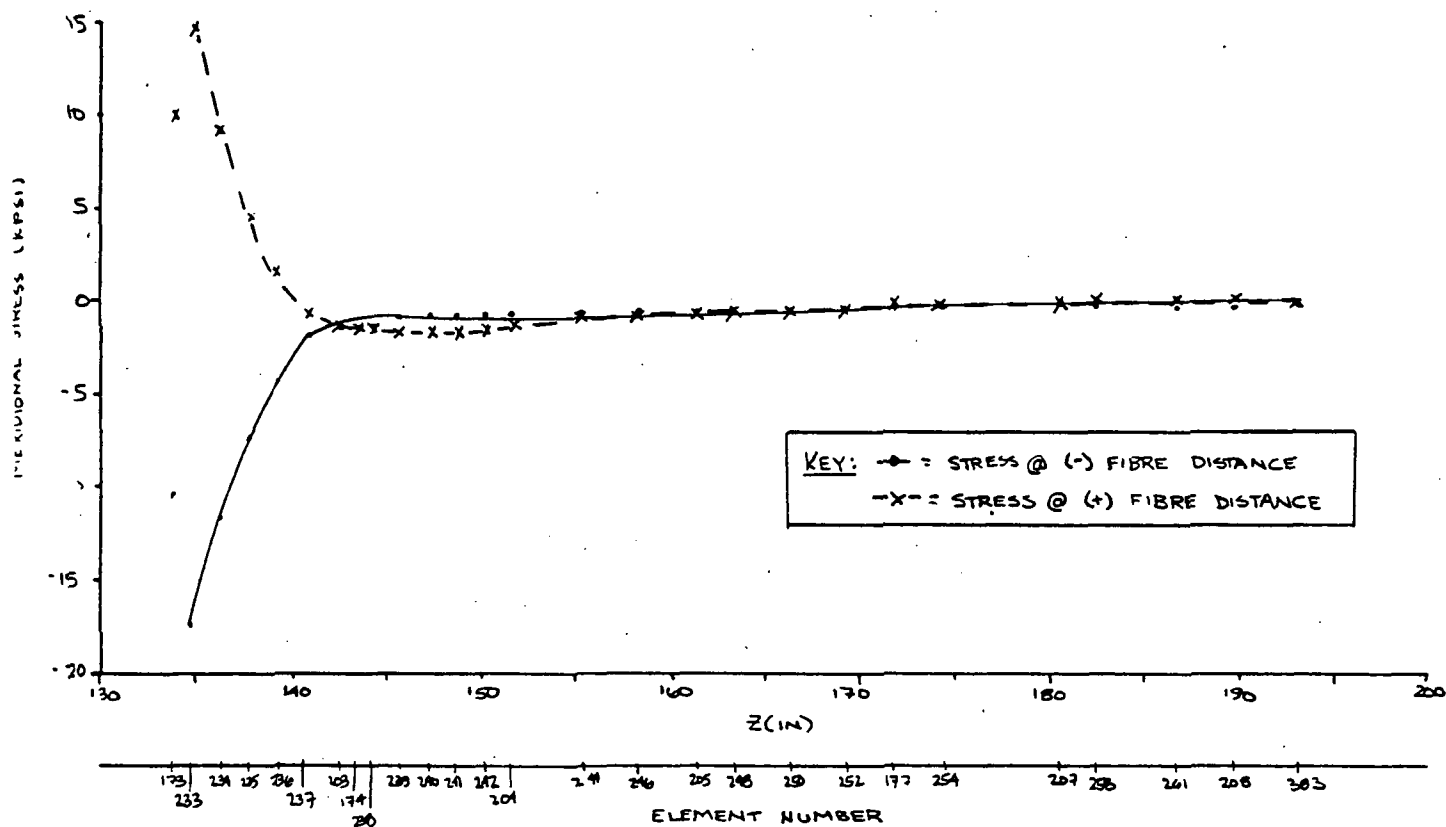


NASTRAN RESULTS FOR THE SLEEC WITH 1G LATERAL LOAD (RUN 2-0)- ALL SEGMENTS



SUBJECT		REPORT NO.	PAGE OF
NASTRAN RESULTS FOR THE SLEEC WITH 1G LATERAL LOAD (RUN 2.0): SEGMENT=1R		DATE	8 AUGUST 195
BY	CHK. BY	WORK ORDER	
		DATE	

MERIDIONAL STRESS VS. Z
OUTB'D SHINGLE
SEC. 1F-1F



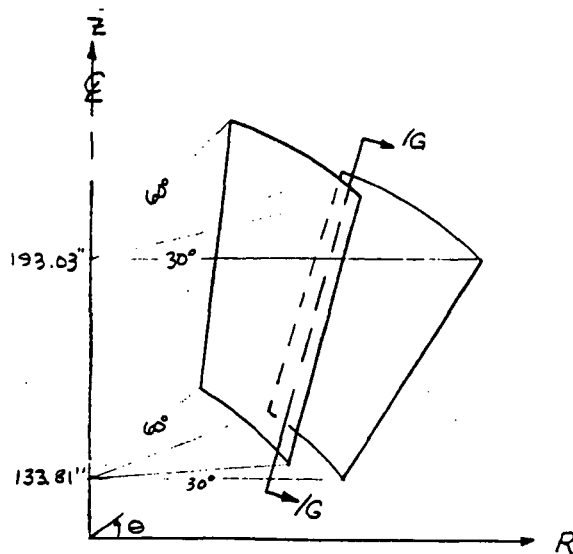
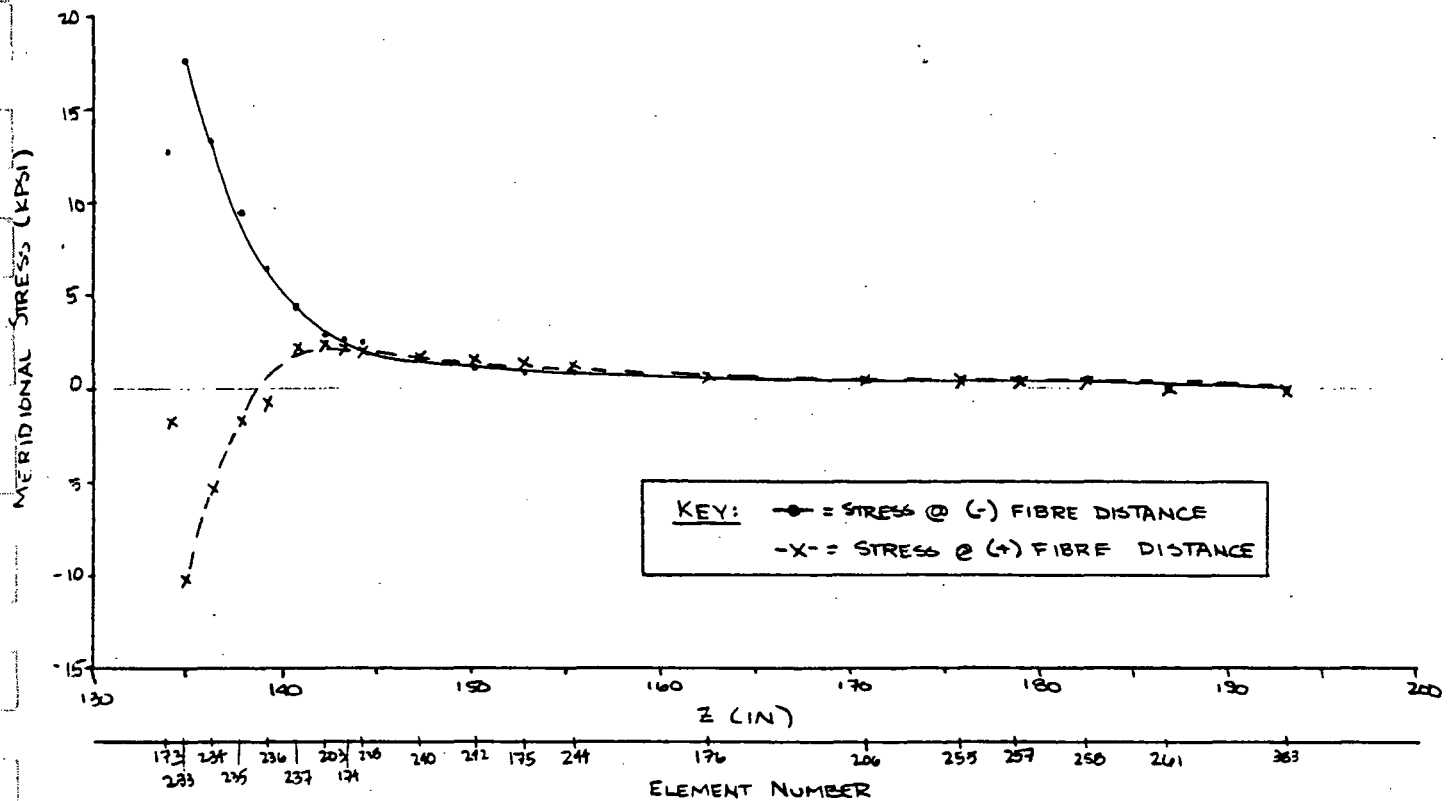
$$M.S. = \frac{70}{17.5} - 1 = \underline{\underline{3.0}}$$

ORIGINAL PAGE-11
OF POOR QUALITY

3.3.10

SUBJECT		REPORT NO.	PAGE OF
NASTRAN RESULTS FOR THE SLEEC WITH 1G LATERAL LOAD (RUN 2.0). SEGMENT 1L		DATE	8 AUGUST 1986
BY		CHK. BY	WORK ORDER
		DATE	

MERIDIONAL STRESS VS. Z
OUTB'D SHINGLE
SEC. 1G-1G



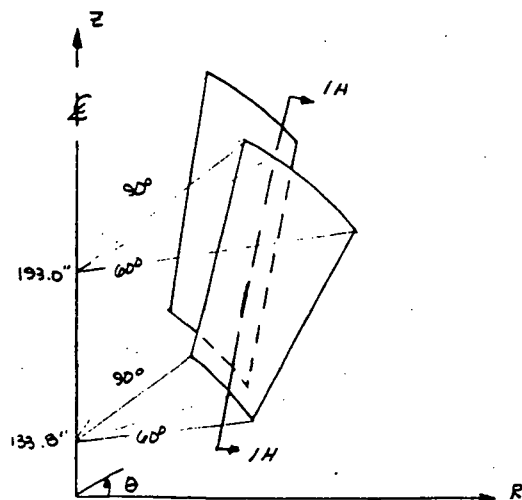
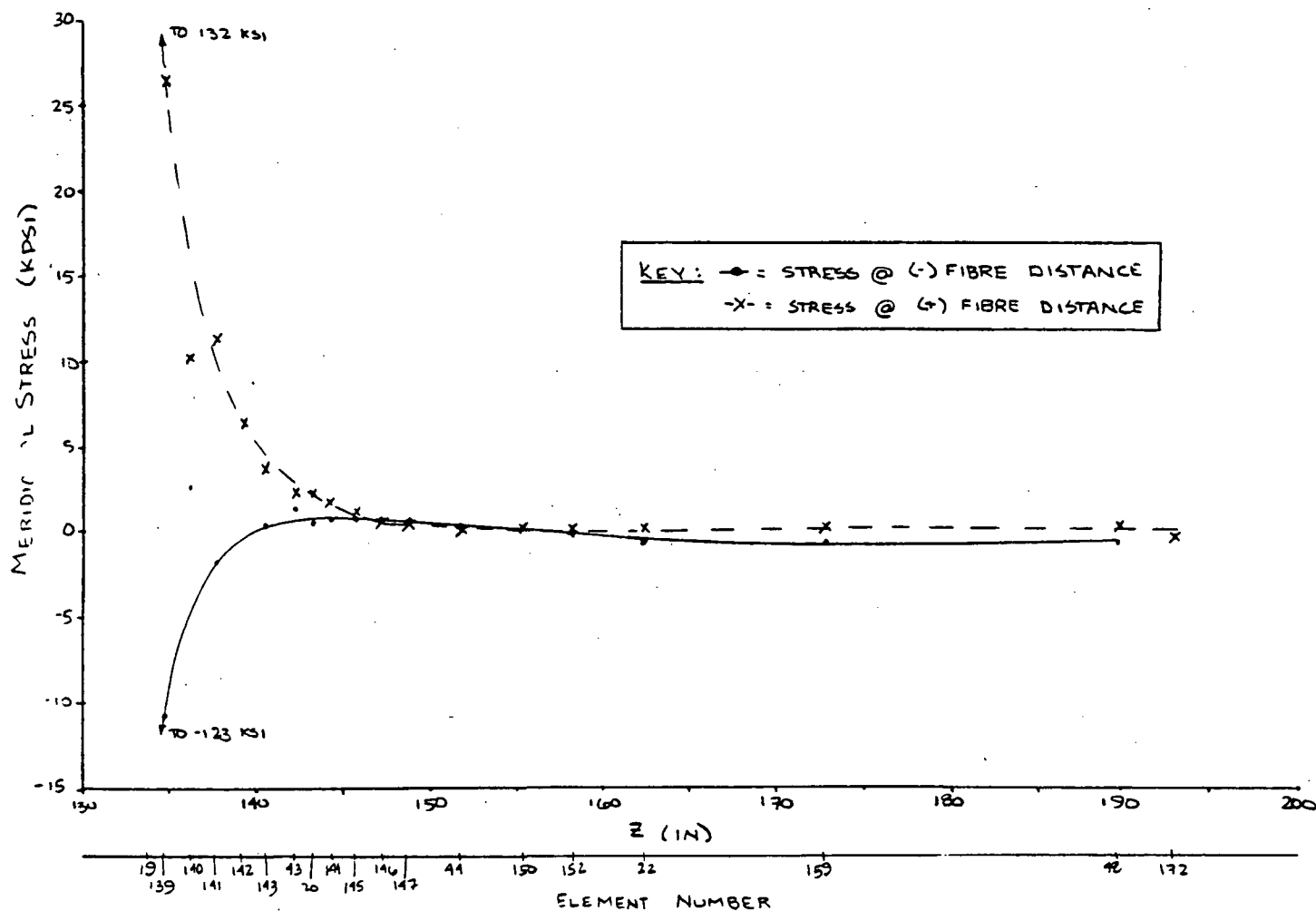
$$M.S. = \frac{70}{17.5} - 1 = \underline{\underline{3.0}}$$

SUBJECT		REPORT NO.	PAGE OF
NASTRAN RESULTS FOR THE SLEEVE WITH 1G LATERAL LOAD (RUN 2.0)		DATE	11 AUGUST 1986
BY		CHK. BY	WORK ORDER
		DATE	

MERIDIONAL STRESS VS. Z

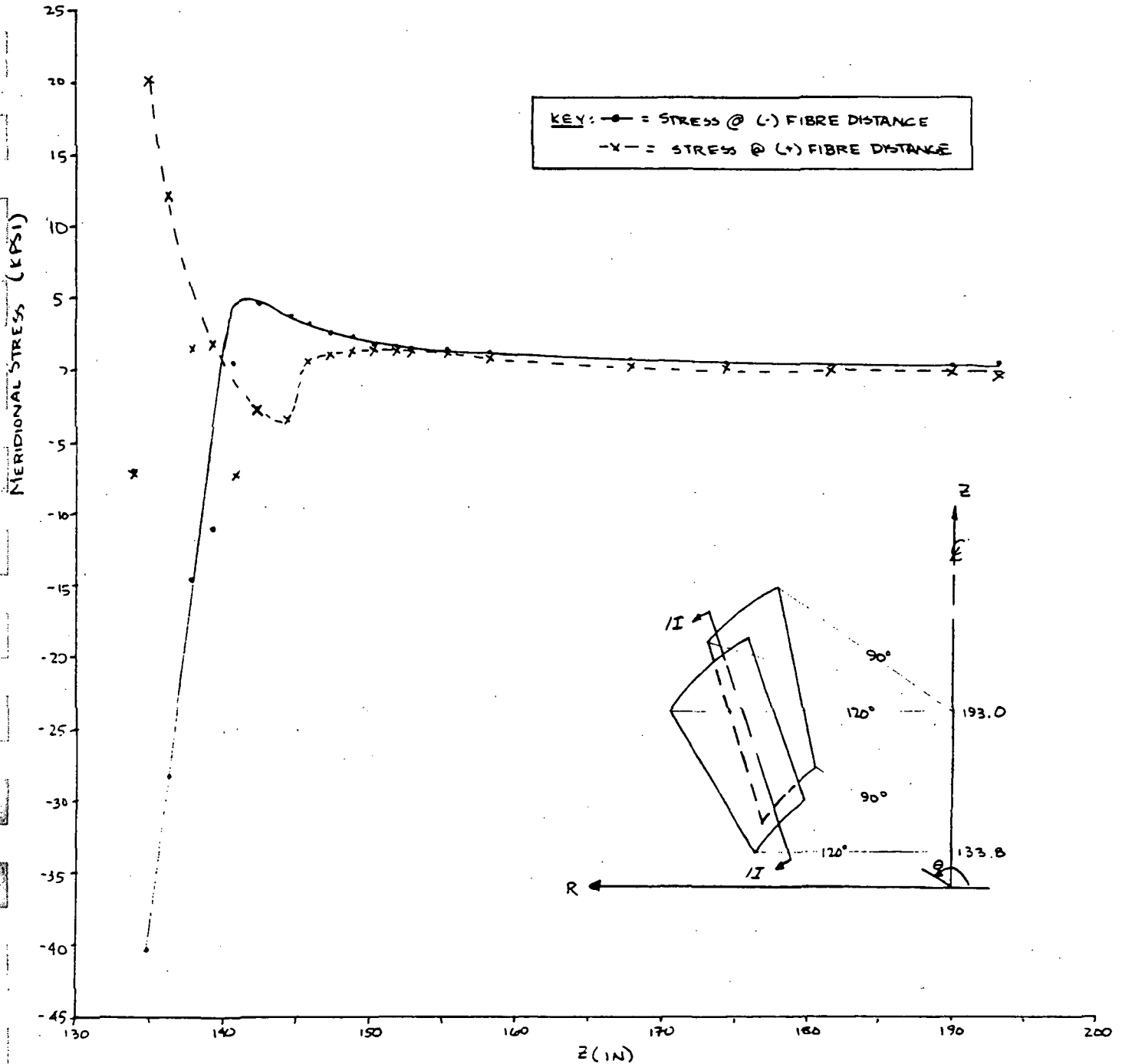
OUTSIDE SHINGLE

SEG. H-1/H



$$M.S. = \frac{70}{71.9} - 1 = \underline{\underline{-0.03}}$$

SUBJECT		REPORT NO.	PAGE OF
NASTRAN RESULTS FOR THE SLEEVE WITH 1G LATERAL LOAD (RUN 2.0)		DATE	11 AUGUST 1986
BY		CHK. BY	WORK ORDER
		DATE	

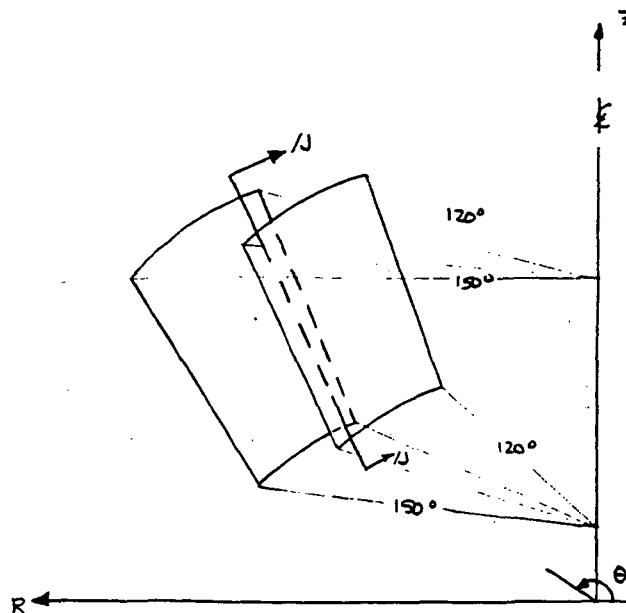
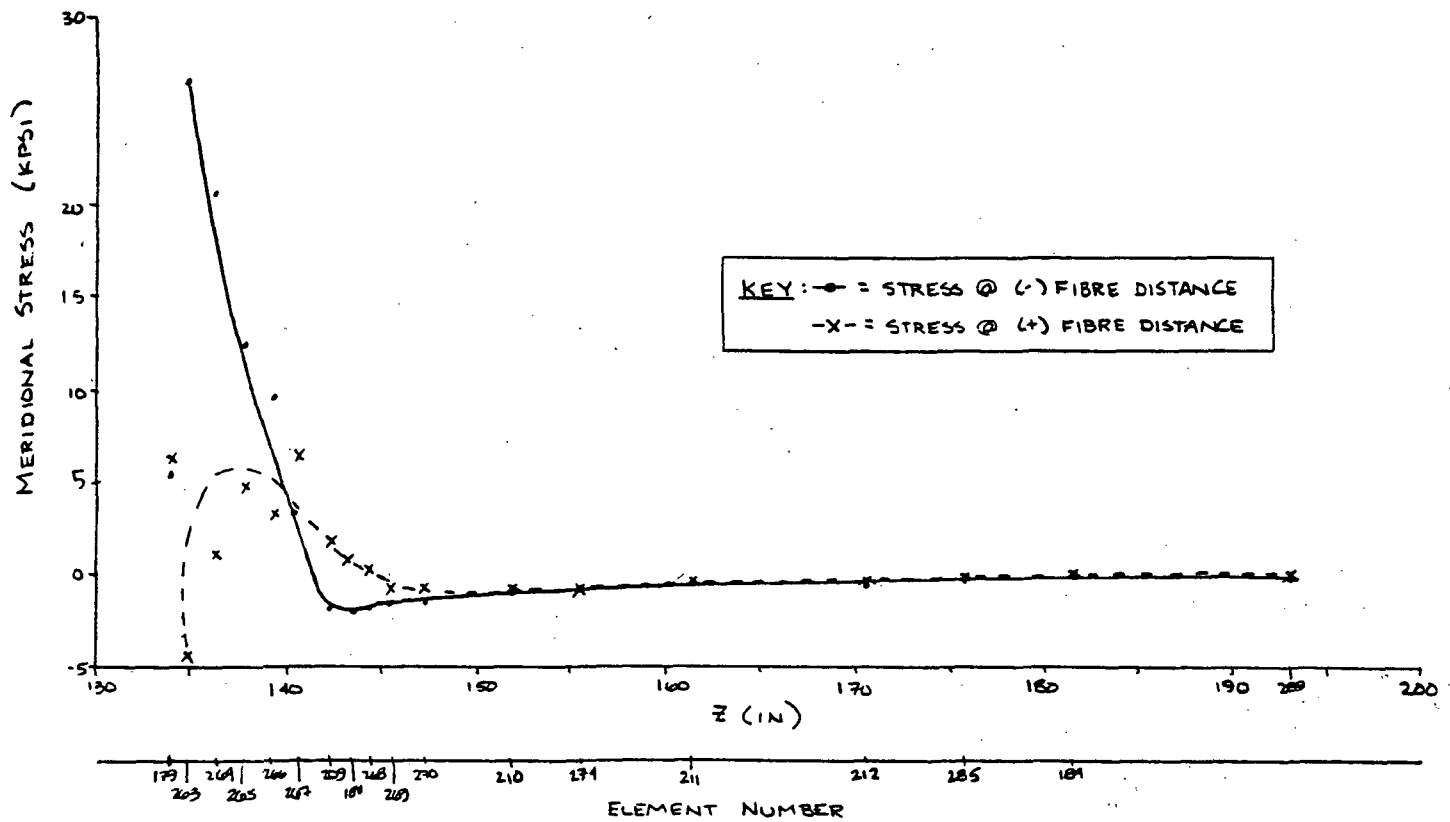
MERIDIONAL STRESS VS. ZOUTB'D SHINGLESEC. 1/1-1/1

ELEMENT NUMBER

$$M.S. = \frac{70}{40.5} - 1 = 0.7$$

REPORT NO.		PAGE	OF
SUBJECT		DATE	
NASTRAN RESULTS FOR THE SLEEC WITH 1G LATERAL LOAD (RUN 2.0) SEGMENT 3R		11 AUGUST 1986	
BY		WORK ORDER	
CHK. BY		DATE	

MERIDIONAL STRESS VS. Z
OUTBOARD SHINGLE
SECTION 11-11



$$M.S. = \frac{70}{26.5} \cdot 1 = \underline{\underline{1.6}}$$

ORIGINAL PAGE
OF POOR QUALITY

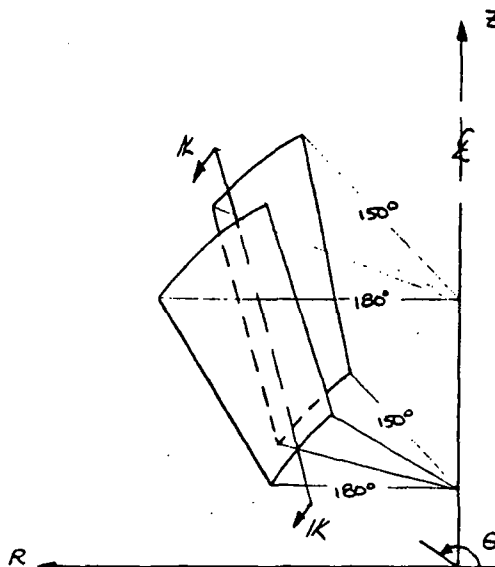
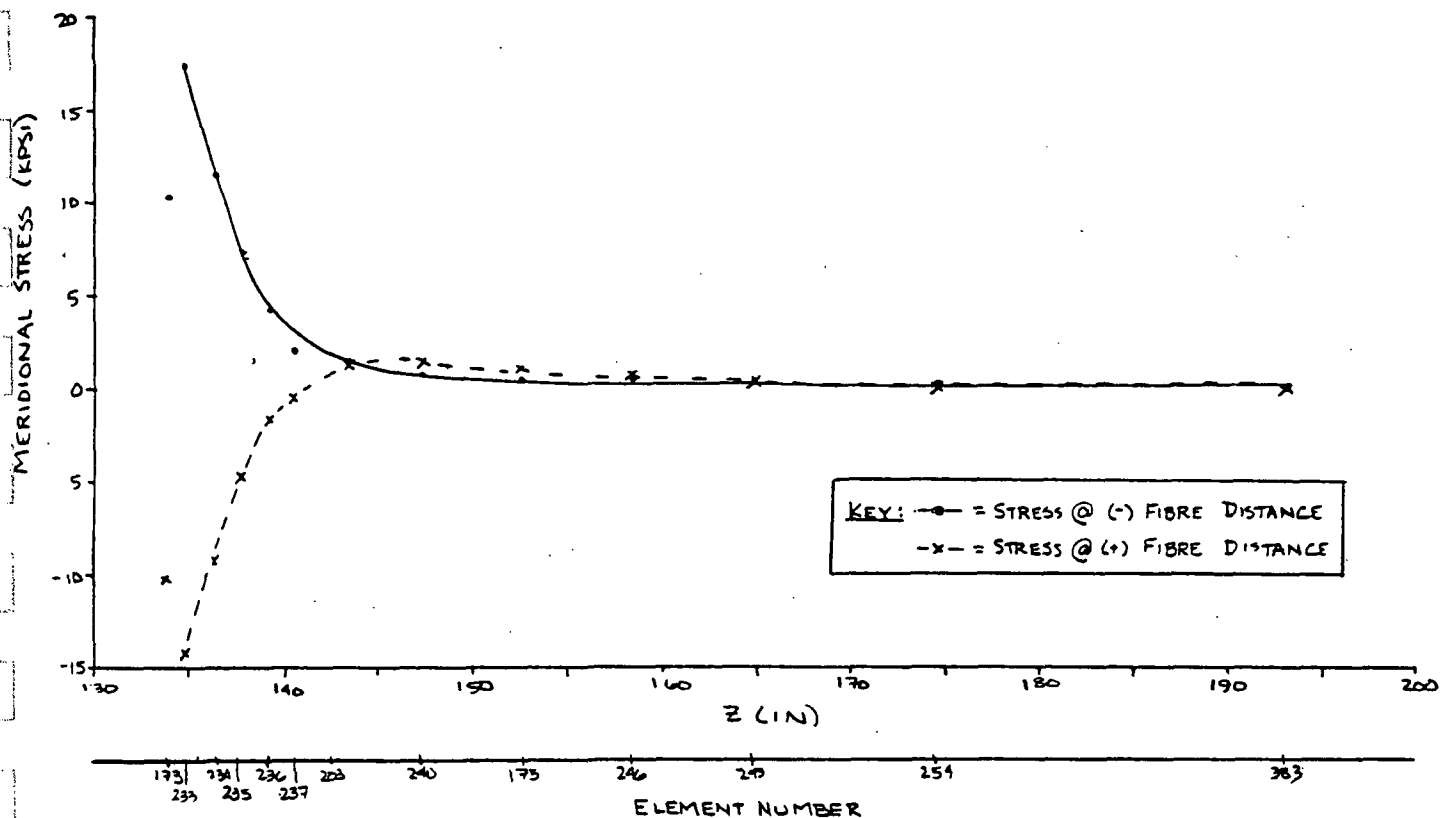
3.3.1A

SUBJECT		REPORT NO.	PAGE OF
NASTRAN RESULTS FOR THE SLEEVE WITH 1G LATERAL LOAD (RUN 2.0)		DATE	11 AUGUST 1986
SEGMENT 3L		WORK ORDER	
BY	CHK. BY	DATE	

MERIDIONAL STRESS .VS. Z

OUTB'D SHINGLE

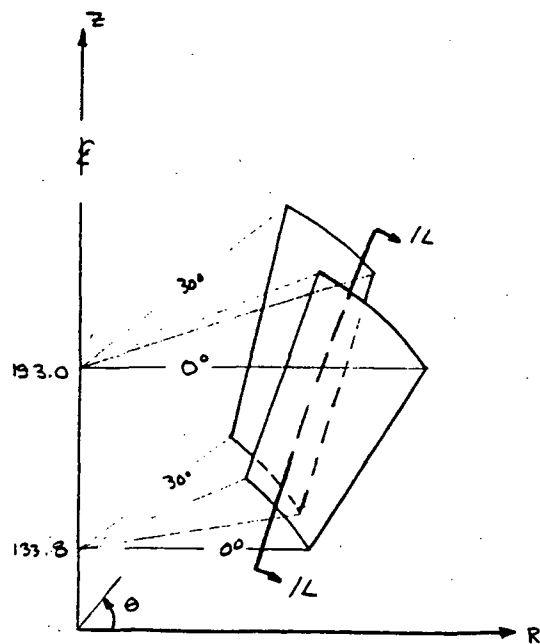
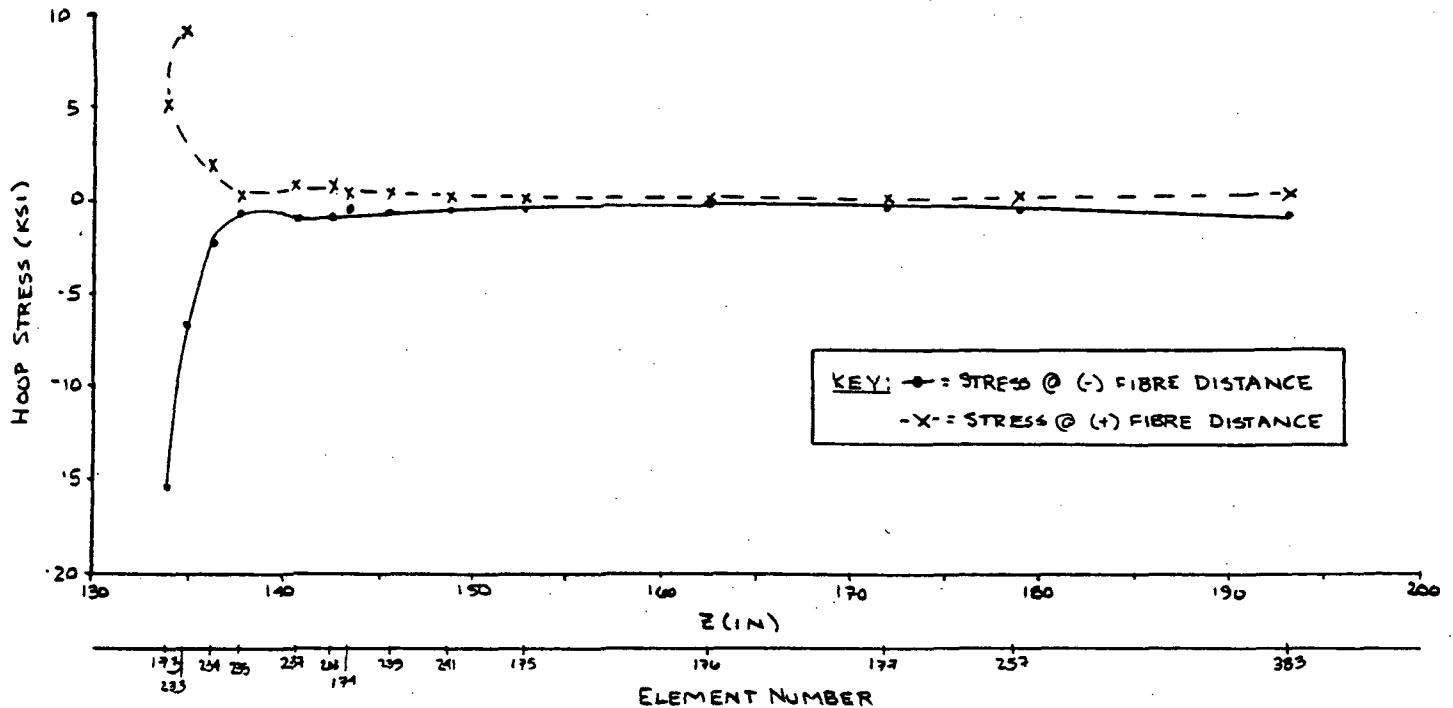
SEC. 1K-1K



$$M.S. = \frac{70}{17.5} - 1 = \underline{\underline{3.0}}$$

REPORT NO.		PAGE OF
SUBJECT		DATE
NASTRAN RESULTS FOR THE SLEEC WITH 1G LATERAL LOAD (RUN 20)		12 AUGUST 198
SEGMENT = 1R		WORK ORDER
BY	CHK. BY	DATE

HOOP STRESS VS. Z
OUTB'D SHINGLE
SEC. 1L-1L



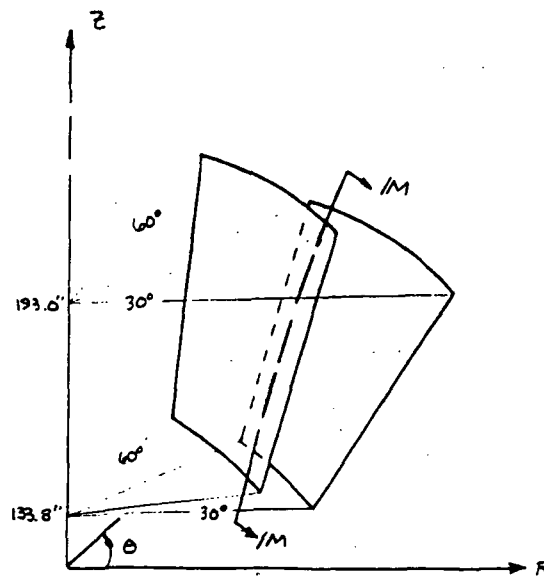
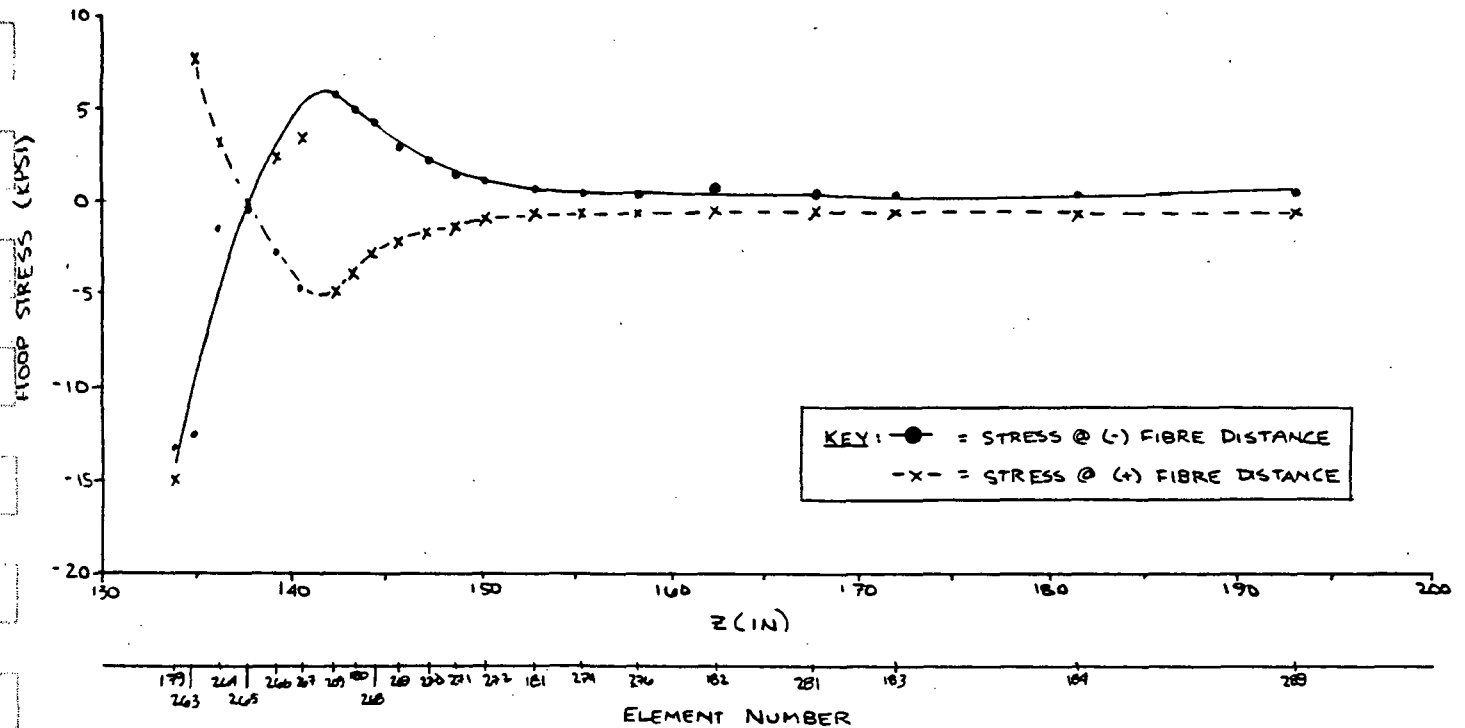
$$M.S. = \frac{70}{15.5} - 1 = \underline{\underline{3.5}}$$

ORIGINAL PAGE IS
OF POOR QUALITY

3.3.16

REPORT NO.		PAGE	OF
SUBJECT		DATE	
NASTRAN RESULTS FOR THE SLEEVE WITH 1G LATERAL LOAD (RUN 2.0)		12 AUGUST 1986	
SEGMENT 1L		WORK ORDER	
BY	CHK. BY	DATE	

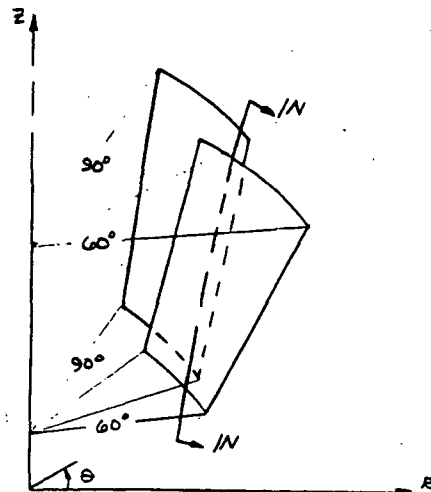
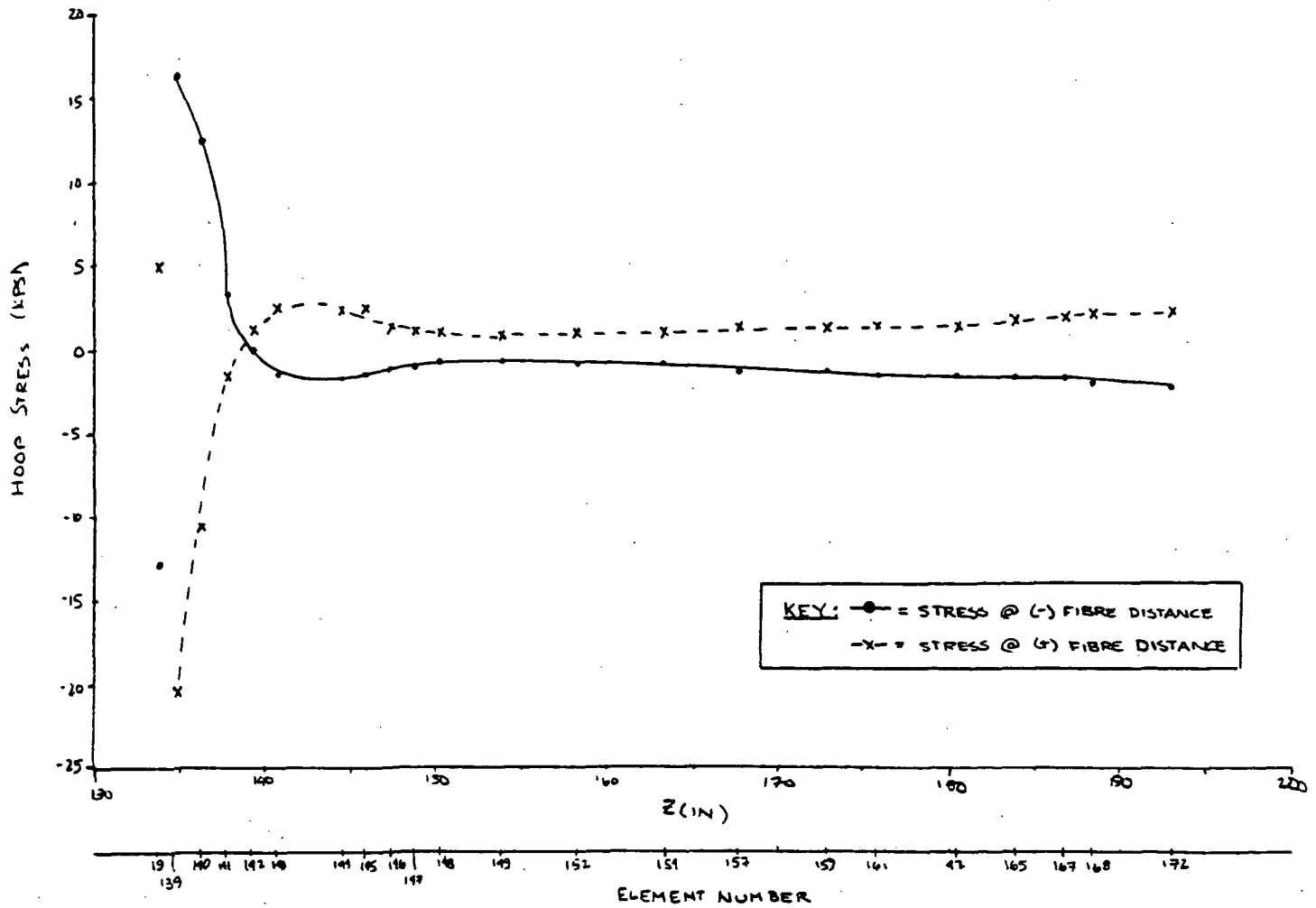
HOOP STRESS .VS. Z
OUTSIDE SHINGLE
SEC. 1M-1M



$$M.S. = \frac{70}{15} - 1 = \underline{\underline{3.7}}$$

REPORT NO.		PAGE	OF
SUBJECT		DATE	
NASTRAN RESULTS FOR THE SLEEC WITH 1G LATERAL LOAD (RUN 2.0)		13 AUGUST 198	
SEGMENT = 2R		WORK ORDER	
BY	CHK. BY	DATE	

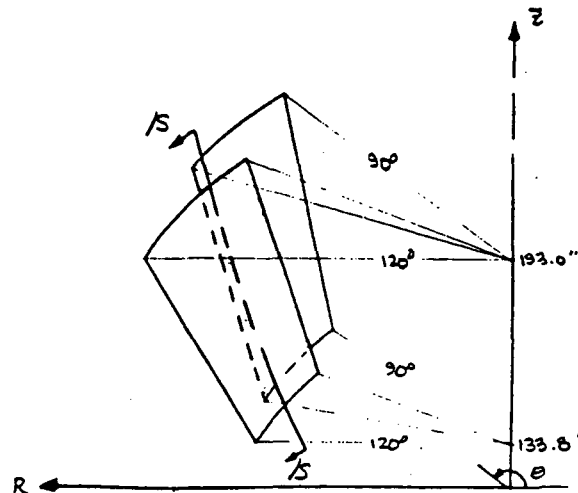
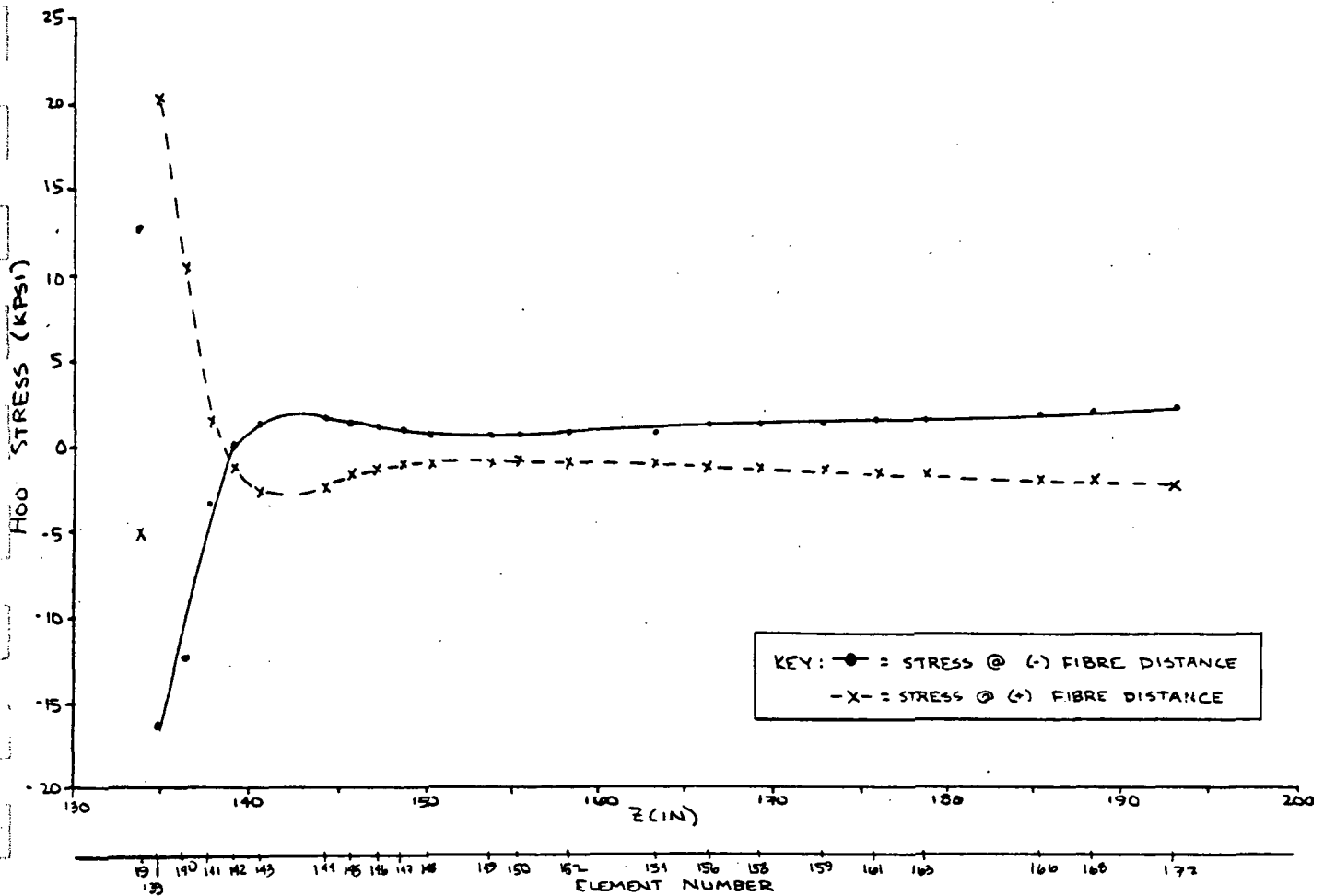
HOOP STRESS VS. Z
OUTR'D SHINGLE
SEC. 1/N-1/N



$$M.S. = \frac{70}{20.5} - 1 = \underline{\underline{2.4}}$$

REPORT NO.		PAGE	OF
SUBJECT		DATE	
NASTRAN RESULTS FOR THE SLEEC WITH 1G LATERAL LOAD (RUN 2.0)		13 AUGUST 1986	
SEGMENT 2, L		WORK ORDER	
BY	CHK. BY	DATE	

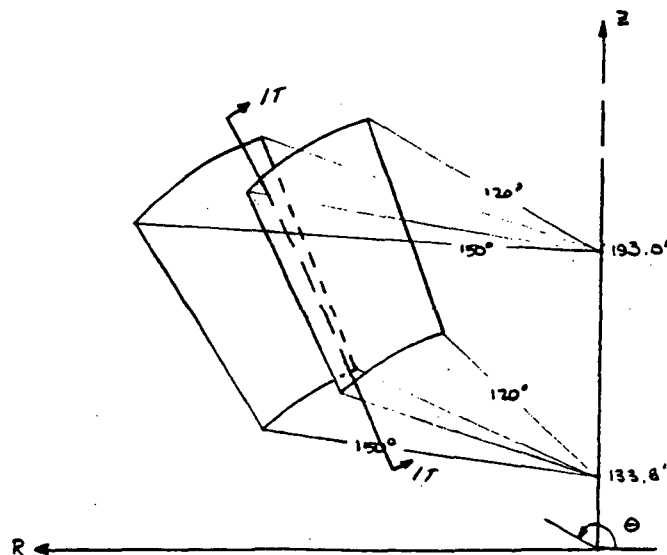
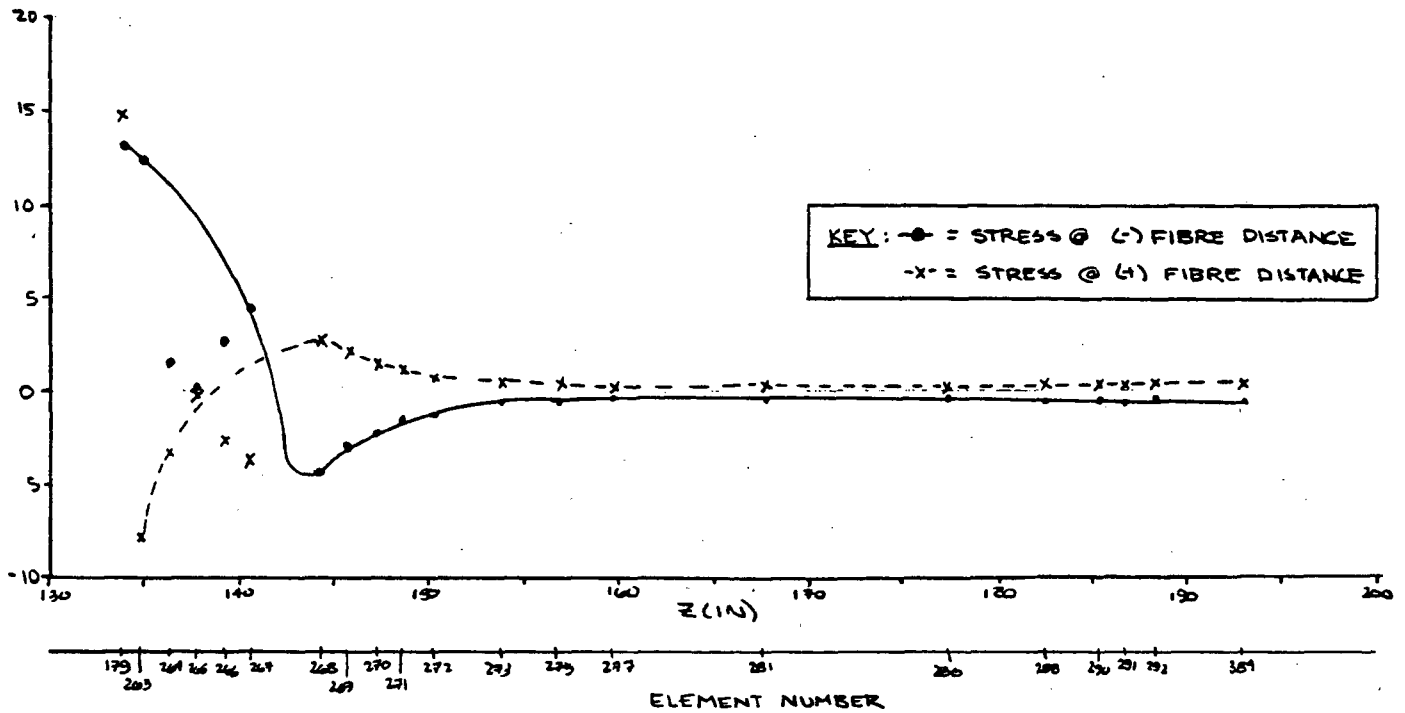
HOOP STRESS VS. Z
OUTB'D SHINGLE
SEC. 15-15



$$M.S. = \frac{70}{20.5} - 1 = \underline{2.4}$$

REPORT NO.		PAGE	OF
SUBJECT		DATE	
NASTRAN RESULTS FOR THE SLEEVE WITH 1G LATERAL LOAD (RUN 20)		13 AUGUST 198	
SEGMENT 3R		WORK ORDER	
BY	CHK. BY	DATE	

HOOP STRESS VS. Z
OUTSIDE SHINGLE
SEC. IT-IT

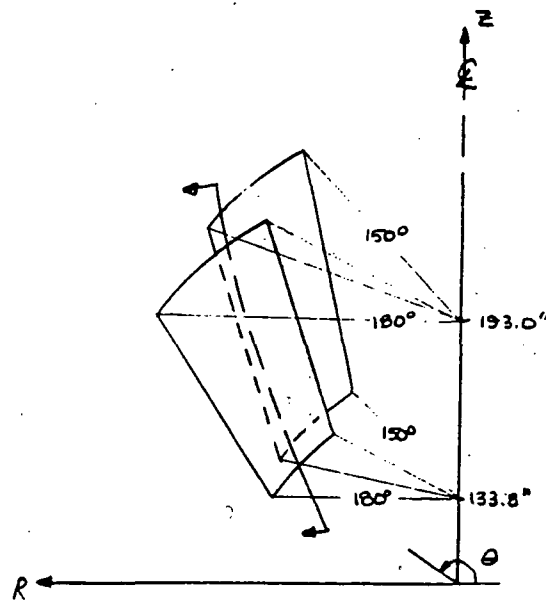
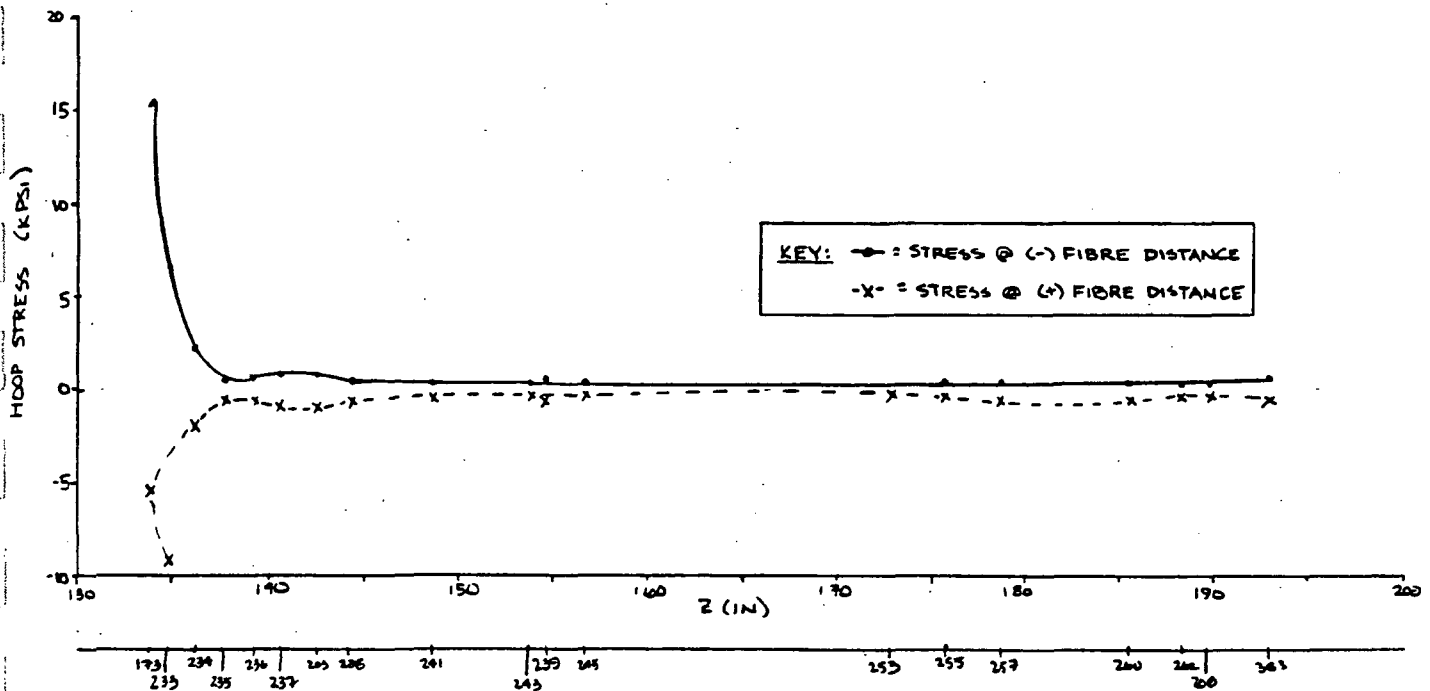


$$M.S. = \frac{70}{14.8} - 1 = 3.7$$

ORIGINAL PAGE IS
OF POOR QUALITY

SUBJECT		REPORT NO.	PAGE OF
NASTRAN RESULTS FOR THE SLEEVE WITH 1G LATERAL LOAD (RUN 2.0)		DATE	13 AUGUST 1986
SEGMENT 3L		WORK ORDER	
BY	CHK. BY	DATE	

HOOP STRESS VS. Z
OUTSIDE SHINGLE
SEC 1U-1U



$$M.S. = \frac{70}{15.5} - 1 = \underline{\underline{3.5}}$$

3.3.2.1

